Thesis for the Master's degree in chemistry

Christian Ahoba-Sam

Ethene Alkylation: Kinetics and Mechanism

60 study points

DEPARTMENT OF CHEMISTRY
Faculty of mathematics and natural sciences

UNIVERSITY OF OSLO 05/2014

ACKNOWLEDGEMENTS

I am grateful to God who is able to do exceedingly abundantly above all through His Son, Jesus Christ who has made it possible for me to come this far, may His name forever be praised. I want to thank the Norwegian Government's Quota Scheme Scholarship for sponsoring my living expenses in Norway in order to have this master's study.

All experimental work has been performed under the supervision of Prof. Unni Olsbye, Assoc. Prof. Stian Svelle and Marius Westgård Erichsen, in the Department of Chemistry, University of Oslo, from August 2012 to May 2014. I am grateful to all of them for allowing me to work with their facilities and to tap into their wealth of knowledge during the period for the success of this work. Particularly, to my main supervisor Unni, I sincerely appreciate her inspiration and in-depth explanations during the period and also to Marius for his support in and out of the lab, and providing me with catalysts for the entire work.

Special appreciation to all members of the catalysis group, for providing a cordial and inspiring learning environment to make my stay worthwhile. Dr. Chavan is acknowledged for helping in the IR spectroscopy. I acknowledge those who helped with proof-reading of this thesis, Reynard and James. Finally, sincere thanks to my dear wife, Rhoda and son Nyansa, for allowing me to spend long hours away from home during the period.

If I have seen further it is by standing on the shoulders of giants. —Isaac Newton

ABSTRACT

Propene and butenes are important chemicals needed for the production of various polymers. Ethene alkylation is one route that can lead to the formation of these monomers. The kinetics and mechanism of this process has not been fully explored so far. The aim of this work is to elucidate the influence of acid strength on the kinetics and mechanism of the titled reaction. Two catalysts, H-SAPO-5 and H-SSZ-24, belonging to the AFI topology with characteristic one-dimensional and large enough pores to minimize transition state restriction have been used in this study. The H-SSZ-24 has stronger Brønsted acidic sites compared to H-SAPO-5.

When ethene was fed over H-SAPO-5, linear butene, propene and iso-butene were the main products. The formation rates of these products followed a second order in ethene at 673 and 748 K. An autocatalytic effect was observed coupled with a decline of linear butenes selectivity as opposed to increasing propene and iso-butene selectivity with increasing ethene conversion. These indicated that linear butenes are the primary product while iso-butene and propene are secondary products. Hence linear butene reactions were further studied.

When linear butenes were fed, no autocatalytic effect was observed and iso-butene, propene and pentenes were the main products. While iso-butene formation was observed to be favored by high temperature and low pressure, the opposite was the case for propene and pentenes. A first order reaction rate in linear butene was found for iso-butene formation and second order for the formation of propene and pentene at 748 and 823 K. The linear butene reactions therefore indicated that while iso-butene is formed from isomerization, propene and pentenes are formed from dimerization-cracking.

To bridge the two reactions, ethene and linear butene were co-reacted. The influence of ethene was mainly observed on the reaction after $\frac{P_{ethene}}{P_{cis-butene}} = 5$ at 748 K. This indicated the importance of linear butenes in the mechanism of ethene alkylation.

When these experiments were repeated over H-SSZ-24, no significant difference in product distribution was observed. However, the difference in acid strength resulted in about 9 to 11 times increase in activity at 748 K compared to that of H-SAPO-5.

LIST OF ABBREVIATIONS IN THIS THESIS

AFI	IZA code for the framework of $AlPO_4$-5, SAPO-5 and SSZ-24
$AlPO_4$	Aluminophosphate (Zeolite material consisting of Al, P and O)
BEA	IZA code for the framework of zeolite Beta
BET	Braunauer-Emmet-Teller
BSE	Back scattered electron
CHA	IZA code for the framework of Chabazite, SAPO-34 and SSZ-13
CT	Contact time
Ea	Intrinsic activation energy
Eapp	Apparent activation energy
EDS	Energy dispersive x-ray spectroscopy
ETD	Everhart-Thornley Detector
FCC	Fluidized catalytic cracking
FER	IZA code for the framework of ferrierite
FTIR	Fourier transform infrared
GC	Gas chromatography
IUPAC	International Union of Pure and Applied Chemistry
IZA	International Zeolite Association
LFD	Large Field detector
MCM	Mobil Composition of Matter
MeAPO	Metal aluminophosphate (A metal containing $AlPO_4$ material)
MFI	IZA code for the framework of ZSM-5

MS	Mass spectrometry
Mtoe	Million tonnes of energy
NMR	Nuclear magnetic resonance
SAPO	Silicoaluminophosphate (Zeolite material consisting of Si, Al, P and O)
SBU	Secondary building unit
SDA	Structure directing agent
SE	Secondary electron
SEM	Scanning electron microscopy
SSD	Solid state detector
SSZ	Standard oil Synthetic Zeolite
TAA	Trialkyl aluminium
TCD	Thermal conductivity detector
TEA	Triethylamine
TMP	Trimethylpentene
TOS	Time on stream
WHSV	Weight hourly space velocity
XRD	X-ray diffraction
VPI	Virgina Polytechnic Institure

TABLE OF CONTENTS

1. INTRODUCTION

During the last century, crude oil has been the main feedstock for the petrochemical industry, for the production of transportation fuel and basic chemicals for the chemical industry. However the increasing demands (for fuels and chemicals) do not match the supply. Therefore, there is now a gradual shift of the use of oil as the all-dominating source of petrochemical feedstock towards coal and natural gas for the same. The International Energy Agency (IEA) 2010 report (see Figure 1.1) shows that coal and natural gas are gradually taking over [1]. For example, between the 1970s and 2008, the world relative supply of oil decreased from 46 to 33 % as compared to the relative increase in the supply of gas and coal from 41 to 48 %.

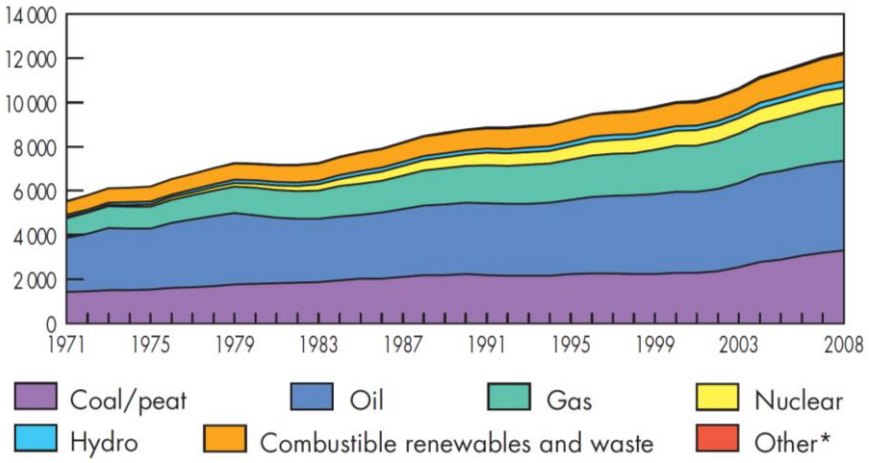

Figure 1.1: The world's total primary energy supply by fuel (Mtoe), evaluation from 1971 to 2008. IEA 2010 annual report [1]

The shift has had an effect on the production of important naphtha co-products such as ethene, propene and butene needed in the petrochemical industries for the production of various polymers which are now in increasingly short supply. Propene for example is used for the production of polypropylene, acrylonitrile and acrylic acids [2]. Iso-butene is converted to methyl-tertiary-butyl-ether to improve the octane number of gasoline among other uses such as polyisobutene, methacrolein and other chemicals [3].

The shift has therefore generated interest in exploring other means of producing ethene, propene and butene. One of such routes is steam cracking, where unreactive alkanes are converted into

reactive alkenes at very high temperatures (> 1000 K) in the presence of steam. Steam cracking of ethane for example produces ethene as the main product [3]. This reaction has received much attention in the United States particularly over the past decade due to the exploration of shale gas (natural gas trapped in shale) which has increased their domestic supply of natural gas to about 95 % of what they need[4]. Currently, many crackers originally meant for naphtha feed are being retrofitted to crack ethane. The cracking of ethane, despite its cheaper cost and abundant feed, produces lesser propene and butene as compared to naphtha feed [5].

Another route to meet the demand of propene and butene production is ethene alkylation reaction. Alkylation involves the transfer of an alkyl group onto another to form longer hydrocarbon chains such as butenes, hexene, octene and so on. Propene for example can be formed from cracking of these longer chains or from other pathways depending on the type of catalyst used. Some catalysts identified and used for alkylation reactions include transition metal complexes, solid acids (inorganic oxides) such as zeolites and metal incorporated into inorganic oxides [6, 7]. Brønsted-acidic zeolites and zeotypes represent one class of materials with potential as ethene alkylation catalysts [8].

The aim of this thesis is to study the influence of acid strength on the kinetics and mechanism of ethene alkylation reactions. A Brønsted-acidic zeolite and zeotype catalysts with large pore sizes and belonging to the same topology (AFI) but with different acid strength will be studied; H-SAPO-5 and H-SSZ-24. The pore size of these catalysts is sufficiently large to allow benzene derivatives and other long chain hydrocarbons to pass through [9, 10]. Per our initial observations, which showed that linear butene was an important product in the process, two alternative mechanisms were studied; the direct alkylation of ethene, and ethene alkylation of a linear butene. As a result, chapter 6 is dedicated to linear butene reactions using cis-2-butene as the feed, chapter 7 to linear butene and ethene co-reactions and then chapter 8 to ethene reactions over both catalysts.

2. CATALYSIS AND ZEOLITES

2.1 CATALYSIS

The history of catalysis dates back to 1814, when Kirchhoff reported on acid hydrolysis of glucose. Other authors followed with various works on catalysis until 1834, when Faraday first investigated why ethylene adsorbs (attaches to surfaces) and deactivates platinum temporarily while sulphur adsorbs and deactivates platinum permanently. His mechanistic study on deactivation and regeneration of catalysts made him the first to have studied catalytic reactions. Berzelius in 1835 defined this process and named it catalysis [11].

A catalyst is defined as a substance that speeds up the rate of a chemical reaction but does not take part in the stoichiometry of the reaction. It provides an alternative pathway for a reaction and as a result lowers the activation energy of the reaction. This occurs as the reactants form bonds with the catalyst, thereby weakening the interatomic bonds, increasing the probability of a favorable orientation of the reactant molecules and also increasing the number of collisions between the reactant molecules. The Figure 2.1 shows the difference in the energy barrier and the pathway between a catalytic (lower) and non-catalytic (upper) reaction pathway. Here, both catalyzed and non-catalyzed products have the same initial and final potential energies. In essence, the catalyst accelerates the equilibrium formation by lowering the activation energy for both forward and backward reactions. Therefore catalysts only affect the kinetics but not the thermodynamics of a reaction [12].

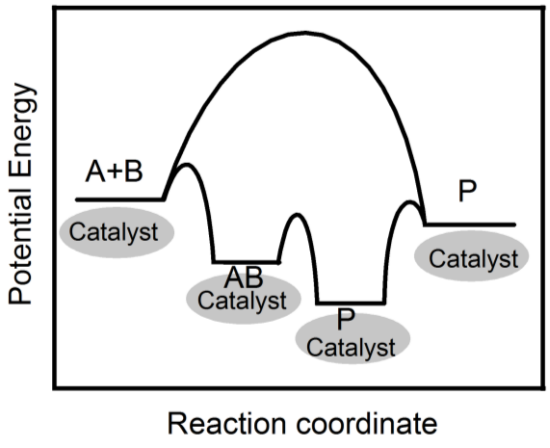

Figure 2.1: Potential energy diagram versus progress of reaction for a non-catalyzed reaction (upper path) and a catalyzed reaction (lower path). Adapted from [12]

2.1.1 Types of Catalysis

A catalyst can be atoms, molecules, larger molecules like enzymes or even solid surfaces. Catalysts usually work by either reduction-oxidation (redox catalyst) or by acid-base reaction or the combination of the two. The redox catalyst involves electron transfer and is usually observed in transition metals or metal complex catalysts. The acid-base catalyst involves mostly proton transfer similar to the Brønsted acid-base concept or in the form of electron pair transfer similar to the Lewis acid-base concept.

Generally, catalysis is classified as either homogeneous or heterogeneous. This distinction is based on the phase in which the reactants and the catalyst are. Homogeneous catalysis is a catalytic reaction where the catalyst and reactants are in the same phase. Example is *Ozonolysis*, where chlorine gas catalyzes the ozone decomposition which causes ozone layer depletion. Heterogeneous catalysis, on the other hand involves catalyst and reactants being in different phases. Example is the *catalytic cracking of crude oil* which is widely used in the petroleum industry, where a zeolite (solid catalyst) catalyzes the cracking of heavy oil fraction into lighter fractions [12, 13].

This project will be based on heterogeneous catalysis; reaction of ethene and cis-2-butene in gaseous phase over solid acids; protonated zeolite and zeotype.

2.2 ZEOLITES AND ZEOTYPES

Zeolite history dates back to the 18th century when A. F. Cronstedt (1756) discovered crystals of aluminosilicates in northern Sweden. Close to two centuries later, it was discovered that the dehydrated form of the aluminosilicate crystals could sieve molecules by selectively adsorbing smaller organic molecules and rejecting larger ones. Zeolites are now known to be microporous crystalline aluminosilicate materials with a one to three dimensional framework structure and molecular-sized pores and cavities, which can allow or disallow molecules from passing through

them based on their sizes or shapes (shape-selectivity). Zeolites are composed of TO_4 tetrahedrals, where the T is aluminium or silicon and O is an oxygen atom. Figure 2.2A shows silicate a typical TO_4 building unit which binds with alumina through the oxygen atom. Figure 2.2B shows a two unit TO_4 which builds up to form a zeolite framework.

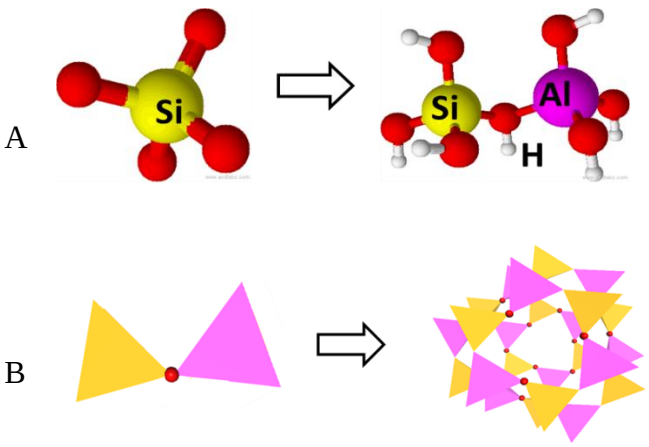

Figure 2.2: The building of zeolites from TO_4 tetrahedrals to form rings with their internal porosity and crystalline structures, adapted from [14]

There is another class of materials which behave in many ways like zeolites and have similar properties, usually referred to as *zeotype*. Zeotypes have the same structure as zeolites but differ in elemental composition. Examples of zeotypes include AlPOs where the T atoms consist of aluminium and phosphorus, and SAPO where the T atoms consist of silicon, aluminium and phosphorus. SSZ-24 and SAPO-5 are examples of zeolite and zeotype respectively, which were used in this project. Zeolites and zeotypes are grouped into different types of frameworks. These frameworks describe the connectivity (topology) of the tetrahedral atoms in their best symmetry as possible. They define the size, shape and volume of the pores, channel system dimension, arrangement of cages and the types of cation sites available. A 3-letter code is assigned to the framework type by the International Zeolite Association according to rules set by IUPAC Commission on Zeolite Nomenclature. The codes are derived from the name of the zeolite or material type. Examples include FAU – **Fau**jasite, LTA – **L**inde **T**ype **A**, MFI- **Z**eolite Socony **M**obil **Fi**ve (from ZSM-5) [15]. As at April 2014, 218 zeolite framework types had been confirmed by the commission [16].

Zeolites and zeotypes can also be classified based on the number of T-atoms forming their ring circumference. Typically, they form 8, 10 and 12 ring structures though larger rings are synthesized (VPI-5 has 18 ring structure). The ring size determines the dimension of the pore. The 8-ring has small-pore between 0.3-0.45 nm; the 10-ring has medium-pore between 0.45-0.60 nm; and the 12-ring has the large-pore up to 0.80 nm pore diameter [17].

The valency of the T atoms can make the structure electrically charged or neutral. If the T atom is silicon throughout, a neutral SiO_2 crystal is formed since Si is tetravalent. The incorporation of aluminium creates a negative charge in the structure since Al is trivalent. On the contrary, in the AlPOs for instance, equal aluminium and phosphorus contents make its structure neutral since P is pentavalent and Al is trivalent. The incorporation of silicon creates a net negative charge. The negative charges are balanced with cation by ion exchange. If the cation is a proton (H^+), then a Brønsted acid zeolite or zeotype is formed [14] often denoted with H- before the name of the zeolite (example is H-SSZ-24). This has been shown in the Figure 2.2A were H on the oxygen forms the O-H bridge between the Si and Al.

The framework type and chemical environment of the zeolite material affect the acidity of zeolites. In terms of Brønsted acidity, two terms, acid strength or acid site density are often used. The *acid strength* of the zeolite defines the relative ease in releasing its proton. This depends on the bond strength of the O-H bond bridging the Si and Al. The weaker the O-H bond the relatively easier it is to release its proton during reaction and hence the stronger the acid zeolite. The *acid site density* defines the concentration or number of acid sites available per gram of material. In zeolites, the number of Al incorporated dictates the number of acid sites available while in SAPOs, the number of Si incorporated does the same. In essence the Si/Al in zeolite and (Al+P)/Si in SAPOs is used to estimate the acid site densities; the lower this ratio, the higher the acid site density [18].

2.2. Applications of Zeolite in catalysis

Zeolites have several applications due to their structural properties. An example is their ion exchange ability due to the accessibility of cation sites which is widely used in the detergent industry. They also have adsorption capacity which is applied in drying, purification and separation. Among these applications of zeolites is shape selectivity and catalytic ability which is used in many hydrocarbon reactions. One of which is the catalytic cracking of large range of oil fractions used in fluidized catalytic cracking (FCC)[17].

The amazing properties of zeolites for catalysis are due to their pore opening, dimension of channels, cation active sites, and space available for reaction intermediates [12, 17]. As stated earlier, their typical pore diameters range between 0.3 to 0.9 nm which is within molecular size range. This makes them allow some molecular species to pass through them and disallow others, a phenomenon referred to as shape selectivity. It has been reported that H-SAPO-34 (CHA topology) which has pore openings of 3.8 Å diameter give superior propene selectivity in ethene alkylation compared to H-ZSM-5 (MFI topology) with 5.3 to 5.6 Å pore diameter[8]. Figure 2.3 shows three main types of shape selectivities with examples. When only the reactants with dimensions smaller than the pore size are allowed into the pores to react, *reactant selectivity* is involved. On the other hand, when only certain transition state or product geometry are allowed through the pores then *transition-state* or *product selectivity* are respectively involved[3].

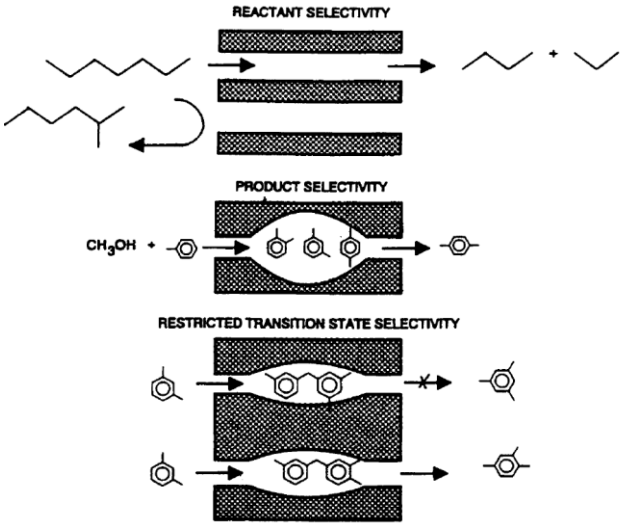

Figure 2.3: The different types of shape selectivities [3]

One of the catalytic applications of zeolites is alkylation of iso-butane to improve the octane number of gasoline production[19]. The octane number is used to describe the efficiency of gasoline in combustion engines. Lower molecular weight alkenes such as propene, butenes and pentenes are used to alkylate the iso-butane. Mineral acids such as HF and H_2SO_4 have been used industrially for iso-butane alkylation. However these catalysts have some drawbacks such as pollution, safety, thermal stability and corrosion related problems. Zeolites on the other hand are non-corrosive, combine high acidity with shape selectivity, have a high surface area and have high thermal stability. Hence much research is being carried out on zeolites as an alternative. The drawback in zeolite usage however is that they lose their activity faster as a result of polymerization or aromatization to form carbonaceous deposits also known as coke within their pores [3, 12]. However zeolites can be regenerated by burning off the coke.

H-SAPO-5 and H-SSZ-24 are example of materials which similarly display the above mentioned characteristics of zeotype and zeolite respectively and were used for studying ethene alkylation reaction in this project. The following section therefore describes these catalysts.

2.3 SAPO-5 and SSZ-24

The history of the $AlPO_4$-5 dates back to 1982 when Wilson et al first synthesised them along with other aluminophophates ($AlPO_4$-n) [20]. The crystal structure was solved a year after [21]. Similar structure was synthesised in 1984 with the incorporation of Si to form silicoaluminophosphates and named SAPO-5 [22]. Thereafter, an all-silica containing and also with low amount of Al zeolite iso-structure of SAPO-5 was synthesized by Nordstrand et al and named SSZ-24 [23].The story of these catalysts continues as more research goes on into their various forms of synthesis, characterization and applications. In recent times, the main route for their synthesis like other zeolite materials has been the hydrothermal techniques. This involves the synthesis with high conditions of temperature and pressure in aqueous solution in a closed system [24]. Various conditions and organic templates which act as structure directing agents (SDA) are employed during synthesis [25]. It has also been reported that several other metals can be incorporated into the $AlPO_4$-5 and SAPO-5 structure to form MeAPO or MeAPSO respectively [26].

2.3.1 SAPO-5 and SSZ-24 Structure

The SAPO-5 and SSZ-24 belong to AFI framework. The three-letter code assigned to their framework by the Structure Commission of the International Zeolite Association (IZA) is AFI derived from **A**luminophosphate-**FI**ve. The letter codes assigned to the zeolitic material are the abbreviations of their names. For example; the SAPO stands for **S**ilicon **A**luminium **P**hosphate and SSZ stands for **S**tandard Oil **S**ynthetic **Z**eolite [15]. The $AlPO_4$-5 like other $AlPO_4$ molecular sieves is made up of a strict alternating P and Al throughout the framework and forms 4, 6 and 12

secondary building units. The rings are viewed as secondary building unit (SBU) when the framework is assumed to be made up of only one SBU. Figure 2.4 shows a layer of the AFI framework. The structure consists of 6-rings connected to three other 6-rings via oxygen bridges to form 4-rings and 12-ring hexagonal arrays. Their construction can also be seen by the composition of the composite building units for the framework. Figure 2.5 shows the composite building units which are *afi*, *bog* and *nsc* (narsarsukite chain) made up of twisted 4 and 6 rings from which the AFI can be constructed. The layers are stacked on top of the each other like mirror images which give rise to a one dimensional channel as shown in Figure 2.6. The 12 membered rings have pore diameter of 0.73 nm and framework density of 16.9T/nm^3. [15-17].

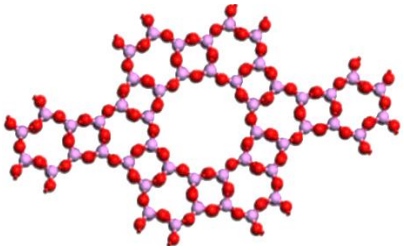

Figure 2.4: A layer of AFI framework, red is O and the purple is alternating Al or P.

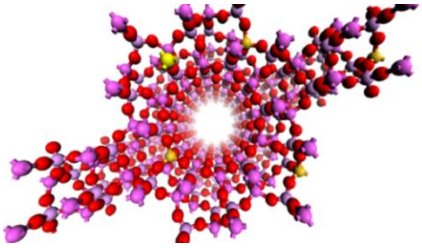

Figure 2.6: The perspective view of the one dimensional channel of AFI framework.

afi ***bog*** ***narsarsukite chain (nsc)***

Figure 2.5 : The composite building units of AFI [15]

Silicoaluminophosphates (SAPO) are made such that there is Si substitution unto aluminophosphate molecular sieves. They are mechanistically considered to be formed via Si substitution for P which creates negative charge [22]. The SSZ-24 as an example of zeolite which is made up of a substitution of Si with Al unto pure silicates which also creates the net negative charge as explained earlier. In Figure 2.6, the yellow ball represents the incorporation of Si into the $AlPO_4$ structure and can also stand for the Al incorporated into pure silica. The negative charges are balanced with cations, and the use of protons creates Brønsted acid sites.

2.3.2 Application of SAPO-5 and SSZ-24 in catalysis

The SAPO-5 and SSZ-24 have shown much interesting properties similar to those described for zeolites earlier. The uniform pore dimension of the AFI framework structure has earlier been shown by Union Carbide to be shape and size selective for separation and catalysis. Butane cracking reaction over various materials showed that though the SAPOs were more active than $AlPO_4$s, they were generally less active compared to their zeolite analogues [22]. Some examples of studies done over the AFI materials to show the sort of molecules their pore sizes can allow are listed below.

- Ito et al[9] studied propene alkylation of biphenyl over H-SSZ-24 with different acid site densities, which showed similar product selectivity with temperature within 423 to 623 K. They reported that the channels in H-SSZ-24 were large enough to accommodate, isomerize and discriminate bulky species such as diisopropylbiphenyl and its isomers.
- Upadhyayula[10] studied the propene alkylation of toluene over H-SAPO-5 also with different acid site densities within 453 to 553 K. They reported that iso-propylbenzene, which was the main product, increased in yield with increasing Si content.
- Westgård Erichsen et al[27] reported on methanol and benzene co-reaction over H-SAPO-5 and H-SSZ-24 in a **m**ethanol-**t**o-**h**ydrocarbon mechanistic study. They also observed high yield of substituted benzenes as products ranging from toluene to hexamethylbenzenes at 523 to 573 K over both catalysts, though the relative amounts of products were not the same and H-SSZ-24 was more than 7 times active than the H-SAPO-5.

H-SAPO-5 and H-SSZ-24 have been chosen for this project because of the above mentioned properties. Their pore diameter can allow reactions with bulky transition states and intermediates to be studied. As a result, a kinetic study of alkylation of the ethene and its oligomers can be studied with possibly fewer restrictions to reactants, transition state or products. Adequate kinetic measurements can help to better understand the mechanistic pathway of ethene alkylation reaction. With their similar structure, single parameter such as acidic strength influence on the mechanism can also be studied. This will help to elucidate the influence of acidic strength on ethene alkylation mechanism.

3. ETHENE ALKYLATION REACTION

3.1 Introduction

Alkylation which was defined earlier to mean the transfer of alkyl groups onto another molecule needs to be distinguished from other terms used in describing ethene reaction mechanism such as dimerization and oligomerization, although they all involve some form of addition of hydrocarbons. Dimerization is used to describe addition of two similar alkenes to form a dimer[28] Oligomerization involves the addition of few alkenes to form relatively short chain hydrocarbons (< 20 C chains) as opposed to polymerization which forms longer chain hydrocarbons [29].

Different types of catalysts have been identified for reactions involving addition of ethene. Transition metal complexes of mainly Ti and Ni (Zr, Hf and Cr have also been reported) coupled with trialkyl aluminium (TAA) are known for ethene oligomerization to produce 1-alkenes. This usually occurs by the formation of an active centre on the metal complex with the TAA, alkene coordination, propagation and chain termination [6, 30]. This process is very selective towards linear 1-alkenes. However, being homogeneous catalysis, it comes with its associated disadvantages such as poor thermal stability, difficulties in product separation and catalyst regeneration [13].

Solid acidic catalysts such as zeolites and zeotypes are known to be efficient in catalyzing addition of ethene by alkylation. The generally accepted mechanism in alkylation is via carbenium ion [3, 31]. Baba and Sawada[32] reported that, H-ZSM-5 showed 90 % ethene conversion and no methane conversion at P_{C2H4}=P_{CH4}= 33.8 kPa and 598 K. Loading H-ZSM-5 with Ag showed a decline in ethene conversion with a corresponding increase in methane conversion. This indicated that protonation of ethene is an important step in the ethene alkylation reaction. Figure 3.1 shows ethylation of ethene via a carbenium ion intermediate (an alkylation process). The first step of

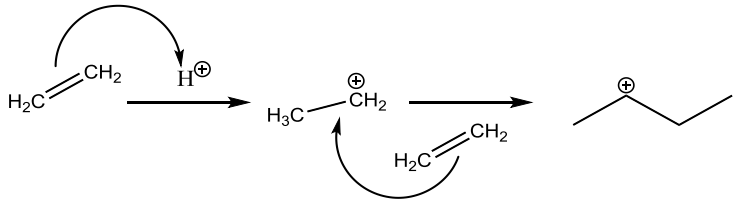

Figure 3.1: Ethylation of ethene via carbenium ion intermediate adapted from [3]

the reaction involves protonation of ethene to form a carbenium ion. Carbenium ion is a positively charged trivalent hydrocarbon usually with the formula R_3C^+. Their stability depends on the number of neighbouring sigma bond electrons which interact with the positive center (or empty orbital) and hence decreases as; tertiary > secondary > primary > methyl [33]. Ethyl cation is a primary carbenium ion and hence has poor stability. The second step is ethylation to form a butene, and then subsequent reaction may follow.

3.2 Ethene alkylation reaction over molecular sieves

The industrial products of interest in the ethene alkylation reaction with regards to this study are mainly propene and isomers of butenes. The trend in the formation of these products can give mechanistic insights to better understand how the reaction works. As a result, this section has been divided into two parts; to follow propene formation from ethene and then, how iso-butene formation is related to linear butenes.

3.2.1 Ethene to propene

Oikawa et al [8] reported of ethene alkylation reaction over small-pore H-SAPO-34 and compared with H-ZSM-5, a medium-pore zeolite at 723 K and 33.3 kPa ethene pressure. It was observed that at comparable conversions, selectivity to propene was higher over H-SAPO-34 than over H-ZSM-5, while it was lower for butenes, and particularly iso-butene formation. This was attributed to the shape selectivity of H-SAPO-34 with 0.45 x 0.41 nm pore size compared to 0.56 x 0.53 nm of H-ZSM-5. Propene has a kinetic diameter of 0.45 nm which fits better in H-SAPO-34 than the 1-butene and iso-butene with kinetic diameters 0.45 and 0.50 nm respectively. This showed that smaller pores prevent the formation of bigger products and that shape selectivity plays significant role in ethene alkylation.

Zhou et al[34] further studied the kinetics of different light alkenes over H-SAPO-34 molecular sieves at 723 K. They observed that the product distribution of ethene and 1-butene fed separately gave propene as the main product in both cases. They reported that ethene conversion showed an autocatalysis (products serve to accelerate reaction rate[35]) which was not seen in propene and 1-butene conversions. At similar WHSVs, the butene and propene conversions were over 9 to 10 times higher than that of ethene which was attributed to the difference in stability of the carbenium ion intermediates. Propene feed on the other hand gave more butene and some ethene, propane, butane and C_5+ as products. This was an indication that the alkylation process of light alkenes involved oligomerization and cracking. The autocatalysis of ethene indicated that ethene alkylates other higher alkenes faster than itself. That implied that ethene dimerization could be the rate determining step in ethene oligomerization while steps that follow are faster. Among the butene isomer products, iso-butene was the least abundant due to the shape selectivity of the H-SAPO-34.

Lin et al[36] reported that out of several molecular sieves with different pore sizes, H-ZSM-5 gave the highest ethene conversion with more propene than butene formation at 723 K. The number of Brønsted acidic protons of H-ZSM-5 was varied by different degrees of proton ion exchanged and also for different Si/Al ratios. Conversion increased while selectivity to propene slightly decreased with increasing number of Brønsted acidic protons. Selectivity to butenes was not significantly affected while aromatics were formed at the expense of propene at high H^+ content. When ethene pressure was varied, the reaction rate depended on ethene by a second order. Further in-situ FT-IR analysis at 573 K with 1.01 kPa ethene showed bands at 2960, 2935 and 2860 cm^{-1} typical of CH_3 and CH_2 stretching vibrations with corresponding 1469 and 1381 cm^{-1} bending vibration after 3 min interaction of ethene and H-ZSM-5. These were ascribed to saturated hydrocarbons due to oligomerization. This therefore led to their speculation that ethene oligomerizes and cracks to form propene.

Earlier, Spoto et al[37] reported on IR of ethene oligomerization over H-ZSM-5. At room temperature and 1.33 kPa ethene partial pressure, they observed bands due to hydrogen bonding between the ethene and the acids at 2974, 1612, 1440 and 1340 cm^{-1} within 10 s time of contact. Successive spectra taken from 7 s to 2 min showed new bands at 2960, 2876, 1469 and 1382cm^{-1} assigned to CH_3 stretching and bending, and also similarly for CH_2 stretching and bending at 2940, 2866, 1460 and 1442 cm^{-1}. These bands indicated hydrocarbon saturation due to protonation and

oligomerization of ethene. Also within this time of contact, there was no band at 1368 cm^{-1} which is usually attributed to -$CH(CH_3)_3$ or -$C(CH_3)_3$, an implication that chain branching was not an initial product of ethene oligomerization though this band appeared after 2 min.

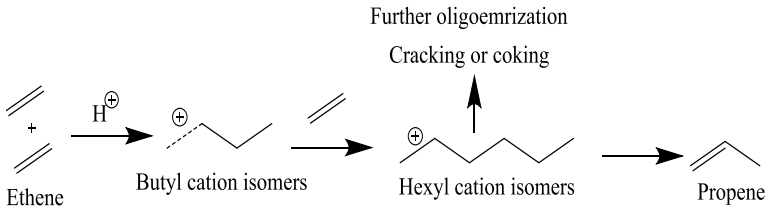

Scheme 3.1: Ethene oligomerization to propene formation

It can therefore be hypothesized from the above discussion that ethene alkylation to form propene proceeds via ethene oligomerization and cracking as summarized in Scheme 3.1. Here, ethene alkylates to butene, hexene and possibly higher alkenes. Cracking of these alkenes produces mainly propene and other possible cracking products. Aside cracking, further oligomerization can lead to the formation of heavy carbonaceous deposits or coke that can block the molecular sieves. This mechanism will therefore be investigated further over the H-SAPO-5 and H-SSZ-24 in this study.

3.2.2 Linear butene to iso-butene

To better understand the formation of iso-butene, linear butene has been reacted over several molecular sieves especially medium pores. However there has been no consensus on the reaction mechanism. So far, three types of mechanisms have been proposed.

Mooiweer et al[38] reported on H-FER (2-D, 10 and 8 membered ring) as a better catalyst compared with H-TON and H-MFI for 1-butene skeletal isomerization in terms of iso-butene yield and catalyst stability at 623 K and 120 kPa-160 kPa. They observed high iso-butene compared with C_5+ which indicated high shape selectivity of H-FER in the skeletal isomerization. They concluded that, due to high energy involved in primary carbenium ion, direct linear butene isomerization to form iso-butene was not likely but rather via dimerization-isomerization-cracking which will involve a

more energetically favourable secondary or tertiary carbenium ion. This constituted *bimolecular* linear butene skeletal isomerization.

Guisnet et al[39] also studied the skeletal isomerization of butene over H-FER at 623 K. When 1-butene was fed and contact time (1/WHSV) varied, iso-butene, propene and pentene were the main products and also appeared as primary products. The formations of pentene and propene were first order while that of iso-butene was 0.5 within 5 to 30 kPa. The apparent activation energy for 1-butene isomerization was 59 kJ/mol. When iso-butene was fed, more linear butenes but fewer propene and pentene selectivities were observed. The formation of linear butene was first order in iso-butene and the apparent activation energy was 42 kJ/mol. They suggested that iso-butene isomerization was not the reverse of linear butene isomerization since different octene isomer intermediates were involved. They concluded that iso-butene formation from linear butene may occur via dimerization, isomerization and cracking since direct isomerization will involve higher energy which is in line with the *bimolecular* linear butene skeletal isomerization pathway suggested earlier.

Scheme 3.3 illustrates a summary of the bimolecular pathway approach. Linear (n-) butenes are protonated, dimerized and then crack or isomerize before cracking. This leads to formation of iso-butene, propene and pentene which are usually the main products. The octene can also crack to produce ethene and hexene which are usually observed as minor products.

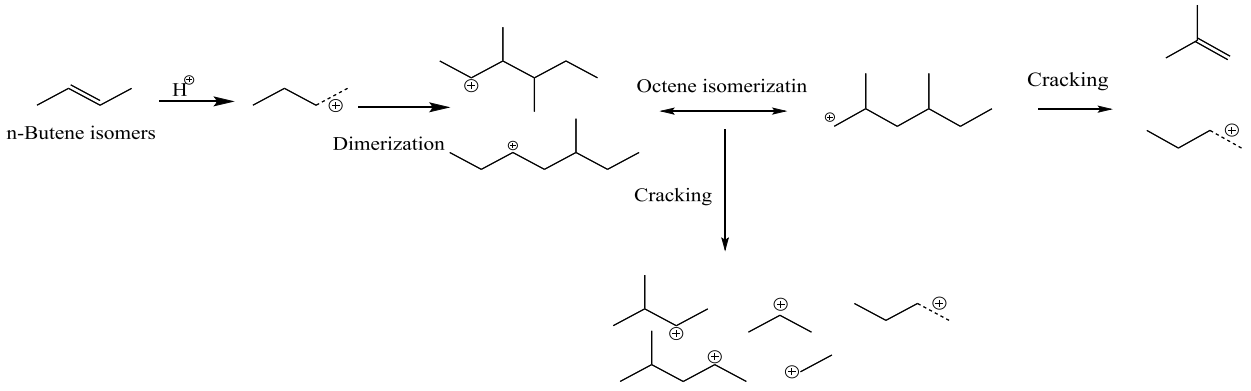

Scheme 3.3: Bimolecular pathway for formation of iso-butene, propene and pentenes

Guisnet et al[40, 41] went further to analyse the influence of coke formation on the mechanism. 1-Butene activity at shorter time on stream (TOS) at 623 K showed skeletal isomerization to iso-butene accompanied by large amount of propene and pentene with small amount of octenes, heptenes and hexenes. However iso-butene slightly increased initially before it decreased while all other products decreased with TOS. They attributed the deactivation to carbonaceous deposit (coke) which was verified with IR as aromatic coke (3085, 3062, 3037, 3000, for C-H stretching and 1524, 1583, 1617 cm^{-1} for C=C). The coke was suggested to partially block the pores which hindered dimerization reactions. They concluded that there is an active aromatic carbenium ion responsible for linear butene monomolecular isomerization rather than protonic zeolite during deactivation. This constitutes the *pseudo-monomolecular* pathway to iso-butene formation.

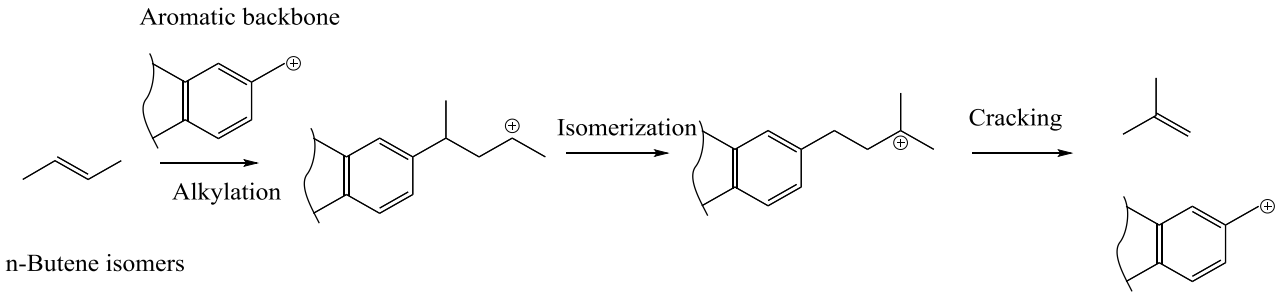

Scheme 3.4: Pseudo-monomolecular pathway to iso-butene formation

Scheme 3.4 illustrates a summary of the pseudo-monomolecular pathway. In this approach the linear (n-) butene isomerizes over an aromatic backbone and cracks to give iso-butenes. This approach limits propene and pentenes formation. In both bimolecular and pseudo-monomolecular pathways, it is proposed that the alkylation was the slowest step whilst isomerization and cracking are fast. Monomolecular linear butenes isomerism to iso-butene formation was ruled out also due to unstable primary iso-butyl carbenium ion intermediate which is suspected to be involved.

Houžvička et al[42, 43] assessed the role of bimolecular pathway for the linear butene skeletal isomerization over several catalysts. They observed that low linear butene partial pressure and high temperature favoured iso-butene and disfavoured propene and pentene formation. The product distribution when linear butene, iso-butene and octene isomers were fed separately was different as shown in Figure 3.2. When linear (n-) butene, iso-butene or 2,4,4-trimethyl-2-pentene (244-TMP) were fed over H-SAPO-11 (and MnAPO-11) at 713 K, the ratios of $(C_5+C_3)/C_4$ were much lower compared with when octenes, methylheptenes and 3,4-dimethyl-2-hexene were fed whilst 2,3,4-

trimethyl-2- pentene lay between the two. This indicated that part of 234-TMP cracks into propene and pentene while what remains isomerizes to 244-TMP which in tend, cracks to form iso-butene. They concluded that bimolecular pathway was less likely since primary dimers of linear butene crack faster than isomerization hence n-butene skeletal isomerization occurs through a *monomolecular* pathway. In addition, iso-butene could alkylate and crack to form propene and pentene.

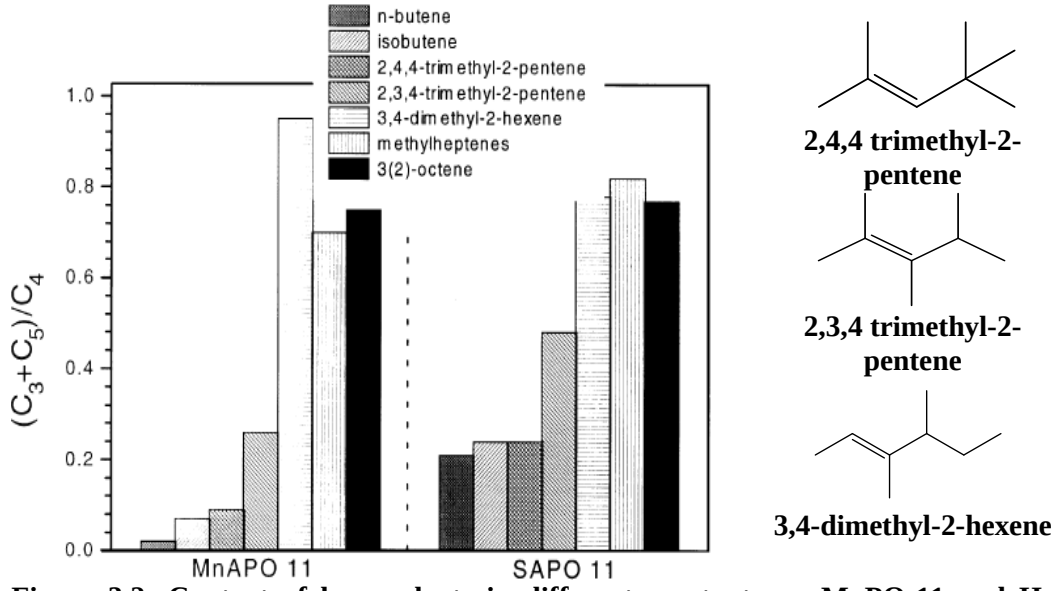

Figure 3.2: Content of by-products in different reactants on MnPO-11 and H-SAPO-11 at 713 K, 1g catalyst, from [42]. The structures of the substituted octene isomers are shown beside at the right

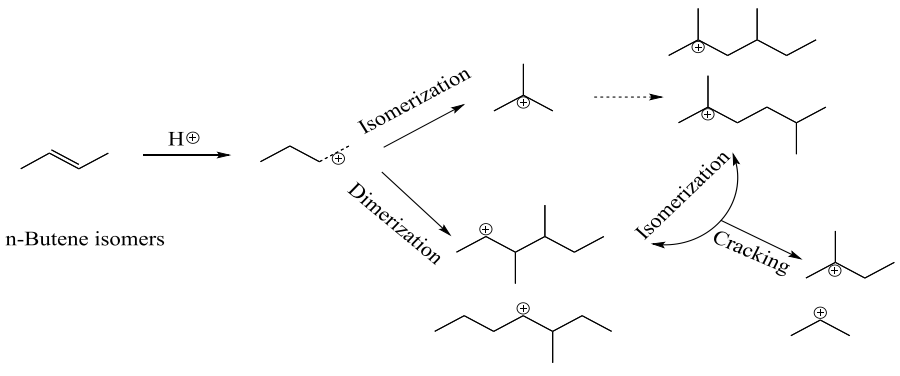

Scheme 3.4: Monomolecular iso-butene formation and bimolecular propene and pentene formation

Scheme 3.4 illustrates a summary of the monomolecular pathway to iso-butene formation and bimolecular pathway to propene and pentene formation. In this approach the linear (n-) butene isomerizes into iso-butene while it dimerizes and cracks to give propene and pentene. The iso-butene can also alkylate and crack to contribute to the propene and pentene formation.

To distinguish between these mechanisms other authors reported on isotopic labelling experiments. Meriaudeau et al [44] reported on isotopic labelling of ^{13}C linear butene over both fresh and aged H-FER at 673 K. They observed that where isobutene selectivity was high, only single labelled ^{13}C was present which favours the monomolecular pathway. At low iso-butene selectivity a mixture of double, single and no labelled ^{13}C isobutene were in the ratio 1:2:1 ratio an indication of some bimolecular reaction. Čejka et al [45] followed by comparing ^{13}C scrambling over CoAlPO-11 (one-dimensional, 3.9x6.3Å) and H-FER (three-dimensional, 4.2x5.4, 3.5x4.8 Å) at 620 K. At similar conversion (about 55 %) only 6 % selectivity showed double or no label isobutene over CoAlPO-11 and 30 % of the same over H-FER. This suggested that only 6 and 30 % unambiguously followed bimolecular pathway for CoAlPO-11 and H-FER respectively. ^{13}C NMR measurement of the labelled iso-butene showed that CH_3:CH_2:C = 1.5:1:1, implying that ^{13}C distributes evenly without any preference. In that case monomolecular pathway is possible through the methyl-cyclopropyl carbocation as shown in Scheme 3.5. They concluded that linear butene isomerization was controlled by '*restricted transition state selectivity'* since CoAlPO-11 was more selective towards monomolecular formation of iso-butene relative to H-FER.

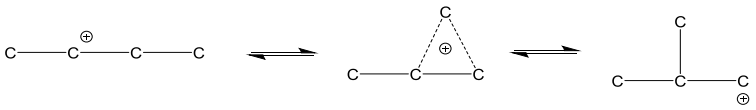

Scheme 3.5: Skeletal isomerization of butene via methyl-cyclopropyl carbocation

The isotopic labelling experiments did not fully distinguish between the mechanisms since both monomolecular and bimolecular pathways were plausible. Domokos et al [29] reported on the kinetics of linear butene skeletal isomerization over H-FER at 623 K. At low 1-butene partial pressure (0.5 kPa), iso-butene selectivity did not show any initial increase with TOS around 40 % conversion which suggested that coke formation did not play a role in the mechanism. However, when the initial increase in iso-butene was observed with TOS at higher pressure (10 kPa), a situation where there should be a drastic change in mechanism, the relative distribution of propene and pentenes did not change. They suggested that extensive oligomerization occurs on fresh catalyst to form less active aromatic species. This reduces consumption of more iso-butenes hence, the observed increase in iso-butene selectivity in aging of the catalyst.

Houžvička et al[46] compared shape selectivity of various pore sizes for linear butene skeletal isomerization and reported that large pore molecular sieves such as H-SAPO-5 were very unstable

for this reaction. They concluded that 10-membered rings were most suitable for skeletal isomerization though a closer look at the kinetics of the large pores was not done. Seo et al[47] also reported that linear butene skeletal isomerization depends more on the molecular sieves structure such that H-FER and clinoptilolite with 10-rings and intersecting 8-rings showed higher iso-butene selectivity compared with H-MFI (10-ring) and H-BEA (12-ring) which were non-selective at 723 K. Villagas et al[48] studied 1-butene dimerization over Beta zeolite of different acid site densities which was obtained by different synthesis time intervals, 24, 96 and 240 h. They observed no activity for the Beta-24 h but similar overall conversions for the Beta-96 and Beta-240, with product range between propene to tetradecane. The zeolite Beta-240 with lower acid site gave more of longer chain alkenes as compared with the zeolite Beta-96 with about twice number of acid site. They concluded that the lesser acids site favoured oligomerization while the more acids favoured cracking.

With all these controversies, closer study of the reaction over unidirectional large pore-sized catalysts might help to better understand the mechanism since the likelihood of restricting transition state will be reduced. This work therefore seeks to systematically follow the reaction by measuring the kinetics over one-dimensional 12-ring molecular sieves with different acid strength. The study will be based on separate reactions of ethene and linear butene and also together over H-SAPO-5 and H-SSZ-24. This will help to understand the mechanism as well as the role of acid strength in the mechanism. We will begin however with the characterization of the molecular sieves used to study these reactions.

4. CHARACTERIZATION OF SAPO-5 AND SSZ-24

4.1 THEORY OF THE EXPERIMENTAL TECHNIQUES

4.1.1 X-ray Diffraction (XRD)

The X-Ray Diffraction (XRD) is one of the oldest and mostly used techniques to characterize catalysts[12]. It helps to identify the phase and the dimension of unit cells in a crystalline material such as zeolites. The X-ray interacts with the crystalline surface to give a diffraction pattern which is like the fingerprint of the substances when the radiation wavelength is similar to the integer multiple of the path length. Materials are described as crystalline when their atoms are arranged in a regular pattern. The smallest three-dimensional repeating unit of a crystal is referred to as unit cell. When an X-ray beam hits the atoms of the crystal and the photon path length is equal to the integer multiple of the beams' wavelength, then the diffractive beams are in phase and constructive interference is produced. As a result the X-ray reflects from a series of parallel planes at an angle Θ as shown in Figure 4.1. Bragg's law relates the wavelength of the radiation (beam), the diffraction angle Θ, and the lattice spacing, d (distance between two lattice planes) as shown in the Figure 4.1 and expressed by Equation 4.1. The lattice spacing is characteristic of a specific material structure [49].

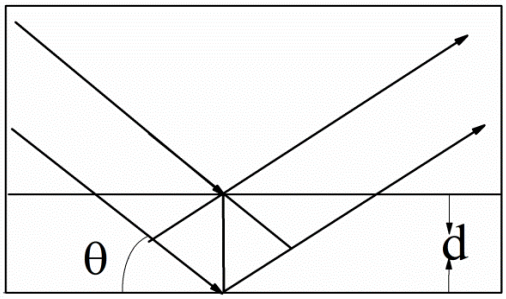

Figure 4.1: Simple schematic representation of photons reflecting from atomic planes. Adapted from [49].

$$n\lambda = 2dsin\,\theta \qquad 4.1$$

As described earlier, zeolites are crystalline and the use of XRD helps to identify their crystalline structure. Powder XRD is mostly used because of the difficulty in growing large enough crystal sizes of zeolites for single crystal XRD. The relative intensity and positions of peaks in the powder diffraction pattern can be compared to known phases which make it easy to identify a known framework. When the pattern do not match any known framework pattern then it is likely to be a novel structure. Series of sharp peaks in the diffractogram are characteristic of crystalline materials while the broadness of the background indicates presence of amorphous material as far as erroneous

sample preparations are avoided. The unit cell dimensions can be determined using the peak position while the peak width helps to determine the crystal size [50].

4.1.2 Scanning Electron Microscopy (SEM)

Scanning Electron Microscope (SEM) is a microscope that uses narrow electron beam at high energy to raster scan a sample to produce its image. The electrons from the beam upon interactions with electrons from the sample produce an image. It helps to view samples in the micrometer to nanometer scale. SEM is a versatile instrument; it gives information about the topology (texture and morphology), elemental analysis, crystalline structure, orientation and chemical composition of the sample.

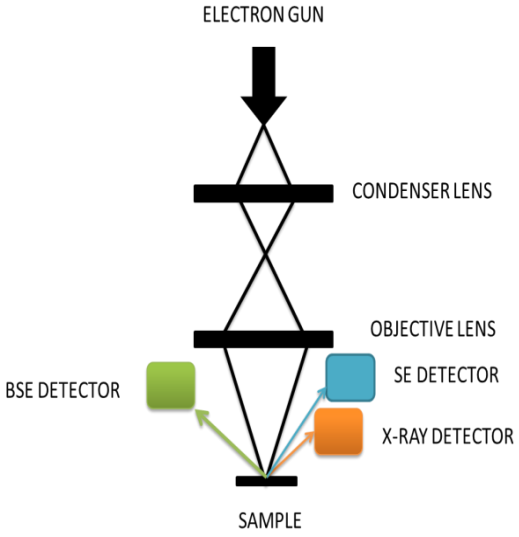

Figure 4.2: Simple schematic representation of SEM operation.

The SEM is arranged in such a way that there are two types of lenses: condenser and objective lenses before the sample as shown in Figure 4.2. Above the lenses is the electron gun which is a filament that shoots electron beams through the lenses to the sample. The modern electron gun is the field emission gun, made of pointed tungsten, W- wire where electrons are generated by magnetic pull. The field emission gun requires high vacuum as they easily get contaminated and corroded. The SEM can operate in two different sets of vacuum, low (~10 Pa) and high (<10 Pa). Sufficient vacuum allows the beam to be generated and controlled. Low vacuum allows observations to be made on samples with non-conductive surfaces because high charge build-up occurs on such surfaces when operating under high vacuum. The sample is usually placed on a stage below the objective lens. Just above the sample are detectors for the various signals to capture

the back signals of the electrons beam to be amplified and viewed. The main types of signals obtained from the SEM are secondary electrons, backscattering electrons and X-ray photons.

The Secondary Electron (SE) signals result from the interactions of the electrons from the surface or near surface of the sample with the electron beam. As a result, their images show the surface structure and shapes of the sample at high resolution and very detailed topological image. The SE gives more emission since they are close to the surface and are not delayed in their emissions. It is detected with the Everhart-Thornley Detector (ETD) in higher vacuum or the Large Field Detector (LFD) in lower vacuum. Back-scattered electrons (BSE) are beam electrons that are reflected from the sample by elastic scattering. BSE gives information about the different chemical composition and their proportions, based on their atomic masses as well as the distribution of different elements in the sample. The BSE requires higher energy than SE since their images are from a fraction of the incident electrons (primary electron beam), and low acceleration voltage will just back scatter very few electrons. BSE are detected by the Solid State Detector (SSD). The BSE are often used in analysis along with the spectra made from the characteristic X-rays. Characteristic X-rays are emitted when the electron beam removes an inner shell electron from the sample, causing a higher-energy electron to fill the lower energy shell and release energy (photon) in the process. These x-rays are characteristic and are used to identify the composition (qualitative) and measure the abundance of elements (quantitative) in the sample. The X-ray is detected with Energy Dispersive Spectrometer (EDS) or the Wavelength Dispersive Spectrometer (WDS). The EDS is much preferred because it is much faster even though it has less resolution [49, 51].

4.1.3 Surface area measurement by N_2 adsorption (BET)

The term adsorption generally means the attachment of a molecule onto a surface (adsorbent). When the molecule attaches the surface with a weak van der Waals interaction the adsorption is described as physisorption. The main principle in surface area measurement is by determining the amount of inert molecules needed to physisorb to a surface to form a monolayer. Nitrogen molecule for instance occupies 0.162 nm^2 at 77 K and knowing the total number of N_2 that can occupy the monolayer layer will give a good estimate of the total surface area of a material. Adsorption

isotherm is a term used to describe the relationship between the amount of adsorbed gas and equilibrium pressure at a constant temperature. The adsorption isotherm derived by Braunaer-Emmet-Teller (BET)[52] provides a relation which can be rearranged into a linear equation used to determine the total surface area as given by Equation 4.2.

$$\frac{p}{v(p_o - p)} = \frac{1}{v_m C} + \frac{(C-1)}{v_m C}\frac{p}{p_o} \qquad 4.2$$

Where p is the partial pressure of the adsorbed species, p_o is the equilibrium/vapour pressure of the adsorbed gas, v is the volume of adsorbed gas, v_m is the volume of gas adsorbed at the first monolayer and C is a constant. A plot of $\frac{p}{v(p_o-p)}$ versus $\frac{p}{p_o}$ gives a straight line, the slope and intercepts of which can be used to find v_m and subsequently used to find the number of molecules adsorbed on the monolayer using the ideal gas law. The total surface area can then be determined when the molecular diameter is known.

This isotherm is valid on the assumption that: (a) adsorbate (adsorbed gas) and adsorptive (gas to be adsorbed) are in equilibrium (b) there is equivalent adsorption site for the first layer (c) second and subsequent layers adsorb on the first adsorbate (d) no adsorbate-adsorbate interactions, (e) adsorption energy for molecules after the first layer are equal to condensation energy as it gets to infinity at the saturation pressure ($p=p_o$). The assumptions made for BET measurement are not strictly applicable to zeolite materials since multilayer adsorption that take place in their pores are very little, however they can be used to compare similar materials. The adsorption isotherm also reveals other characteristics of the material. For example, hysteresis loops where adsorption and desorption curves do not coincide due to capillary condensation in mesoporous structures [12, 53, 54].

4.1.4 Fourier Transform Infrared Spectroscopy (FTIR)

When a molecule interacts with photons, transition in vibration and rotational energy levels of the molecules can occur. When the molecule absorbs infrared light (IR range ~ 5-12500 cm^{-1}), the molecular vibrations and rotations are excited which changes the dipole moment. The excited molecular vibration that causes changes in dipole moments is that only seen by IR signal. This can

be described using a simple harmonic oscillator (Figure 4.3) for a diatomic molecule shown in Equation 4.3 below, where ν is the frequency, k is the force constant and μ is the reduced mass. This relation implies that stronger bond and lighter mass have higher vibration frequencies [49, 55].

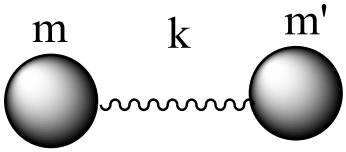

$$\nu = \frac{1}{2\pi}\sqrt{\frac{k}{\mu}} \quad , \quad \mu = \frac{m * m'}{m + m'} \qquad 4.3$$

Figure 4.3: Ball and spring model of the simple harmonic oscillator adapted from [56]

Figure 4.4 is a simple schematic diagram of how the FTIR instrument operates. The IR light emitted from a source is split in the beamsplitter into two directions and are reflected back to meet at the beamsplitter. The movement of one of the mirrors creates a variable total path length which creates constructive and destructive interference called interferogram. The interferogram passes through the sample as different characteristic wavelengths are absorbed and detected as energy versus time variables. The Fourier transform mathematical expression is used to convert this relation into intensity versus frequency spectra. FTIR spectra of zeolites are usually presented as absorbance versus wavenumber ($\tilde{\nu}$), which is the reciprocal of wavelength and proportional to frequency [57].

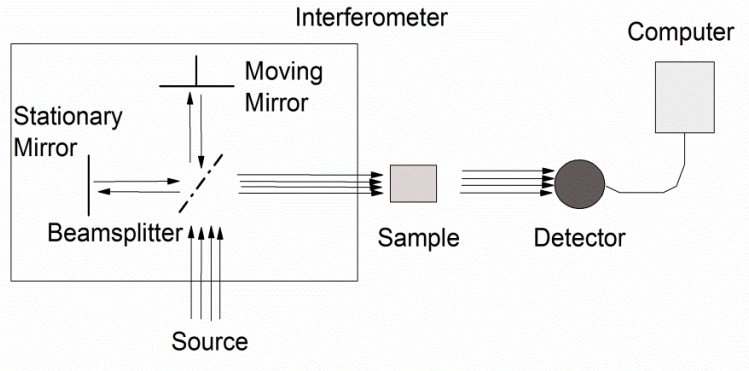

Figure 4.4: Simple schematic representation of FTIR operation adapted from [57]

IR is used in catalysis to study the nature of adsorbed species on the catalytic sites[55]. The interaction between the probe molecule and the acid sites of zeolites gives valuable information about the acid strength. The weak base carbon monoxide (CO) is usually used as probe molecule which adsorbs at low temperature conditions, though several others can be used as well. The CO interacts through H-bonding with the surface hydroxide groups, upon which frequency bands are shifted to lower wavenumbers. The relative shift in v(OH) is an indication of the acid strength[12, 49, 55].

4.2 EXPERIMENTAL

The catalysts used for this study are H-SAPO-5 and H-SSZ-24. H-SAPO-5 and Na-SSZ-24 samples used were obtained from M. Westgård Erichsen. These catalysts have been hydrothermally synthesized and characterized described in [27, 53, 58]. Note that the SSZ-24 used in this work was made in the same manner but a different batch from what was characterized in those reports. The Na-SSZ-24 sample was calcined and ion exchanged (see Section 4.2.1) before characterization.

4.2.1 Ion exchange and calcination

The Na-SSZ-24 was calcined to remove the structure directing agent used during the synthesis. The calcination was done with 25% O_2 in N_2 flow at an increment of 1 K/min till 823 K and stayed constant for 10 hours as described in [27]. The sample was ion exchanged in order to replace Na^+ with proton using excess of 1 M NH_4NO_3 (1 g of catalyst to 1.6 g of NH_4NO_3) over 348 K water bath for two hours. This was repeated twice before a second calcination was done to remove NH_3 to obtain H-SSZ-24.

4.2.2 Powder X-ray Diffraction

Powder X-ray diffraction was used for phase identification and to determine the relative crystallinity of the catalysts. The Powder XRD measurement was done using a Bruker D8 Discover diffractometer with Bragg-Brentano geometry using Cu Kα radiation with a wavelength, λ=1.5406 Å. The samples were prepared by mixing with isopropanol on a glass plate and the liquid portion allowed to evaporate in order to attain flat surface. The samples having been catalytically tested, were gently grinded before the mixing in order to have a random orientation. Diffractograms were measured for 2 theta range between 2-60^o using 2 min count time and step size of 0.021^o.

4.2.3 Scanning Electron Microscopy

The scanning electron microscopy was used to determine particle size and the morphology as well as the elemental composition of the two catalysts. This was done using FEI Quanta 200 FEG-ESEM. The SEM was equipped with Everhart-Thornley Detector (ETD), Large Field Detector (LFD), Solid State Detector (SSD) and Energy Dispersive Spectrometer (EDS). Microscopy was done around 10 mm working distance with up to 20 kV acceleration voltage. Samples were placed on a circular sample holder covered with carbon tape (to stick) and air blown to get rid of loose particles in order to avoid sample detaching in vacuum, before they were set into the microscope. All the images were taken at low vacuum because the samples were non-conducting.

4.2.4 BET Surface area Measurement

The surface area measurement was done using BEL BELSORP-mini II instrument. 50 mg sample mass was used for each experiment. The samples were preheated under vacuum at 353 K for 1 hour and 573 K for 4 hours to remove any moisture and any other adsorbate before adsorption measurement. N_2 adsorption and desorption were done at 77 K by placing the sample cells in liquid N_2.

4.2.5 Fourier Transform Infrared Spectroscopy (FTIR)

A CO-adsorption FTIR was done to distinguish the acid strength of the two catalysts using the Vertex 80 instrument with MCT (mercury cadmium telluride) detector in transmission mode. The samples were prepared by grinding gently to ensure homogeneity and pressed into a self-supporting disk. The disk was placed in a gold envelope with openings at both sides to allow transmission through the disk sample. The enveloped sample was placed in a quartz cell with KBr windows and pretreated under vacuum at 423, 573 and 723 K for an hour each to remove any moisture and other adsorbates. The sample was cooled to ambient temperature and 4 kPa of CO was gradually

introduced into the cell stepwise. The sample was cooled with liquid N_2 and spectra collected at regular intervals. Desorption of CO was followed at liquid N_2 temperature (77 K) by successive lowering of the coverage by pumping. Spectra were collected at each successive stage. All spectra were corrected for water and CO_2.

4.3 RESULTS AND DISCUSSION

4.3.1 Powder X-ray Diffraction of H-SAPO-5 and H-SSZ-24

Figure 4.5 shows the X-ray diffraction pattern of the H-SAPO-5 and H-SSZ-24 catalysts. The aim of the XRD was to ascertain that the zeolites used belong to the AFI topology. Hence this was compared with an AFI XRD pattern of AlPO-5[59]. The diffraction pattern showed pure AFI structures for all the samples. This implied that the structures of both catalysts were the same.

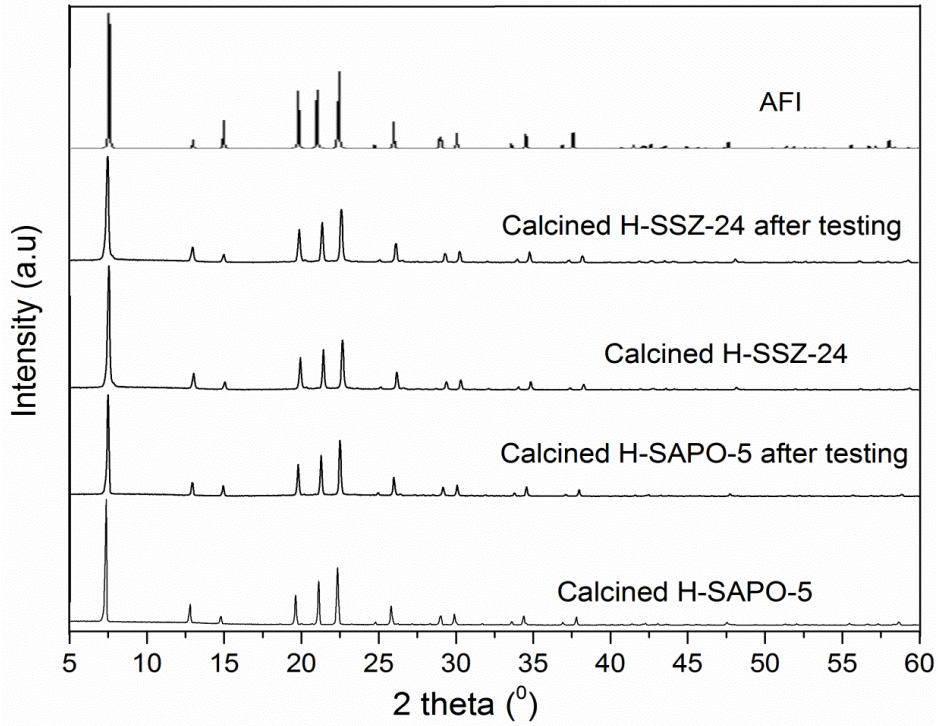

Figure 4.5: Powder XRD patterns of used and unused H-SAPO-5 and H-SSZ-24 after calcination. These are compared with AFI ($AlPO_4$-5)

The XRDs were done not only for the ion exchanged and calcined catalyst but also for the tested catalyst as well. This was done to ascertain that the catalyst remain intact after testing and re-calcination at 823 K in the presence of oxygen. The diffractogram indicated that there was no significant change in the structure of the catalysts after testing. This was not surprising since other works [60, 61] have reported that both catalysts thermal stability (>900 K) is above 823 K, the calcination temperature employed here.

4.3.2 Scanning Electron Microscopy of H-SAPO-5 and H-SSZ-24

The Figures 4.6 and 4.7 shows the micrograph of the H-SAPO-5 and H-SSZ-24 respectively. The H-SAPO-5 shows clear hexagonal crystals with close to 2 μm size. It was however difficult obtaining a nice image for the H-SSZ-24. This was because they form much smaller crystals of about 0.2 μm. However, both catalysts are expected to have similar structure and shape since their XRD's were similar (see Figure 4.5). A closer look revealed that the H-SSZ-24 forms aggregates between 1 to 2 μm size which has been observed elsewhere [62]. The sizes of the H-SAPO-5 and H-SSZ-24 were also similar to those reported by Westgård Erichsen et. al [27, 58].

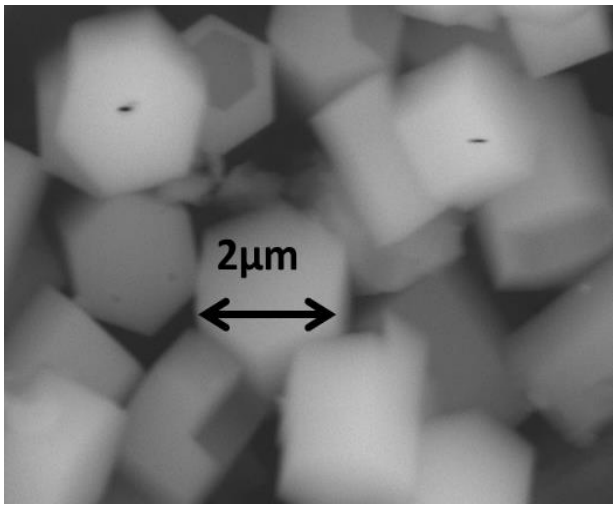

Figure 4.6: SEM image of H-SAPO-5

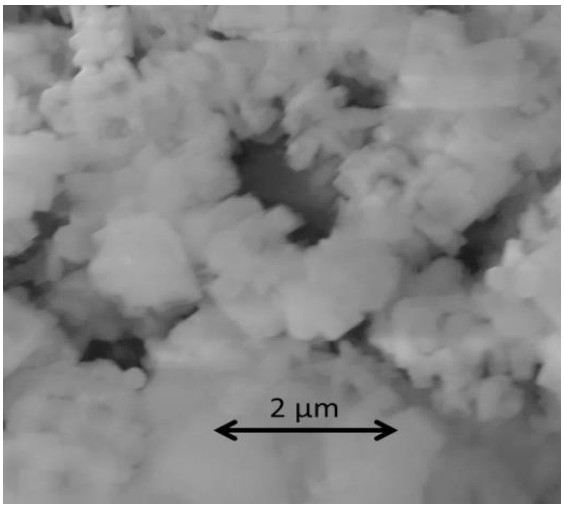

Figure 4.7: SEM image of H-SSZ-24

Table 4.1: The elemental analysis (atomic %) from the EDS and acidic densities of the H-SAPO-5

	1	2	3	4	5	6	Average
Al	23	22	24	25	27	26	25
P	28	29	29	32	36	34	31
Si	0.8	0.4	0.5	0.9	0.7	1.0	0.7
(Al+P)/Si	64	128	106	63	90	60	85±43

The Tables 4.1 shows the elemental analysis obtained from the Energy Dispersive Spectrometer (EDS) of the SEM for the H-SAPO-5 taken at 6 different spots. The averages of the elemental composition were 25:31:0.7 for the Al:P:Si which gave a (Al+P)/Si ratio of 85. The difference between the least and highest ratios for the six measurements from the average was about 43 (50 %). The P content in particular

was consistently higher than the Al in all the 6 measurements. This was not expected because in a strictly 1Al:1P in $AlPO_4$-5 framework, Si replaces P in order to create the positive charge in the SAPO, which implies that there should be more Al compared to P. Hence the higher P content than Al may not strictly represent the true content. Moreover, the amount of Si was very low and also deviated from its average about 43%, close to the 50 % deviation in the average of (Al+P)/Si ratio. It is possible therefore that the uncertainties in the measurement could be due to relatively low sensitivity to Si and perhaps poor calibration of the instrument to P. Hence these values will be used for comparison purposes and rather than taken as the actual chemical composition amount. Table 4.2 shows the elemental analysis obtained for the H-SSZ-24 sample. Here, an average of 48:0.9 for the Si:Al was observed which gave a Si/Al ratio of 55±10. The deviation in the average of the ratios was 18 % in the H-SSZ-24 which was narrower compared with the H-SAPO-5 measurements.

Table 4.2: The elemental analysis from the EDS and acidic densities of the H-SSZ-24

	1	2	3	4	5	6	Average
Si	52	49	46	47	47	47	48
Al	0.9	1.1	0.8	0.8	0.9	0.8	0.9
Si/Al	58	45	58	59	52	59	55±10

The EDS analysis from the two catalysts showed that the number of acid sites in the H-SSZ-24 will be about one-half (1/55:1/85) of H-SAPO-5 acid sites based on their averages, although the deviations indicate that limits between one to three times more acid sites is possible. Note that the reciprocal of the calculated ratios are representative of available acid sites. Westgård Erichsen et. al[27] in a similar analysis reported 1/35 and 1/80 as the acid site densities for H-SSZ-24 and H-SAPO-5 respectively. The acid site density in the H-SAPO-5 was similar in both observations but different in the H-SSZ-24. The difference in the H-SSZ-24 acid site densities is not surprising since they are different synthesis batch and slight differences may occur during each production.

4.3.3 BET Surface area Measurement of H-SAPO-5 and H-SSZ-24

The N_2 adsorption was used to determine and compare the surface area of the catalysts as well as their pore size distribution. Figure 4.8 shows the adsorption isotherms for H-SAPO-5 and H-SSZ-24. The isotherms resemble type I BET isotherms according to the IUPAC classifications[54] which is often observed in zeolites[12]. The accessible micropore volume dictated uptake which implies that the samples are microporous materials with relatively small external surfaces.

Table 4.3 shows the BET calculated surface areas of the catalysts. The surface area of the H-SAPO-5 was 338 m^2/g whilst that of the H-SSZ-24 was 233 m^2/g. The surface area of the H-SAPO-5 was thus 105 m^2/g more than that of the H-SSZ-24. Westgård Erichsen et. al [27] obtained 340 and 284 m^2/g for the H-SAPO-5 and H-SSZ-24 respectively. The surface area of H-SAPO-5 was about the same, however the H-SSZ-24 was much smaller. The lower H-SSZ-24 surface area compared to the H-SAPO-5 could be due to formation of aggregates observed in SEM image in Figure 4.7. There is also a possibility that defects can occur in the structure which may play a role in the lowering of the surface area. These defects if present are expected to be revealed with FTIR measurements.

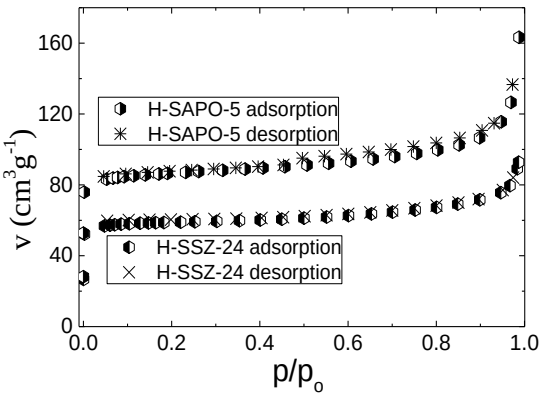

Figure 4.8: The adsorption isotherms for the H-SAPO-5 and H-SSZ-24

Table 4.3: BET surface area (m^2/g) of H-SAPO-5 and H-SSZ-24

H-SAPO-5	H-SSZ-24
338	233

4.3.4 Fourier Transform Infrared Spectroscopy of H-SAPO-5 and H-SSZ-24

Figure 4.9 shows the FT-IR spectra of CO adsorption over H-SAPO-5, from 3800 to 3200 cm^{-1} for the OH stretching region and from 2250 to 2050 cm^{-1} for the CO stretching region. The plots in

each case are separated into two just to show when there was a significant change in the CO adsorption with the top showing more CO coverage and bottom for lower CO coverage though the measurements were continuously taken at regular intervals. The bottom black curve corresponds to the activated sample without any CO adsorption, whilst the dark fading gray curves correspond to the successive increase of CO coverage with the lightest gray as the highest coverage.

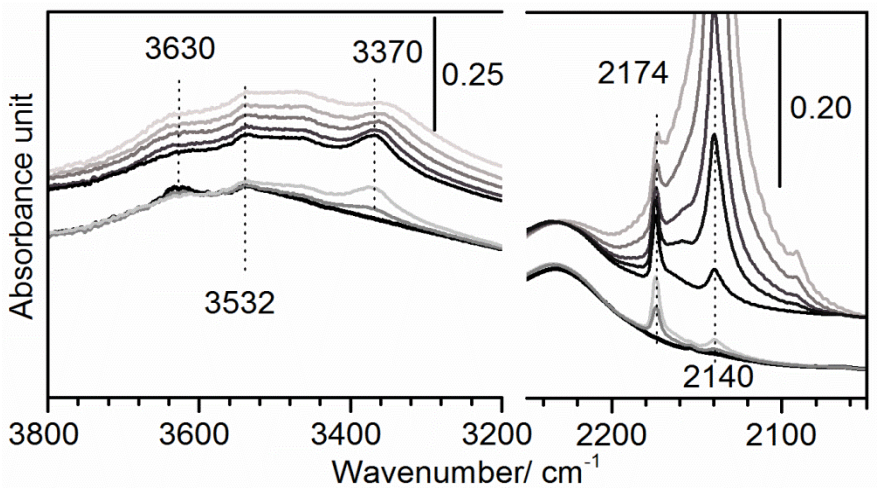

Figure 4.9: The FT-IR of increasing dosage of CO on H-SAPO-5. The bottom black curve corresponds to activated sample while the fading gray curves correspond to increasing dosage of CO.

The activated sample showed OH bands at 3630 and 3532 cm^{-1}. These bands are typical of OH bridging in Si-O(H)-Al in the 12 and 6 rings in H-SAPO-5 structure respectively which has been reported in other works [58, 63-65]. No peak was observed at 3677-3780 cm^{-1} which is usually assigned to terminal P-OH and Al-OH [58, 63, 65]. Upon CO adsorption, the 3630 cm^{-1} band gradually eroded whilst 3370 cm^{-1} band grew and the peak at 3532 cm^{-1} relatively remained. The 2140 cm^{-1} band is attributed to liquefied CO and 2174 cm^{-1} to physisorbed CO at the Brønsted acid site. No CO peak was observed between 2200 and 2190 cm^{-1} which is usually assigned to defects[66]. Hence there were no observable peaks for defects in the CO-adsorption for H-SAPO-5 sample.

The Figure 4.10 shows the FT-IR spectra of CO adsorption over H-SSZ-24. Similar to the explanation above, the plots represent a continuous measurement but for clarity, they are separated into regions and this time with insertion A and B. The plot style (colour grading) is also the same as described for the adsorption over H-SAPO-5 above. The activated H-SSZ-24 showed four main OH stretching bands at 3747, 3680, 3612 and 3489 cm^{-1}. The very intense peak at 3747 cm^{-1} with

shoulder peak 3730-40 cm^{-1} is typical of isolated silanol at the external surface and terminal Si-OH respectively, whilst those of 3612 and 3489 cm^{-1} are for the OH bridging Si-O(H)-Al groups in the 12 ring and 6 rings respectively as reported in other experiments [27, 63]. The peak broadening at 3489 cm^{-1} is attributed to hydrogen bonding between silanols to form a nest of SiOH [67, 68].

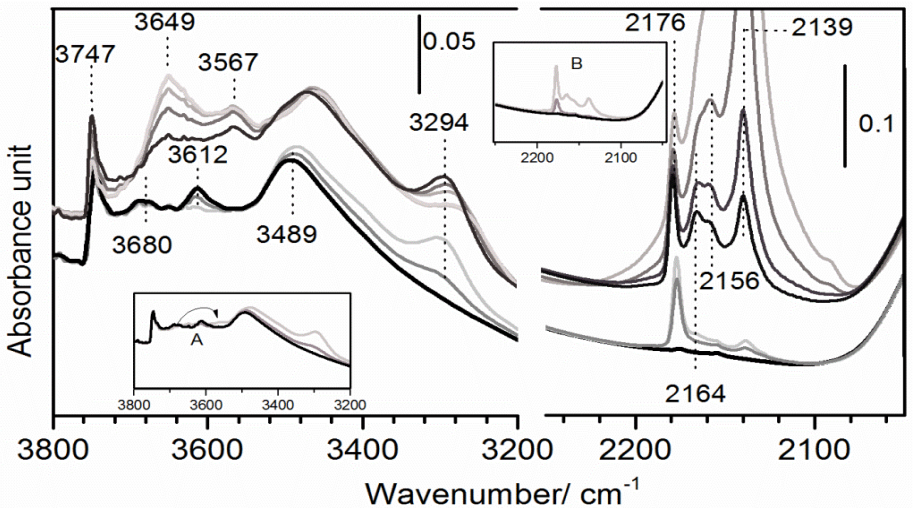

Figure 4.10: The FT-IR of increasing dosage of CO on H-SSZ-24. The bottom black curves correspond to the activated sample while the fading gray curves correspond to increasing dosage of CO. Insertion A and B: shows the shift of the 3680 band to 3567 cm^{-1} and the corresponding 2164 cm^{-1} band.

When CO was adsorbed, the bands shifted at the OH region as follows: 3612 cm^{-1} to 3294cm^{-1}, 3680 cm^{-1} to 3567 cm^{-1}, 3747 $cm^{-1}$to 3649 cm^{-1} and the 3489 cm^{-1} slightly to 3484 cm^{-1}. At the CO region, 2139 cm^{-1} is attributed to liquefied CO while the 2176 cm^{-1} is attributed to the physisorbed CO at the Brønsted acid site. The band due to silanol was observed at 2156 cm^{-1}[68, 69]. However there appeared another peak at 2164 cm^{-1}. This interaction is more obvious upon closer look at the insertions in the Figure 4.10. The eroding of the band at 3680 cm^{-1} corresponded to the formation of the 2164 cm^{-1} band which was much intense at lower CO coverage compared to the silanol peaks at 3649 cm^{-1} and corresponding 2156 cm^{-1}. Once again, no peak was observed between 2250 and 2190 cm^{-1}.

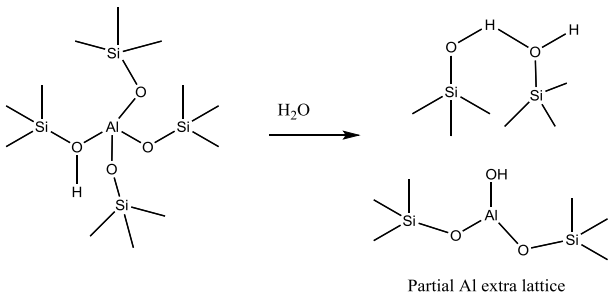

Scheme 4.1: Hydrolysis of SiO(H)Al to form silanol and partial aluminium extra lattice, adapted from [68]

The broad peak around 3680 cm^{-1} was difficult to assign though it was suspected to be a sort of AlO-H according to other reports (peak around 3680-65 cm^{-1}) [66, 68, 70, 71]. Ballingger et al [71] reported that the 3680 cm^{-1} (broadness ranges 3688-3672 cm^{-1}) peak in alumina persist when pretreated at 475 to 800 K which was attributed to isolated hydroxides. However, Zecchina et al [68] attributed the peak at 3670-3665 cm^{-1} range in ZSM-5 to a *'partial Al extra lattice'* (see Scheme 4.1) which are located at the external surface. Their conclusion was based on higher acidic strength of the '*partial Al extra lattice'* compared to that of silanol and γAl_2O_3 on CO interaction. The silanol shoulder peak we observed at 3720-30 cm^{-1} for the terminal SiOH and CO adsorption peak at 2164 cm^{-1} correlated well with their observations at 3725 and 2164 cm^{-1} respectively. Though we could not assign the specific hydroxide to this peak, we speculate that it is a form of aluminium hydroxide (Al-OH). This also can be the reason why the surface area of H-SSZ-24 was significantly lower than that of H-SAPO-5.

Table 4.4: The CO induced shift of Si-O (H)-Al Bands

	Δv(OH) (cm^{-1})	Δv(CO) (cm^{-1})
H-SAPO-5	-260	+31
H-SSZ-24	-318	+33

The aim of the FTIR was to compare the acidic strength of the catalysts used in this project. The acidity measurement is based on the O-H--CO interaction at low temperature with acidic site which causes a shift in the frequencies (or wave number = v) of OH and CO stretching bands. By definition, the stronger the acid, the easier its protons interact due to weaker O-H bond. As a result stronger acids are expected to appear at lower frequencies and larger shifting of these bands when CO (base) adsorbs [72]. Table 4.4 shows the shift induced by the CO adsorption on the Brønsted acid sites, SiO(H)Al. The maximum Δv(OH) in the H-SAPO-5 was -260 cm^{-1} whilst that in the H-SSZ-24 was -318 cm^{-1}. Also at the CO region, the Δv(CO) were +31 cm^{-1} and +33 cm^{-1} in the H-SAPO-5 and H-SSZ-24 respectively. This implied that the H-SSZ-24 had stronger Brønsted acid sites compared to the H-SAPO-5 and corresponds well with the data of *Westgård Erichsen et. al*[27]. Moreover, while there was only one type of hydroxides (bridging SiO(H)Al) observed in the H-SAPO-5, there were some others observed in the H-SSZ-24 and has been attributed to SiOH and 'AlOH' which displayed some acidity. The appearance of the 'Al-OH' and Si-OH at the OH band

region in the H-SSZ-24 suggested that they possess some extra sites which exhibit Brønsted acidity. However the silanol with $\Delta\nu$(OH) shift of -98 cm $^{-1}$ and alumina with Δv(OH) of -113 cm $^{-1}$ shifts upon CO adsorption implied that the extra acidic strength in H-SSZ-24 was far less than the observed OH bridging of the SiO(H)Al in the 12 rings of H-SSZ-24 with Δv(OH) of -318 cm $^{-1}$ shift and that of H-SAPO-5 with -260 cm $^{-1}$ shift.

4.4 SUMMARY OF CHARACTERIZATION

The two catalysts used in this work, H-SAPO-5 and H-SSZ-24 have been characterized by Powder X-ray diffraction, Scanning electron microscopy, BET surface area measurement by N_2 adsorption and in-situ FTIR with CO adsorption. The Powder XRD showed that the two materials belong to the AFI topology. The SEM showed that the hexagonal crystals of the H-SAPO-5 was about 2 μm while the H-SSZ-24 was about 0.2 μm though they formed aggregates up to 2 μm. The EDS helped to estimate the (Al+P)/Si ratio of the H-SAPO-5 as 85±43 and Si/Al ratio for the H-SSZ-24 as 55±10. This implied that the H-SSZ-24 had about one and half more acidic sites than H-SAPO-5.

The N_2 adsorption showed that the two catalysts were microporous with surface area of 338 m^2/g and 233 m^2/g for H-SAPO-5 and H-SSZ-24 respectively. The FTIR of CO adsorption showed that the maximum v(OH) shift in the H-SAPO-5 was -260 cm^{-1} and -318 cm^{-1} in H-SSZ-24. This indicated that the H-SSZ-24 had stronger Brønsted acid sites compared to the H-SAPO-5. Moreover, while there was only one type of Brønsted acid site observed for the H-SAPO-5, the H-SSZ-24 showed some other type which displayed relatively weak acid strength.

5. CATALYTIC TESTING: THEORY AND EXPERIMENTAL

In order to elucidate the mechanism of ethene alkylation over the just characterized H-SAPO-5 and H-SSZ-24 at Chapter 4, a number of experiments were performed in a reactor to measure the kinetics of the reaction. The kinetic measurements have been reported in Chapters 6 to 8. This chapter therefore seeks to describe the theoretical background of the experimental techniques used in the catalytic testing followed by the general experimental procedure.

5.1 REACTOR THEORY

Chemical processes operate in our everyday life. These processes can be quantified and compared by understanding the kinetics and reactor (reaction house) design in which they occur. There are different types of reactor models or designs available such as continuously stirred tank, batch and plug-flow reactors. Based on the principle of mass conservation, reactions may be quantified using these models. This implies that the total masses that is; input, output, produced and consumed must balance and therefore every factor and steps involved in the reaction in a reactor are important [73, 74]. In heterogeneous catalysis, the reaction occurs in series of five steps[11]. These are:

- diffusion of molecules into the catalyst porous structure/surface
- adsorption of molecule onto the surface
- reaction at the surface
- desorption of products from the surface
- diffusion out of the catalyst surface into the bulk.

All these steps can affect the rate measurements one way or the other and hence, the theoretical background of the reactor used in this thesis and how these steps influence kinetics is addressed below.

5.1.1 Reaction-Plug flow reactor

Fixed-bed reactors are widely used in heterogeneous catalysis in both laboratory and on industrial scale[75]. This reactor is one in which the solid catalysts are stationary on a grate (bed) with fluid reactant flowing through. The fixed-bed reactor can be modeled to operate like an ideal plug-flow reactor. Here, it is assumed there is no temperature and diffusion gradient (which is usually true with lab scale reactors) and the entire fluid that enters the reactor flow at the same velocity as illustrated in Figure 5.1. Consider a fluid flowing into a plug-flow reactor with Q flow rate in a volume *V* and a concentration of reactant c_o. When there is a reaction within a volume *dV*, at a rate r, the output concentration becomes c_0-*dc*. If the rate of reaction and the rate at which products appear at the outlet is constant (steady state conditions) then a mass balance can be written as shown below.

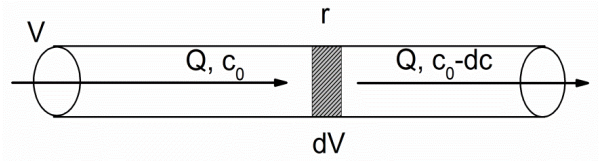

Figure 5.1: Plug-flow adopted from [73]

Mass balance	$\text{Input} + \text{product} = \text{output}$ $Qc_0 + rdV = Q(c_0 - dc)$	5.1
Rearranged	$rdV = -Qdc,$ $\frac{dV}{Q} = -\frac{dc}{r}$	5.2
If the conversion at the end of the reactor is given as *X*	$X = \frac{c_o - c}{c_o}$	5.3
Differential of *X* with *c*	$\frac{dX}{dc} = -\frac{1}{c_o}$ $dc = -c_o\, dX$	5.4
Substitution of 5.4 into 5.2, integral in the total volume of the reactor	$\frac{1}{Q}\int_0^V dV = c_o \int_o^X dX\, /r$	5.5
When rate is independent (of *X*) at low conversion	$\frac{V}{Q} = c_o \frac{X}{r}$	5.6

The *V/Q* (volume over flow) is equivalent to the average residence time of the reactants on the catalyst. Usually the mass of the catalyst is used instead of the volume in the rate expression and is used to define the contact time as mass of catalyst over the (total) flow rate. The mass of flow rate

per mass of catalyst is also referred to as weight hourly space velocity (WHSV). It can be assumed that at very low contact times conversions will be far lower than equilibrium composition and the rate measurement will mainly be the primary or initial reactions as secondary and subsequent reactions are suppressed.

An ideal plug-flow reactor must operate under continuous steady-state, constant conditions of temperature and pressure without diffusion limitation. As a rule of thumb, the diameter of the reactor must be more than 10 times the catalyst diameter to eliminate reactor wall influence on the flow pattern. The length of bed per catalyst diameter must be about 50 to minimize axial gradients. However, the higher this value, the higher the temperature gradient and pressure drop hence a compromise must be reached. Working at low conversion, high flow rate and using a diluent with high thermal conductivity at high temperature helps to maintain isothermal conditions [73, 76].

5.1.2 Kinetics

Kinetics concerns the rate at which chemical reactions occur and their dependence on macroscopic parameters such as concentration, pressure, temperature, volume and the presence or absence of catalyst. Usually, only one parameter is varied while the rest are kept constant. The change in rate of reaction with such parameters helps to understand the reaction at the molecular level with the aim of describing the reaction mechanism.

Consider a reaction between A and B to produce C and D as shown in Equation 5.7, with v representing stoichiometric coefficient, the rate of the reaction, r can be expressed as the appearance of the products or disappearance of the reactants in terms of concentration of the reactants and products, where k_{for} and k_{back} are the rate constant for the forward and backward reactions respectively. Equation 5.8 shows the differential rate of the example in Equation 5.7, where n is number of moles and V is the volume. The rate can also be expressed in terms of partial pressures (p) in the case of gases as they are related to concentration by the ideal gas law ($p = \frac{n}{V}RT$).

$$v_a A + v_b B \overset{k_{for}/k_{back}}{\longleftrightarrow} v_c C + v_d D \quad 5.7$$

$$r \equiv -\frac{1}{v_a}\frac{dn_A}{Vdt} = -\frac{1}{v_b}\frac{dn_B}{Vdt} = \frac{1}{v_c}\frac{dn_C}{Vdt} = \frac{1}{v_d}\frac{dn_D}{Vdt} \quad 5.8$$

$$r = k_{for} p_A^{\alpha} p_B^{\beta} - k_{back} p_C^{\gamma} p_D^{\sigma} \quad 5.9$$

When the rate is expressed as shown in Equation 5.9, it is referred to as the rate law for the reaction, where α, β, γ and σ are the order of reaction with respect to the reactants and products of which they are raised to. The overall order of reaction is equal to α+ β+γ + σ. When dynamic equilibrium is reached, the rate of the forward reaction will be equal to the rate of the backward reaction and the overall rate is zero. Hence low conversions, usually below 10 % of equilibrium conversion where the rate of backward reaction is negligible is important to measure kinetics of the forward reaction.

The overall rate law of a mechanism consists of elementary steps, each describing what happens at the microscopic level. An elementary reaction can be a unimolecular, bimolecular or termolecular (which is seldom) where single, two or three molecules (that is 1, 2 or 3 molecularity) respectively are involved. The order of reaction in elementary reactions is equal to the respective molecularity. The example in Equation 5.7 comprises of two elementary steps, the forward and backward reactions, and each step is bimolecular if the stoichiometric coefficients are equal to 1. In catalysis, adsorption and desorption are also considered as elementary steps. If we consider a first order forward reaction such as shown in Equation 5.10, the differential and integral rate law can be written as shown in Equations 5.11 and 5.12 respectively.

$$A \rightarrow Product \quad 5.10$$

$$r = -\frac{dp_A}{dt} = kp_A \quad 5.11$$

$$ln\frac{p_A}{p_{A0}} = -kt, \;\; or \;\; p_A = p_{A0} e^{-kt} \quad 5.12$$

Temperature dependence of the rate is also a valuable parameter to study for understanding reaction mechanisms. Arrhenius proposed a relation between the rate constant (k) and temperature (T) as shown in Equation 5.13, where A is the pre-exponential factor proportional to the frequency of collision, Ea is the activation energy and R is the gas constant. This equation can be use to estimate the Ea by comparing reaction rates with varied temperatures. The Ea is defined as the minimum

kinetic energy reactants require to form a product. Hence the exponential part of the Arrhenius law describes the fraction of collision that has enough energy to cause a reaction to occur.

$$k = Ae^{-\frac{Ea}{RT}} \qquad 5.13$$

Usually the overall rate law for a reaction can be obtained experimentally. Determining the mechanism from the rate law is quite problematic since it may consist of several elementary steps. One can obtain more than one mechanism that is consistent with the rate law. In most cases one must make an educated guess. Some approximations can also be made. One of such is to use the rate-determining-step (rds) approach. The rds is the slowest step among all the elementary steps in the mechanism and this step always appear at the numerator of the rate law. The second is the steady-state-approximation (ssa). The ssa assumes that concentrations of intermediates are very low and that variation of intermediates is independent of time such that $\frac{\mathrm{d(intermediate)}}{\mathrm{dt}} = 0$. In that case the intermediates have high rate constants and react very fast [12, 77, 78].

5.1.3 Adsorption

In heterogeneous catalysis, the reactants interact with the catalyst surface before the reaction takes place. As defined earlier, the binding of the reactants to the surface of the catalyst is termed as adsorption which can be classified into physisorption and chemisorption based on their adsorption enthalpies. Physisorption is characterized by van der Waal interaction or the lacks of true chemical bond (no electron sharing) between the reactants and the catalyst surface, usually associated with enthalpies between 5- 30 kJ/mol. When the reactants form a chemical bond with the catalyst surface, then the adsorption is chemisorption which is associated with enthalpies above 30 kJ/mol.

Adsorption enthalpy is always expected to be exothermic since entropy is lost upon adsorption, and only negative enthalpy can make Gibbs free energy negative, that is the adsorption is feasible according to $\Delta G = \Delta H - T\Delta S$. The relationship between surface coverage (θ) by the reactant (gas) and partial pressure of the gas (p) at constant temperature is termed *isotherm*. This is credited to Irving Langmuir (1891-1957) as being the first to give a quantitative theory of gas adsorption and

provided the basis for the kinetics of catalytic reaction. The Langmuir adsorption isotherm can be derived based on the following assumptions: the catalysts have uniform adsorption sites, adsorbed molecules do not interact with each other, only monolayer is allowed and desorption is allowed.

Molecule *A* at equilibrium with an active site *	$A + * \leftrightarrow A*$	5.14
θ_A is coverage of *A* and θ_* is free site	$k_{for} p_A \theta_* = k_{back} \theta_A$ $\theta_A = \frac{number\ of\ \ site\ \ adsorbed\ by\ A}{number\ of\ sites\ availble}$	5.15
K is equilibrium constant	$\theta_* + \theta_A = 1\ and\ \frac{k_{for}}{k_{back}} = K$	5.16
Substitution of 5.16 into 5.15 and rearranged	$Kp_A = \frac{\theta_A}{1-\theta_A}$	5.17
Langmuir adsorption isotherm for associative single gas.	$\theta_A = \frac{Kp_A}{1+Kp_A}$	5.18
Fraction of empty site	$\theta_* = \frac{1}{1+Kp_A}$	5.19

Equations 5.14-5.19 show the derivation of the Langmuir adsorption isotherm for a non-dissociative gas. In the case of dissociative adsorption, as expressed in Equation 5.20, the coverage expression changes as shown in Equation 5.21. Relationships can also be derived for competitive adsorption where two or more different reactants compete for the same site as shown in Equations 5.22 to 5.25.

Dissociative adsorption	$A_2 + 2* \leftrightarrow 2A*$	5.20
Langmuir adsorption isotherm for dissociative gas.	$\theta_{A_2} = \frac{\sqrt{Kp_A}}{1+\sqrt{Kp_A}}$	5.21
Equilibrium constant for *A* is K_A Equilibrium constant for *B* is K_B	Same as (5.14) $A + * \leftrightarrow A*$ $B + * \leftrightarrow B*$	5.22
Adsorption isotherm for *A* in a competitive adsorption.	$\theta_A = \frac{K_A p_A}{1+K_A p_A + K_B p_B}$	5.23
Adsorption isotherm for *B* in a competitive adsorption	$\theta_B = \frac{K_B p_B}{1+K_A p_A + K_B p_B}$	5.24
Generalized adsorption isotherm	$\theta_i = \frac{K_i p_i}{1+\sum_j^N K_j p_j}$	5.25

When competitive adsorption occurs before surface reaction between the adsorbates (adsorbed gases), the mechanism is often described as using the *Langmuir-Hinshelwood* kinetic model. This

has been shown using Equations 5.14, 5.22 and 5.26, while 5.27 shows the rate expression. There is another situation where one of the reactants reacts with an adsorbate directly from the gaseous phase without adsorbing at the surface. This mechanism is represented by *Eley-Rideal* kinetic model, and has also been shown using Equations 5.14 and 5.28, with 5.29 showing the rate expression.

Assuming the surface reaction is the slowest step	$A* + B* \rightarrow C* + *$	5.26
Langmuir-Hinshelwood mechanism rate expression	$r = k_{for}\,\theta_A\theta_B$	5.27
Assuming this is the slowest step	$A* + B \rightarrow C*$	5.28
Eley-Rideal mechanism rate expression	$r = k_{for}\,\theta_A p_B$	5.29

However it should be noted that sometimes the molecules can adsorb very strongly on the surface such that they completely cover the surface. Such species is referred to as the **M**ost **A**bundant **R**eaction **I**ntermediate (MARI). MARI approximations help to simplify the overall rate expression when elementary reactions are assumed to reach fast equilibrium except the one which determines the rate (rate determining step). All other coverage is approximated to be zero except the MARI coverage. When the adsorption is very weak or when relatively high temperatures are used such that the molecules are weakly bound to the surface and reaction equilibrium is shifted towards gas phase, near empty surface approximation are assumed[12]. Another term used in adsorption is the sticking coefficient. This describes the fraction of collisions that lead to successful adsorption which is expressed in Equation 5.30 and it is dependent on temperature[35, 77].

$$\text{Sticking coefficient} = \frac{rate\ of\ adsorption\ of\ particles\ on\ the\ surface}{rate\ of\ collision\ of\ particle\ on\ the\ surface} \qquad 5.30$$

5.1.3.1 Apparent activation energy

The temperature dependence of the rate constant was earlier given in Equation 5.13. When there is coverage due to adsorption, the apparent (measured) activation energy (Eapp) may deviate from the intrinsic activation energy (Ea) for the reaction. Temperature differentiation of the logarithm of the rate from the Arrhenius expression gives Equation 5.31. Using the thermodynamics relation

$lnK = -\frac{\Delta G}{RT}$ and Equation 5.29 for example, a relationship can be derived between the Ea and the coverage assuming there is no backward reaction [12].

	$$Eapp = -R\frac{dlnr}{d\left(\frac{1}{T}\right)} = RT^2\frac{dlnr}{dT}$$	5.31
Substitution of 5.29 into 5.31, and evaluated	$$Eapp = RT^2\left\{\frac{Ea_{for}}{RT^2} + \frac{\Delta H_A}{RT^2} - \frac{\Delta H_A K_A p_A}{(1+K_A p_A)}\right\}$$ $$Eapp = Ea_{for} + (1-\theta_A)\Delta H_A$$	5.32

5.1.4 Diffusion in porous materials

Transportation of gases over porous materials is a potential problem during testing[12]. The molecular transport can be described by Fick's first law[77], given as :

$$J = -D\frac{dc}{dz} \qquad 5.33$$

Where J is the molar flux, D is diffusion coefficient and dc/dz is the concentration gradient. When the rate of reaction is faster than gas diffusion in and out of the pores, then reaction is diffusion controlled. In that case, the diffusion is the rate determining step and this introduces error in measuring the kinetics of the reaction. An effective factor, Ƞ, can be used to describe the diffusion phenomenon relative to when there are no diffusion limitations[12] given as:

$$\eta = \frac{effective\ reaction\ rate}{reaction\ rate\ when\ diffusion\ is\ absent} \qquad 5.34$$

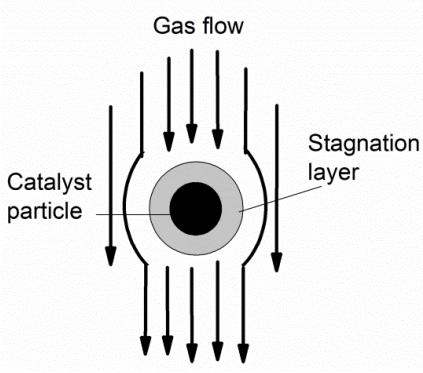

Figure 5.2: Stagnant layer of gas formed around a catalyst particle adopted from [12].

Working with small catalyst particles minimizes the intra-particle gradient (internal diffusion). Catalysts are usually pressed, crushed and sieved into pellets of equal sizes before they are tested. The pellet size is very important in the diffusion. Gas molecules flowing through the catalyst bed usually forms a stagnant layer around the catalyst particles as shown in Figure 5.2. The stagnant molecules poses external diffusion limitations while molecules which need to go through the pores are internally limited especially when the catalyst is very active.

External diffusion can be determined when different flow of reactants is used at the same space velocity (WHSV). When the conversions are found to be independent of gas velocity then external diffusion is minimal. Internal diffusion on the other hand can be determined when different particle sizes are used under the same conditions. When the conversions are independent on particle size, then internal diffusion is minimized [12, 35, 76]. An alternative is to use an Arrhenius plot; that is log of the reaction rate versus reciprocal of temperature. Generally, temperature dependence of diffusion controlled reaction rate ($\sim T^{3/2}$) is not so high compared to exponential dependence of the chemical reaction ($e^{-Ea/RT}$)[35]. Hence exponential dependence of the rate on temperature implies minimal internal diffusion.

5.2 GAS CHROMATOGRAPHY AND DETECTORS

5.2.1 Gas chromatography (GC)

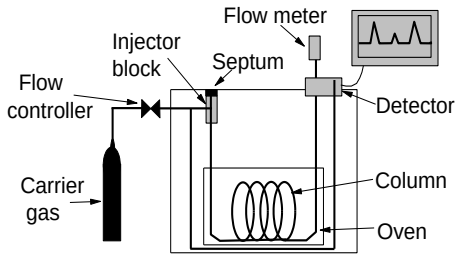

Figure 5.3: Schematic diagram of a GC adapted from [79]

Chromatography is a separation method used to separate a solute sample between a mobile and a stationary phase[79]. In gas chromatography (GC), the *mobile phase* is a gas such as He, Ar or N_2 often called carrier gas. The *stationary phase* is either a wide-bore (2-4 mm diameter and 2-6 m long) containing particulate material (packed) or coated open tubular (capillary) column. Capillary columns (about 150-300 µm internal diameter and 30-100 m long) are more efficient in separation since they have a long column which increases resolution. Figure 5.3 is a schematic diagram of a GC. When the sample is injected into the GC, they are carried through a capillary column by the carrier gas. Different compounds are separated when they interact with the stationary phase and elute depending on the degree of interaction; the higher the chemical affinity between the stationary phase and the compound, the longer its retention time. The order of elution usually depends on the boiling points. Non-polar stationary phase separates non-polar solutes whilst polar stationary phase better separates polar solutes. An oven surrounds the column which helps to control temperature and vapour pressure in the column, keep the solutes in gas phase and speed up elution at high

temperatures. Longer columns give better separation though retention time becomes longer. Volatile solutes are required since non-volatile solutes will condense and degrade the column. Detectors used with the GC include thermal conductivity detector (TCD), flame ionization detector (FID), electron capture detector (ECD) and mass spectrometry (MS).

5.2.2 Thermal conductivity detector (TCD)

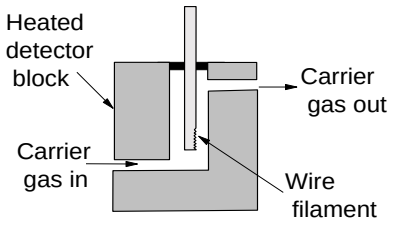

Figure 5.4: Schematic diagram of a TCD for GC adapted from [79]

Thermal conductivity detector (TCD) was used widely in the analysis of eluent from the GC in this work. Figure 5.4 is a schematic diagram for a TCD of a GC. The TCD operates based on the thermal conductivity of the mobile phase. Helium is mostly used as the mobile phase because it has a high thermal conductivity. The mobile phase passes over a tungsten-rhenium wire filament as it exits the column. The electrical resistance of the filament depends on temperature which is related to the thermal conductivity of the mobile phase that flows over it. When the solute exits from the column, the thermal conductivity of the mobile phase is decreased and the temperature of the filament also decreases resulting in increment of its (filament) resistance. There is a reference cell through which only the mobile phase passes, this compensates for any flow, temperature and pressure variations. The difference in the resistance is then detected by a Wheatstone bridge circuit and measured as a signal. The TCD can detect any solute with different thermal conductivity other than the carrier gas, hence referred to as a universal detector. It is also nondestructive and gives a linear response to solute concentration. TCDs are however not as sensitive as other popular detectors [79].

5.2.3 Mass Spectrometry (MS)

The coke analysis was done with a GC-MS. The effluent from the GC is introduced directly into the MS ionization chamber. All the effluent are ionized and separated according to their mass-to-charge

ratio. Here, each solute undergoes its characteristic fragmentation to give a spectrum of ion intensity to mass-to-charge ratio for each compound and helps to identify the solute. A chromatogram is obtained using the total ion current detected. A specific mass-to-charge ratio can also be monitored[79].

5.3 EXPERIMENTAL

5.3.1 Catalytic testing

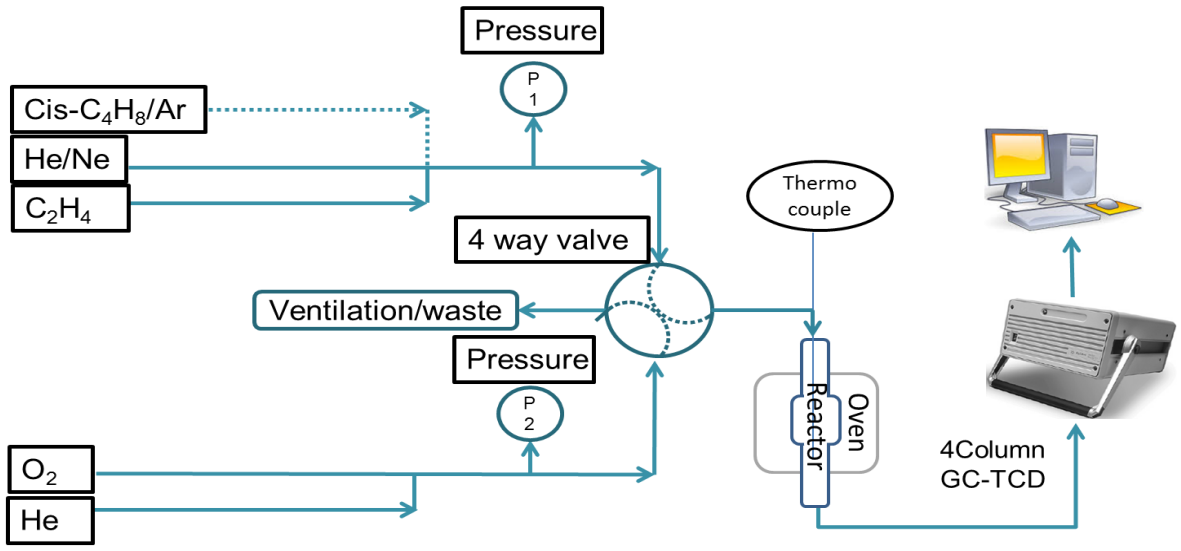

Figure 5.5: Set-up for the catalytic test

The reactor set-up is as shown in Figure 5.5. All the tests were done using a fixed bed reactor with 4 or 6 mm inner bed diameter depending on the amount of catalyst used. A thermocouple was placed in the reactor just on top of the bed to monitor the reaction temperature. The type of gas that flows into the reactor and the ventilation was controlled by a 125 series nitrogen-piloted four-way valve from Humphrey. The ethene, cis-2-butene (9 % in argon) and inert (10 % of neon in helium) gases flow lines were joined together into one slot in the four-way valve. The oxygen and helium flow lines were joined together into the second slot of the valve. The other two slots were connected to the reactor and the vent. Each of the two flow lines that go into the valve was equipped with pressure gauge to monitor the total gas pressure that flows into the reactor. The reactor was placed in an oven which was well insulated to ensure stable internal temperature. Temperature profiling was done to obtain the region where temperature was highest and stable to place the catalyst bed. This was done by varying the position of the thermocouple in a reactor in the oven at a constant oven set temperature (see Appendix C). The catalyst bed was therefore placed at 8 cm from the top of the oven. The line that connected the reactor to the GC was heated by a heating coil and insulated to avoid condensation of products.

Agilent 3000 micro Gas Chromatograph (GC) equipped with thermal conductivity detectors (TCD) were used for all analysis. Analytes were injected into the GC via 1/8 inches Swagelok connectors. The GC contained four different columns, each connected to a TC detector that together allows analysis of C_1-C_{10} compounds. All the 4 columns used He as carrier gas. The columns were baked at 453 K for A and 433 K for B to D with He for 300 runs (33 h) to remove any column contaminant before it was first used for measurement. Table 5.1 shows the types of column, dimensions as well as the temperature and pressure programing used for the analysis.

Table 5.1: Types of column in the micro GC with their temperature and pressure control

Channel	Column (Dimension) (m x mm x μm)	Temperature Control/ K			Pressure Control	
		Sample inlet	Injector	Column	Equilibration time/s	Column Pressure /kPa
A	MolSieve (10 x 0.32 x 12)	353	333	353	15	172
B	Plot U (8 x 0.32 x 30)	353	343	343	60	172
C	Alumina (10 x 0.32 x 8)	353	353	418	60	241
D	OV-1 (8 x 0.15 x 2)	353	353	418	60	241

Two different gas mixtures from AGA were used for calibration of the GC. The first mixture was composed of He, Ar, ethene, ethane, propane, propene and all C_4 compounds while the second contained He, Ar, CO, CO_2, methane, ethane, ethene, propane and propene. Each peak was well integrated for consistency in their peak area measurements before used for further analysis. While the second mixture peak areas correlated well with the labelled (manufacture) composition, the first mixture did not. When the response factors were calculated for each peak, the second calibration mixture was consistent with tabulated literature[80] values while the first calibration mixture was not. Hence all the C_4+ hydrocarbons response factors were calculated using tabulated values from literature [80]. The relative retention times for the C_{5+} peaks were estimated by flowing He gas through liquid C_{5-8}s (listed in Appendix A) compounds under ice-bath. Blank tests (without catalyst) of ethene (99.5 %) were done at temperatures from 323 to 823 K. There was no measurable ethene conversion at these conditions. However, when blank test for cis-2-butene (99.0 %) was done, up to 5 % 1-butene and trans-2-butene were formed at 823 K. Moreover, 1-butene, cis-2-butene and trans-2-butene selectivities were always found to be equivalent to their thermodynamic equilibrium composition (see Appendix F) and hence were put together and referred to as linear butenes. The thermodynamics calculations were done using Standard Reference values from NIST Database [81].

The catalysts in powdery form were pressed, gently crushed and sieved into pellets between 250 and 420 μm sizes to minimize internal diffusion during testing. The catalyst pellets were calcined with O_2 at 823 K for 1 h on stream to get rid of any moisture and organic matter before lowering to the reacting temperature for testing. The calcination was done in the same way after each test to regenerate the catalyst (see Appendix I for activity before and after regeneration). The primary aim of this project was to measure the kinetics of the ethene oligomerization reaction and to determine the mechanism. Three types of experiment were done:

- Linear butene reactions (using cis-2-butene as feed)
- ethene and linear butene co-reactions
- ethene reactions

Parameters such as temperature, pressure and contact time variations were of importance. The reaction temperature ranged from 673 to 823 K with 748 K as standard temperature. Ethene partial pressure ranged from 6.7 to 66.7 kPa with 33.3 kPa as standard while cis-2-butene partial pressure ranged from 0.9 to 8.1 kPa with 4.5 kPa as standard. The total pressure was kept around 100 kPa. The partial pressures were varied by varying the reactants and inert gas (He/Ne) flow. The reactor effluent was measured after 2 min time on stream to ensure constant pressure of reactant in the reactor as well as constant peak area value in the GC [82]. Measurements were made at standard conditions in between each varied parameter within a particular set of experiment. The standards were used to normalize some conversions for deactivation of the catalyst (see Appendix D). The variations of the parameters were done in a randomized manner, for example temperature was varied in the order; 748, 673, 748, 823, 748, 698, 748, 798, 748, 723, 748, 773 and 748 K. This was to ensure that trend of activity and selectivity does not follow deactivation of the catalysts with time on stream as was done elsewhere [83]. At each specific condition, five measurements were made to ensure precision.

Another aim was to compare the influence of acid strength on the mechanism. Hence testing was done over H-SAPO-5 and then repeated over H-SSZ-24 for comparison. The ethene conversion observed over the H-SAPO-5 was below 2 % at 3 ml/min ethene flow rate per 300 mg for the highest contact time. This was good for kinetic studies since several subsequent reactions were suppressed so that primary or initially formed products can predominantly be studied. The challenge then is larger peaks which can overshadow smaller peaks in the column and also that some peaks will be below the detection limit of the GC. However, with a four column micro GC, different

ranges of products were eluted in different columns. Clearly well separated peaks were mostly observed.

External diffusion was checked with different flow rates at the same contact time. It was observed that external diffusion was minimal (see Appendix E). To check for internal diffusion, Arrhenius plot for ethene reaction was used. The influence of internal diffusion was also found to be minimal which is further illustrated later in chapter 8 with an exponential rate dependence on temperature. Mass balance was analysed by running reactants through a cold (373 K) reactor of a deactivated catalyst after testing to obtain the amount of feed under relatively similar reaction conditions. Retained products or coke were analysed by dissolving deactivated catalyst in HF as was done elsewhere[84]. CH_2Cl_2 was added to the solution and then separated into aqueous and organic phase. The organic phase was fetched using syringe and then injected into a GC-MS.

5.3.2 Calculations based on GC analyses and reaction conditions

The calculations for the conversion, selectivity, yield, mass balance and rates were based on GC response and reaction conditions. The integrated peak areas from the GC were treated mathematically into concentrations. The response factors, k_i for a compound i with volume % V_i, were calculated as shown in Equation 5.35 by using an average of 10 peak areas with deviation within 2 % (GC's uncertainty). The volume % of any analyte was then calculated by the product of a k factor and its peak area.

$$k_i = \frac{Volume\ \%\ of\ i\ (V_i)}{Average\ Peak\ Area\ for\ i} \qquad 5.35$$

The conversion is used to quantify the amount of reactants that transform in a chemical process. The conversion was calculated in terms of carbon %. The volume % is equivalent to concentration of the gas from the ideal gas law ($PV=nRT$), at constant temperature and pressure conditions. The volume % multiplied by the number of carbons in a compound (N) is equivalent to the carbon % (C %) of analyte. The conversion %, X was calculated from the effluent as;

$$X = \frac{\sum(V_i \times N_i)}{\sum(V_i \times N_i) + \sum(V_{rxt} \times N_{rxt})} \times 100\% \quad 3.36$$

where, *rxt* is for the reactants in effluent and *i* for the products. All conversions were calculated based on the effluent. Conversion can also be calculated as;

$$X' = \frac{reactants\ (mol)_{\ in} - reactants\ (mol)_{out}}{reactants\ (mol)_{\ in}} \times 100\%$$

$$X' = \frac{C\ (reactants) \times V_{\ in} - C\ (reactants) \times V_{out}}{C\ (reactants) \times V_{\ in}} \times 100\% \quad 5.37$$

where C is the concentration and V is the total volume. If the moles of the inert gas that goes through the reactor do not change, then the concentration and volume can be expressed as;

$$\frac{C(inert)_{in}}{C(inert)_{out}} = \frac{V_{out}}{V_{in}} \quad 5.38$$

When the Equation 5.37 is divided through by V_{in} and Equation 5.38 substituted, a simple way of calculating the conversion *X'* is obtained as shown in Equation 5.39.

$$X' = \frac{C\ (reactants)_{\ in} - C\ (reactants)_{out} \times \frac{C(inert)_{in}}{C(inert)_{out}}}{C\ (reactants)_{in}} \times 100\% \quad 5.39$$

The mass balance was analysed by comparing conversions using the two formulas that is *X* and *X'*.

Selectivity is used to quantify the proportion of product formed in relation with all products. Selectivity %, *Sj* was calculated for a product *j* as;

$$S_j = \frac{V_j \times N_j}{\sum V_i \times N_i} \times 100\% \quad 5.40$$

Yield is used to quantify the amount of individual products formed in the reaction. The yield %, *Yj* was calculated for a product *j* with *Sj* selectivity as;

$$Y_j = \frac{X \times S_j}{100} \quad 5.41$$

The rate of reaction for the formation of *j* was calculated as;

$$rate\ = \frac{Y_j \times flow\ rate\ (\frac{\mu mol}{s})}{catalyst\ mass\ (g)} \quad 5.42$$

Weight hourly space velocity WHSV was calculated as

$$\text{WHSV} = \frac{\text{mass of gas flow}(\frac{\text{g}}{\text{h}})}{catalyst\ mass(g)} \quad 5.43$$

Contact time (CT) was calculated as:

$$\text{CT} = \frac{catalyst\ mass(g)}{\text{mass of total gas flow}(\frac{\text{g}}{\text{h}})} \quad 5.44$$

Accumulated reactant gas per catalyst mass, ARG was calculated as;

$$ARG = \frac{TOS_x \times mol\ of\ gas\ flow\ (reactant) \times \sum_{TOS_0}^{TOS_x} conversion}{catalyst\ mass} \quad 5.45$$

6. LINEAR BUTENE REACTIONS

This chapter describes the kinetics of linear butene using cis-2-butene as the feed over the two catalysts. The first part will consist of all results over H-SAPO-5 followed by those over H-SSZ-24. The discussions will first be based on the observations over H-SAPO-5 and thereafter a comparison will be made with the observations over H-SSZ-24 to elucidate the influence of acid strength on the mechanism.

6.1 RESULTS

6.1.1 Cis-2-butene conversion over H-SAPO-5

6.1.1.1 Catalytic activity versus time on stream

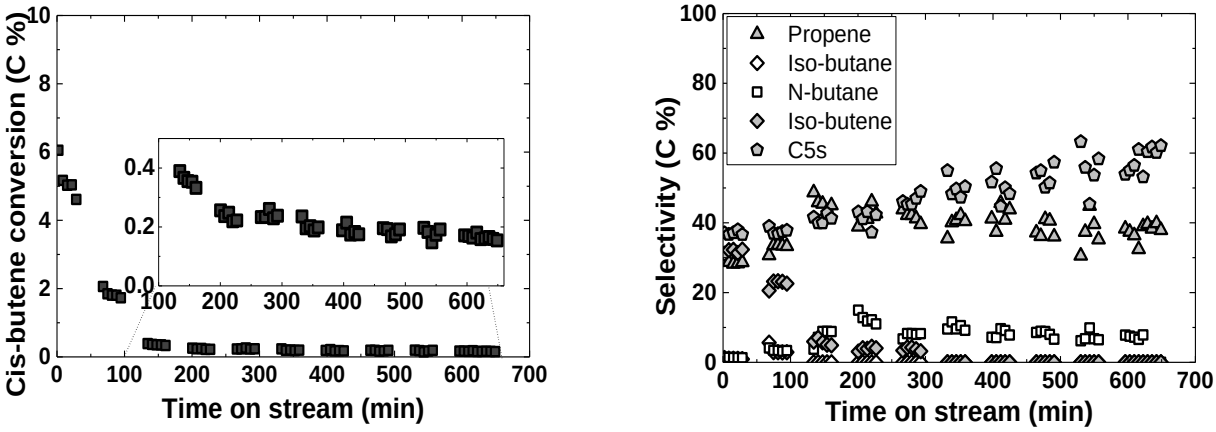

Figure 6.1: Catalytic activity of H-SAPO-5 versus time on stream, Conversion (left) and Selectivity (right): H-SAPO-5 mass = 50 mg, $P_{Cis\text{-}2\text{-}butene}$= 4.5 kPa, $Flow_{total}$=100 ml/min, T= 673 K, WHSV= 0.59 h^{-1}

Figure 6.1 shows the activity of cis-2-butene feed versus time on stream (TOS) over H-SAPO-5 at 673 K, 4.5 kPa cis-2-butene partial pressure and 0.59 h^{-1} WHSV. Conversion decreased rapidly from 2 min to 130 min and then remained relatively stable below 1% conversion with TOS. The insertion shows a magnified version between 100 and 500 min. All linear butenes were considered

as reactants and iso-butene as a product. The linear butenes were grouped together because they easily isomerize as was explained in the experimental section (Section 5.3.1) during the cis-2-butene blank test. At initial TOS, selectivities to propene, iso-butene and C_5s (mostly pentene isomers) were 29, 31 and 37 % respectively. The propene and C_5s selectivities increased with TOS to 40 and 62 % respectively. Iso-butene selectivity declined rapidly in a similar trend as conversion with TOS such that at 333 min it was below detection. This suggests that deactivation does not influence iso-butene positively under these conditions. N-butane and iso-butane were observed as minor products. Selectivity to n-butane increased from 1 to 11 % between 2 and 346 min and then declined to 8 % at about 623 min TOS. Iso-butane only showed up between 2 and 95 min with selectivities up to 3 %. It appeared that alkanes especially n-butane was high at the time when the catalyst had severely deactivated at 673 K. Coke analysis of the deactivated sample showed no soluble coke.

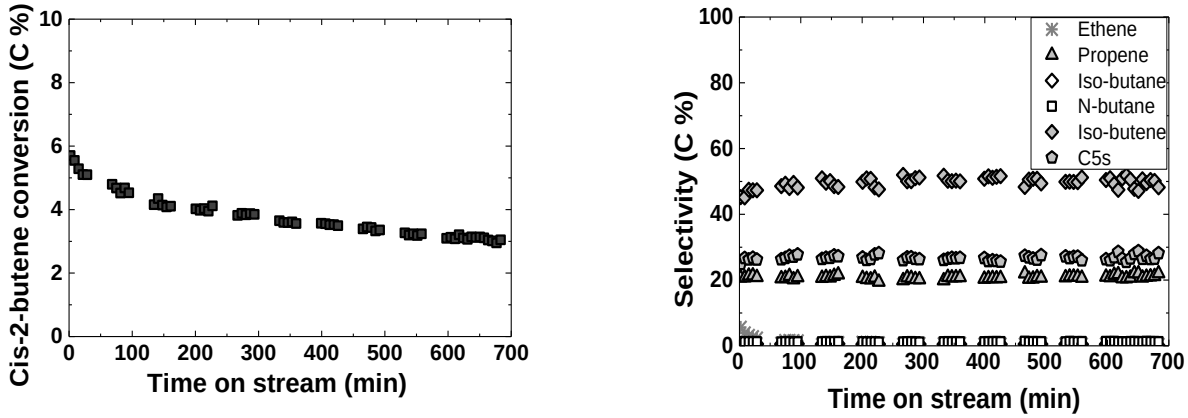

Figure 6.2: Catalytic activity of H-SAPO-5 versus time on stream, Conversion (left) and Selectivity (right): H-SAPO-5 mass= 50 mg, $P_{Cis\text{-}2\text{-}butene}$= 4.5 kPa, $Flow_{total}$= 100 ml/min, T= 748 K, WHSV = 0.59 h^{-1}

The H-SAPO-5 activity over TOS was also studied at 748 K at similar conditions as was done at 673 K. Figure 6.2 shows the activity of cis-2-butene feed reaction versus TOS over H-SAPO-5 at 748 K. Conversion decreased from 6 to 3 % with TOS. The decrease was less rapid as compared to the reaction at 673 K. Selectivities to iso-butene, C_5s (see Appendix G for C_5s composition) and propene were 44, 28 and 21 % respectively and remained relatively stable with TOS. The selectivity at 748 K varied very slightly compared to that observed at 673 K. Some iso-butane and n-butane were also observed at 748 K with total selectivity up to 2 % over TOS. In addition, some ethene was observed with selectivity that declined rapidly from 5 to 1 % initially and remained at 1 % over the TOS.

Furthermore, the catalytic activity was studied at 823 K under similar conditions as was done at 673 and 748 K. Figure 6.3 shows the activity of cis-2-butene feed versus TOS over H-SAPO-5 at 823 K. The conversion decreased from 9 to 4 % within the 2 to 653 min TOS studied. The deactivation at 823 K was less rapid similar to the activity at 748 K with TOS compared to that at 673 K. Selectivity at 823 K to iso-butene, C_5s (see Appendix G for C_5s composition) and propene were relatively stable around 71, 15 and 12 % respectively with TOS. Ethene, iso-butane and n-butane were also observed with about 3 % total selectivity with TOS. The selectivities to the alkanes (n-butane and iso-butane) at 748 and 823 K were far less compared to those observed at 673 K, where deactivation was fastest. This suggests that alkane formation and deactivation are directly related.

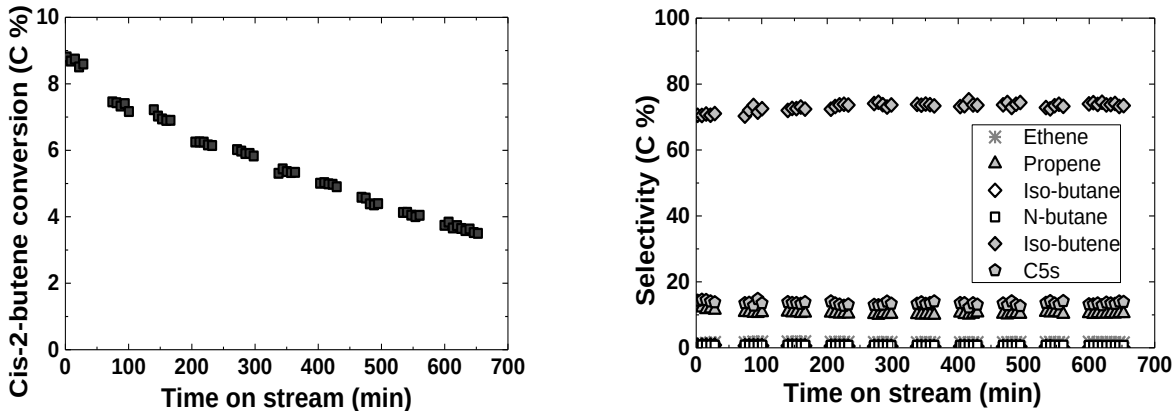

Figure 6.3: Catalytic activity of H-SAPO-5 versus time on stream, Conversion (left) and Selectivity (right): H-SAPO-5 mass = 50 mg, $P_{Cis\text{-}2\text{-}butene}$= 4.5 kPa, $Flow_{total}$ =100 ml/min, T = 823 K, WHSV = 0.59 h^{-1}

6.1.1.2 Contact time variation at 748 K

To compare the product distribution with cis-2-butene conversions the contact time was varied over H-SAPO-5. Figure 6.4 shows a plot of selectivity versus cis-2-butene conversion during contact time variation over H-SAPO-5 at 748 K, 4.5 kPa partial pressure and 0.12-1.17 h^{-1} WHSV. 50 mg catalyst was used with total flow variation from 20 to 200 ml/min. The cis-2-butene to total gas flow rates ratio was kept constant at 0.045 to maintain the 4.5 kPa cis-2-butene partial pressure at different flow rates. Note that the Std. (crossed symbols) in the Figure 6.4 represents standard contact time (0.019 h.g/g), while the others (opened symbols) are for different contact times. Only the main products are represented since the total minor products were generally less than 5 % at 748

K. The selectivities of the main products at conversions between 3 and 20 % varied slightly compared to the selectivities below 3 %. Selectivity to iso-butene was about 52 %, while that of C_5s and propene were 28 and 20 % respectively as conversion decreased from 20 to 3 %. This implies that the ratio of C5s/propene approached 28/20 (~1.4) which is quite close to the 5/3 (~1.7) carbon ratios of the two products as lower conversions are approached. It appeared that, at increasing conversions, the ratio between C_5s and propene approached unity.

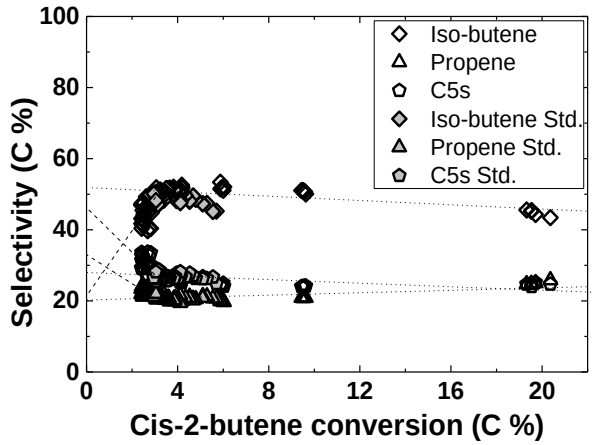

Figure 6.4: Selectivity versus Cis-2-butene conversion at different contact times:

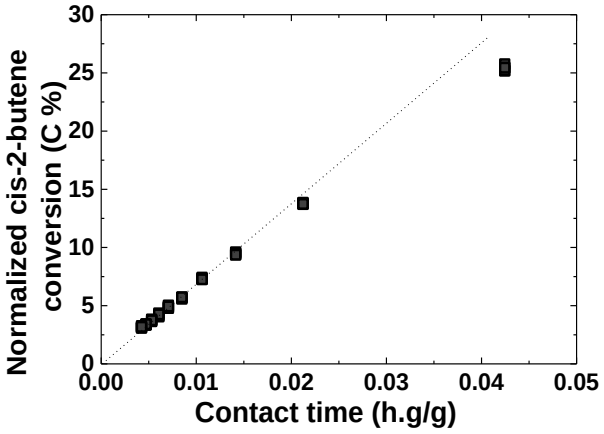

Figure 6.5: Cis-2-butene conversion versus contact time:

H-SAPO-5 mass = 50 mg, $P_{Cis\text{-}2\text{-}butene}$= 4.5 kPa, $Flow_{total}$=20-200 ml/min, WHSV = 0.12-1.17 h^{-1}, T= 748 K, The Std. represents standard conditions measured in-between contact time variations.

Below 3 % conversion, C_5s and propene selectivities increased while that of iso-butene decreased. This suggested that iso-butene is formed from different pathway compared with the C_5s and propene. When these selectivities were extrapolated to 0 % conversion, the iso-butene approached 22 % while the C_5s and propene approached 47 and 32 % respectively. The selectivity above 20 % at 0 % conversion suggests that the main products are formed directly from linear butenes. Here also, the ratio of C5s/propene approached 1.4 similar to their ratios as conversion decreased from 20 to 3 %. This also suggests that the C_5s and propene may be from a common intermediate probably a C_8, though no C_8s were observed.

Figure 6.5 shows the normalized conversion of cis-2-butene versus contact time (CT). The conversion increased linearly with contact time. When the conversion was extrapolated to 0 h CT,

the conversion approached 0 %. The implication of this graph will be discussed later in Chapter 7 and 8 in comparison with ethene reactions.

6.1.1.3 Effect of cis-2-butene partial pressure on activity

The effect of cis-2-butene partial pressure over H-SAPO-5 was studied between 0.9 and 8.1 kPa cis-2-butene partial pressures with WHSV ranging from 0.12 to 1.17 h^{-1} at temperatures 673, 748, and 823 K. 50 mg catalyst was used while cis-2-butene flow rate was varied between 0.9 to 8.1 ml/min to vary its partial pressure. The total gas flow rate was held constant at 100 ml/min to maintain constant contact time. The original conversions obtained were below 10 % but were normalized for rate calculations.

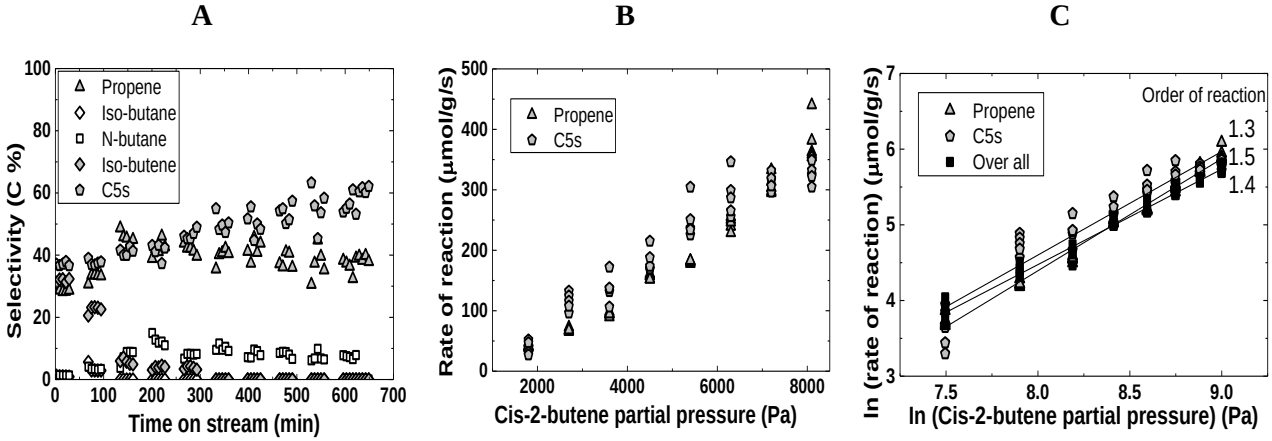

Figure 6.6: Effect of cis-2-butene partial pressure on selectivity (A), rate (B) and log-log plot of (B) as (C): H-SAPO-5 mass= 50 mg, $Flow_{total}$= 100 ml/min, $P_{cis\text{-}2\text{-}butene}$=1.8-8.1 kPa, T = 673 K, WHSV= 0.23-1.17 h^{-1}

Figure 6.6A shows the selectivity versus cis-2-butene partial pressure at 673 K. The selectivity to C_5s and propene dominated throughout as they increased from about 33 to 43 % and 34 to 47 % respectively with partial pressure. Iso-butene mainly appeared at the initial partial pressure with 11 % selectivity and disappeared. Meanwhile, selectivity to n-butane decreased from 19 to 6 % between 1.8 and 5.4 kPa and increased to 9 % at 8.1 kPa. Note that at this temperature, the catalyst deactivated much severely, coupled with n-butane formation and subsequent disappearance of iso-butene just as was observed over TOS (Figure 6.1). Figure 6.6B shows the rate of formation for C_5s

and propene versus cis-2-butene partial pressure at 673 K. The rate of formation of the products increased linearly with pressure. The orders of reaction were obtained by plotting a logarithmic version of the graph in Figure 6.6B and the overall rate using logarithm of rate versus logarithm of cis-2-butene partial pressure as shown in Figure 6.6C. The reaction orders within 1.8 to 8.1 kPa were 1.3, 1.5 and 1.4 for the overall, propene and C_5s formation rates respectively.

Similar experiment was repeated at 748 K. The results are presented in Figure 6.7. Figure 6.7A shows the selectivity versus cis-2-butene partial pressure. The selectivity to iso-butene was highest at 0.9 kPa and decreased from 80 to 21 % at 8.1 kPa partial pressure. The C_5s and propene selectivities on the other hand increased with partial pressure, from 6 to 38 % and 5 to 33 % respectively. Some minor selectivity to ethene, iso-butane and n-butane were also observed with total selectivity ranging between 1 to 5 % with partial pressure.

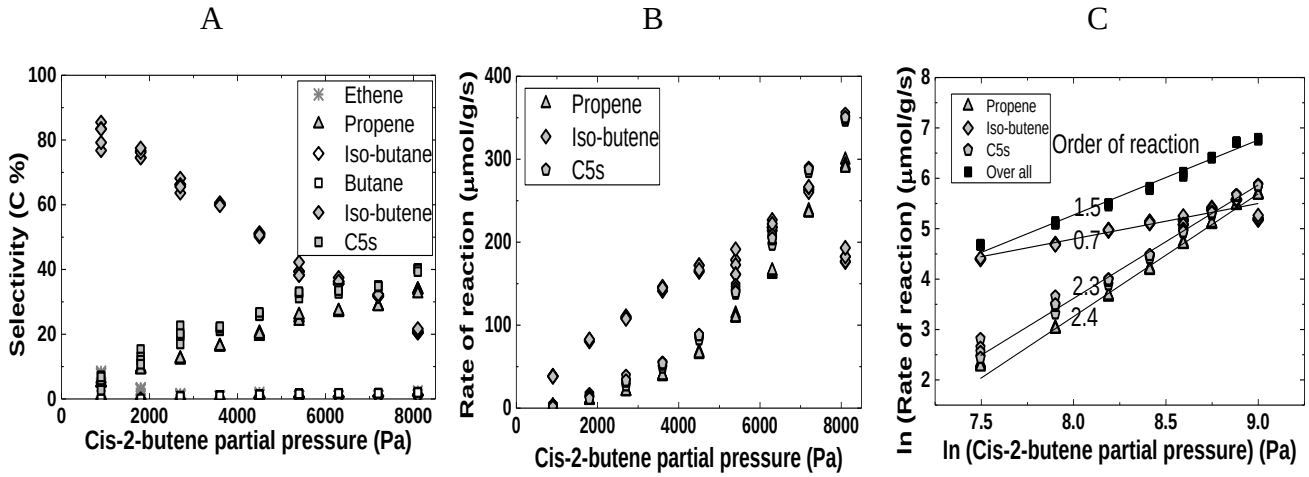

Figure 6.7: Effect of cis-2-butene partial pressure on selectivity (A), rate (B) and log-log plot of (B) as (C): H-SAPO-5 mass= 50 mg, $Flow_{total}$= 100 ml/min, $P_{cis\text{-}2\text{-}butene}$=0.9-8.1 kPa, T = 748 K, WHSV= 0.12-1.17 h^{-1}

Figure 6.7 B shows the rate of formation of the main products versus cis-2-butene partial pressure at 748 K. The rate of formation of iso-butene increased linearly with partial pressure except at 8.1 kPa where it declined. Below 6.3 kPa, iso-butene formation rate was more than the formation rate of C_5s and propene. C_5s formation rate was slightly higher than that of propene, and both increased exponentially with partial pressure. The logarithmic form of Figure 6.7B and the overall rate using logarithm of both rate and cis-2-butene partial pressure have been shown in Figure 6.7C. The

reaction orders were 1.5, 0.7, 2.4 and 2.3 for the overall, iso-butene, propene and C_5s formation rates respectively.

Furthermore, the effect of cis-2-butene partial pressure was studied at 823 K under similar conditions as stated above except temperature. Figure 6.8A shows the selectivity versus cis-2-butene partial pressure. The selectivity to iso-butene was very high at 0.9 kPa and decreased from 90 to 50 % at 8.1 kPa partial pressure. The C_5s and propene selectivities on the other hand were much less and increased from 5 to 23 % and 2 to 21 % respectively with partial pressure. Some minor selectivity to ethene, iso-butane and n-butane were also observed which total selectivity ranged between 1 to 5 % with partial pressure similar to what was observed at 748 K. By comparison, iso-butene was favored by low cis-2-butene partial pressures and high temperatures.

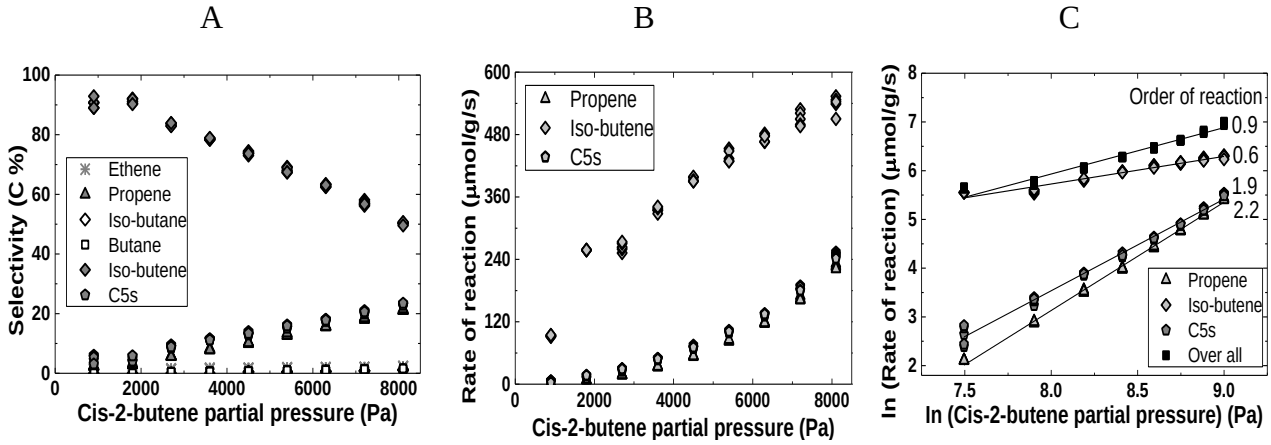

Figure 6.8: Effect of cis-2-butene partial pressure on selectivity (A), rate (B) and log-log plot of (B) as (C): H-SAPO-5 mass= 50 mg, $Flow_{total}$= 100 ml/min, $P_{cis\text{-}2\text{-}butene}$=0.9-8.1 kPa, T = 823 K, WHSV= 0.12-1.17 h^{-1}

Figure 6.8B shows the rate of formation of the main products versus cis-2-butene partial pressure at 823 K. The rate of formation of iso-butene increased linearly whilst that of C_5s and propene increased exponentially with partial pressure. This was very similar to the observation at 748 K except that the rates were higher at 823 K. The logarithm of both the rate versus cis-2-butene partial pressure has been shown in Figure 6.8C. The reaction orders were 0.9, 0.6, 2.2 and 1.9 for the overall reaction, iso-butene, propene and C_5s formation rates respectively. The order of reaction at 748 and 823 K were the same when they are taken to the first significant figure. The first order dependence of iso-butene formation on cis-2-butene too suggested that they are formed through a pathway which differs from that for C_5s and propene with second order dependence.

6.1.1.4 Effect of temperature on activity

The effect of the reaction temperature on the cis-2-butene reaction was studied over H-SAPO-5 to see its effects on selectivity, rate and also to estimate the activation energy. This was done between 673 to 748 K, at 4.5 kPa cis-2-butene partial pressure and of 0.58 h^{-1} WHSV. 50 mg catalyst and 4.5 ml/min cis-2-butene flow rate were used. The original conversions observed for all temperatures were below 10 % but were normalized for calculating the rate. Figure 6.9A shows the selectivity versus temperature. The selectivity to iso-butene increased slowly from 23 to 27 % at initial temperatures between 673 and 723 K but rapidly afterwards to 70 % at 823 K. At similar temperatures, C_5s and propene selectivities relatively stayed around 37 and 30 initially but rapidly declined after 723 K to 15 and 13 % respectively with temperature which indicates that high temperature favours the formation of iso-butenes. A total of 3 % selectivity to ethene, iso-butane and n-butane were observed roughly throughout the various temperatures.

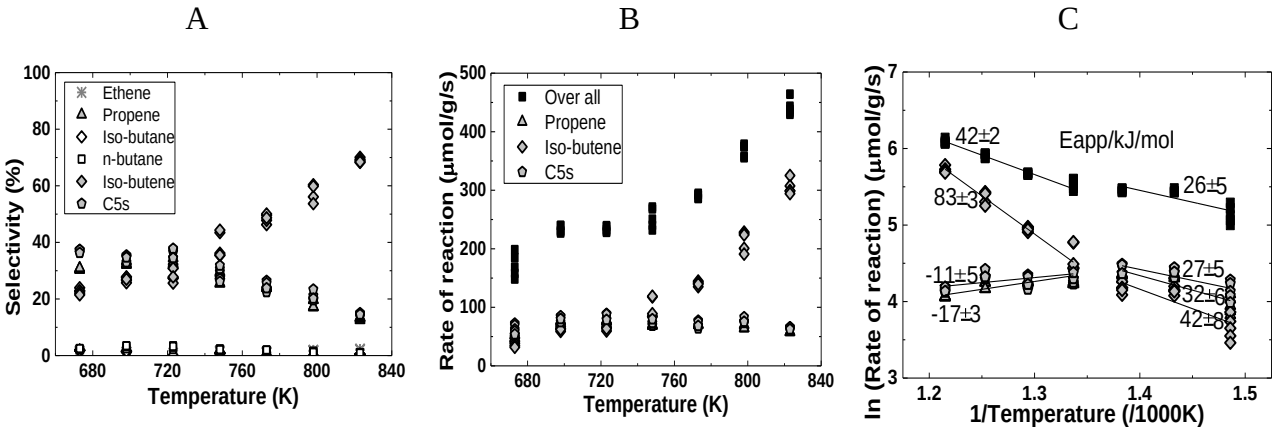

Figure 6.9: Effect of temperature on selectivity (A), rate (B) and log-log plot of (B) as (C): H-SAPO-5 mass=50 mg, $Flow_{total}$= 100 ml/min, $P_{cis\text{-}2\text{-}butene}$=4.5 kPa, T = 678-823 K, WHSV= 0.59 h^{-1}

Figure 6.9B shows the rate of reaction versus temperature. The trends in the various rates varied mainly at two temperature regions. These regions can be classified as low temperature range between 673 and 723 K and high temperature range between 748 and 823 K. In low temperature region, iso-butene, C_5s and propene formations increased slowly with temperature. In the high temperature region, the formation rate of iso-butene increased exponentially whilst that of C_5s and propene decreased with temperature. The deviation at high temperature suggested suppression of C_5s plus propene formation pathway in favour of the iso-butene. The overall reaction rate increased with temperature though it was slower at the low temperature region. It is also possible that

deactivation at lower temperature conditions affected the overall rate and iso-butene formation particularly, as they were observed to rapidly disappear at 673 K (Figure 6.1).

Furthermore, a linearized version of the plot in Figure 7.8 B was plotted by taking the logarithm of the rate versus the reciprocal of the temperature and is shown in Figure 7.8 C. Multiplication of the slope of the straight lines by gas constant (R=8.314 J/K/mol) gives the apparent activation energy. The apparent activation energies for the overall reaction, iso-butene, C_5s and propene formation rates at lower temperature region were 26±5, 42±8, 27±5 and 32±6 kJ/mol respectively. At the high temperature region, the apparent activation energies for the overall reaction, iso-butene, C_5s and propene formation rates were 42±2, 83±3, -11±5 and -17±3 kJ/mol respectively. The error margins were evaluated from standard deviation calculation. The similarities in the apparent activation energies of C_5s and propene supported the view that they may be formed from a common intermediate which differs from that of iso-butene.

6.1.2 Cis-2-butene conversion over H-SSZ-24

6.1.2.1 Catalytic activity versus time on stream

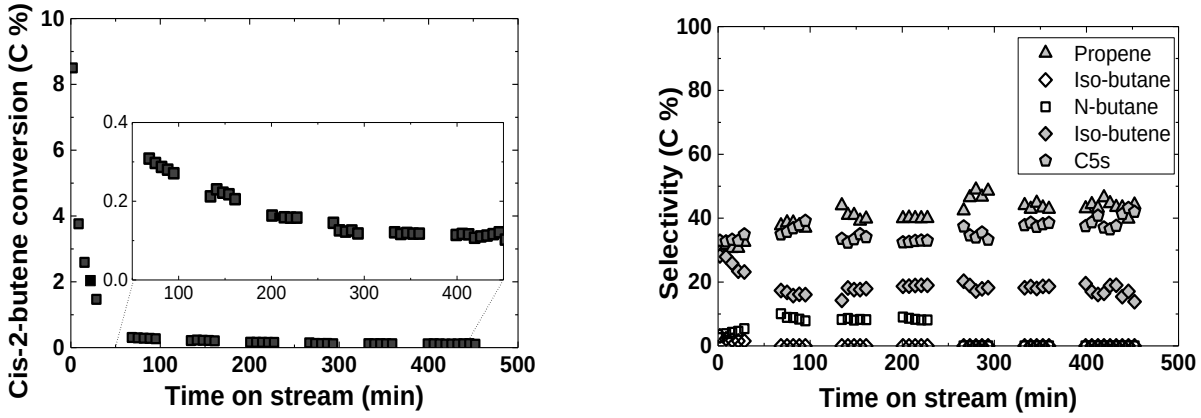

Figure 6.10: Catalytic activity of H-SSZ-24 versus time on stream, Conversion (left) and Selectivity (right): H-SSZ-24 mass = 5 mg, $P_{Cis\text{-}2\text{-}butene}$= 4.5 kPa, $Flow_{total}$=140 ml/min, T = 673 K, WHSV = 8.2 h^{-1}

Figure 6.10 shows the conversion and selectivity plot against time on stream (TOS) using the H-SSZ-24 at 673 K, 8.2 h^{-1} WHSV and 4.5 kPa cis-2-butene partial pressure. The insertion shows a magnified version between 100 and 450 min. Cis-2-butene conversion decreased sharply particularly at the beginning with time on stream from 9 % at 2 min to 0.3 % at 68 min then to 0.1 at 452 min. At 2 min TOS, selectivities to propene, iso-butene and C_5s (pentene isomers) were 30, 28 and 33 % respectively. The propene and C_5s selectivities increased slightly with TOS to 44 and 42 % respectively. Iso-butene selectivity declined to 13 % at 452 min with initial rapid decrease similar to that of the conversion. Selectivity to n-butane increased from 3 to 8 % between 2 and 228 min and then disappeared. Iso-butane only showed up at the first 29 min with selectivities from 3 to 2 %. Coke analysis was done on the deactivated H-SSZ-24 similar to what was done over H-SAPO-5. Similarly, no soluble coke was observed.

The H-SSZ-24 activity versus TOS was studied at 748 K at similar conditions. Figure 6.11 shows the activity of cis-2-butene feed versus TOS at 748 K. Cis-2-butene conversion decreased rapidly from 9 to 0.6 % with TOS, though less rapidly compared to the reaction at 673 K. The main products were iso-butene, C_5s and propene with nearly similar selectivities. Selectivities to iso-butene initially increased from 26 to 41 % between 2 and 75 min and remained fairly stable with

TOS. C_5s and propene varied slightly with TOS with selectivity ranging from 30 to 35 and 26 to 33 % respectively. Minor selectivity to ethene, iso-butane and n-butane were observed. Ethene and iso-butane total selectivities were 3 % but disappeared after 29 min. n-Butane with 2 % selectivity remained stable with TOS.

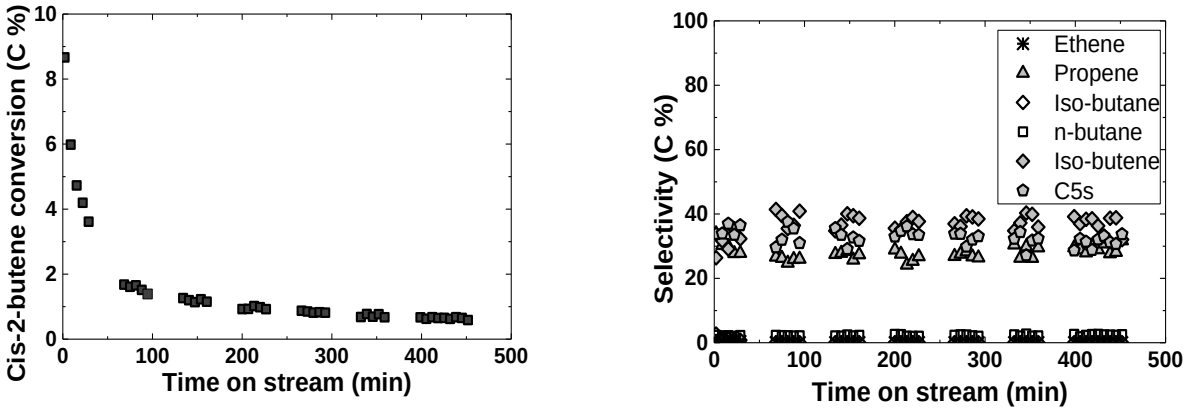

Figure 6.11: Catalytic activity of H-SSZ-24 versus time on stream, Conversion (left) and Selectivity (right): H-SSZ-24 mass = 5 mg, $P_{Cis\text{-}2\text{-}butene}$= 4.5 kPa, $Flow_{total}$=140 ml/min, T = 748 K, WHSV = 8.2 h^{-1}

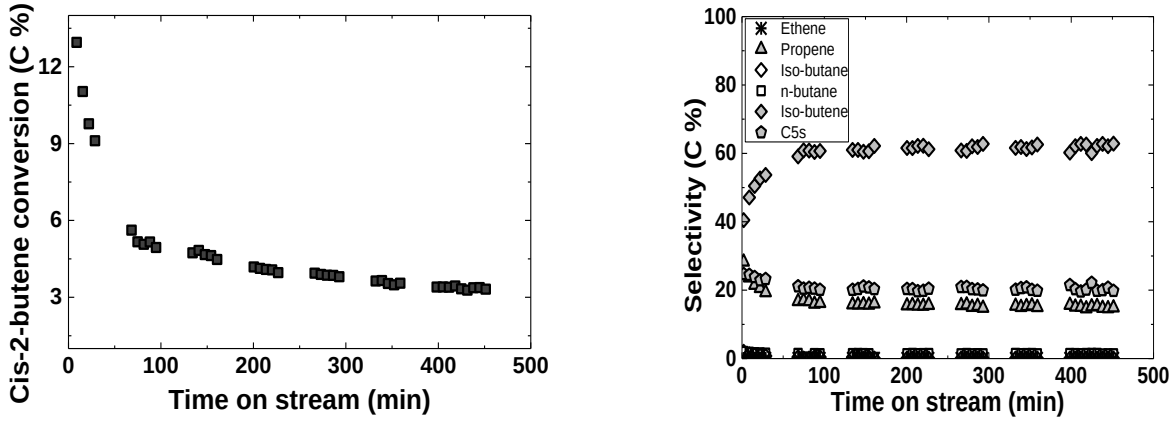

Figure 6.12: Catalytic activity of H-SSZ-24 versus time on stream, Conversion (left) and Selectivity (right): H-SSZ-24 mass = 5 mg, $P_{Cis\text{-}2\text{-}butene}$= 4.5 kPa, $Flow_{total}$=140 ml/min, T = 823 K, WHSV = 8.2 h^{-1}

Similar experiment was repeated at 823 K and is shown in Figure 6.12. The conversion rapidly decreased initially from 13 to 5 % within the 2 to 68 min TOS after which the decrease was less rapid to 3 % at 451 min. A comparison of the deactivation of H-SSZ-24 at the three temperatures shows that the rate of deactivation decreased with increasing temperature. At 823 K, the main products were iso-butene, C_5s and propene. Selectivities to iso-butene increased at initial TOS, from 40 to 59 % between 2 and 68 min but gently afterwards to 63 % at 451 min. In the period of time,

selectivity to propene initially decreased from 28 to 19 % and slowly to 15 %. The C_5s slowly decreased from 24 to 20 % with TOS. Minor selectivities to ethene, iso-butane and n-butane were observed. Ethene and n-butane selectivities were each fairly stable with TOS from 2 to 1 %. 2 % iso-butane selectivity was observed initially but gradually disappeared after 160 min.

6.1.2.2 Contact time variation at 748 K

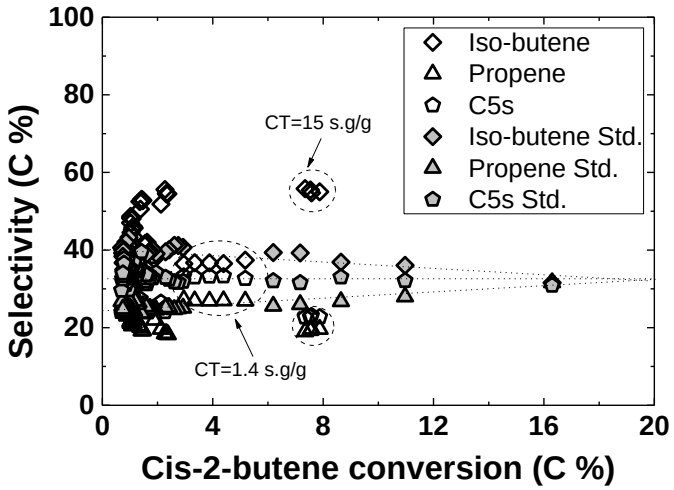

Figure 6.13: Selectivity versus Cis-2-butene conversion at different contact times over H-SSZ-24: H-SSZ-24 mass = 5 mg, $P_{Cis\text{-}2\text{-}butene}$= 4.5 kPa, T= 748 K, $Flow_{total}$= 20-200 ml/min WHSV = 1.2-11.7 h^{-1}. The Std. represents standard conditions measured in between contact time variations.

Figure 6.13 shows a plot of selectivity versus cis-2-butene conversion during contact time variation over H-SSZ-24 at 748 K. This was done at different flow rates but constant cis-2-butene to inert flow rate ratios so that the 4.5 kPa partial pressure was maintained. 5 mg catalyst was used with total flow variation from 20 to 200 ml/min. At the standard (Std.) contact time (0.0006 h.g/g CT = 2.16 s.g/g CT), the selectivity of iso-butene increased with decreasing conversion and approached 40 % at 0 % conversion. Propene selectivity on the other hand decreased with decreasing conversion and approached 24 % while C_5s was relatively stable at 33 %. This gives a C_5s/propene ratio of about 1.4 similar to what was observed over H-SAPO-5. Also, the C5s/propene ratio approached unity at 16 % conversion over H-SSZ-24 similar to the observation over H-SAPO-5. Moreover, over both catalysts, the standard contact times gave more than 20 % selectivities to the main products. When the contact time variation components over the H-SSZ-24 are considered, selectivities at 8 % conversion (circled) were observed for the highest contact time at 15 s.g/g CT, while selectivities around 4 % conversions were observed for the lowest contact time at 1.4 s.g/g contact time. At other contact time variations where conversions were below 2 %, the selectivities were relatively scattered and showed no strict trend. Hence, the contact time variation over H-SSZ-

24 did not show a clear trend in selectivities versus conversion, except for the standard contact times.

6.1.2.3 Effect of cis-2-butene partial pressure on activity

The effect of cis-2-butene partial pressure over H-SSZ-24 was also studied at 673, 748, and 823 K temperatures between 1.6 and 6.4 kPa cis-2-butene partial pressures. The total gas flow rate was held constant at 140 ml/min while cis-2-butene and inert flow rates were varied. 5 mg catalyst was used with 2.3-9 ml/min cis-2-butene flow to give 2.9 to 11.7 h^{-1} WHSV. The original conversions measured and used for the rate calculations for the different pressure at each temperature were below 10 %.

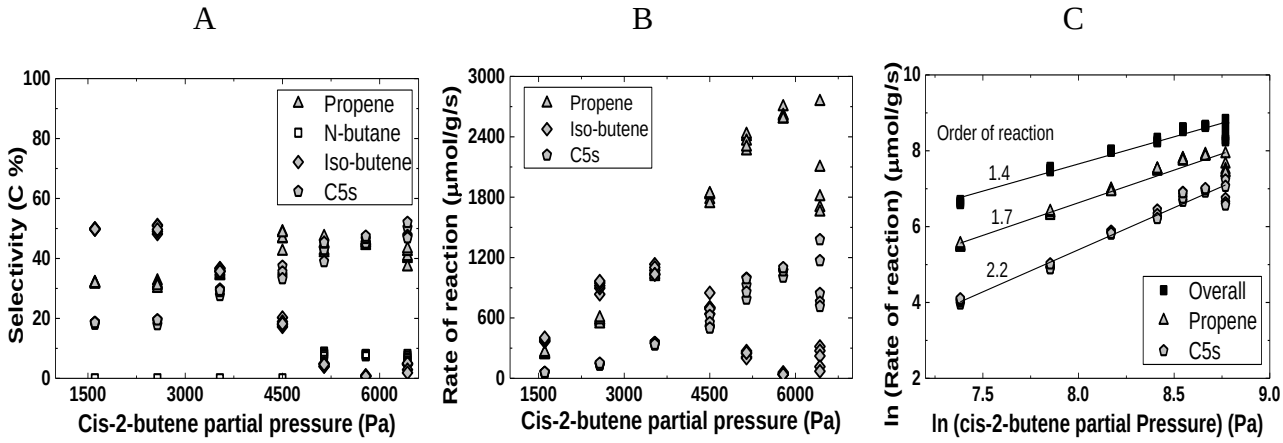

Figure 6.14: Effect of cis-2-butene partial pressure on selectivity (A), rate (B) and log-log plot of (B) as (C): H-SSZ-24 mass= 5 mg, $P_{Cis\text{-}2\text{-}butene}$= 1.6-6.4 kPa, $Flow_{total}$= 140 ml/min, T 673 K, WHSV = 2.9-11.7 h^{-1}

Figure 6.14A shows the effect of cis-2-butene partial pressure on selectivity at 673 K. At 1.6 kPa partial pressure, iso-butene selectivity was highest with 50 % followed by propene and C_5s with 32 and 18 % selectivities respectively. The selectivity of iso-butene rapidly decreased to about 2 % with increasing partial pressure. The C_5s and propene selectivities on the other hand increased to 47 and 43 % respectively with partial pressure. Note that the propene selectivity was more than C_5s selectivity at lower pressure but reduced at high pressure. Meanwhile, about 8 % selectivity to n-butane showed up between 5.1 and 6.4 kPa. This was at the pressure when iso-butene selectivity

was very low. The trend in the selectivity versus cis-2-butene partial pressure at 673 K was similar for the reactions over both H-SSZ-24 and H-SAPO-5 with the rapid disappearance of iso-butene as the catalyst rapidly deactivated.

Figure 6.14B shows the rate of reaction of formation for iso-butene, C_5s and propene versus cis-2-butene partial pressure at 673 K. The rate of formation of the C_5s and propene increased exponentially with pressure. Iso-butene formation rate initially increased linearly from 1.6 to 3.5 kPa but declined afterwards. To estimate the orders of reaction, logarithms of the rate of reaction and cis-2-butene partial pressures were plotted for the C_5s formation, propene formation and overall reaction as shown in Figure 6.14C. The iso-butene was not included because their rate rapidly declined with pressure at 673 K. The reaction orders within 1.6 to 6.4 kPa were 1.4, 1.7 and 2.2 for the overall, propene and C_5s formations rates respectively.

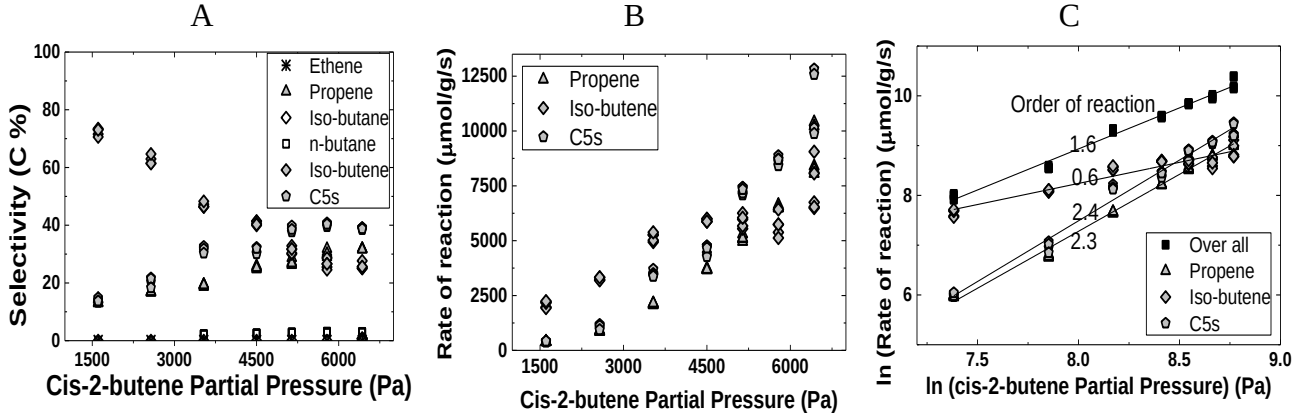

Figure 6.15: Effect of cis-butene partial pressure on selectivity (A), rate (B) and log-log plot of (B) as (C): H-SSZ-24 mass = 5 mg, $P_{Cis\text{-}2\text{-}butene}$= 1.6-6.4 kPa, $Flow_{total}$= 140 ml/min, T = 748 K , WHSV = 2.9-11.7 h^{-1}

Figure 6.15A shows the selectivity versus cis-2-butene partial pressure at 748 K. At 1.8 kPa partial pressure, selectivity to iso-butene was 72 % but rapidly decreased to 26 % at 6.4 kPa. The C_5s and propene selectivities increased with partial pressure, from 14 to 39 % and 14 to 32 % respectively. Once again, iso-butene formation was favored at low pressure at 748 K just as was observed over H-SAPO-5. The ratio of C_5s to propene also increased with pressure. Some minor selectivity to ethene, iso-butane and n-butane were also observed which total selectivity stayed around 3 % between 3.5 to 6.4 kPa partial pressure. Figure 6.15B shows the rate of reaction for the formation of the main products versus cis-2-butene partial pressure at 748 K. The rate of formation of iso-butene increased linearly between 1.6 and 4.5 kPa then began to level off with increasing partial pressure.

C_5s and propene formation rates increased exponentially with partial pressure. The logarithmic form of Figure 6.15B plus the overall rate were plotted to obtain the order of reaction. Figure 6.15C shows the logarithm of reaction rates versus logarithm of cis-2-butene partial pressure. The reaction orders obtained were 1.6, 0.6, 2.3 and 2.4 for the overall, iso-butene, propene and C5s formation rates respectively.

Figure 6.16A shows selectivity versus cis-2-butene partial pressure at 823 K. Iso-butene selectivity decreased with partial pressure, from 85 to 44 %. C_5s and propene selectivities on the other hand increased from 7 to 28 % and 6 to 24 % respectively with partial pressure. Minor selectivities to ethene, iso-butane and n-butane were also observed, the total selectivity of which varied between 1 to 4 % with partial pressure similar to what was observed at 748 K. The effects of cis-2-butene partial pressure over the H-SSZ-24 at 748 and 823 K were very similar. In all, iso-butene was favored at low cis-2-butene partial pressures as well as high temperature. This was also similar to the observations over H-SAPO-5.

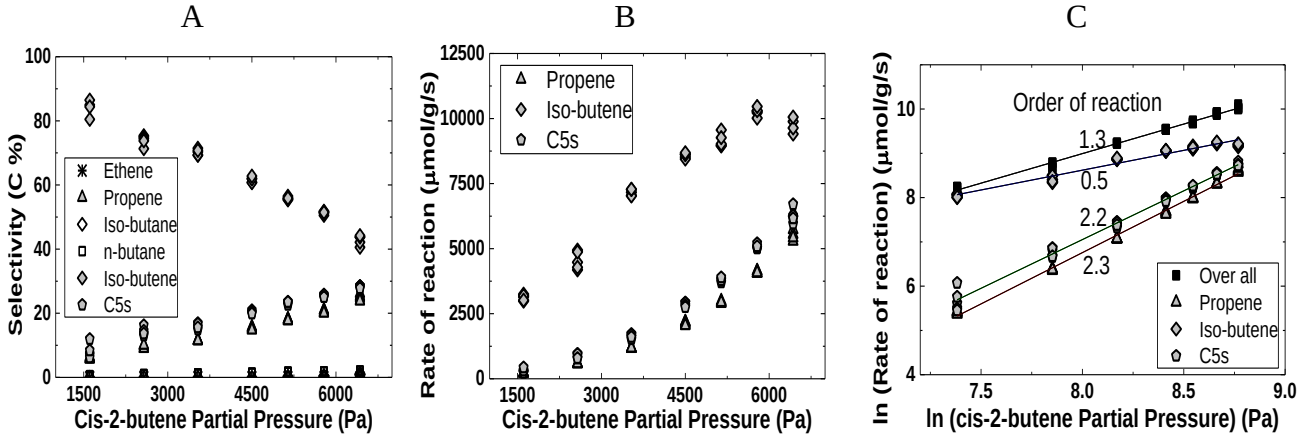

Figure 6.16: Effect of cis-butene partial pressure on selectivity (A), rate (B) and log-log plot of (B) as (C): H-SSZ-24 mass = 5 mg, $P_{Cis\text{-}2\text{-}butene}$= 1.6-6.4 kPa, $Flow_{total}$= 140 ml/min, T = 823 K, WHSV = 2.9-11.7 h^{-1}

Figure 6.16B shows the rate of formation of the main products versus cis-2-butene partial pressure at 823 K. The rate of formation of iso-butene increased linearly between 1.6 and 5.8 kPa partial pressure but dropped off afterwards. C_5s and propene rate of formation exponentially increased with partial pressure. This was very similar to the observation at 748 K. The logarithm of the reaction rates versus logarithm of cis-2-butene partial pressure were plotted and are shown in Figure 6.16C.

The reaction orders were 1.3, 0.5, 2.3 and 2.2 for the overall reaction, iso-butene, propene and C_5s formation rates respectively. The order of reaction at 748 and 823 K were also similar.

6.1.2.4 Effect of temperature on activity

The effect of reaction temperature on the reaction was studied over H-SSZ-24 between 673 to 823 K. This was done at 4.5 kPa cis-2-butene partial pressure and of 8.2 h^{-1} WHSV. 6.3 ml/min ethene flow rate over 5 mg catalyst were used. At 8.2 h^{-1} WHSV the original conversions observed at the varied temperatures stayed below 10 %.

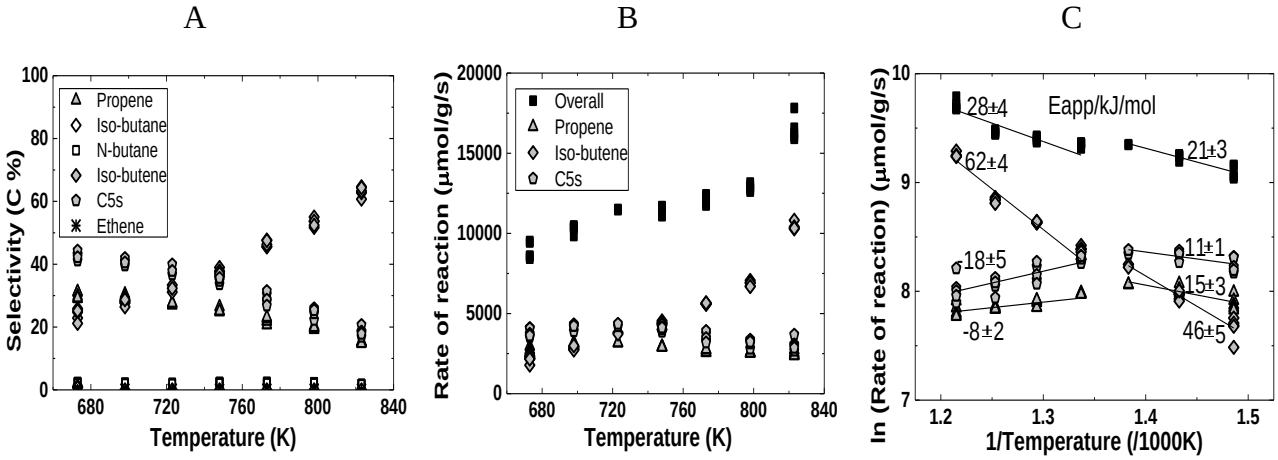

Figure 6.17: Effect of temperature on selectivity (A), rate (B) and log-log plot of (B) as (C): H-SSZ-24 mass=50 mg, $Flow_{total}$= 140 ml/min, $P_{cis\text{-}2\text{-}butene}$= 4.5 kPa, T = 673-823 K, WHSV= 8.2 h^{-1}

Figure 6.17A shows effect of the temperature on product selectivity over H-SSZ-24. The effect of temperature was distinct at low (678-723 K) and high (748 -823 K) temperature regions, just as it was observed over H-SAPO-5. The selectivity to iso-butene slowly increased from 23 to 33 % at low temperature region and rapidly increased to 64 % at high temperature region. C_5s selectivities decreased slightly from 43 to 38 % at low temperature region and rapidly at high temperature region to 18 %. Similarly propene selectivity initially decreased slowly from 31 to 27 % and then rapidly to 15 %. Obviously, temperature favoured iso-butene formation over H-SSZ-24 just as was observed over H-SAPO-5 (see Figure 6.9). Also the selectivity to C_5s to propene ratios also decreased with temperature over H-SSZ-24. Though this difference was observed over H-SAPO-5,

it was more significant over H-SSZ-24. A total of 3 % selectivity to ethene, iso-butane and n-butane were observed with varying temperature.

Figure 6.17B shows the rate of the overall reaction as well as that for the formation of the main products versus temperature. The various rates varied at the two temperature regions. At low temperature region, the rate of reaction increased slowly with temperature. At high temperature region, only the iso-butene formation rate among the products increased exponentially with temperature. On the other hand, C_5s and propene formation rates decreased with temperature at the high temperature region. The overall reaction rate generally increased with temperature. The apparent activation energies were estimated by plotting the logarithm of the reaction rate versus the reciprocal of the temperature and are shown in Figure 6.17C. The apparent activation energies with respect to the overall reaction/products, iso-butene, C_5s and propene formation rates at lower temperature region were 21±3, 46±5, 11±1 and 15±3 kJ/mol respectively. At the high temperature region, the apparent activation energies for the overall reaction, iso-butene, C_5s and propene formation rates were 28±4, 62±4, -18±5 and -8±2 kJ/mol respectively. Once again, apparent activation energies in C_5s and propene were nearly the same at the different regions while that of iso-butene was much different. This followed similar trend to the observation over H-SAPO-5. However, the apparent activation energies observed over H-SSZ-24 were generally lower than those over H-SAPO-5.

6.2 Discussion

Generally it was observed that iso-butene, propene and C_5s (mostly pentene isomers) were the main products, with selectivities above 20 % as linear butene conversions approached 0 % over both H-SAPO-5 and H-SSZ-24 (Figures 6.4 and 6.13). This suggested that the iso-butene, propene and C_5s were the primary products formed from linear butenes. The C_5s/propene selectivities were observed to be about 1.4 at 0 % conversions which is roughly equivalent to the molar amount of C_3 and C_5 an indication that propene and C_5s were formed from a common C_8 intermediate. Generally, an approximately second order of reaction was observed for propene and C_5s formation while that of iso-butenes was approximately first order. This indicated that iso-butene followed a pathway different from the pathway to propene and C_5s. Apparent activation energy values confirmed this by giving distinct values for the propene and C_5s as compared to that of the iso-butenes especially between 748 to 823 K (Figures 6.9 and 6.17). Iso-butene selectivity was favoured at low pressure and high temperature. Similar temperature and pressure effect has also been observed by several groups over medium pore molecular sieves [29, 42, 85].

The main aim of this part of the thesis is to examine the role of linear butenes in ethene alkylation. In this discussion, the first section will be based on the kinetics and mechanism over H-SAPO-5. The next will be based on the influence of acid strength on the mechanism based on comparisons of the kinetics over H-SSZ-24 and that of H-SAPO-5.

6.2.1 Linear butene reaction over H-SAPO-5

So far, three mechanisms have been discussed in literature as the possible route from linear butene skeletal isomerisation to iso-butene, which are; bimolecular[38, 39], pseudo-monomolecular[40, 41] and monomolecular[42, 43] pathways. All these mechanisms agree that propene and pentene are formed via dimerization and cracking of linear butene. It is important to note that most of these observations were made over medium pore size molecular sieves (10 membered rings), different from the large pore (12 membered ring) used in this work.

Our observations showed that propene and C_5s formation depended on cis-2-butene approximately second order and first order with respect to iso-butene formation over H-SAPO-5 at 748 and 823 K. Per this observation, the bimolecular pathway formation of propene and pentene agrees with literature suggestions. However, in terms of the iso-butene formation, the first order dependence on cis-2-butene at 748 and 823 K, implied that their formation are not likely to be a bimolecular reaction over H-SAPO-5. This is so because if dimerization and cracking to form propene and pentene were second order then dimerization, isomerisation and cracking to form iso-butene must also be a second order reaction. It is therefore suggested that linear butene isomerisation to iso-butene over H-SAPO-5 is unlikely to be a bimolecular reaction.

Our observations also showed that the H-SAPO-5 deactivated over time on stream which was accompanied by n-butane formation especially at low temperatures. Generally, the deactivation did not show significant positive influence on iso-butene formation (Figure 6.1-6.3). At 673 K, iso-butene quickly disappeared with time on stream (Figure 6.1). Coke analysis of the deactivated catalysts indicated that there was no soluble coke formed within the H-SAPO-5, however the rapid hydrogenation of linear butene to form n-butane indicated that the coke formed would be aromatic in nature. A spectroscopic data by Andy et al[41] had shown that linear butene over H-FER during deactivation (within 30-1200 min TOS) was associated with aromatics formation. In view of this, it is suggested that heavy aromatics might have been formed in H-SAPO-5 which did not directly catalyse iso-butene formation contrary to the pseudo-monomolecular pathway. Domokos et. al.[29] also suggested that aromatics do not positively influence iso-butene formation over H-FER, but rather pore size restricts oligomerization as the catalyst pores are blocked with coke.

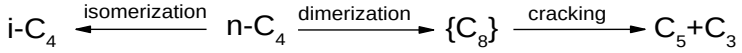

Scheme 6.1

In view of this, we will focus on the monomolecular formation of iso-butene as the plausible pathway over H-SAPO-5. Scheme 6.1 shows a simplified version of the two competing pathways for linear butene reactions; isomerization leading to iso-butene formation or dimerization-cracking leading to propene and pentene. As stated earlier, the observed approximately equi-molar amount of C_5s and propene at decreasing conversions coupled with similar trends at contact time, pressure and temperature conditions strongly suggested that they (propene and pentenes) were formed from cracking of a common octene (C_8) intermediate. Villegas et al[48] reported octene selectivity up to

30 % over H-Beta zeolites at 473 K and 20 MPa. Though no C_8 was observed in our case, probably due to rapid cracking at the chosen reaction conditions, we can speculate that the propene and pentenes were formed from an octene intermediate. Mass balance of 1.0±0.1 (mostly <10 % conversion) for the reaction at 673, 748 and 823 K indicated that almost all products were accounted for within 2 to 600 min time on stream (shown in Appendix H).

Based on our data, reaction sequence can be predicted for linear butene reaction. For simplicity, we will focus on the primary (or initial) products. First of all, linear butenes (n-C_4) adsorbs on a Brønsted acid site (HB) as shown in Equation 6.1. In our FT-IR measurements (Figure 4.9), it was observed that CO adsorbed at only Brønsted acid sites and no defects were observed in the H-SAPO-5. However, during testing (Figures 6.1-6.3, 6.6-6.9) it was observed that iso-butene formation was always favoured at increasing temperature compared to C_5s and propene. The reverse occurred at decreasing temperature in favour of C_5s and propene selectivity. This opposite trend in selectivity indicated a possible second site other than just the Brønsted acid site which aids in the dimerization process such that site discrimination occurs at varying temperatures. This second site probably adsorbs weakly and is less favoured as temperature increases. It has also been reported that pure $AlPO_4$-5 show some activity to n-butane[22] and cumene (at 723 K and 100 kPa)[63] cracking even though at a very low activity compared to H-SAPO-5. It is therefore suspected that there could be a second site close to the Brønsted acid sites where some cis-2-butene weakly adsorbs which is more sensitive to temperature. The nature of this site is not known, however we shall refer to it as a 'Lewis acid site' (L) even though no defects were observed in the CO adsorption experiment of the H-SAPO-5 sample. Equation 6.2 illustrates cis-2-butene adsorbing on an L site, nearby HB.

$$n - C_4 + HB = n - C_4HB \qquad 6.1$$

$$n - C_4 + L = n - C_4L \qquad 6.2$$

The linear butene adsorbed on the Brønsted acid sites either isomerizes to iso-butene as illustrated by Equation 6.3 or dimerizes with the adsorbate at the 'Lewis site' to C_8 (octene isomers) also illustrated by Equation 6.4. Wichterlovâ et al[86] reported that Brønsted sites promote isomerization while the combination of Brønsted and Lewis acid sites promote dimerization and cracking of linear butenes over H-FER at 620 K. This was demonstrated when zeolite which had been dehydroxylated

by different temperature calcination created Lewis acid sites, showed an improved propene and C_5s yield but a lowered iso-butene yield.

$$n - C_4HB \rightarrow i - C_4HB \quad 6.3$$

$$n - C_4HB + n - C_4L \rightarrow C_8HB + L \quad 6.4$$

We can consider that no further alkylation occurs after the initial reactions (Equations 6.1-6.4). The next step is desorption of iso-butene shown in Equation 6.5 and the C_8 cracking on desorption into propene and pentene shown in Equation 6.6 to give their products.

$$iC_4B = i{-}C_4 + HB \quad 6.5$$

$$C_8HB = C_3 + C_5 + HB \quad 6.6$$

If we assume that all the adsorption and desorption steps are in fast equilibrium, that is Equations 6.1, 6.2, 6.5 and 6.6, then coverage, θ can be written using Langmuir adsorption isotherm as follows;

$$\theta_{n-C_4HB} = \frac{K_1 P_{n-C_4}}{1 + K_1 P_{n-C_4} + K_{-5} P_{i-C_4} + K_{-6} P_{C_8}} \quad 6.7$$

$$\theta_{i-C_4HB} = \frac{K_{-4} P_{i-C_4}}{1 + K_1 P_{n-C_4} + K_{-5} P_{i-C_4} + K_{-6} P_{C_8}} \quad 6.8$$

$$\theta_{C_8HB} = \frac{K_{-6} P_{C_8}}{1 + K_1 P_{n-C_4} + K_{-5} P_{i-C_4} + K_{-6} P_{C_8}} \quad 6.9$$

$$\theta_{HB} = \frac{1}{1 + K_1 P_{n-C_4} + K_{-5} P_{i-C_4} + K_{-6} P_{C_8}} \quad 6.10$$

$$\theta_{n-C_4L} = \frac{K_2 P_{n-C_4}}{1 + K_2 P_{n-C_4}} \quad 6.11$$

$$\theta_L = \frac{1}{1 + K_2 P_{n-C_4}} \quad 6.12$$

where, P is partial pressure, K is adsorption and K_ is desorption equilibrium constants respectively. Also, the θ_{HB} and θ_L represent free Brønsted and 'Lewis' adsorption sites respectively. For simplicity, the C_3 and C_5s are put together as C_8. Note that the equilibrium/rate constants are written such that Equations 6.1- 6.6 corresponds to 1-6 subscripts respectively.

We can therefore derive rate expressions for the formation of iso-butene if we consider the isomerization as the slowest step and for C_8 if the dimerization is the slowest step. These rates are given below, where k represents the rate constant.

$$\frac{d(i-C_4)}{dt} = k_3\theta_{n-C_4HB} = k_3K_1P_{n-C_4}\theta_{HB} \quad 6.13$$

$$\frac{d(C_8)}{dt} = k_4\theta_{n-C_4HB}\theta_{n-C_4L} = k_4K_1K_2P_{n-C_4}{}^2\theta_{HB}\theta_L \quad 6.14$$

These rate expressions fit well with our observations on the dependence on cis-2-butenes over the H-SAPO-5; first order for the iso-butene and second order for the C_8s. If this rate expression is true, then the rate of formation of the C_8s divided by the rate of formation iso-butene should increase with cis-2-butene partial pressure given as;

$$\frac{rate\ of\ C_8\ formation}{rate\ of\ i-C_4\ formation} = \frac{k_5K_1K_2P_{n-C_4}{}^2\theta_{HB}\theta_L}{k_3K_1P_{n-C_4}\theta_{HB}} = \frac{k_5K_2P_{n-C_4}\theta_L}{k_3} \quad 6.15$$

Figure 6.18 shows the graph when the rate of C_8 (=C_3 +C_5s) formation is divided by the rate of iso-butene formation versus cis-2-butene partial pressure at 748 and 823 K over H-SAPO-5. The C_8/i-C_4 rate ratios roughly increased linearly with cis-2-butene partial pressure, except that it was more enhanced at 748 K. This is not surprising since the adsorption equilibrium constants are usually high at lower temperatures due to less contribution of loss of entropy[87] (more about this later). It is therefore reasonable that the ratio was enhanced at 748 than 823 K. The observations in Figures 6.6-6.9 which showed that iso-butene was favoured at high temperature and low partial pressure correlates very well with the rate expression for C_8/i-C_4. Increasing cis-2-butene partial pressure favours dimerization and disfavours isomerization and vice versa. Increasing reaction temperature limits adsorption and therefore dimerization is disfavoured and iso-butene formation is relatively increased.

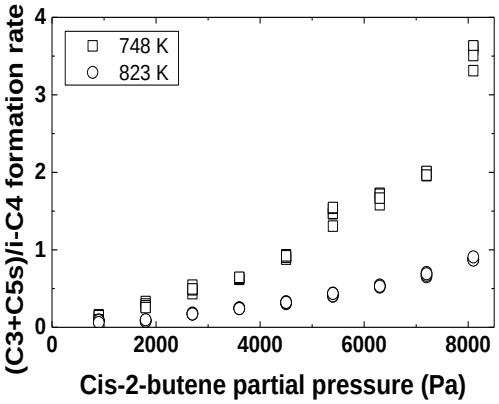

Figure 6.18: C_8s/i-C_4 formation rates versus cis-2-butene partial pressure: H-SAPO-5 mass= 50 mg, WHSV= 0.23-1.17 h^{-1}

Furthermore, the rate of formation expressions can be differentiated to give a relationship between the apparent activation energy (Eapp), the intrinsic activation energy (Ea), the coverage (θ) and the adsorption enthalpies (ΔH) if we assume that the pre-exponential factor and entropy are not strictly dependent on temperature[12]. From Equation 6.13, the relation can be derived for iso-butene formation as follows;

$$Eapp\ (iC_4) = \frac{RT^2 dln(iC_4)}{dT} = RT^2\left\{\frac{Ea_3}{RT^2} + \frac{\Delta H_1}{RT^2} - \frac{\Delta H_1 \theta_{n-C_4HB}}{RT^2} - \frac{\Delta H_{-5}\theta_{i-C_4HB}}{RT^2} - \frac{\Delta H_{-6}\theta_{C_8HB}}{RT^2}\right\}$$

$$Eapp(iC_4) = Ea_3 + \left(1 - \theta_{n-C_4HB}\right)\Delta H_1 + \Delta H_5\theta_{i-C_4HB} + \Delta H_6\theta_{C_8HB} \qquad 6.16$$

Note that when the desorption enthalpies, -ΔH_ are reversed they become adsorption enthalpies, +ΔH. Likewise a relationship for the C_8 formation Eapp can be derived from Equation 6.14 as;

$$Eapp(C_8) = \frac{RT^2 dln(C_8)}{dT} = RT^2\left\{\frac{Ea_4}{RT^2} + \frac{\Delta H_1}{RT^2} + \frac{\Delta H_2}{RT^2} - \frac{\Delta H_1 \theta_{n-C_4HB}}{RT^2} - \frac{\Delta H_{-5}\theta_{i-C_4HB}}{RT^2} - \frac{\Delta H_{-6}\theta_{C_8HB}}{RT^2} - \frac{\Delta H_2\theta_{n-C_4L}}{RT^2}\right\}$$

$$Eapp(C_8) = Ea_4 + \left(1 - \theta_{n-C_4HB}\right)\Delta H_1 + (1 - \theta_{n-C_4L})\Delta H_2 + \Delta H_5\theta_{i-C_4HB} + \Delta H_6\theta_{C_8HB} \qquad 6.17$$

These expressions can be used to predict the apparent activation energies at high coverage and low coverage based on temperature. De Moor et al[87] reported that increasing temperature reduces the adsorption equilibrium over zeolites due to the contribution of entropy (ΔS) which is enhanced at high temperature. This has been shown in Figure 6.19. Longer chain hydrocarbons adsorb stronger at lower temperatures due to higher dispersion forces (related to enthalpy ΔH) though some entropy is lost. However at high temperature, the effect of the lost ΔS on Gibbs free energy (ΔG = ΔH-TΔS) is enhanced which leads to low adsorption equilibrium constant and therefore lowers adsorption.

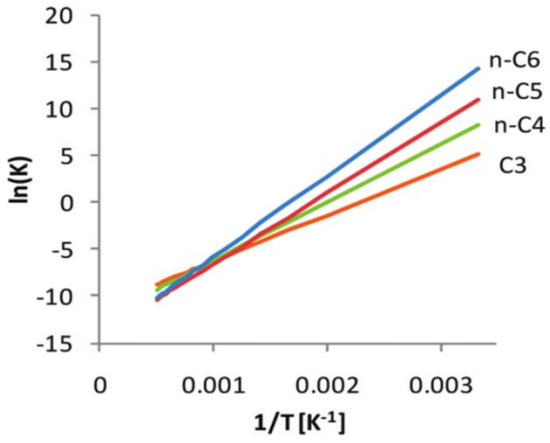

Figure 6.19: van't Hoff plot showing iso-equilibrium points for adsorption from Figure 1 of [87]

We can therefore predict the influence of coverage on the Eapp based on Equations 6.16 and 6.17. The $\Delta H_5\theta_{i-C_4HB} + \Delta H_6\theta_{C_8HB}$ component poses negative influence while $(1-\theta_{n-C_4HB})\Delta H_1$ component poses positive influence on the measured activation energy since adsorption is exothermic. At low temperature, the Eapp(i-C_4) for iso-butene will be Ea_3 (intrinsic activation energy for isomerization) decreased by $\Delta H_5\theta_{i-C_4HB} + \Delta H_6\theta_{C_8HB}$ and increased by $(1-\theta_{n-C_4HB})\Delta H_1$ since there is relatively high coverage. It is expected that overall, low temperature should result in low Eapp(i-C_4). At high temperature, coverage will be relatively low, and the influence of the adsorption enthalpies is also low which implies that the Eapp(i-C_4) should be relatively high. When we consider similar analysis for the C_8 expression, since the $\Delta H_5\theta_{i-C_4HB} + \Delta H_6\theta_{C_8HB}$ poses negative influence and the $(1-\theta_{n-C_4HB})\Delta H_1 + (1-\theta_{n-C_4L})\Delta H_2$ poses positive influence, it is not so clear to assign the general trend by considering only the Equation 6.17 since each opposing sign has two coverage components and therefore could roughly cancel out each other. However, if we compare the two apparent activation energy expressions, Equations 6.16 and 6.17, the differences are Ea_3 for iso-butene and $Ea_4 + (1-\theta_{n-C_4L})\Delta H_2$ for C_8. In that case, as far as coverage is concerned, C_8 formation Eapp is expected to increase at high coverage which is lower at temperature, and decrease at higher temperature when there in low coverage. Hence the effect of temperature on the magnitude of Eapp for the formation of the C_8 is expected to be in opposite order compared with that of iso-butene.

Table 6.1: Summary of apparent activation energies over H-SAPO-5 in kJ/mol

Temperature range/K	Iso-butene	Propene	C_5s
673-723	42±8	32±6	24±5
748-823	83±3	-17±3	-11±5

Table 6.1 shows a summary of the apparent activation energies for the formation of iso-butene, propene and C_5s over H-SAPO-5. This is in agreement with the analysis done above. The Eapp for iso-butene was 83 kJ/mol at high temperature and 42 kJ/mol at the lower temperature regions. Propene and C_5s Eapp were -17 and -11 kJ/mol in high and 32 and 24 kJ/mol in low temperature regions. These differences in the apparent activation energies at different temperatures were estimated because the rate of formation of the iso-butene and propene plus C_5s diverged with temperature. These divergences in rate were also observed by different authors over H-ZSM5[85] and H-FER[29] between 523 and 773 K. The deviation of the propene and C_5s trend with temperature can be due to the effect of entropy on the formation of octene at high temperatures. The Eapp over H-SAPO-5 of iso-

butene was generally higher than that of C_5s and propene. This suggests that the intrinsic activation energy of iso-butene may be higher than that required for dimerization and cracking. This is reasonable if we consider that iso-butene is formed from methyl-cyclopropyl carbocation as was predicted using ^{13}C NMR measurement[45]. Cyclopropyl is highly strained[33] which will require high energy to form than linear butene dimerization.

6.2.2 Influence of acid strength on linear butene reactions (H-SAPO-5 and H-SSZ-24 compared)

H-SSZ-24 was observed to possess stronger Brønsted acidity with about one-half more acid site density compared to H-SAPO-5 (Section 4.3). The activity of H-SSZ-24 was observed to be much higher than the acid sites density difference compared to that over H-SAPO-5 (Section 6.2.2). The previous discussion was based on the kinetics and mechanism of linear butene over H-SAPO-5. It was proposed that over H-SAPO-5, iso-butene is formed from linear butene isomerization while the propene and pentene (C_5s) were from dimerization and cracking of linear butenes. In this Section a comparison is made to elucidate the influence of acid strength on the proposed mechanism.

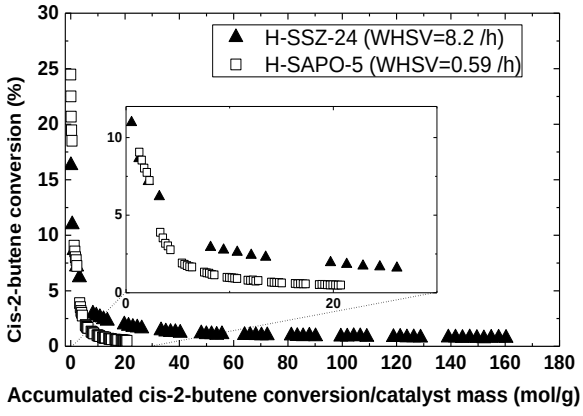

Figure 6.20: Cis-2-butene conversion versus accumulated ethene over 650 min TOS: $P_{Cis\text{-}2\text{-}butene}$= 4.5 kPa, T= 748 K.

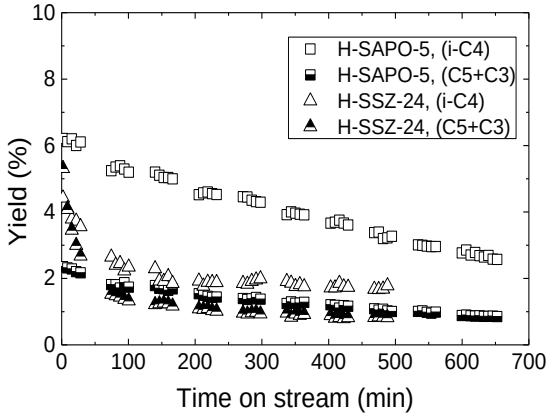

Figure 6.21: Yield versus TOS: $P_{Cis\text{-}2\text{-}butene}$= 4.5 kPa, T= 823 K

To compare the activity and deactivation of the two catalysts, the cis-2-butene selectivity versus accumulated conversions per catalyst mass over TOS has been plotted and shown in Figure 6.20. Below 5 % conversions, both catalysts deactivate at similar trends. The WHSV for the two catalysts

to make equivalent cis-2-butene conversions at 748 K, suggest that H-SSZ-24 is about 14 times more active than H-SAPO-5. Considering their acid densities to be about $\frac{H-SSZ-24}{H-SAPO-5} = 1.5$, it can be inferred that the acid strength of H-SSZ-24 increased the activity by at least 9 times than that of H-SAPO-5.

It was also observed that over H-SSZ-24 at 748 and 823 K, iso-butene selectivity initially increased as the catalyst deactivated and then leveled off with TOS (Figures 6.11 and 6.12). Upon initial observation, it appeared that deactivation favoured iso-butene formation over H-SSZ-24 contrary to the observations over H-SAPO-5. Hence the yield of iso-butene and C_5s plus propene versus time on stream, at 823 K over H-SAPO-5 and H-SSZ-24 is plotted and shown in Figure 6.21. At initial TOS the yield of the C_5s plus propene decreased a little more than that of iso-butene. It must be noted that at the same TOS over H-SSZ-24, propene selectivity was slightly higher than C_5s with some minor ethene observed which quickly declined when C_5s became more than propene (Figure 6.12). This suggested that oligomerization and cracking occur faster on fresh catalyst. After 29 min, deactivation affected both isomerization and dimerization-cracking in a similar pattern especially where the yield of C_5s plus propene should even decrease, if deactivation really disfavoured their formation relative to iso-butene formation or if a substantial change in mechanism occurred. Hence we can conclude that the heavy (aromatic) coke formed in H-SAPO-5 and H-SSZ-24 as a result of deactivation does not play catalytic role in linear butene isomerization within our working conditions. Rather, on fresh catalysts, both dimerization-cracking and isomerization pathways compete closely. However as the catalyst deactivates, less sites may be available for dimerization-cracking and isomerization is advantaged.

To compare the competition between isomerization and dimerization-cracking over H-SAPO-5 and H-SSZ-24, the ratio of C_5s plus propene over iso-butene versus cis-2-butene conversion have been plotted and shown in Figure 6.22 based on the contact time variation experiments. Since the contact time variation over H-SSZ-24 did not show a clear trend (Section 6.1.2.2), only the standard contact time is used together with all the data for H-SAPO-5. Generally, the dimerization-cracking step was higher over H-SSZ-24, about one-half more than over H-SAPO-5 especially at increasing conversions. Over H-SAPO-5, the dimerization-cracking to isomerization ratio was around 1 until below 2 % conversion where it appeared to increase. H-SSZ-24 on the other hand showed a ratio of about 1.5 to 2 in favour of dimerization-cracking over isomerization pathway.

Clearly H-SSZ-24 favoured dimerization-cracking over isomerization compared to H-SAPO-5. The trend as conversion approached 0 % is widely scattered particularly over H-SSZ-24 such that either both mechanisms are influenced roughly at the same extent over both catalysts or due to increase in the uncertainty of the measurement at low conversions. The estimated $\frac{C_5s+C_3}{i-C_4} = 1.5$ over H-SSZ-24 and $\frac{C_5s+C_3}{i-C_4} = 1$ over H-SAPO-5 correlates well with the acid site densities of the two catalysts. This indicates that the slight difference in the two pathways observed over the catalysts can be attributed to their number of acid sites rather than their acid strength.

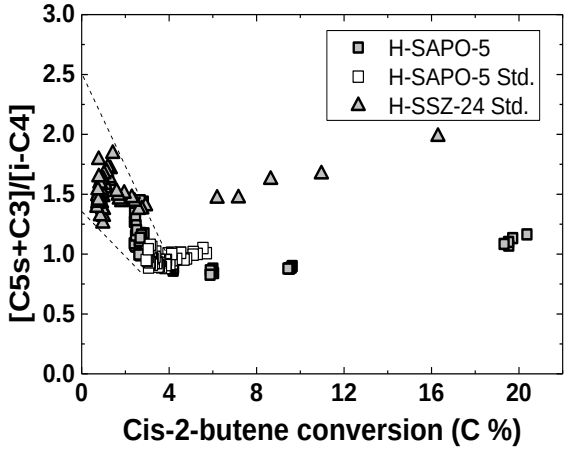

Figure 6.22: (C5s+C3)/i-C4 versus cis-2-butene conversion: $P_{Cis\text{-}2\text{-}butene}$ = 4.5 kPa, T= 748 K

Despite the difference in the relative amount of the pathways discussed above over the two catalysts, their ratios followed similar trend with conversions. Could this similar trend imply that the reactions were operating under thermodynamics control such that the products distribution is similar over both catalysts? To analyze this, our observations can be compared with the thermodynamics of the inter-conversion of iso-butene to propene and pentene. If we consider a reaction such as in Equations 6.18, then a quotient, Q can be calculated as illustrated in Equation 6.19 based on the concentration of the propene, C_5s and iso-butene formed during the temperature variation experiments. The thermodynamic equilibrium constant, K can be calculated as shown in Equation 6.20 from Gibbs free energy (ΔG) values using standard reference values[81].

$$i - C_4 = C_3 + C_5 \qquad 6.18$$

$$Q = \frac{[C_3][C_5]}{[i - C_4]} \qquad 6.19$$

$$Keq = e^{-(\Delta G_{C3} + \Delta G_{C4} - \Delta G_{i-C4})/RT} \qquad 6.20$$

Figure 6.23 shows a plot of K and Q versus temperature. The thermodynamics calculation favours dimerization-cracking pathway as temperature increases. However, the reaction quotient showed the reverse of thermodynamics trend. This indicates that kinetics rather than thermodynamics controlled the reaction over both catalysts. Moreover, the Q for the reaction over both H-SAPO-5 and H-SSZ-

24 showed the same trend as well as about the same magnitude, which confirms that the reaction is the same over both catalysts.

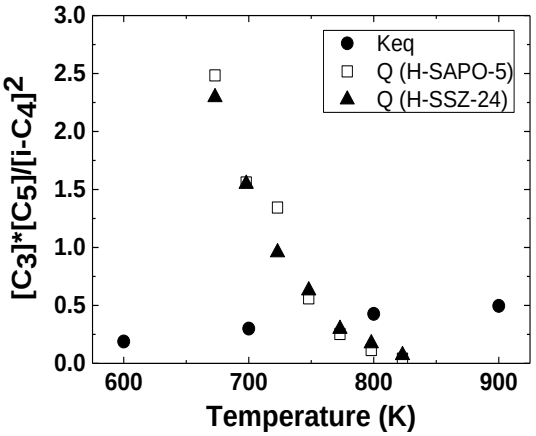

Figure 6.23 : Q, and K versus temperature

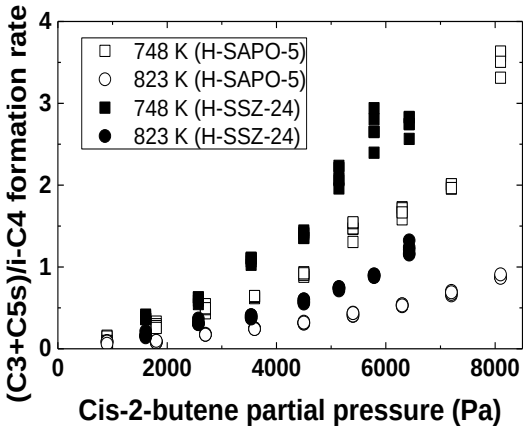

Figure 6.24: C8s/i-C4 formation rates versus cis-2-butene partial pressure

The cis-2-butene partial pressure variation experiment showed that the trends in rate of formation of products as well as the order of reactions of the main products over H-SSZ-24 (Section 6.1.2.3) were similar to that over H-SAPO-5. Figure 6.24 shows the fraction of the rates of formation for C_5s plus propene over iso-butene versus cis-2-butene partial pressure over H-SSZ-24 and H-SAPO-5. Similar relatively linear dependence on the cis-2-butene was obtained over both H-SSZ-24 and H-SAPO-5. The trends when temperature was varied over both catalysts were also similar. This also indicates that the mechanism as suggested over H-SAPO-5 is the same over H-SSZ-24. The rate constant over both catalyst was calculated based on the pressure experiments at 748 K and is shown in Table 6.2. The rate constant was 11 times higher over H-SSZ-24 for the formation of propene and C_5s each and 7 times higher for iso-butene than over H-SAPO-5. These rate constant ratios over the two catalysts confirm the idea that H-SSZ-24 favours dimerization-reaction over isomerization by a ratio equivalent to their acid site density compared to H-SAPO-5. The overall rate constant was 9 times higher over H-SSZ-24 compared to that of H-SAPO-5. This was the same estimated ratio for their activity and was earlier attributed to the difference in the acid strength.

Over H-SAPO-5, the effect of temperature on the rate was mainly attributed to the differences in coverage that occurred at different temperature ranges which led to the differences in the apparent activation energy (Eapp). Table 6.3 shows a summary of the apparent activation energies for the

formation of iso-butene, propene and C_5s over H-SSZ-24 and H-SAPO-5. It is expected that the Eapp would follow similar pattern if the mechanism over both catalysts are the same. At high coverage, propene and C_5s' Eapp decreased while at low coverage the iso-butene Eapp decreased. The Eapp over both H-SSZ-24 and H-SAPO-5 therefore followed a similar pattern.

Table 6.2: Reaction rate constant at 748 K for the formation of main products over H-SAPO-5 and H-SSZ-24

	Unit	H-SAPO-5	H-SSZ-24	$\frac{k\ over\ H-SSZ-24}{k\ over\ H-SAPO-5}$
$k_{overall} = \frac{overall\ reaction\ rate}{P_{C_2}^{1.5}}$	μmol/(gsPa$^{1.5}$)	5.5 x10^{-3}	4.8 x10^{-2}	9
$k_{iC4} = \frac{rate\ of\ i-C_4 formation}{P_{n-C_4}}$	μmol/(gsPa)	1.9 x10^{-1}	1.3	7
$k_{C3} = \frac{rate\ of\ C_3 formation}{P_{n-C_4}^{2}}$	μmol/(gsPa^2)	1.5 x10^{-5}	1.8 x10^{-4}	11
$k_{C5s} = \frac{rate\ of\ C_5 s formation}{P_{n-C_4}^{2}}$	μmol/(gsPa^2)	2.1 x10^{-5}	2.3 x10^{-4}	11

Table 6.3: Summary of apparent activation energies over H-SAPO-5 and H-SSZ-24

Temperature Range/K	H-SAPO-5			H-SSZ-24		
	Iso-butene	Propene	C5s	Iso-butene	Propene	C5s
673-723	42±8	32±6	24±5	46±8	15±3	11±1
748-823	83±3	-17±3	-11±5	62±4	-8±2	-18±5

Generally the Eapp were relatively lower over H-SSZ-24 compared to those over H-SAPO-5. This difference could either be due to the difference in adsorption enthalpies or intrinsic activation energies over both catalysts. However, since both catalysts have different adsorption enthalpies due the differences in acid strength, it is likely that differences in the Eapp are as a result of the differences in adsorptions. Moreover, the differences between the Eapp for each product at the different temperature ranges were relatively lower over H-SSZ-24 than H-SAPO-5. Once again, this could be due to the differences in the ability of the two catalysts to adsorb. With the generally high activity of H-SSZ-24 observed, it can be inferred that it adsorbs better and therefore has lower discrimination of coverage at the different temperature regions compared with the H-SAPO-5.

6.3 SUMMARY

The kinetics of cis-2-butene activity over H-SAPO-5 studied showed that the primary products were iso-butene, pentenes and propene. A first order with respect to iso-butene and second order with respect to pentenes and propene formations were observed which suggested that two competing pathways were involved in the mechanism with linear butene; monomolecular isomerization to iso-butene or dimerization-cracking to pentene and propene. The formation of iso-butene was not favoured by coke formation especially at lower temperatures suggesting that aromatic formation do not play a major role in their formation. Kinetic rate expressions were deduced which corresponded well with our observations. High temperature and low cis-2-butene partial pressure favoured isomerization relative to the dimerization-cracking pathway. The apparent activation energies were distinct at two different temperature ranges; iso-butene = 83 kJ/mol, propene= - 17 kJ/mol, pentene= -11 kJ/mol between 748 and 823 K, and then iso-butene = 42 kJ/mol, propene= 32 kJ/mol, pentene= 24 kJ/mol between 673 and 723 K. These differences were mainly attributed to differences in coverage on adsorption enthalpies at different temperatures.

Repeat of these experiments over H-SSZ-24 showed that generally, the rate of cis-2-butene activity is about 9 times more than over H-SAPO-5 which was equal to the overall rate constant ratio between the two catalysts at 748 K. This was attributed to the difference in acid strength between the two catalysts. The product distribution at equivalent conversions was not significantly different over both catalysts when the kinetic parameters were varied. The apparent activation energy over H-SSZ-24 were; iso-butene = 62 kJ/mol, propene = - 8 kJ/mol, pentene = -18 kJ/mol between 748 and 823 K, and then iso-butene = 46 kJ/mol, propene = 15 kJ/mol, pentene = 11 kJ/mol between 673 and 723 K. These were generally lower than what was observed over H-SAPO-5 though the influences of coverage due to difference in temperature followed similar trends. This suggested that acid strength did not significantly discriminate between the isomerization and dimerization-cracking pathways. Therefore, the proposed reaction pathway for linear butene skeletal isomerization is the same over both H-SSZ-24 and H-SAPO-5.

7. ETHENE AND LINEAR BUTENE CO-REACTIONS

This chapter describes the kinetics of cis-2-butene and ethene co-reactions. This was to help ascertain the role of the two co-reactants in the mechanism. Observations over H-SAPO-5 are reported first, followed by those over H-SSZ-24. Discussions based on the observations over H-SAPO-5 will be made first followed by a comparison with the observations over H-SSZ-24 to elucidate the influence of acid strength on the mechanism.

7.1 Results

*7.1.1 Conversion of co-feed over H-SAPO-*5

7.1.1.1 Catalytic activity of co-feed versus time on stream

The activity of H-SAPO-5 was tested with co-reaction between ethene and cis-2-butene. Two main partial pressures were used; $\frac{P_{ethene}}{P_{cis-2-butene}}$ equal to about 2 and 5.

Ethene (10 kPa) and cis-2-butene (4.5 kPa)

Figure 7.1 shows the activity when 4.5 kPa cis-2-butene and 10 kPa ethene were co-fed over H-SAPO-5 versus time on stream (TOS) at 673 K. This was done with 50 mg catalyst 4.5 ml/min cis-2-butene and 10 ml/min ethene flow to give a WHSV of 3.9 h^{-1}. The conversion of the co-feed decreased from 2.5 % at 2 min to 0.1 % at 614 min. The decrease was more rapid between 2 min and 68 min, similar to what was observed at 673 K when only cis-2-butene was fed over H-SAPO-5. At 2 min TOS, the main products were iso-butene, propene and C_5s. Iso-butene selectivity decreased from 28 to about 1 % with TOS. The decrease in iso-butene selectivity was less rapid with the co-feed reaction than when cis-2-butene was fed alone over H-SAPO-5. C_5s varied slightly with TOS with selectivities between 40 and 30 %. Propene selectivities increased from 30 to 49 %

with TOS. The co-feed reaction showed slightly more propene selectivity than C_5s which was the opposite when cis-2-butene was fed alone. Selectivities to n-butane and iso-butane were also observed. Selectivity to n-butane increased from 2 to 11 % with TOS. Iso-butane was observed between 2 and 226 min with selectivities varying from 1 to 7 %.

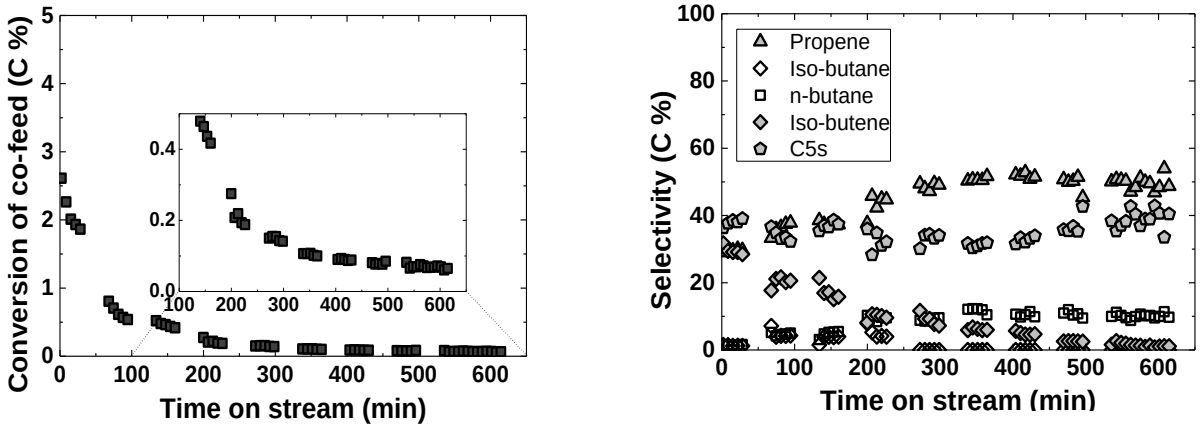

Figure 7.1: Catalytic activity of H-SAPO-5 versus time on stream, Conversion (left) and Selectivity (right): H-SAPO-5 mass = 50 mg, $P_{Cis\text{-}2\text{-}butene}$= 4.5 kPa, P_{Ethene}= 10 kPa, $Flow_{total}$= 100 ml/min, T = 673 K, WHSV = 3.9 h^{-1}

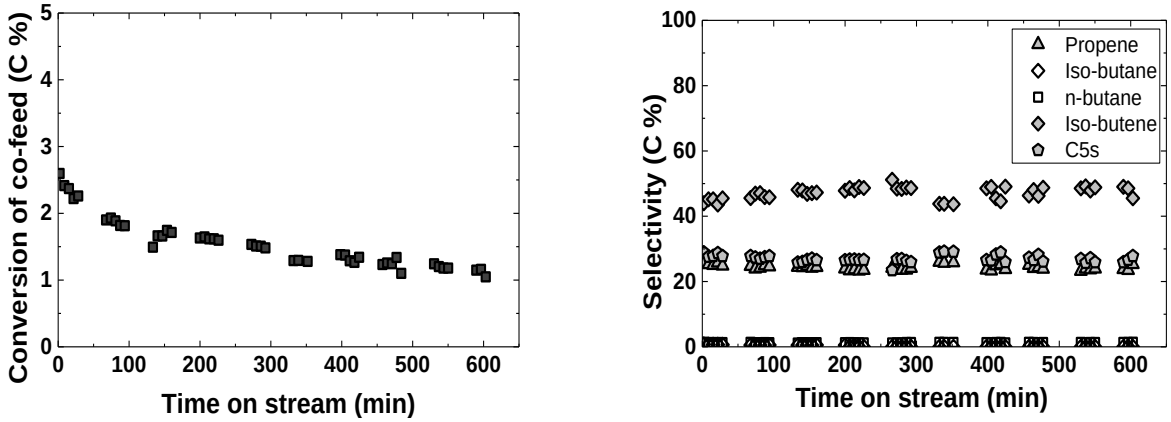

Figure 7.2: Catalytic activity of H-SAPO-5 versus time on stream, Conversion (left) and Selectivity (right): H-SAPO-5 mass = 50 mg, $P_{Cis\text{-}2\text{-}butene}$= 4.5 kPa, P_{Ethene}= 10 kPa, $Flow_{total}$= 100 ml/min, T = 748 K, WHSV = 3.9 h^{-1}

The next, was to test H-SAPO-5 activity under similar conditions at 748 K. Figure 7.2 shows the activity of co-feed versus TOS over H-SAPO-5 at 748 K. Conversion decreased from 2.6 to 1 % with TOS. The initial conversion at 748 K was about the same as was observed at 673 K, however the decline with TOS was less rapid at 748 K. Selectivities to the main products at 748 K also varied slightly for the 2 to 603 min TOS studied. The selectivities varied from 43 to 50 % for iso-butene, 26 to 29 % for C_5s and 24 to 26 % for propene with TOS. Some iso-butane and n-butane were observed which remained around 1 % each with TOS.

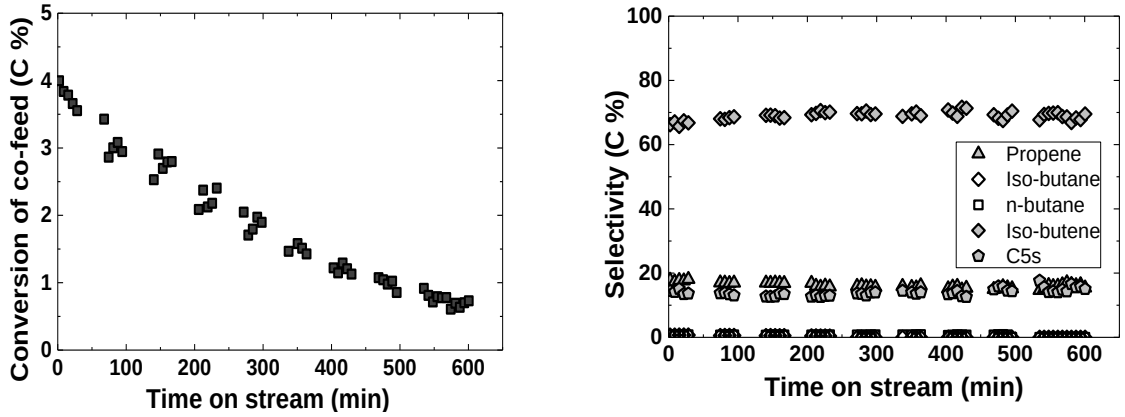

Figure 7.3: Catalytic activity of H-SAPO-5 versus time on stream, Conversion (left) and Selectivity (right): H-SAPO-5 mass = 50 mg, $P_{Cis\text{-}2\text{-}butene}$= 4.5 kPa, P_{Ethene}= 10 kPa, $Flow_{total}$= 100 ml/min, T = 823 K, WHSV = 3.9 h^{-1}

Thirdly, the catalytic activity was tested at 823 K under similar conditions as was done at 673 K and 748 K. Figure 7.3 shows the activity of co-feed versus TOS over H-SAPO-5 at 823 K. The conversion decreased from 4 to 1 % within 2 to 601 min TOS. At 823 K, the initial conversion was twice the conversion at 748 K, however deactivation was slightly rapid compared to the conversion curve at 748 K but not as rapid as was observed at 673 K. Selectivities to the main products were relatively stable over the TOS studies. The selectivities stayed around 67, 15 and 16 % for iso-butene, C_5s and propene respectively. These selectivities differ from the observation made at 748 K by a higher iso-butene and a lower C_5s and propene selectivities. Minor selectivities of about 2 % to iso-butane and n-butane were observed.

Ethene (20 kPa) and cis-2-butene (3.6 kPa)

Figure 7.4 shows the activity when 3.6 kPa cis-2-butene and 20 kPa ethene were co-reacted over H-SAPO-5 versus time on stream (TOS) at 673 K. This was done with 50 mg catalyst 0.9 ml/min cis-2-butene and 5 ml/min ethene flow to give a WHSV of 1.6 h^{-1}. The conversion decreased from 4.6 to 0.2 % between 2 min and 563 min TOS. This decrease was less rapid compared to the co-reaction between 4.5 kPa cis-2-butene and 10 kPa ethene partial pressures at 673 K.

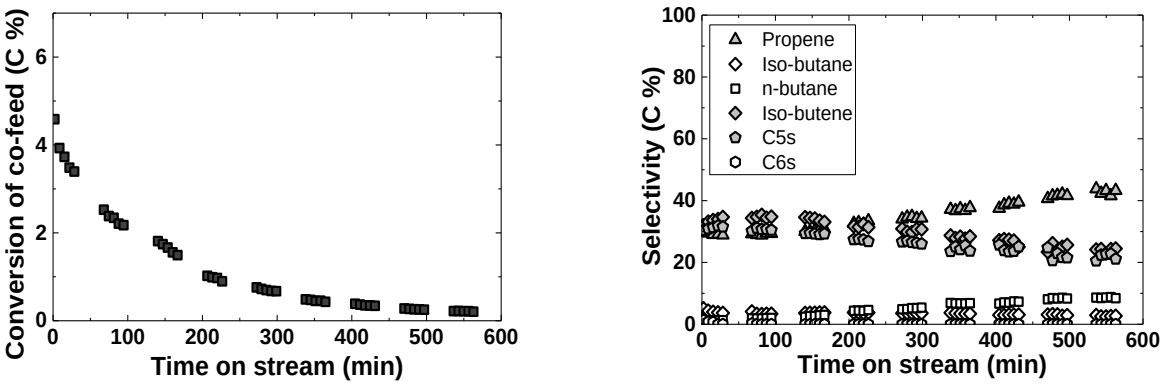

Figure 7.4: Catalytic activity of H-SAPO-5 versus time on stream, Conversion (left) and Selectivity (right): H-SAPO-5 mass = 50 mg, $P_{Cis\text{-}2\text{-}butene}$= 3.6 kPa, P_{Ethene}= 20 kPa, $Flow_{total}$= 25 ml/min, T = 673 K, WHSV = 1.6 h^{-1}

The main products were iso-butene, propene and C_5s throughout the TOS studied. Iso-butene and C_5s selectivity increased slightly from 32 to 34 % and 30 to 31 % at initial TOS but decreased to 24 and 21 % at 563 min respectively. Propene selectivity on the other hand increased from 30 to 43 % within 2 to 563 min TOS. The trends in iso-butene and C_5s selectivities were rather similar and differed from that of propene with TOS. This observation was different from the co reaction when 4.5 kPa cis-2-butene and 10 kPa ethene partial pressures were fed at 673 K where iso-butene selectivity rapidly declined opposite to the C_5s and propene with TOS. Also, the C_5s trends were opposite to that of the propene trend. This indicates that the influence of ethene is larger at the $\frac{P_{ethene}}{P_{cis-2-butene}} = \frac{20}{3.9}$ than at the $\frac{P_{ethene}}{P_{cis-2-butene}} = \frac{10}{4.5}$ which leads to an increase in propene formation relative to C_5s and iso-butene formations at 673 K. It is also important to note that, with the observed less rapid deactivation here, iso-butene selectivity was 24 % even at 0.2 % conversion at 563 min. This differed from when there was a rapid deactivation in the $\frac{P_{ethene}}{P_{cis-2-butene}} = \frac{10}{4.5}$ reactions with about 10 % iso-butene selectivity at 206 min TOS with 0.2 % conversion (Figure 6.1). This indicates that the more cis-2-butene concentration, the faster the deactivation. Selectivities to n-butane and iso-butane were also observed. Selectivity to n-butane increased from 1 to 8 % while that to iso-butane decreased from 5 to 3 % with TOS.

Figure 7.5 shows the activity of co-reaction between 3.6 kPa cis-2-butene and 20 kPa ethene over H-SAPO-5 versus TOS at 748 K. Conversion decreased from about 5 to 2 % with TOS. The initial conversion at 748 K was about the same as was observed at 673 K, however the decrease with TOS

was less rapid at 748 K. The selectivity to iso-butene increased gradually from 42 to 57 %. Selectivities to C_5s decreased gradually from 21 to 17 % and 34 to 24 % for propene with TOS. Some minor amount of iso-butane and n-butane were observed with total selectivities around 3 to 2 % with TOS. The selectivity to propene was more than C_5s selectivity for all TOS studied. The iso-butene selectivity increased throughout all TOS which was contrary to the observations at 673 K. Selectivity to the minor products was much less at 748 K than at 673 K.

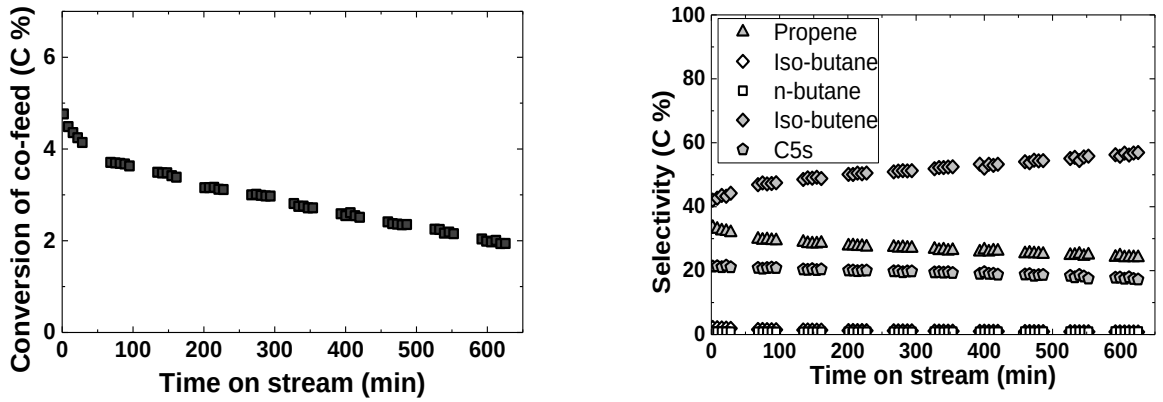

Figure 7.5: Catalytic activity of H-SAPO-5 versus time on stream, Conversion (left) and Selectivity (right): H-SAPO-5 mass = 50 mg, $P_{Cis\text{-}2\text{-}butene}$= 3.6 kPa, P_{Ethene}= 20 kPa, $Flow_{total}$= 25 ml/min, T = 748 K, WHSV = 1.6 h^{-1}

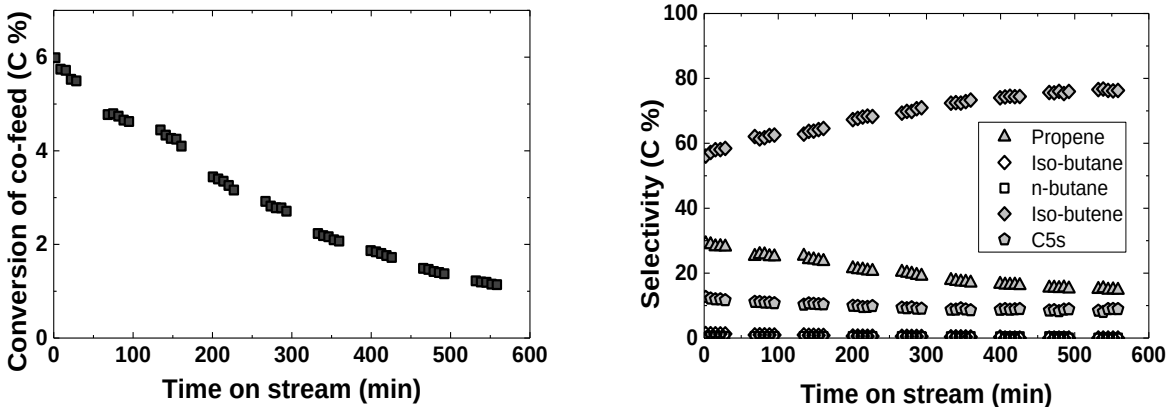

Figure 7.6: Catalytic activity of H-SAPO-5 versus time on stream, Conversion (left) and Selectivity (right): H-SAPO-5 mass = 50 mg, $P_{Cis\text{-}2\text{-}butene}$= 3.6 kPa, P_{Ethene}= 20 kPa, $Flow_{total}$= 25 ml/min, T = 823 K, WHSV = 1.6 h^{-1}

The next, was to test H-SAPO-5 activity under similar conditions at 823 K. Figure 7.6 shows the activity of co-feed reaction versus TOS over H-SAPO-5 at 823 K. The conversion decreased from 6 to 1 % within 2 to 558 min TOS. The decrease was less rapid at 748 K than at 823 K. The trend of selectivities with TOS at both temperature were however similar. The selectivity to iso-butene

increased gradually from 56 to 76 %. Selectivities to C_5s and propene decreased gradually from 13 to 9 % and 29 to 15 % respectively with TOS. Iso-butane and n-butane total selectivities were up to 2 % with TOS. The main difference at the two temperatures was the relative selectivities: iso-butene was higher and C_5s and propene were lower at the higher temperature.

7.1.1.2 Contact time variation at 748 K

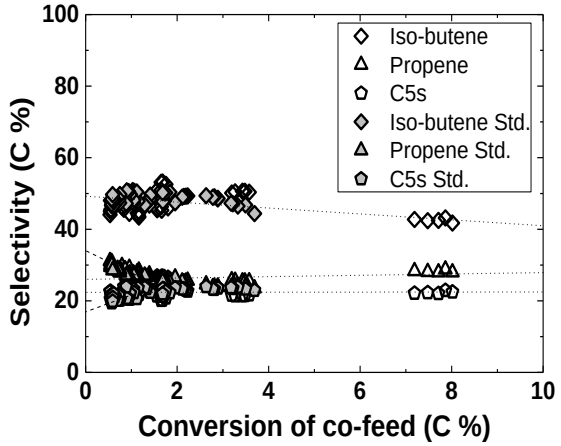

Figure 7.7: Selectivity versus Co-feed conversion at different contact times over H-SAPO-5:

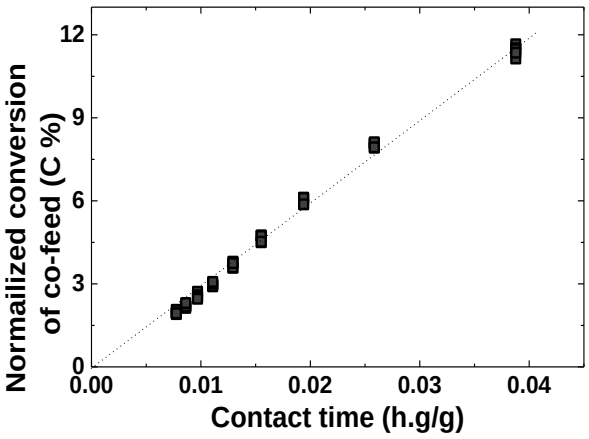

Figure 7.8: Normalized conversion versus contact time:

H-SAPO-5 mass = 50 mg, $P_{Cis\text{-}2\text{-}butene}$= 4.5 kPa, P_{Ethene}= 10 kPa, $Flow_{total}$= 20-100 ml/min, T = 748 K, WHSV = 0.8-3.9 h^{-1}. The Std. represents standard conditions measured in-between contact time variations.

The influence of contact time on the co-feed reaction over H-SAPO-5 at 748 K was studied. This was done at 4.5 kPa cis-2-butene and 10 kPa ethene partial pressures, nearly 1:2 ratios within 0.9 to 3.9 h^{-1} WHSVs. The total flows were varied at constant ratio of cis-2-butene: ethene: inert gases over 50 mg catalyst. Figure 7.7 shows the selectivity versus co-feed conversion over H-SAPO-5. Generally, the selectivity of iso-butene stayed around 49 % and varied very slightly with conversions even at varied contact times. Propene and C_5s selectivities stayed around 29 and 22 % respectively between 1 to 8 % conversions. As conversions approached 0 %, the propene selectivity approached 34 % while that of C_5s approached 17 %. This indicated that propene selectivity relative to iso-butene and C_5s increased as compared to when cis-2-butene was fed alone over H-SAPO-5 (Figure 6.4). Figure 7.8 shows the normalized conversion of co-feed versus contact time. The

conversion increased linearly with contact time similar to what was observed when cis-2-butene was feed alone (Figure 6.5).

7.1.1.3 Effect of cis-2-butene partial pressure on co-feed reaction activity

The effect of cis-2-butene partial pressure on the co-feed reaction over H-SAPO-5 was studied between 0.9 and 8.1 kPa cis-2-butene partial pressures, while ethene partial pressure was kept constant at 10 kPa. This was done by keeping ethene flow constant at 10 ml/min and varying cis-2-butene flow within 0.9 to 8.1 ml/min over 50 mg catalyst such that the WHSV ranged from 2.9 to 4.9 h^{-1}. The total gas flow rate was held constant at 100 ml/min to maintain constant contact time. Under these conditions, three different experiments were done at 673, 748, and 823 K temperatures. The original conversions obtained and used for rate calculations were below 5 %.

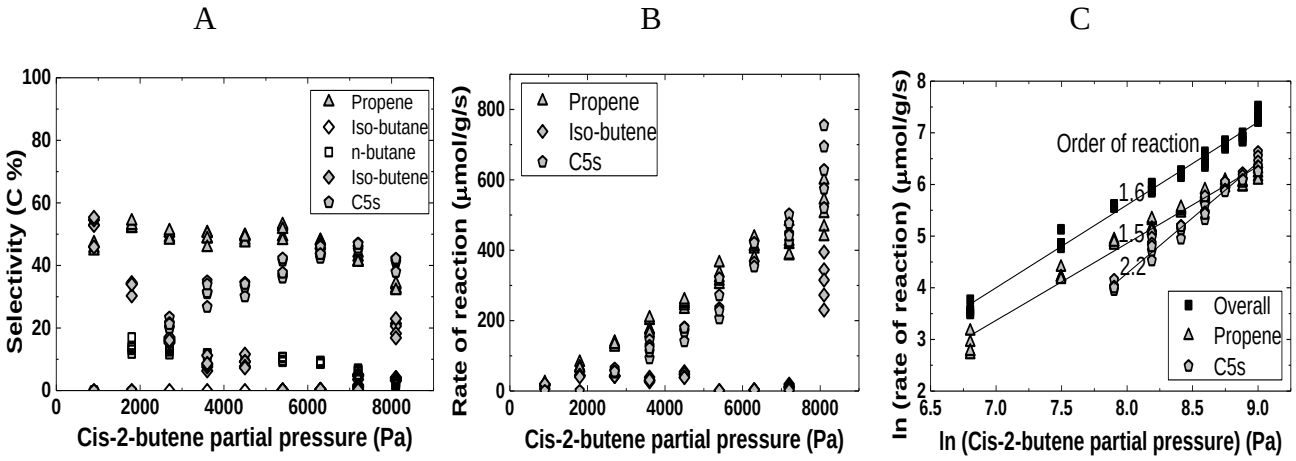

Figure 7.9: Effect of cis-butene partial pressure on selectivity (A), rate (B) and log-log plot of (B) as (C): H-SAPO-5 mass = 50 mg, $P_{Cis\text{-}2\text{-}butene}$= 0.9-8.1 kPa, P_{Ethene}= 10 kPa, $Flow_{total}$= 100 ml/min, T = 673 K, WHSV = 2.9-4.9 h^{-1}

Figure 7.9A shows the selectivity versus cis-2-butene partial pressure at 673 K. Selectivity to propene decreased from 54 to 32 % with cis-2-butene partial pressure. C_5s selectivity increased from 20 to 42 % within 2.7 to 8.1 kPa. No C_5s selectivity was observed below 2.7 kPa cis-2-butene partial pressure, that is when $\frac{P_{ethene}}{P_{cis-2-butene}} > 4$. As the cis-2-butene pressure increased, selectivity to C_5s appeared and eventually became slightly more than propene selectivity after 6.3 kPa. 46 % iso-

butene selectivity decreased rapidly and disappeared with pressure. Iso-butene selectivity appeared again at 8.1 kPa, which could be due to low influence of deactivation at the time it was measured. Selectivity to n-butane decreased from 16 to 3 % between 1.8 and 8.1 kPa while iso-butane appeared within 7.2 to 8.1 kPa with about 5 % selectivity. Figure 7.9B shows the rate of formation for the main products versus cis-2-butene partial pressure at 673 K. The rate of formation of C_5s and propene linearly increased with cis-2-butene partial pressure. The rate of formation of iso-butene was initially linear between 0.9 and 4.5 kPa and then disappeared and reappeared at 8.1 kPa. Figure 7.9C shows logarithm of the rate of reaction versus logarithm of cis-2-butene partial pressure. The iso-butene was not included because of the rapid disappearance of its rate. The reaction orders within 1.8 to 8.1 kPa were 1.6, 1.5 and 2.2 for the overall reaction, propene and C_5s formations rates respectively.

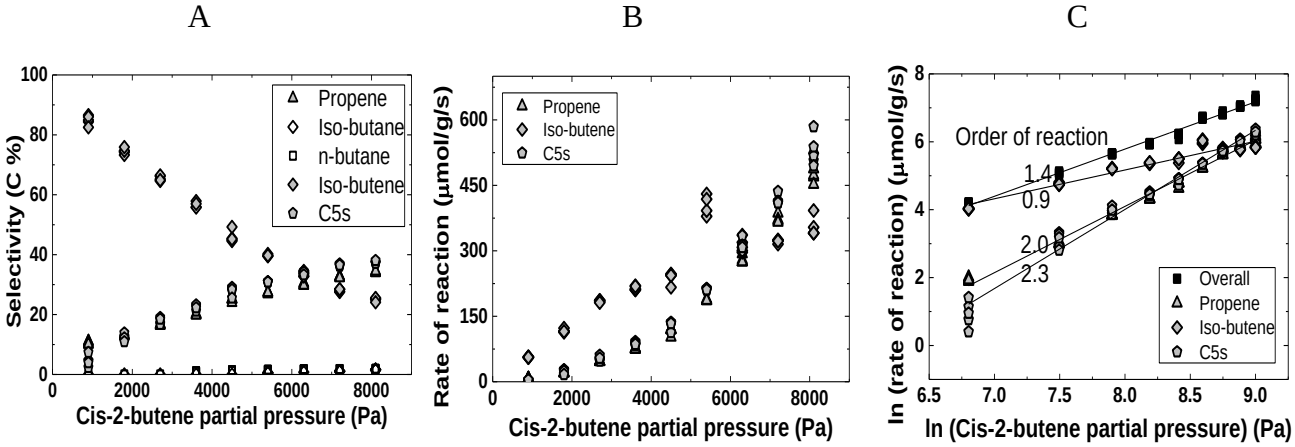

Figure 7.10: Effect of cis-butene partial pressure on selectivity (A), rate (B) and log-log plot of (B) as (C): H-SAPO-5 mass = 50 mg, $P_{Cis\text{-}2\text{-}butene}$= 0.9-8.1 kPa, P_{Ethene} = 10 kPa, $Flow_{total}$= 100 ml/min, T = 748 K, WHSV = 2.9-4.9 h^{-1}

Figure 7.10A shows the selectivity versus cis-2-butene partial pressure at 748 K. The selectivity to iso-butene decreased from 84 to 24 % within 0.9 and 8.1 kPa partial pressures. The C_5s and propene selectivities on the other hand increased with partial pressure, from 5 to 38 % and 11 to 34 % respectively. Some minor amount of iso-butane and n-butane were also observed with total selectivity which varied between 1 to 3 % with partial pressure. Figure 7.10B shows the rate of formation of the main products versus cis-2-butene partial pressure at 748 K. The rate of formation of iso-butene linearly increased with partial pressure between 0.9 and 5.4 kPa and then leveled off. The iso-butene formation rate was higher than the formation rate of C_5s and propene below 6.3 kPa. C_5s and propene formation rates increased exponentially with partial pressure. Figure 7.10C shows logarithm of the rate of reaction versus logarithm of cis-2-butene partial pressure. The reaction

orders were 1.4, 0.9, 2.0 and 2.3 for the overall, iso-butene, propene and C_5s formations rates respectively.

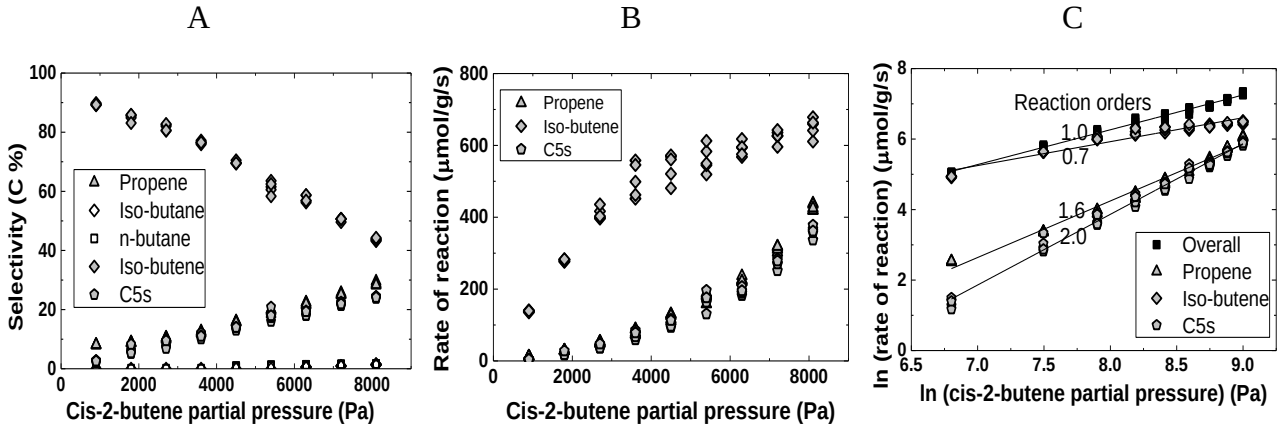

Figure 7.11: Effect of cis-2-butene partial pressure on selectivity (A), rate (B) and log-log plot of (B) as (C): H-SAPO-5 mass = 50 mg, $P_{Cis\text{-}2\text{-}butene}$= 0.9-8.1 kPa, P_{Ethene}= 10 kPa, $Flow_{total}$= 100 ml/min, T = 823 K, WHSV = 2.9-4.9 h^{-1}

Figure 7.11A shows the selectivity versus cis-2-butene partial pressure at 823 K. The selectivity patterns were similar to that observed at 748 K within the 0.9 to 8.1 kPa cis-2-butene partial pressures. The selectivity to iso-butene decreased from 89 % to 44 % with cis-2-butene partial pressure. C_5s and propene selectivities increased from 3 to 24 % and 8 % to 28 % respectively with cis-2-butene partial pressure. Some minor amount of iso-butane and n-butane were observed with total selectivity which varied between 1 to 3 % within 4.5 to 8.1 kPa cis-2-butene partial pressure. Figure 7.11B shows the rate of formation of the main products versus cis-2-butene partial pressure at 823 K. The C_5s and propene rate of formations increased exponentially with partial pressure. Iso-butene formation rate increased linearly within 0.9 and 3.6 kPa after which it gradually levelled off with partial pressure. Figure 7.11C shows logarithm of the rate of reaction versus logarithm of cis-2-butene partial pressure. The reaction orders were 1.0, 0.7, 1.6 and 2.0 for the overall, iso-butene, propene and C_5s formation rates respectively.

7.1.1.4 Effect of ethene partial pressure on co-feed reaction activity

Effect of ethene partial pressure on the co-feed reaction over H-SAPO-5 was studied between 4 and 40 kPa ethene partial pressures, while cis-2-butene partial pressure was kept constant at 4.5 kPa.

This was done by keeping cis-2-butene flow constant at 0.9 ml/min and varying ethene flow within 1 to 10 ml/min over 50 mg catalyst such that the WHSV ranged from 0.5 to 2.9 h^{-1}. The total gas flow rate was held constant at 25 ml/min to maintain constant contact times. Three different experiments were done at 673, 748 and 823 K temperatures under these conditions. The original conversions obtained and used for rate calculations were below 6 %.

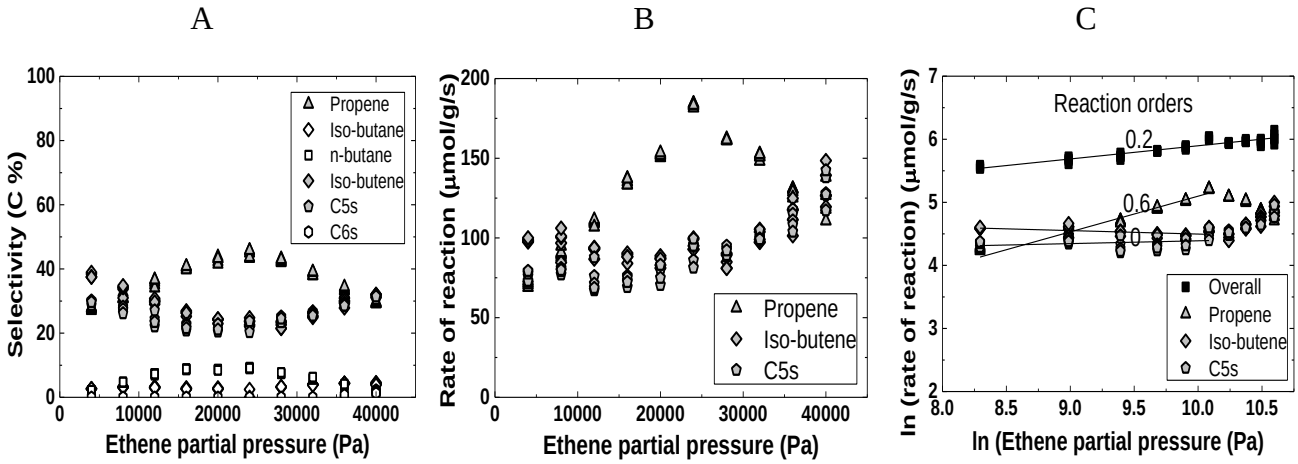

Figure 7.12: Effect of ethene partial pressure on selectivity (A), rate (B) and log-log plot of (B) as (C): H-SAPO-5 mass = 50 mg, $P_{Cis\text{-}2\text{-}butene}$= 3.6 kPa, P_{Ethene}= 4-40 kPa, $Flow_{total}$= 25 ml/min, T = 673 K, WHSV = 0.5-2.9 h^{-1}

Figure 7.12A shows the selectivity versus ethene partial pressure at 673 K. Selectivity to propene increased from 27 to 45 % between 4 and 24 kPa and then decreased to 30 % at 40 kPa. Iso-butene and C_5s selectivity decreased from 30 to 20 % and 38 to 22 % respectively within 4 to 24 kPa and then increased again to 31 and 32 % at 40 kPa. Note that propene selectivity was mostly higher than C_5s and iso-butene except at 40 kPa ethene partial pressure, though a deviation occurred at 24 kPa. Selectivity to n-butane varied between 2 and 9 % in a pattern similar to the propene selectivity. Iso-butane selectivity on the other hand varied between 2 and 5 in a pattern similar to the iso-butene selectivity. Some C_6s were also observed at 40 kPa with up to 2 % selectivity.

Figure 7.12B shows the rate of reaction of formation for the main products versus ethene partial pressure at 673 K. The rate of formation of C_5s and iso-butene appeared to be independent on ethene pressure except after 24 kPa where they started to increase linearly with ethene partial pressure. Propene on the other hand showed rapid linear increase between 4 and 24 kPa and then a sharp decrease with ethene partial pressure. Figure 7.12C shows log-log plot of the rate of reaction versus ethene partial pressure at 673 K. The reaction order for the overall reaction was 0.2 within 4

and 40 kPa ethene partial pressures. Due to the rapid change that occurred after 24 kPa, the reaction order with respect to the product formations were estimated for ethene partial pressures between 4 to 24 kPa. The reaction orders between 4 and 24 kPa were 0 each with respect to C_5s and iso-butene formations and 0.6 with respect to propene formation.

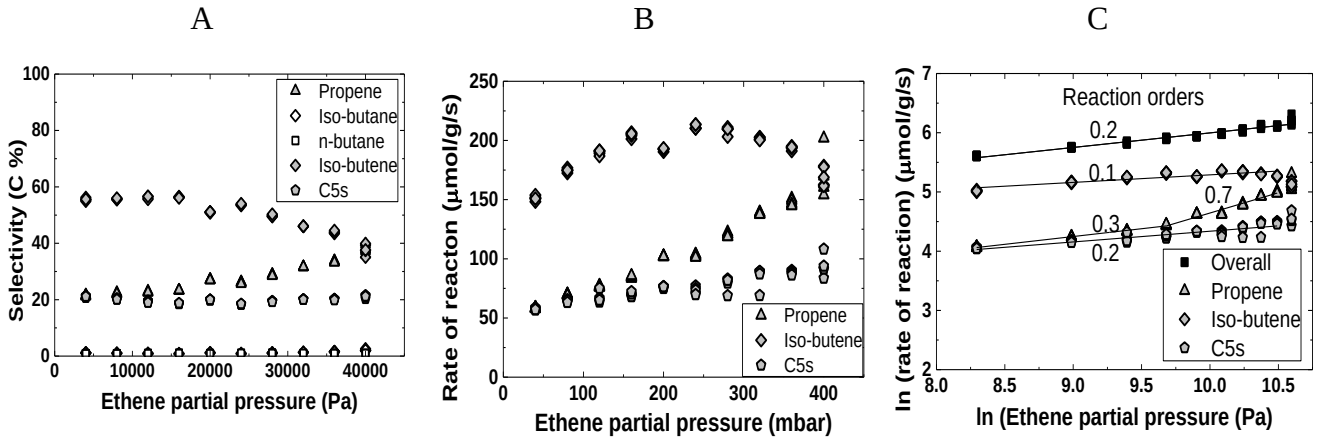

Figure 7.13: Effect of ethene partial pressure on selectivity (A), rate (B) and log-log plot of (B) as (C): H-SAPO-5 mass = 50 mg, $P_{Cis\text{-}2\text{-}butene}$= 3.6 kPa, P_{Ethene}= 4-40 kPa, $Flow_{total}$= 25 ml/min, T = 748 K, WHSV = 0.5-2.9 h^{-1}

Figure 7.13A shows the selectivity versus ethene partial pressure at 748 K. The selectivity to iso-butene stayed around 55 % between 4 and 24 kPa and then decreased to 38 % with ethene partial pressure. C_5s selectivity was about 20 % which remained roughly constant with ethene partial pressure. Propene selectivity increased slightly from 22 to 38 % ethene partial pressure. Some minor amount of iso-butane and n-butane were observed with total selectivity of about 3 % throughout the ethene partial pressure studied. Figure 7.13B shows the rate of formation for the main products versus ethene partial pressure at 748 K. Iso-butene formation rate increased initially between 4 and 24 kPa and then decreased with ethene pressure. The reaction rates for the formation of C_5s appeared to be stable within the ethene partial pressure studied. Propene formation rate increased linearly with ethene pressure. Figure 7.13C shows logarithm of the rate of reaction versus the logarithm of ethene partial pressure. The overall order of reaction was 0.2 the same as observed at 673 K. In order to obtain a good fit for the reaction orders for formation, the pressure range between 4 and 36 kPa was considered. At this pressure range, iso-butene was 0.1 and 0.2 for C_5s. Propene was 0.3 between 4 and 16 kPa but 0.7 between 16 and 36 kPa. This suggested that, the influence of ethene on the main products is more at 673 K than at 748 K.

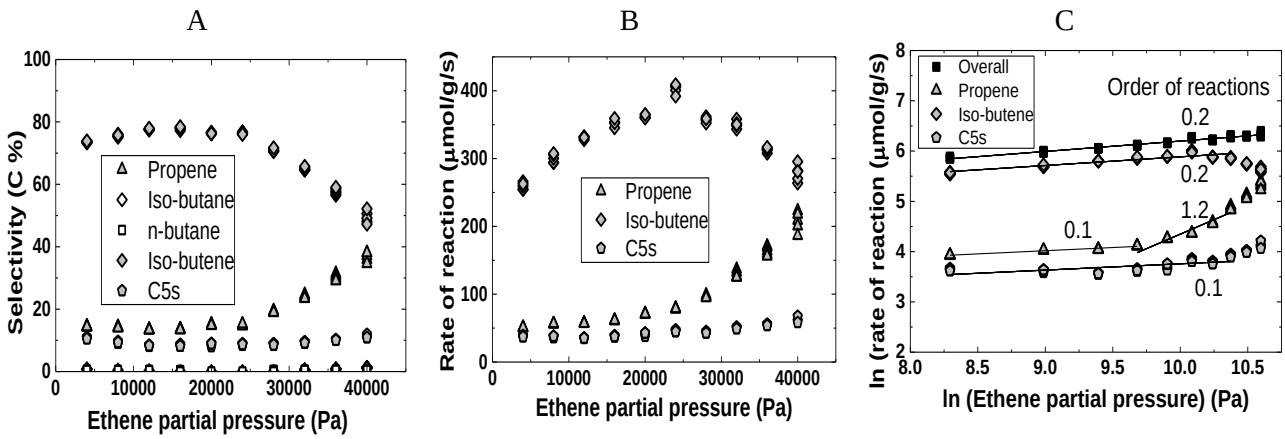

Figure 7.14: Effect of ethene partial pressure on selectivity (A), rate (B) and log-log plot of (B) as (C): H-SAPO-5 mass = 50 mg, $P_{Cis\text{-}2\text{-}butene}$= 3.6 kPa, P_{Ethene}= 4-40 kPa, $Flow_{total}$= 25 ml/min, T = 823 K, WHSV = 0.5-2.9 h^{-1}

Furthermore, the effect of ethene partial pressure was studied at 823 K. Figure 7.14A shows the selectivity versus ethene partial pressure. The selectivity to iso-butene remained fairly stable between 4 and 24 kPa and then decreased from 76 to 50 % with ethene partial pressure. Propene selectivity remained fairly stable within similar partial pressures as iso-butene and then increased from 15 to 35 % with ethene partial pressure. C_5s selectivity of about 11 % remained fairly constant with ethene partial pressure. Some minor amount of iso-butane and n-butane were observed with total selectivity which varied between 1 to 3 % with ethene partial pressure. Figure 7.14B shows the rate of formation for the main products versus ethene partial pressure at 823 K. Iso-butene formation rate increased initially between 4 and 24 kPa and then decreased with ethene pressure. The reaction rates for the formation of C_5s once again appeared not to be affected by ethene partial pressure. Propene formation rate was also stable initially until 24 kPa where it increased rapidly with ethene pressure. Figure 7.14C shows logarithm of the rate of reaction versus the logarithm of ethene partial pressure. The overall order of reaction was 0.2 same as was observed at 673 and 748 K. The reaction orders between 4 and 32 kPa were 0.2 and 0.1 with respect to the formations of iso-butene and C_5s. The reaction order with respect to propene formation was 0.1 between 4 and 16 kPa and 1.2 between 16 and 32 kPa. This was also similar to the reaction orders at 748 K.

7.1.1.5 Effect of temperature on co-feed activity

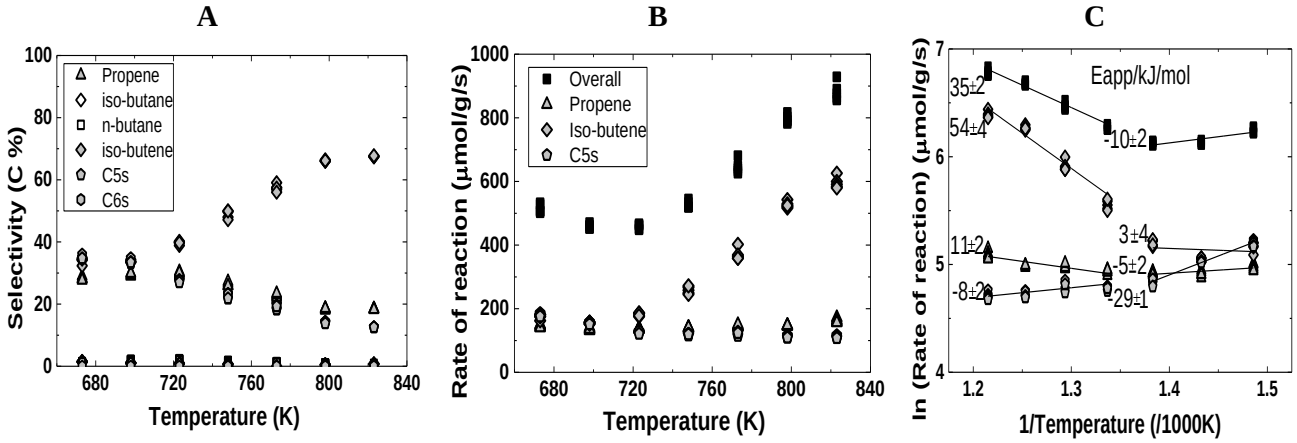

Figure 7.15: Effect of temperature on selectivity (A), rate (B) and log-log plot of (B) as (C): H-SAPO-5 mass = 50 mg, $P_{Cis\text{-}2\text{-}butene}$= 4.5 kPa, P_{Ethene}= 10 kPa, $Flow_{total}$ = 60 ml/min, T = 673-823 K, WHSV = 2.3 h^{-1}

The effect of the reaction temperature on the co-reaction between 4.5 kPa cis-2-butene and 10 kPa ethene partial pressures was studied over H-SAPO-5. This was done using 2.7 ml/min cis-2-butene and 6 ml/min ethene flows over 50 mg catalysts, such that the WHSV was 2.3 h^{-1}, where original conversions were below 10 %. Figure 7.15A shows the selectivity versus temperature. Selectivity to iso-butene increased slowly at initial temperatures between 673 and 723 K (low temperature) from 34 to 40 % and then rapidly to 68 % between 748 to 823 K (high temperature). At similar temperature range, C_5s selectivities decreased slowly from 35 to 27 % and then rapidly to 13 %. Selectivity to propene stayed relatively stable at the initial low temperatures, but rapidly declined at high temperatures from 20 to 18 %. A total of about 3 % selectivity to iso-butane and n-butane were observed throughout the various temperatures.

Figure 7.15B shows the rate of reaction versus temperature. The trends in the various rates varied at the two temperature regions. At low temperature region, the overall reaction rate decreased with temperature, but then increased rapidly at the high temperature region. Iso-butene formation rate showed mild temperature effect at low temperature region, but exponentially increased at high temperature region. Propene formation rate was slightly affected while C_5s formation rate decreased with temperature. A linearized version of the plot in Figure 7.15B was obtained by plotting the logarithm of the rate versus the reciprocal of the temperature as shown in Figure 7.15C. The apparent activation energies for the overall reaction, iso-butene, C_5s and propene formation rates at

lower temperature region were -10±2, 3±4, -29±1 and -5±2 kJ/mol respectively. At the high temperature region, the apparent activation energies for the overall reaction, iso-butene, C_5s and propene formations rates were 35±2, 54±4, -8±2 and 11±2 kJ/mol respectively.

7.1.2 Conversion of co-feed over H-SSZ-24

7.1.2.1 Catalytic activity of co-feed versus time on stream

The activity of H-SSZ-24 was tested with co-reaction between ethene and cis-2-butene. Two main partial pressures were used similar to the experiments done over H-SAPO-5. Two ratios were of interest; $\frac{P_{ethene}}{P_{cis-2-butene}} = \frac{2.2}{1}$, and $\frac{P_{ethene}}{P_{cis-2-butene}} = \frac{5.6}{1}$. This was done at 673, 748 and 823 K.

Ethene (10 kPa) and cis-2-butene (4.5 kPa)

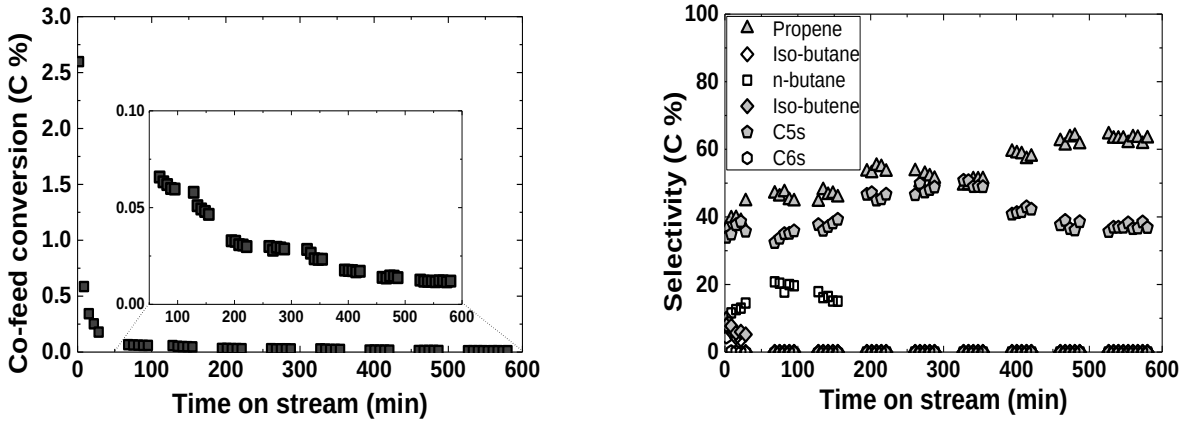

Figure 7.16: Catalytic activity of H-SSZ-24 versus time on stream, Conversion (left) and Selectivity (right): H-SSZ-24 mass = 5 mg, $P_{Cis-2-butene}$= 4.5 kPa, P_{Ethene}= 10 kPa, $Flow_{total}$= 100 ml/min, T = 673 K, WHSV = 39 h^{-1}

Figure 7.16 shows the activity when 4.5 kPa cis-2-butene and 10 kPa ethene were co-fed over H-SSZ-24 versus time on stream (TOS) at 673 K. This was done with 50 mg catalyst and 4.5 ml/min cis-2-butene and 10 ml/min ethene flow to give a WHSV of 39 h^{-1}. The conversion of the co-feed at 2 min TOS was 2.6 % but rapidly decreased to 0.06 % at 68 min. The conversion further decreased to 0.01 % at 580 min. Though, cis-2-butene fed alone gave a rapid decline of activity at the initial 68 min at 673 K, the co-feed reaction deactivation was much more. This deactivation with conversion below 0.1 % made it difficult to do further analysis of the co-feed reaction at 673 K over

H-SSZ-24 for any long TOS. At 2 min TOS, the respective selectivities were 8 % to iso-butene, 34 % to C_5s, 37 % to propene, 10 % to iso-butene and 8 % to n-butene.

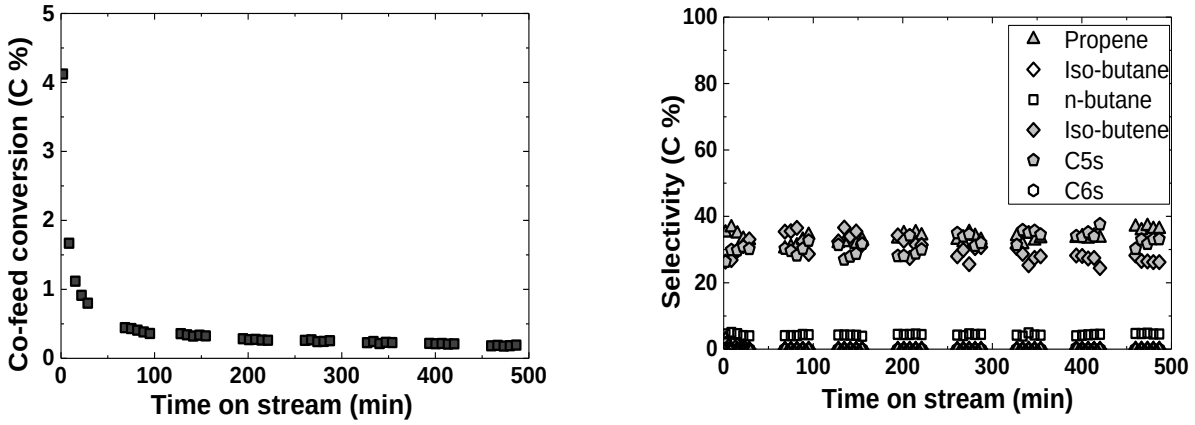

Figure 7.17: Catalytic activity of H-SSZ-24 versus time on stream, Conversion (left) and Selectivity (right): H-SSZ-24 mass = 5 mg, $P_{Cis\text{-}2\text{-}butene}$= 4.5 kPa, P_{Ethene}= 10 kPa, $Flow_{total}$= 100 ml/min, T = 748 K, WHSV = 39 h^{-1}

The next, was to test H-SSZ-24 activity at 748 K under similar conditions as was done at 673 K. Figure 7.17 shows the activity of co-feed versus TOS over H-SSZ-24 at 748 K. Conversion decreased rapidly from 4.4 to 0.8 % within the first 29 min then gradually to 0.2 % with TOS. Selectivities to propene and C_5s stayed around 36 and 30 % with TOS. Iso-butene selectivity also showed some slight increase from 26 % to 35 and then decreased back to 26 % with TOS. Minor selectivities to iso-butane, n-butane and C_6s were observed. The iso-butane and C_6s only appeared at the initial TOS with up to 5 % selectivity. N-butane selectivity however stayed around 5 % selectivity with TOS.

Thirdly, the catalytic activity was tested at 823 K under similar conditions. Figure 7.18 shows the activity of co-feed versus TOS over H-SSZ-24 at 823 K. The conversion decreased from 9 to 0.3 % within 2 to 586 min TOS. At 823 K, the initial conversion was about twice the conversion at 748 K, however deactivation was equally rapid compared to that 748 K. At 2 min TOS, the selectivities to iso-butene, propene and C_5s were 32, 44 and 18 % respectively. Propene to C_5s selectivity ratio at 2 min was quite high but reduced with TOS. The iso-butene selectivity increased to 54 %, while propene declined to 26 % at 68 min. These selectivities including the C_5s remained relatively stable after 68 min TOS. The selectivities at 823 K differ from the observation made at 748 K by a higher

iso-butene and a lower C_5s and propene selectivities. A total of 6 % selectivities to iso-butane, n-butane and C_6s were observed at 2 min which decreased and disappeared with TOS, except n-butane which increased slightly and was observed throughout.

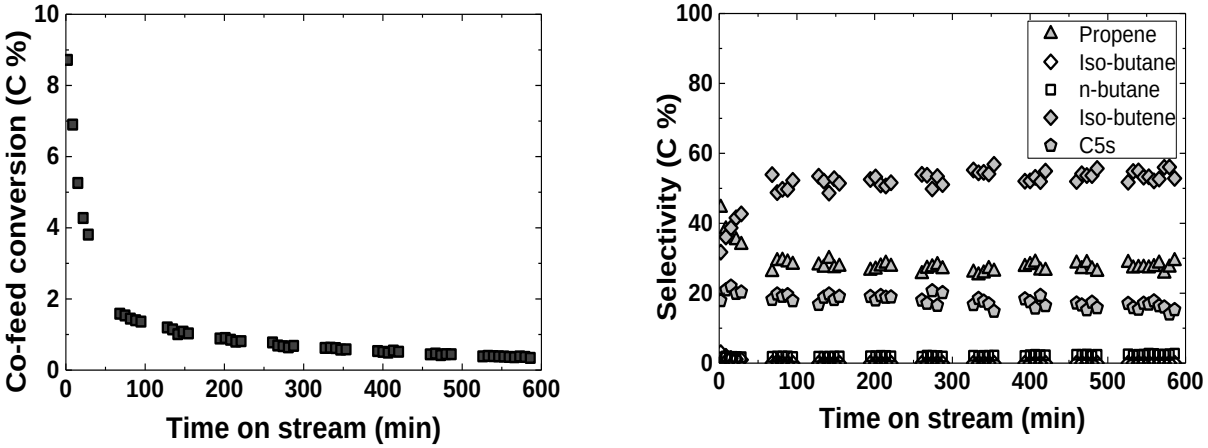

Figure 7.18: Catalytic activity of H-SSZ-24 versus time on stream, Conversion (left) and Selectivity (right): H-SSZ-24 mass = 5 mg, $P_{Cis\text{-}2\text{-}butene}$= 4.5 kPa, P_{Ethene}= 10 kPa, $Flow_{total}$= 100 ml/min, T = 823 K, WHSV = 39 h^{-1}

Ethene (20 kPa) and cis-2-butene (3.6 kPa)

Figure 7.19 shows the activity of co-reaction between cis-2-butene at 3.6 kPa and ethene at 20 kPa versus TOS over H-SSZ-24 at 748 K. Conversion decreased rapidly from 8 to 0.14 % with TOS. This showed a higher initial conversion, but more rapid deactivation compared to the co-reaction between 4.5 kPa cis-2-butene and 10 kPa ethene partial pressures. Selectivity to iso-butene increased from 25 to 75 % with TOS. Selectivity to propene decreased from 39 to 15 % while C_5s slightly decreased from 19 to 11 % with TOS. Some minor selectivities to propane, iso-butane, n-butane and C_6s were observed at the initial TOS mainly between 2 to 29 min except n-butane which eventually disappeared at 221 min. At 2 min TOS, the selectivities were 3, 5, 3 and 6 % to propane, iso-butane, n-butane and C_6s respectively. As was suggested earlier, the alkane formation implied hydrogen transfer which may lead to hydrocarbon deposits in the form of aromatic. This could account for the rapid deactivation within the initial TOS.

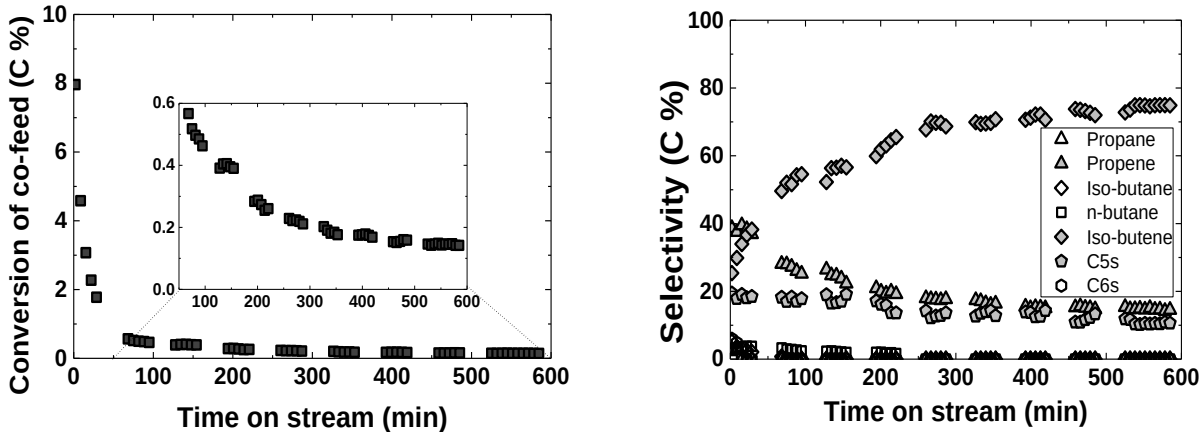

Figure 7.19: Catalytic activity of H-SSZ-24 versus time on stream, Conversion (left) and Selectivity (right): H-SSZ-24 mass = 5 mg, $P_{Cis\text{-}2\text{-}butene}$= 3.6 kPa, P_{Ethene}= 20 kPa, $Flow_{total}$= 25 ml/min, T = 748 K, WHSV = 16 h^{-1}

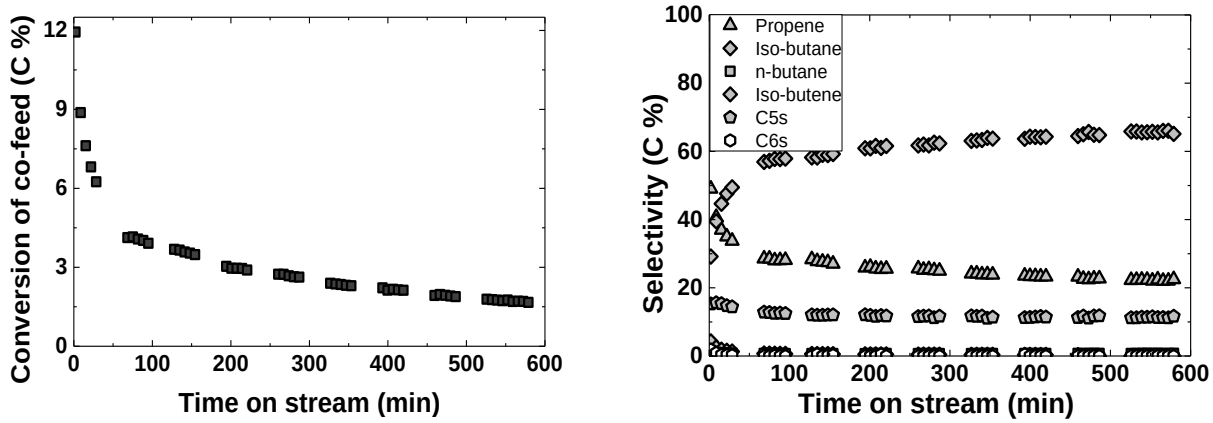

Figure 7.20: Catalytic activity of H-SSZ-24 versus time on stream, Conversion (left) and Selectivity (right): H-SSZ-24 mass = 5 mg, $P_{Cis\text{-}2\text{-}butene}$= 3.6 kPa, P_{Ethene}= 20 kPa, $Flow_{total}$= 25 ml/min, T = 823 K, WHSV = 16 h^{-1}

Figure 7.20 shows the activity of co-feed versus TOS over H-SSZ-24 at 823 K. The conversion decreased from 12 to about 2 % within 2 to 586 min TOS. The deactivation trend was similar to that at 748 K, though the initial conversion was more at 823 K. The trends of the selectivities at 823 K were also similar to that at 748 K. Selectivity to iso-butene initially increased rapidly between 2 and 68 min from 29 to 57 % and then slowly to 65 % with TOS. Propene selectivity initially decreased rapidly between 2 and 68 min from 49 to 29 % and then slowly to 22 % with TOS. Selectivity to C_5s decreased slightly from 15 to 12 % with TOS. Minor selectivities to iso-butane, n-butane and C_6s were observed. At 2 min, 4 % selectivity to iso-butene was observed which decreased with TOS. Selectivity of n-butane stayed at 1 % throughout the TOS studied. 2 % selectivity to C_6s was observed at 2 min TOS but quickly decreased with TOS.

7.1.2.2 Contact time variation at 748 K

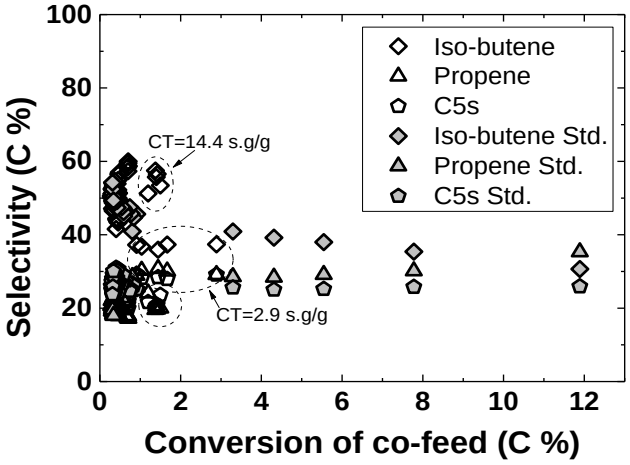

Figure 7.21: Selectivity versus conversion of co-feed over H-SSZ-24 at different contact times: H-SSZ-24 mass = 5 mg, $P_{Cis\text{-}2\text{-}butene}$= 4.5 kPa, P_{Ethene}= 10 kPa , $Flow_{total}$= 20-100 ml/min, T = 748 K, WHSV = 7.8-39.1 h^{-1}

The influence of contact time on the co-feed reaction over H-SSZ-24 at 748 K was studied at similar conditions used over H-SAPO-5 except the catalysts mass that were changed in order to get comparable conversions. The partial pressures were 4.5 kPa cis-2-butene and 10 kPa ethene, ratios within 7.8 to 39 h^{-1} WHSVs. The total flows were varied between 20 and 100 ml/min but with a constant fraction of cis-2-butene, ethene and inert gases over 50 mg catalyst to maintain constant reactants' partial pressures. Figure 7.21 shows selectivity versus co-feed conversion over H-SSZ-24 at varied contact times (CT). Generally, selectivities to the main products, iso-butene, propene and C_5s at conversions below 1 % were very scattered such that a clear trend cannot be deduced. Unfortunately, most of the measurements were made at this conversion as the H-SSZ-24 deactivated rapidly on time stream at 748 K (Figure 7.17). Moreover, the main products selectivity fell outside the selectivity of the highest and the lowest contact times similar to the observations when cis-2-butene was fed alone (Figure 6.13). Although no strict trends could be deduced at conversions below 1 %, iso-butene selectivity was around 40 % at 3 % conversions and decreased slightly with increasing conversion. Meanwhile propene and C_5s selectivities were around 30 % at 3 % conversion. While propene increased slightly with conversion, C_5s was relatively stable.

7.1.2.3 Effect of cis-2-butene partial pressure on co-feed reaction activity

The effect of cis-2-butene partial pressure on the co-feed reaction over H-SSZ-24 was studied between 0.9 and 8.1 kPa cis-2-butene and 10 kPa ethene partial pressure just as was done over H-SAPO-5. Cis-2-butene flow was varied between 0.9 and 8.1 ml/min whilst ethene was kept at 10 ml/min over 5 mg of H-SSZ-24 such that the WHSV ranged from 29 to 49 h^{-1}. The total gas flow rate was held constant at 100 ml/min to maintain constant contact times. Under these conditions, three different experiments were done at 673, 748, and 823 K temperatures. However, since the co-feed reaction over H-SSZ-24 deactivated much rapidly, only those at 748 and 823 K are reported (See Appendix F for 673 K). The original conversions obtained and used for rate calculations were below 10 %.

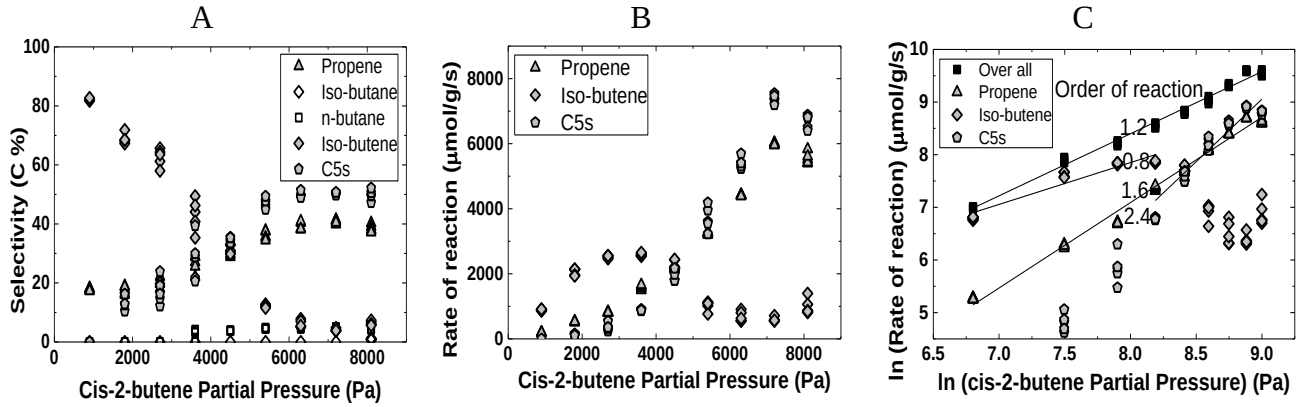

Figure 7.22: Effect of cis-butene partial pressure on selectivity (A), rate (B) and log-log plot of (B) as (C): H-SSZ-24 mass = 5 mg, $P_{Cis\text{-}2\text{-}butene}$= 0.9-8.1 kPa, P_{Ethene}= 10 kPa, $Flow_{total}$=100 ml/min, T = 748 K, WHSV = 29-49 h^{-1}

Figure 7.22A shows the selectivity versus cis-2-butene partial pressure at 748 K. The selectivity to iso-butene decreased rapidly from 82 to 6 % within 0.9 and 8.1 kPa partial pressures. The C_5s and propene selectivities on the other hand increased with partial pressure, from 0 to 50 % and 18 to 40 % respectively. Some minor amount of iso-butane and n-butane were also observed with total selectivity varying between 3 and 5 % within 3.6 to 8.1 kPa cis-2-butene partial pressure. Figure 7.22B shows the rate of formation of the main products versus cis-2-butene partial pressure at 748 K. The rate of formation of iso-butene increased linearly between 0.9 and 3.6 kPa and then declined with partial pressure. The iso-butene formation rate was more than the formation rate of C_5s and propene below 4.5 kPa cis-2-butene pressure. The rates of formation of C_5s and propene increased exponentially with partial pressure. Figure 7.22C shows logarithm of the rate of reaction versus

logarithm of cis-2-butene partial pressure. The overall reaction order was 1.2 and 1.6 for propene formation between 0.9 and 8.1 kPa cis-2-butene partial pressures. The order of reaction with respect to iso-butene formation was 0.8 between 0.9 and 3.6 kPa while that of C_5s was 2.4 between 3.6 and 8.1 kPa. Iso-butene was estimated for at low pressure because of the frequent bending at high pressure. C_5s were estimated for at high pressure because of the relatively low rates at the low pressure.

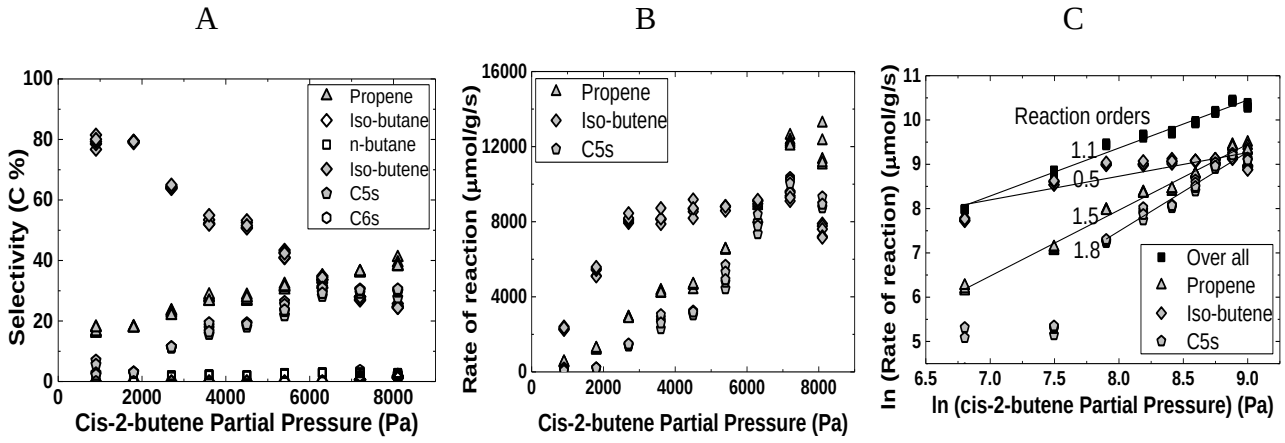

Figure 7.23: Effect of cis-2-butene partial pressure on selectivity (A), rate (B) and log-log plot of (B) as (C): H-SSZ-24 mass = 5 mg, $P_{Cis\text{-}2\text{-}butene}$= 0.9-8.1 kPa, P_{Ethene}= 10 kPa, $Flow_{total}$= 100 ml/min, T = 823 K, WHSV = 29-49 h^{-1}

Figure 7.23A shows the selectivity versus cis-2-butene partial pressure at 823 K. The selectivity to iso-butene decreased from 80 to 24 % with partial pressure. The C_5s and propene selectivities on the other hand increased with partial pressure, from 7 to 31 % and 16 to 38 % respectively. Note that at 823 K, propene selectivity was more than C_5s selectivity throughout the partial pressure used, which differ from the observation at 748 K, where the reverse was observed after 4.5 kPa. Some minor amount of iso-butane, n-butane and C_6s were observed up to 7 % total selectivity. Figure 7.23B shows the rate of reaction of formation of the main products versus cis-2-butene partial pressure at 823 K. The C_5s and propene rate of formations increased exponentially with partial pressure. Iso-butene formation rate increased linearly within 0.9 and 4.5 kPa after which it levelled off with partial pressure. Figure 7.23C shows logarithm of the rate of reaction versus logarithm of cis-butene partial pressure. The reaction orders for the overall reaction, iso-butene and propene were 1.1, 0.5 and 1.5 respectively within 0.9 to 8.1 kPa partial pressure. Reaction order with respect to the formation of C5s was 1.8 within 2.7 and 8.1 kPa partial pressures.

7.1.2.4 Effect of ethene partial pressure on co-feed reaction activity

Effect of ethene partial pressure on the co-feed reaction between 4 kPa cis-2-butene and varied ethene from 8 to 40 kPa partial pressures over H-SSZ-24 was studied just as was done over H-SAPO-5. Cis-2-butene flow was kept at 0.9 ml/min and ethene flow varied from 2 to 10 ml/min over 5 mg catalysts such that the WHSV ranged from 7.8 to 29 h^{-1}. The total gas flow rate was held constant at 25 ml/min to maintain constant contact time. Three experiments were done at different temperatures, but due to the rapid deactivation at 673 K (Appendix H), only those at 748 and 823 K are reported just as was done when cis-2-butene was the varying parameter. The original conversions obtained and used for rate calculations were below 10 %.

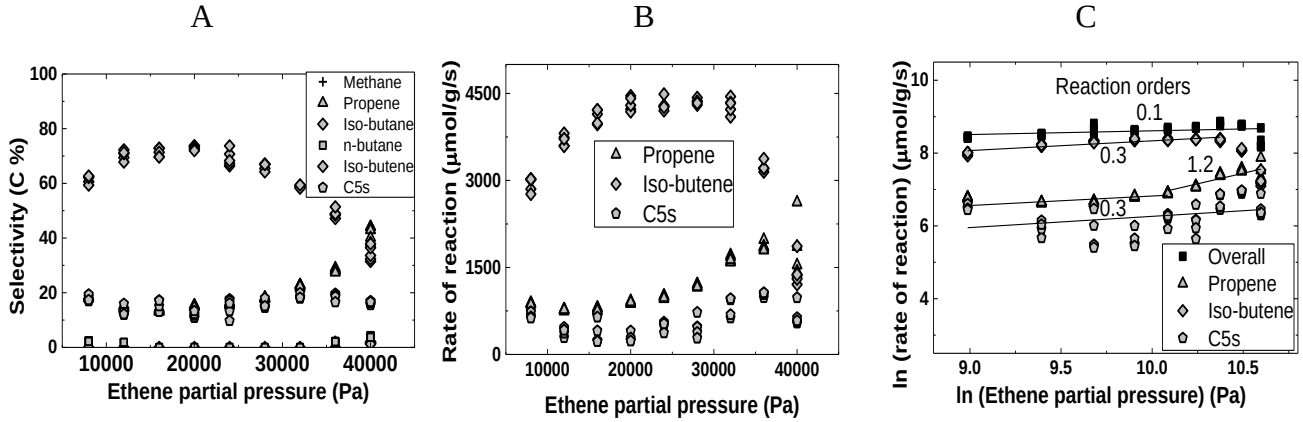

Figure 7.24: Effect of ethene partial pressure on selectivity (A), rate (B) and log-log plot of (B) as (C): H-SSZ-24 mass = 5 mg, $P_{Cis\text{-}2\text{-}butene}$= 3.6 kPa, P_{Ethene}= 8-40 kPa, $Flow_{total}$= 25 ml/min, T = 748 K, WHSV = 7.8-29 h^{-1}

Figure 7.24A shows the selectivity versus ethene partial pressure at 748 K. The selectivity to iso-butene increased slightly from 61 to 73 % between 8 and 20 kPa and then decreased to 34 % with ethene partial pressure. C_5s selectivity varied from 20 to 16 % with partial pressure. Propene selectivity initially decreased slightly from 19 to 13 % between 8 and 16 kPa and then increased linearly with partial pressure. Some minor amount of methane, iso-butane and n-butane were observed especially between 36 and 40 kPa with total selectivity of about 6 %. Figure 7.24B shows the rate of formation for the main products versus ethene partial pressure at 748 K. Iso-butene formation rate initially increased between 8 and 32 kPa and then decreased with ethene partial pressure. The reaction rates for the formation of C_5s appeared to be bending slightly in opposite direction to the iso-butene with partial pressure studied. Propene formation rate decreased at initial

partial pressures and then linearly increased after 16 kPa partial pressure. Figure 7.24C shows logarithm of the rate of reaction versus the logarithm of ethene partial pressure. The order of reaction for the overall reaction was 0.1 and 0.3 for C_5s between 8 and 40 kPa partial pressures. The order of reaction with respect to iso-butene formation was 0.3 between 8 and 32 kPa. The order of reaction with respect to propene formation between 8 and 24 kPa was 0.3 and 1.2 between 24 and 40 kPa.

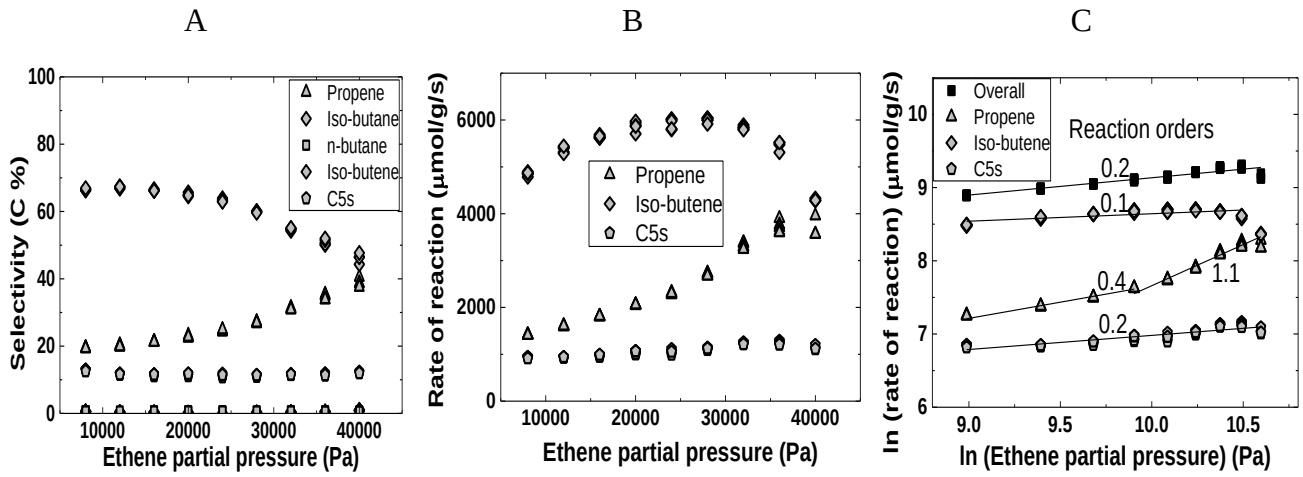

Figure 7.25: Effect of ethene partial pressure on selectivity (A), rate (B) and log-log plot of (B) as (C): H-SSZ-24 mass = 5 mg, $P_{Cis\text{-}2\text{-}butene}$= 3.6 kPa, P_{Ethene}= 8-40 kPa, $Flow_{total}$= 25 ml/min, T = 823 K, WHSV = 7.8-29 h^{-1}

Furthermore, the effect of ethene partial pressure was studied at 823 K under similar conditions as stated above. Figure 7.25A shows the selectivity versus ethene partial pressure. The selectivity to iso-butene remained fairly stable between 8 and 20 kPa and then decreased from 65 to 46 % with partial pressure. Propene selectivity gently increased from 20 to 38 % with partial pressure. C_5s selectivity stayed fairly constant around 12 % with ethene partial pressure. Some minor amount of iso-butane and n-butane were observed with total selectivity less than 2 %. Figure 7.25B shows the rate of reaction of formation for the main products versus ethene partial pressure at 823 K. Iso-butene formation rate increased with partial pressure between 8 and 28 kPa and then decreased. The reaction rates for the formation of C_5s remained constant with increasing ethene partial pressure. Propene formation rate increased gently between 8 and 20 kPa and then rapidly with partial pressure. Figure 7.25C shows logarithm of the rate of reaction versus the logarithm of ethene partial pressure. The order of reaction for the overall reaction and C_5s formation rates was 0.2 each between 8 and 40 kPa ethene partial pressures. The reaction order with respect to iso-butene

formation was 0.1 between 4 and 38 kPa partial pressures. The reaction orders with respect to propene formation between 8 and 20 kPa was 0.4 and then between 20 and 40 kPa was 1.1.

7.1.2.5 Effect of temperature on co-feed activity

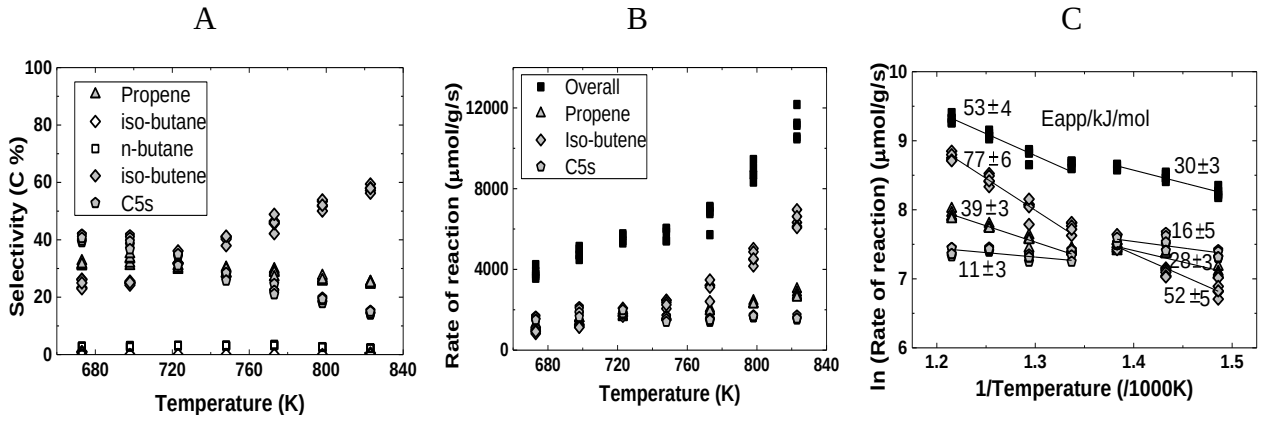

Figure 7.26: Effect of temperature on selectivity (A), rate (B) and log-log plot of (B) as (C): H-SSZ-24 mass = 5 mg, $P_{Cis\text{-}2\text{-}butene}$= 4.5 kPa, P_{Ethene}= 10 kPa $Flow_{total}$= 60 ml/min, T = 673-823 K, WHSV = 23 h^{-1}

The effect of the reaction temperature on the co-reaction was done over H-SSZ-24 under similar conditions used over H-SAPO-5 except difference in WHSV. 6 ml/min ethene and 2.7 ml/min cis-2-butene were used over 5 mg catalysts to give a WHSV of 23 h^{-1}. Ethene and cis-2-butene partial pressures were 10 and 4.5 kPa close to a 2: 1 ratio. Figure 7.26A shows the selectivity over H-SSZ-24 versus temperature. Selectivity to iso-butene increased linearly with temperatures from 25 to 58 %. C_5s and propene on the other hand decreased with temperature from 40 to 15 % and 31 to 25 % respectively. Propene to C_5s selectivity ratio increased with increasing temperature such that after 723 K, propene was more than C_5s. About 3 % selectivity to n-butane was observed throughout while 1 % iso-butane was observed at the initial temperatures. Figure 7.26B shows the rate of reaction over H-SSZ-24 versus temperature. The overall rate increased slowly between 673 and 748 K, and then rapidly with temperature. The rate of iso-butene formation increased slowly at the lower temperature region and then exponentially at the high temperature region. The rate of C_5s formation increased slightly at the lower temperature region but levelled off at high temperature region. Propene on the hand increased with temperature at all temperature regions. Figure 7.26C shows logarithm of the rate of reaction versus the reciprocal of temperature. The apparent activation

energies for the overall reaction, iso-butene, C_5s and propene formations rates at lower temperature region were 30±3, 52±5, 16±5 and 28±3 kJ/mol respectively. At the high temperature region, the apparent activation energies for the overall reaction, iso-butene, C_5s and propene formation rates were 53±4, 77±6, 11±3 and 39±3 kJ/mol respectively.

7.2 Discussion

At chapter 6, the role of linear butene in ethene alkylation reaction over H-SAPO-5 and H-SSZ-24 were examined and two competing pathways were proposed; isomerization to iso-butene and dimerization-cracking to propene and pentenes. In this chapter, we examined the role of linear butene and ethene in the mechanism over these catalysts. Particularly, how much does ethene influence the reaction when linear butenes are formed? The next section therefore examines this based on kinetic observations made over H-SAPO-5 and then followed by a comparison over H-SSZ-24.

7.2.1 Ethene and Linear butene co-reaction over H-SAPO-5

Generally, it was observed that the co-reaction over H-SAPO-5 showed propene, iso-butene and C_5s as the main products especially at 748 and 823 K, irrespective of the varying conditions. The trend in product distribution was quite similar to what was observed when cis-2-butene was fed alone except that propene in most cases was more abundant than C_5s in the co-reaction especially with increasing ethene partial pressure. In the cis-2-butene reactions, it was suggested that over fresh catalysts, some few C_5s further crack into propene and ethene. In the co-feed reaction, ethene is considered as a reactant and this comparison cannot be made directly. However, at $\frac{P_{ethene}}{P_{cis-2-butene}} > 5$, propene selectivity was higher than C_5s selectivity over the entire TOS even as the catalyst deactivated (Figures 7.4-7.6). This indicated there were extra propene produced aside those from the linear butene dimerization-cracking in the co-reaction.

When contact times were varied at 748 K (Figure 7.7), iso-butene, propene and C_5s were the main products with selectivities above 10 % as conversions approached 0 %. Moreover the conversions approached 0 % at 0 h.g/g contact times similar to the observations when cis-2-butene was fed alone (Figure 6.5). The main difference therefore between the selectivities for the co-feed compared with the cis-2-butene reactions is the increase in the selectivity to propene formation. When cis-2-butene partial pressures were varied in the co-reaction, propene and C_5s formations were second

order while iso-butene formation was first order at 748 and 823 K. When ethene partial pressures were varied, the reaction rate's dependence on ethene was generally low especially $\frac{P_{ethene}}{P_{cis-2-butene}} < 5$. Propene formation was first order between 24 and 40 kPa at 748 K. At 673 K propene dependence on ethene was first order between 4 and 24 kPa while at 823 K, this dependence was observed after 24 kPa. As a result, the general increase in the amount of propene is most likely to be due to ethylation of linear butene and cracking to form extra propene aside the usual dimerization-cracking of linear butene.

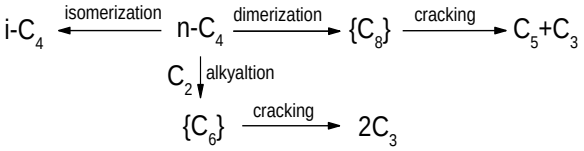

Scheme 7.1

To generate a reaction sequence for the co-reaction, we can summarize the pathway for the initial products formation for the co-reaction as shown in Scheme 7.1. By this scheme, an additional pathway alkylation-cracking has been added to the two pathways when linear butene reacts alone. This implies that rate expressions generated earlier in the linear butene reactions will change slightly for iso-butene and C_5s in terms of coverage while that for propene is expected to be affected even more by the additional pathway. For simplicity and continuity, we will use the assumptions and Equations derived earlier for linear butene reactions. Where amendments are made, they will be stated. Ethene can adsorb either on a Brønsted or 'Lewis' site. It has been reported that the heat of adsorption increases with chain length with about 5 kJ/mol per carbon [88] on amorphous silica and about 12 kJ/mol per carbon on H-MFI zeolite[89]. While these measurements were done for alkanes and alkenes over the amorphous silica, only alkanes were measured over H-MFI because of the faster reactivity of alkenes. If we assume that relative heat of adsorption per carbon follow similar trends over the H-SAPO-5 for alkenes, then ethene will most probably compete less for the Brønsted site compared to any adjacent site which we assumed earlier (Section 6.2.1) to be a sort of 'Lewis acid site'. This is also reasonable with our observations since, the formation of iso-butene which occurs mainly at the Brønsted site[86] was not much affected when ethene was fed. Hence we will consider that the ethene adsorbs on a 'Lewis site' (Equation 7.1) near a Brønsted site which has adsorbed a linear butene. Then the two react to form a C_6 given by Equation 7.2. We can also assume here that the alkylate cracks on desorption as given by Equation 7.3 since the amount of C_6s observed was very low.

$$C_2 + L = C_2L \qquad 7.1$$

$$n - C_4HB + C_2L \rightarrow C_6HB + L \quad 7.2$$

$$C_6HB = 2C_3 + HB \quad 7.3$$

If we consider the adsorption and desorption steps to be at equilibrium just as was done for the linear butene reactions, then the coverage can be written as:

$$\theta_{C_2L} = \frac{K_7 P_{C_2}}{1 + K_2 P_{n-C_4} + K_7 P_{C_2}} \quad 7.4$$

$$\theta_{HB} = \frac{1}{1 + K_1 P_{n-C_4} + K_{-5} P_{i-C_4} + K_{-6} P_{C_8} + K_{-9} {P_{C_3}}^2} \quad 7.5$$

$$\theta_L = \frac{1}{1 + K_2 P_{n-C_4} + K_7 P_{C_2}} \quad 7.6$$

Note that the equilibrium/rate constants in Equations 7.1, 7.2 and 7.3 corresponds to 7, 8 and 9 respectively as part (or continuation) of Equations 6.1 to 6.6 at chapter 6 (Section 6.2.1). We can recall that the propene formation rate as part of C_8 in the linear butene reaction was given as:

$$\frac{d(C_8)}{dt} \cong \frac{d(C_3)'}{dt} = k_4 \theta_{n-C_4HB} \theta_{n-C_4L} = k_4 K_1 K_2 {P_{n-C_4}}^2 \theta_{HB} \theta_L \quad 6.14$$

The rate of formation of propene in the co-reaction can then be written as;

$$\frac{d(C_3)}{dt} = k_4 \theta_{n-C_4HB} \theta_{n-C_4L} + k_8 \theta_{n-C_4HB} \theta_{C_2L} = k_4 K_1 K_2 {P_{n-C_4}}^2 \theta_{HB} \theta_L + k_8 K_1 K_7 P_{C_2} P_{n-C_4} \theta_{HB} \theta_L \quad 7.7$$

By this, it is expected that propene will depend on cis-2-butene second order when the first part of Equation 7.7 is dominating and first order when the second part dominates. This correlates well with our observations (Figures 7.9-7.14).When the propene formation rate from the co-reaction is divided by that from the linear butene reaction, a linear relation that depends on ethene and inverse to linear butene pressure is obtained as illustrated in Equation 7.8.

$$\frac{rate\ of\ C_3\ from\ co-feed}{rate\ of\ C_3\ from\ n-butene} = 1 + \frac{k_8 K_7 P_{C_2}}{k_4 K_2 P_{n-C_4}} \quad 7.8$$

A plot of the rate of propene formation from the co-reaction divided by that from linear butene reaction versus ethene partial pressure at a constant cis-2-butene pressure (4.5 kPa) and temperatures of 673, 748 and 823 K over H-SAPO-5 are shown in Figure 7.27. The ratio of the propene rates increased linearly at different ethene partial pressure range at the different temperatures; the lower the temperature the higher the effect of ethene. This can be attributed to an

increase in ethene adsorption at the catalyst surface per collision at lower temperature (increase in sticking co-efficient). At 673 K, the effect of ethene reached maxima at 24 kPa and then gently declined with ethene pressure. It was observed that at similar partial pressures, propene formation rate declined sharply while both C_5s and iso-butene selectivity gently increased after the 24 kPa (Figure 7.12). One possibility is ethylation of propene into C_5s, but the gentle rise in C_5s formation does not correspond to the rather sharper decline of propene, as well as this cannot explain the increase in iso-butene formation. It is also possible that at 673 K, high ethene concentration could lead to further ethylation of C_6s to C_8s or ethene dimerizes and isomerizes therefore allowing some iso-butene and C_5s formation to increase to catch up with propene. This may sound contradictory to the earlier assumed cis-2-butene adsorption at mostly Brønsted acid sites at the expense of ethene, however, at low temperature sticking co-efficient is increased, and increasing ethene concentration on surface increases the chances of ethene adsorbing on Brønsted acid sites as well. As a results, the reaction can become complex and subsequent reactions could occur. However all this possibilities seems to be limited to reactions at 678 K since at other higher temperatures this was not observed. Also, the observed decrease in propene and increasing iso-butene formation rates after 24 kPa suggests that ethylation of iso-butene at such a high ethene concentration is less likely.

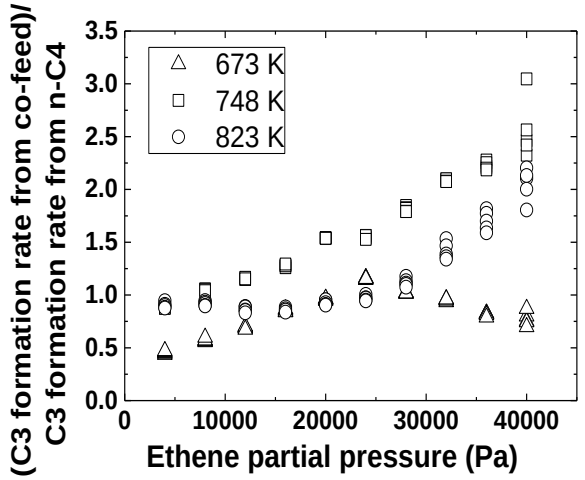

Figure 7.27: Propene formation rates from co-feed/n-butene versus ethene partial pressure over H-SAPO-5: H-SAPO-5 mass= 50 mg, $P_{cis\text{-}2\text{-}butene}$= 4.5 kPa

Furthermore, to interpret the apparent activation energies (Eapp), the formation rates were differentiated to obtain a relation between the intrinsic activation energy (Ea), coverage (θ) and enthalpies of adsorption (ΔH). These have been shown in Equations 7.9 to 7.11.

$$Eapp(iC_4) = Ea_3 + \left(1 - \theta_{n-C_4HB}\right)\Delta H_1 + \Delta H_5\theta_{i-C_4HB} + \Delta H_6\theta_{C_8HB} + \Delta H_9\theta_{C_6HB} \quad 7.9$$

$$Eapp(C_5) = Ea_4 + \left(1 - \theta_{n-C_4HB}\right)\Delta H_1 + (1 - \theta_{n-C_4L})\Delta H_2 + \Delta H_5\theta_{i-C_4HB} + \Delta H_6\theta_{C_8HB} - \Delta H_7\theta_{C_2L} + \Delta H_9\theta_{C_6HB} \quad 7.10$$

$$Eapp(C_3) = Ea_4 + Ea_8 + 2\left(1 - \theta_{n-C_4HB}\right)\Delta H_1 + (1 - 2\theta_{n-C_4L})\Delta H_2 + 2\Delta H_5\theta_{i-C_4HB} + 2\Delta H_6\theta_{C_8HB} + (1 - 2\theta_{C_2L})\Delta H_7 + 2\Delta H_9\theta_{C_6HB} \quad 7.11$$

Table 7.1: Summary of apparent activation energies over H-SAPO-5 for co-feed

Temperature range/K	Iso-butene	Propene	C5s
673-723	3±4	-5±6	-29±5
748-823	54±4	11±3	-8±2

Table 7.1 shows a summary of the Eapp for the co-reaction. When we compare these with those obtained for the linear butene feed reactions (Table 6.1), it is expected that the extra coverage due to ethylation of linear butene will lead to some differences in the Eapp. Iso-butene for instance, has $\Delta H_9\theta_{C_6HB}$ term which contributes negatively to lower the Eapp value particular at low temperature range when coverage was expected to be high. C_5s' Eapp expression has $\Delta H_9\theta_{C_6HB}$ term which contributes negatively and $\Delta H_7\theta_{C_2L}$ term which contributes positively on increasing coverage. However since, the adsorption enthalpies are higher for longer chains[87], the influence of $\Delta H_9\theta_{C_6HB}$ term is expected to be higher and hence more negative Eapp was observed in the lower temperature range. The Eapp expression for propene has several coverage parameters that negatively affect its value more than that of C_5s. However the Eapp for propene was relatively more positive compared to C5s, because of the presence of Ea_8 which makes it still show a more positive Eapp compared to that of C_5s.

7.2.2 Influence of acid strength on co-feed reactions (H-SAPO-5 and H-SSZ-24 compared)

Figure 7.28 shows a comparison of the co-reaction activity over H-SAPO-5 and H-SSZ-24; conversion of co-feed versus the amounts of co-feed conversion accumulated per gram catalyst over 550 min TOS at 748 K. Even at 10 times H-SSZ-24 WHSV, initial co-feed conversion was more than twice that of H-SAPO-5. The H-SSZ-24 showed a faster deactivation than H-SAPO-5 at initial time on streams though they eventually crossed at a point. After this point the deactivation rates were similar. It is also important to note that the product distribution over H-SSZ-24 at 748 K showed roughly an equal selectivity to iso-butene, propene and C_5s over the TOS (Figure 7.17) which was different from what was observed over H-SAPO-5 (Figures 7.2) where iso-butene

selectivity was distinctly higher than propene and C_5s selectivities. This difference is likely to be due to the rapid deactivation of the H-SSZ-24 at 748 K. Hence, the co-feed reaction showed more influence of deactivation on selectivity over H-SSZ-24 than over H-SAPO-5.

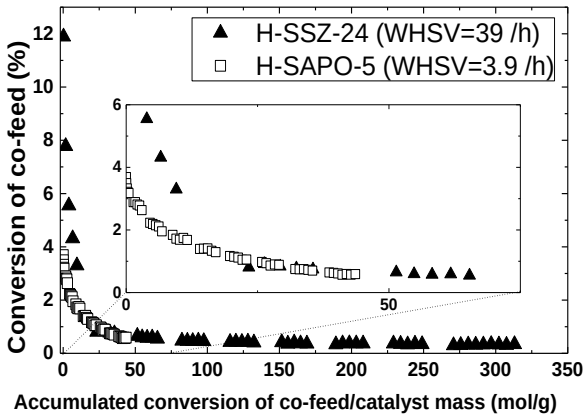

Figure 7.28: Conversion of co-feed over H-SAPO-5 and H-SSZ-24 versus accumulated ethene per catalyst mass over 550 min TOS: P_{Ethene}= 10 kPa, $P_{Cis\text{-}2\text{-}butene}$= 4.5 kPa, T= 748 K

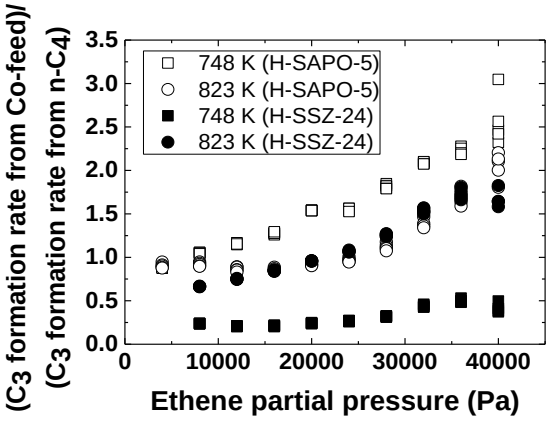

Figure 7.29: Propene formation rates from co-feed over that from cis-2-butene versus ethene partial pressure over H-SAPO-5 and H-SSZ-24: $P_{cis\text{-}2\text{-}butene}$= 4.5 kPa

Over H-SAPO-5, reaction between ethene and cis-2-butene was suggested to be responsible for the extra formation of propene aside those from dimerization-cracking of linear butene. Over H-SSZ-24, pressure variation of ethene and cis-2-butene showed similar results as was observed over H-SAPO-5. The main difference was the difference in activity which was also observed when cis-2-butene was fed alone. This suggested that just like linear butene reaction was similar over both catalysts, so is the co-reaction. Figure 7.29 shows a plot of propene from co-feed divided by propene from cis-2butene versus ethene partial pressure over H-SAPO-5 and H-SSZ-24 at 748 and 823 K. This plot was based on Equation 7.8 which compares the rate expressions derived for the co-feed reaction and compared with that of linear butene reaction. The propene formation rate over H-SSZ-24 increased with ethene partial pressure though was mild at 748 K. The influence of ethene over H-SSZ-24 was less at 748 K than at 823 K which was the reverse over H-SAPO-5. One can attribute this difference to the difference in adsorption equilibrium constants at different temperatures (see Figure 6.19). Note that Equation 7.8 had ethene adsorption constant K_7 in the numerator and cis-2-butene adsorption constant K_2 in the denominator. K_2 is expected to be much higher than K_7 based on the view that adsorption increases with chain length at lower temperature [87] such that the denominator can dominate until a high ethene concentration. However, since the

influence of temperature on adsorption is expected to be relatively similar over both catalysts, this possibility is less likely to account for the difference. The second possibility is basically due to the high influence of deactivation over H-SSZ-24 selectivity at 748 K. At 823 K, where H-SSZ-24 selectivities were less affected by deactivation, their trends appear to be similar to that of H-SAPO-5 at 748 K. Hence the difference illustrated in Figure 7.29 over the two catalysts was mainly due to the influence of deactivation at 748 K.

Table 7.2: Summary of apparent activation energies over H-SAPO-5 and H-SSZ-24

Temperature range/K	H-SAPO-5			H-SSZ-24		
	Iso-butene	Propene	C5s	Iso-butene	Propene	C5s
673-723	3±4	-5±6	-29±5	52±5	28±3	16±5
748-823	54±4	11±3	-8±2	77±5	39±3	11±3

Table 7.2 shows the apparent activation (Eapp) over H-SAPO-5 and H-SSZ-24. Generally, the Eapp for the co-feed over H-SSZ-24 were higher than those observed over H-SAPO-5. This was rather the opposite in the cis-2-butene experiments though the relative differences in the Eapp at the two temperature regions were similar. It is important to note that the difference in the WHSVs for the two set of experiment over the two catalysts were not the same. While for the cis-2-butene experiments, H-SSZ-24 WHSV was about 14 times that of H-SAPO-5, in the co-feed experiments the WHSV was about 10 times. This might have affected the relative coverage for the co-reaction compared to the linear butene reaction over the two catalysts particularly since the co-feed reaction had longer contact time (H-SAPO-5=47 and H-SSZ-24=4.7 s.g/g) than the cis-2-butene reactions (H-SAPO-5=31 and H-SSZ-25=2.2 s.g/g). This could have resulted in the differences in the magnitude of the Eapp for the co-feed and linear butene reactions. The trend in the Eapp were however similar for the co-feed reaction over both catalysts. Moreover, relative differences between the Eapp at the two temperature ranges for each product were lesser over H-SSZ-24 than H-SAPO-5 similar to what was observed for the linear butene reaction. This, similar to the conclusion for the linear butene reactions, could be due to lesser discrimination for H-SSZ-24 adsorption since it adsorbs faster (and stronger) than H-SAPO-5. Based on our Eapp expressions from Equations 7.8-7.11, we inferred that the differences observed for the activation energies (Eapp) at the different temperature ranges for H-SAPO-5 were mainly due to the relative coverage and its associated adsorption enthalpies. This is also expected for H-SSZ-24 though relatively lower compared with that of H-SAPO-5. One important component in the expressions which contribute positively to the Eapp is $\left(1-\theta_{n-C_4HB}\right)\Delta H_1$. The adsorption enthalpy, ΔH_1 is the only component that is associated

with Brønsted acid site and also contributes positively to the Eapp. Since H-SSZ-24 has stronger acid sites, they are expected to have a higher adsorption enthalpy than that of H-SAPO-5. Another component that could positively contribute to the Eapp for C_5s and propene is $\Delta H_7 \theta_{C_2L}$. However, this component is not found in the Eapp expression for iso-butene formation which also saw a significant increase over H-SSZ-24. Hence the differences in the Eapp can be attributed mainly to the difference in adsorptions which is inherently due to the difference in Brønsted acid strength of the catalysts.

7.3 SUMMARY

Co-reaction between linear butene and ethene over H-SAPO-5 showed similar primary products as was observed in linear butene reactions. The main difference was an increase is propene formation which was attributed to an extra alkylation-cracking pathway in addition to the linear butene dimerization-cracking pathway. The influence of ethene was mostly observed at $\frac{P_{ethene}}{P_{cis-2-butene}} > 4$ at 748 and 823 K, though it was observed at lower ratio at 673 K. Propene formation depended on ethene by roughly first order while C_5s and iso-butene were mostly zero order depending on the $\frac{P_{ethene}}{P_{cis-2-butene}}$ ratio. The high concentration of ethene needed to make extra propene coupled with other main products formed indicated their (propene) formation is via alkylation cracking. The apparent activation energies were distinct at two different temperature ranges; iso-butene = 3 kJ/mol, propene= -5 kJ/mol, pentene= -29 kJ/mol between 673 and 723 K, and then iso-butene = 54 kJ/mol, propene= 11 kJ/mol, pentene= -8 kJ/mol between 748 and 823 K. These were slightly different from that observed for the linear butene reactions and were mainly attributed to the additional adsorption of ethene and hexene which generally reduced the activation energies in the co-reaction. A kinetic scheme was proposed which correlated well with our observations.

Over H-SSZ-24, similar effect of ethene was observed at comparable conversions, hence similar mechanism was proposed over H-SSZ-24. The apparent activation energies at the two different temperature ranges were; iso-butene = 52 kJ/mol, propene= 28 kJ/mol, pentene= 16 kJ/mol between 673 and 723 K, and then iso-butene = 77 kJ/mol, propene= 39 kJ/mol, pentene= 11 kJ/mol between

748 and 823 K. The differences in the Eapp over the two catalysts were mainly attributed to the difference in Brønsted acid strength which in tend produces stronger adsorption over stronger sites. Although the apparent activation energy this time was more than that of the H-SAPO-5 which is the reverse in the linear butene reactions, difference in coverage as a result of the relative difference in WHSV for the respective experiments could be the reason. The trends in the Eapp however, were similar in both cases over both catalysts.

8. ETHENE REACTIONS

So far, linear butene reaction and co-reaction with ethene have been shown in Chapters 6 and 7. This chapter therefore seeks to connect the mechanism from ethene as reactants to what has earlier been discussed, first of all over H-SAPO-5 and then over H-SSZ-24.

8.1 Results

8.1.1 Ethene conversion over H-SAPO-5

8.1.1.1 Catalytic activity versus time on stream

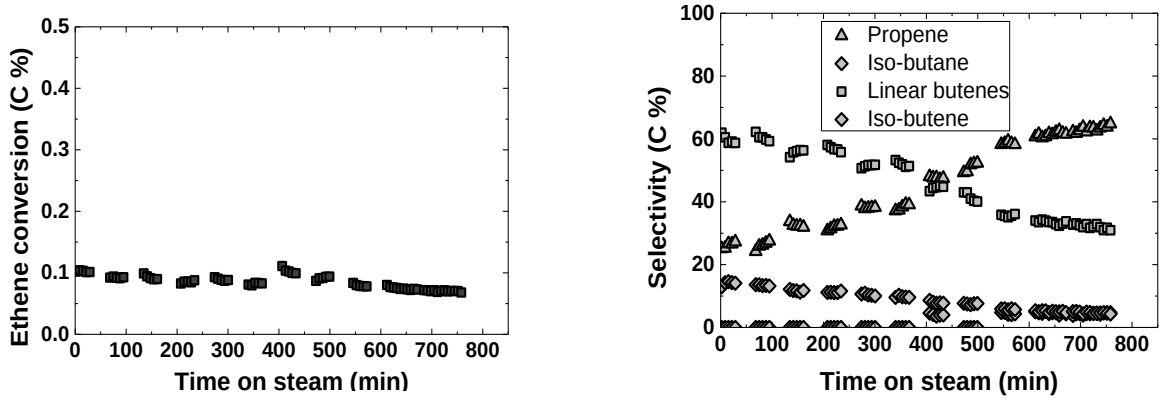

Figure 8.1: Catalytic activity of H-SAPO-5 versus time on stream, Conversion (left) and Selectivity (right), H-SAPO-5 mass=200 mg, $Flow_{total}$= 15ml/min, P_{Ethene}= 33.3 kPa, T= 673 K, WHSV = 0.58 h^{-1}.

Figure 8.1 shows the conversion and selectivity plot against time on stream (TOS) over H-SAPO-5 at 673 K, 0.58 h^{-1} WHSV and 33.3 kPa ethene partial pressure. The conversion observed was 0.1% and deactivated very gently. It must be noted that, lower temperatures than 673 K were used but the conversions were even much lower. The major products observed were linear butenes, propene, and iso-butene. The selectivity to linear butenes was 62 % at 2 min and declined to 31 % with TOS. The selectivity to propene on the other increased from 25 to 65 %. This suggested that propene depends on butene formation since it increased while the later decreased. The iso-butene decreased slowly from 14 to 4 % with TOS. About 5 % selectivity to iso-butane was observed after 400 min.

Figure 8.2 shows the conversion and selectivity versus TOS over H-SAPO-5 at 748 K, 0.47 h^{-1} WSHV and 33.3 kPa ethene partial pressure. About 0.4 % ethene conversion was observed at 2 min and slightly decreased to 0.3 % with TOS. The main products were similar to those observed at 673 K though the trend of selectivities was different. The linear butenes selectivity was 48 % followed by propene at 31 % and then iso-butene at 19 % at 2 min TOS. These selectivities remained relatively constant over the 540 min TOS. About 2 to 5 % total selectivity to methane and C_5s were observed as minor products over the TOS. The selectivity to methane was either equal or more than that of C_5s which suggested that their formations were independent since their approximate ratio was far less than $5C_5$s:1methane, a situation suggesting they were not formed from C_6 cracking. Hence the methane was probably formed from cracking of ethene.

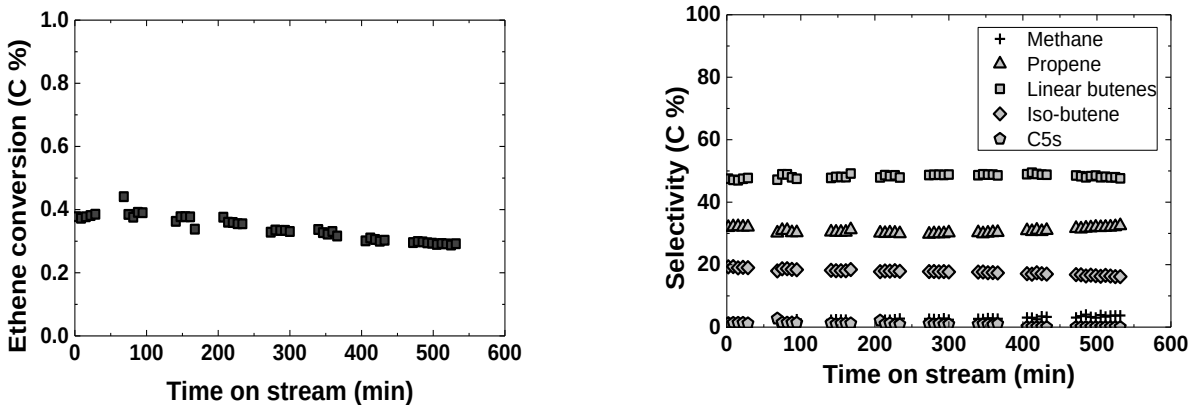

Figure 8.2: Catalytic activity of H-SAPO-5 versus time on stream, Conversion (left) and Selectivity (right), H-SAPO-5 mass=300 mg, $Flow_{total}$= 15ml/min, P_{Ethene}= 33.3 kPa, T= 748 K, WHSV = 0.47 h^{-1}

The selectivity variation at 748 K was mild compared to what was observed at 673 K. Propene selectivity for example at 748 K was about half of what was observed at 673 K. Though their WHSV differ slightly, the reaction at 748 K with slightly longer contact time (~1/WSHV) was expected to allow for subsequent secondary reaction. Since the reaction with slightly more contact time rather showed less changes in the selectivity over the TOS, the difference observed can be attributed mainly to the difference in temperatures suggesting that lower temperature favoured propene formation.

8.1.1.2 Contact time variation at 748 K

Figure 8.3 shows ethene conversion versus contact time over H-SAPO-5 at 748 K and 33.3 kPa ethene partial pressure between 0.23 to 0.78 h^{-1} WHSV. 300 mg catalyst mass was used with 3 to 10 ml/min ethene flow rate. The fraction of ethene to the total gas flow (1/3) was kept constant to maintain a constant pressure. The ethene conversion was very slow at the initial contact times (CT) between 0.3 and 0.4 h.g/g but rapidly increased after this CT. This is an indication of autocatalysis [35], a situation where a product helps to increase reaction rate. When the conversions were extrapolated to 0 h CT, the conversion approached 0.1 % rather than 0 % probably due to uncertainty in the measurement at such a low conversion.

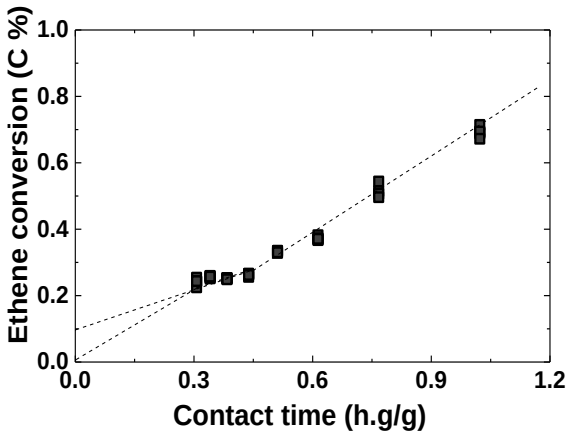

Figure 8.3: Ethene conversion versus contact time

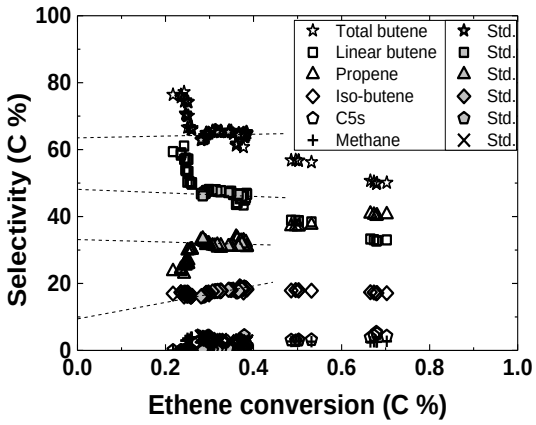

Figure 8.4: Selectivity versus ethene conversion

H-SAPO-5 mass=300 mg, $Flow_{total}$= 9-30 ml/min, P_{Ethene}= 33.3 kPa, T=748 K, WHSV= 0.23-0.78 h^{-1}. The Std. represents standard conditions measured in-between contact time variations.

Figure 8.4 shows the selectivity versus ethene conversion for different contact times over H-SAPO-5 at 748 K. The standard (Std.) contact time (=0.61 h.g/g) over the entire time on stream was included. Also total butenes selectivity was included in the plot to compare it trends with that of other products. Generally the selectivity of linear butenes was highest at 0.2 % conversion and declined from about 61 to 36 % with increasing conversion. Selectivity to propene followed which rather increased from 22 to 40 % with conversion. Note that, below 0.3 % conversion, there was a sharp decline of linear butenes selectivity and a corresponding sharp increase in propene selectivity. This indicates that propene is a secondary product formed from linear butenes. Iso-butene selectivity on the other hand of about 17 % increased very slightly with conversion. A closer look at the standard contact time that is within 0.3 and 0.4 % conversion, showed an increase in iso-butene relative to both the linear butenes and total butenes. Even though at other contact times iso-butene

selectivity was relatively stable, the increase at the standard contact time hints a possible formation of iso-butene from linear butenes. Minor selectivity to methane and C_5s were observed. Whiles methane selectivity stayed around 2 %, C_5s increased from 1 to 5 % with conversion.

8.1.1.3 Effect of ethene partial pressure on activity

The effect of ethene partial pressure over H-SAPO-5 was studied between 6.7 to 66.7 kPa ethene partial pressures at 673 K and 0.23 to 1.05 h^{-1} WHSV. The total gas flow was held constant at 15 ml/min while ethene flow was varied to vary it partial pressure. Figure 8.5A shows the selectivity versus ethene partial pressure. The selectivity to linear butenes and iso-butenes decreased from about 45 to 36 % and 15 % to 6 % respectively between 33.3 and 40 kPa after which they ascended up to about the same starting selectivities. Propene on the other hand increased from 40 % to 59 % between 33.3 and 40 kPa and decreased thereafter to 30 %. Some minor products such as iso-butane, n-butane and methane were also observed with selectivities noticeable from 33.3 kPa.

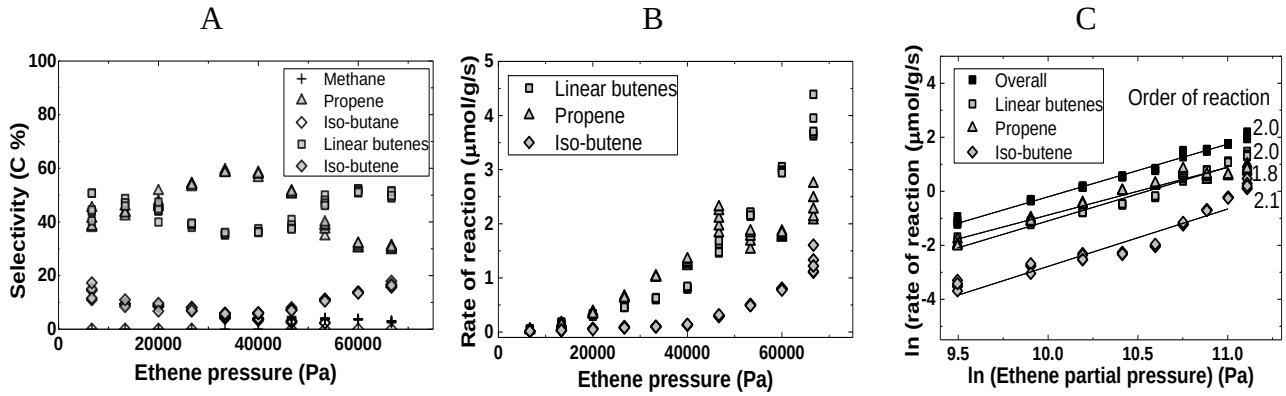

Figure 8.5: Effect of ethene partial pressure on selectivity (A), rate (B) and log-log plot of (B) as (C): H-SAPO-5 mass=200 mg, $Flow_{total}$= 15 ml/min, P_{Ethene}= 6.7-66.7 kPa T = 673 K, WHSV= 0.12-1.16 h^{-1}

Figure 8.5B shows the rate of formation of the main products versus ethene partial pressure at 673 K. The rate of formation of the linear butenes and iso-butene increased exponentially with pressure. The rate of formation for propene increased exponentially until 46.7 kPa when it leveled off. The reaction orders were obtained by plotting logarithm of reaction rate versus the logarithm of ethene partial pressure as shown in Figure 8.5C. The orders of reaction were estimated within 13.3-60 kPa

pressure range. The reaction orders for the overall, linear butene, propene and iso-butene formation rates were 2.0, 2.0, 1.8 and 2.1 respectively.

Figure 8.6A shows the selectivity versus ethene partial pressure at 748 K under similar conditions as was done at 673 K. The selectivity to the main products, linear butenes, propene and iso-butene varied very slightly with pressure. Selectivity to linear butenes and iso-butenes decreased slightly from 50 to 42 % and 16 to 12 % respectively between 13.3 and 40 kPa after which they ascended back to about the same starting selectivities. Selectivity to propene was relatively stable around 36 %. Selectivity to methane was observed to be 9 % maximum at 40 kPa and gradually declined to 3 %.The selectivities to the main products showed less variation with pressure compared to the reaction at 673 K.

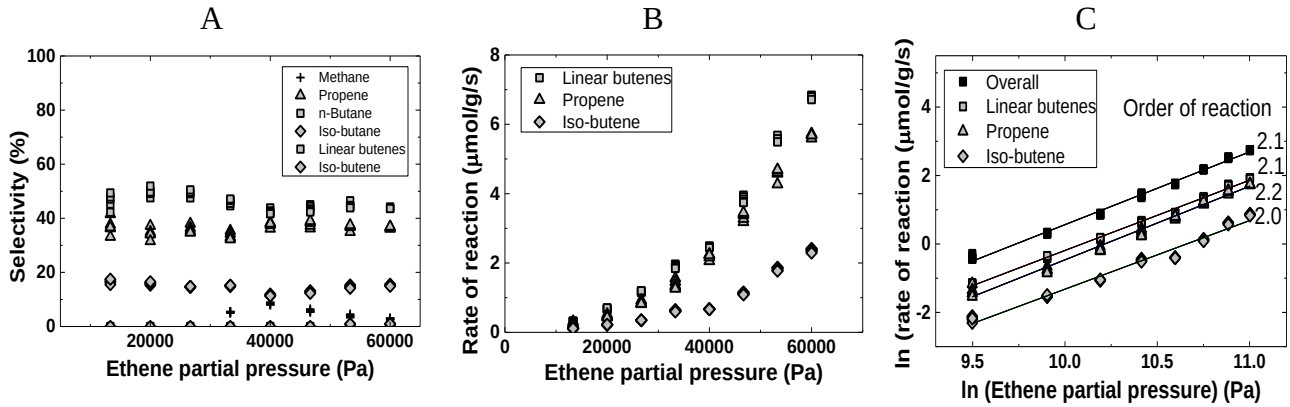

Figure 8.6: Effect of ethene partial pressure on selectivity (A), rate (B) and log-log plot of (B) as (C): H-SAPO-5 mass=200 mg, $Flow_{total}$= 15 ml/min, P_{ethene}= 13.3-60 kPa, T = 748 K, WHSV= 0.23-1.05 h^{-1}

Figure 8.6B shows the rate of formation for the main products versus ethene partial pressure at 748 K. The rate of formation of the products increased exponentially with pressure. A linear form of the graph in Figure 8.6B was plotted using logarithm of reaction rate versus logarithm of ethene partial pressure as shown in Figure 8.6C including the rate of the overall reaction to obtain the order of reaction. The reaction orders within 13.3-60 kPa were 2.1, 2.1, 2.2 and 2.0 for the overall reaction, linear butene, propene and iso-butene formation rates respectively. The reaction orders were just slightly higher than was observed at 673 K.

8.1.1.4 Effect of temperature on activity

The effect of the reaction temperature on the reaction was studied over H-SAPO-5 to analyse its effects on the selectivity and reaction rate in order to estimate the activation energy. This was done at 33.3 kPa ethene partial pressure, WHSV of 0.47 h^{-1} and between 673 to 823 K. 200 mg catalysts was used with 4 ml/min ethene flow rate. Figure 8.7A shows the selectivity versus temperature. The selectivity to linear butenes decreased from 60 % to 38 %, whilst propene and iso-butene selectivities increased from 25 to 36 % and 14 to 19 % respectively with temperature. This further indicates the dependence of propene and iso-butene on linear butenes. About 6 % selectivity to methane was observed between 773 and 823 K.

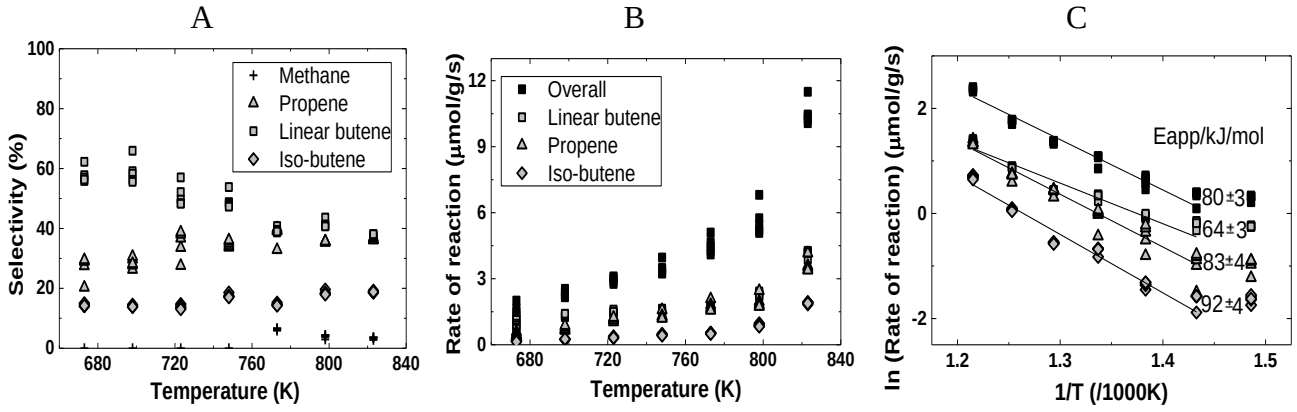

Figure 8.7: Effect of temperature on selectivity (A), rate (B) and log-log plot of (B) as (C): H-SAPO-5 mass=200 mg, $Flow_{total}$= 12 ml/min, P_{Ethene}= 33.3 kPa, T = 673-823 K, WHSV= 0.47 h^{-1}

Figure 8.7B shows the rate of reaction versus temperature. The overall reaction and the main products formation rates increased exponentially with temperature. Note that the rate's exponential dependence on temperature implied the reaction was not internal diffusion limited [35] as was discussed at the experimental section (Section 5.3.1). This exponential increase with temperature for all products differed from the reaction cis-2-butene and co-feed reactions where after 673 K, propene and iso-butene rates clearly moved in opposite pattern. This gives a hint that when ethene is the only reactant, iso-butene and propene formations are limited by ethene dimerization. To estimate the apparent activation energies, the logarithm of the rate versus the reciprocal of the temperature was plotted shown in Figure 8.7C. The apparent activation energy from the Arrhenius plot estimated from 698 to 823 K for the overall reaction, linear butene, propene and iso-butene formation rates were 80±3, 64±3, 83±4, and 92±4 kJ/mol respectively. Note that the rate between

673 and 698 K appeared not to differ and which deviated when the apparent activation energy was estimated, hence the 673 K rates were not included for a better correlation.

8.1.2 Ethene conversion over H-SSZ-24

8.1.2.1 Catalytic activity versus time on stream

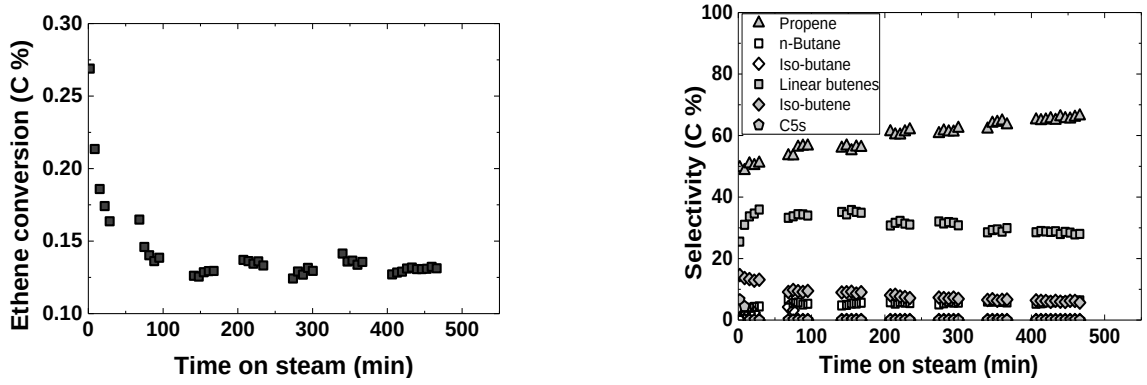

Figure 8.8: Catalytic activity of H-SSZ-24 versus time on stream, Conversion (left) and Selectivity (right), H-SSZ-24 mass=20 mg, $Flow_{total}$= 21 ml/min, P_{Ethene}= 33.3 kPa, WHSV = 8.1 h^{-1}, T= 673 K

Figure 8.8 shows the conversion and selectivity plot versus TOS using the H-SSZ-24 at 673 K, 8.1 h^{-1} WHSV and 33.3 kPa ethene partial pressure. Ethene conversion decreased initially from 0.3 % to about 0.1 % within 2 to 88 min and then remained relatively stable with TOS. The products observed were propene, linear butenes, iso-butene, and some butane, iso-butane and C_5s. Selectivity to propene increased from 49 to 66 % with TOS. Linear butene selectivity increased initially from 23 to 36 % within 2 to 29 min and then decreased slowly to 28 % with TOS. Selectivity to iso-butene decreased slowly from 15 to 7 % with TOS. About 6 % butane selectivity was observed, which remained relatively constant throughout the TOS. Up to 4 % selectivity to iso-butane was observed in the first 75 min TOS. C_5s selectivity up to 7 % was only observed at the initial time (2-9 min). When the selectivities are compared at 673 K between the two catalysts (Figures 7.1 and 7.8), the major products and their trend with TOS are similar though their relative amounts (selectivity %) differs.

Figure 8.9 shows the conversion and selectivity plot versus TOS using the H-SSZ-24 catalyst at 748 K and 33.3 kPa ethene partial pressure. Ethene conversion decreased rapidly from about 0.5 to 0.2 % between 2 to 95 min after which it decreased gently to 0.1 % with TOS. The main products were linear butene, propene and iso-butene, with some minor n-butane, C_5s and C_6s. The linear butenes selectivity increased from 23 to 58 % whilst propene selectivity decreased from 67 % to 29 % with TOS. Iso-butene selectivity also increased with TOS from 7 to 19 %. These observations were different from what was observed at 673 K, where propene selectivity rather increased whilst linear butene and iso-butene decreased with TOS. The selectivities to the n-butane, C_5s and C_6+ were mostly observed at the initial TOS between 2 to 29 min with 6 % total selectivity.

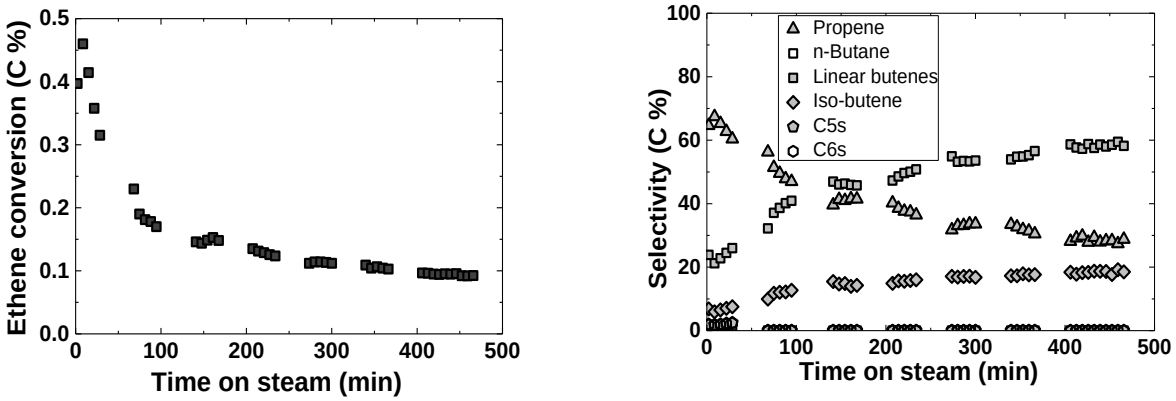

Figure 8.9: Catalytic activity of H-SSZ-24 versus time on stream, Conversion (left) and Selectivity (right), H-SSZ-24 mass=20 mg, $Flow_{total}$= 21 ml/min, P_{Ethene}= 33.3 kPa, WHSV = 8.1 h^{-1}, T= 748 K

When we compare the selectivities at 748 K between the two catalysts (Figures 8.2 and 8.9), the product selectivities varied a lot with the H-SSZ-24. This which could be due to the rapid deactivation observed over the H-SSZ-24 compared with that over H-SAPO-5. After the rapid deactivation in the H-SSZ-24 (95 min TOS), the trend variation minimized as the selectivities to the major products stabilized similar to what was observed over H-SAPO-5. The effect of deactivation on selectivity was therefore more important over H-SSZ-24 than H-SAPO-5.

8.1.2.2 Contact time variation at 748 K

Over the H-SSZ-24, a wider range of WHSV from 0.7 to 11.6 h^{-1} was studied at 748 K and 33.3 kPa ethene partial pressure. The wider range was used because H-SSZ-24 showed high activity and a

narrow range might not be sufficiently representative. To obtain the wider range, three different masses of the catalyst were used because the mass flow controller of ethene flow is limited just between 1 to 10 ml/min. 20, 30, and 100 mg of catalyst were used. The fraction of ethene to total gas flow was kept at 1/3 to maintain the 33.3 kPa ethene partial pressure. Figure 8.11 shows the normalized conversion versus contact time over H-SSZ-24. The ethene conversion increased relatively slower between 0.02 to 0.08 h but increased rapidly with contact time (CT) afterward. When the conversion was extrapolated to 0 % h CT, the slower part approached 0 % while the rapid part approached negative conversion. This was an indication of autocatalytic effect similar to what was observed over the H-SAPO-5.

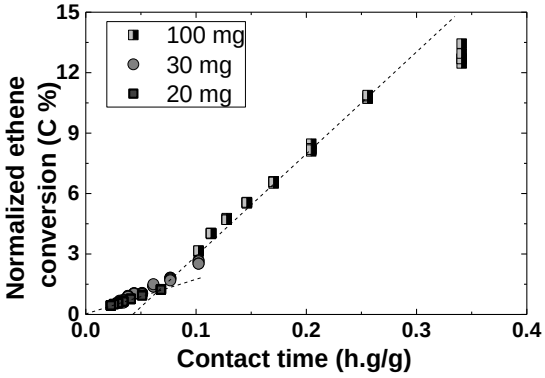

Figure 8.11: Normalized ethene conversion versus contact time

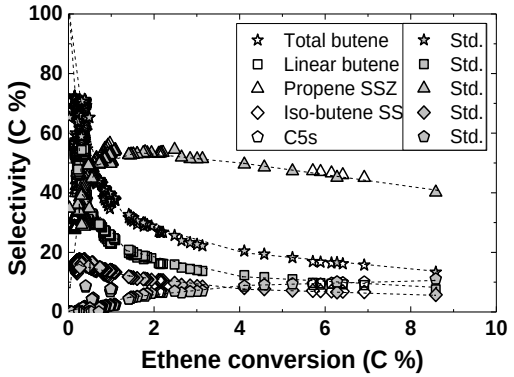

Figure 8.12: Selectivity versus ethene conversion

H-SSZ-24 mass=20, 30, 100 mg, $Flow_{total}$= 9-30 ml/min, P_{Ethene}= 33.3 kPa WHSV= 0.70-11.64 h^{-1}. The Std. represents standard conditions measured in-between contact time variations.

Figure 8.12 shows selectivities versus ethene conversion over H-SSZ-24. Linear butene selectivity once again rapidly decreased from 54 to 32 % with conversion in a similar trend as the total butenes. Iso-butene also decreased with conversion though not very rapid compared to the way total or linear butenes declined. Meanwhile propene selectivity increased rapidly at initial conversions but levelled off and eventually decreased with conversion. Below 1 % conversion, the rapid increase in the linear butene corresponded with the rapid decrease of propene. At the conversion when propene selectivity levelled off, C_5s selectivity also gradually increased. Although iso-butene selectivity this time slightly declined with conversion, it is important to note that propene as well declined as well as more C_5s are formed. Hence it is possible that above 1 % conversion the reaction becomes more complex. When selectivities were extrapolated to 0 % conversion, linear butene selectivity merges with the total butene selectivity which approaches 100 % and propene approaches 0 %. Iso-butene however showed a quick turn at low conversions (<0.4 %) and can either follow propene to 0 % or some selectivity below 10 %. While it is clear that propene is a

secondary product formed from linear butenes which is a primary product, it is not very certain from this experiment, the stand of iso-butene though it hints towards been a secondary product also formed from linear butenes.

8.1.2.3 Effect of ethene partial pressure on activity

The effect of ethene partial pressure over H-SSZ-24 was studied between 16.7 to 41.7 kPa ethene partial pressures at 673 and 748 K with WHSV between 4.7 to 11.6 h^{-1} where conversions were below 1 %. Figure 8.13A shows the selectivity versus ethene partial pressure at 673 K. Selectivities to linear butenes and iso-butene decreased from 24 to 21 % and 7 to 6 % between 16.7 and 25 kPa and then ascended to 31 and 14 % respectively with pressure. Propene selectivity at similar pressures increased from 63 to 66 % and decreased to 49 %. Selectivity for n-butane and iso-butane were about 6 and 3 % respectively. The n-butane remained relatively stable at all pressures whilst 3 % iso-butane selectivity appeared between 33.3 to 41.7 kPa.

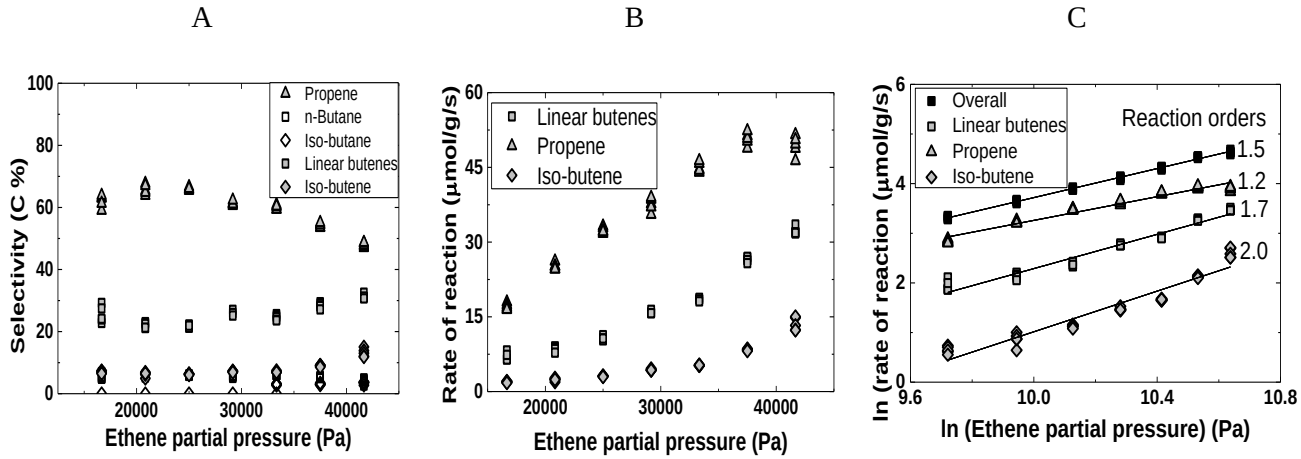

Figure 8.13: Effect of ethene partial pressure on selectivity (A), rate (B) and log-log plot of (B) as (C): H-SSZ-24 mass=20 mg, $Flow_{total}$= 24 ml/min, $Flow_{total}$= 12-30 ml/min, P_{Ethene}= 16.7-41.7 kPa, T = 673 K, WHSV= 4.7-11.6 h^{-1}

Figure 8.13B shows the rate of formation of the main products versus ethene partial pressure at 673 K. The rate of formation of the linear butenes and iso-butene increased exponentially with pressure. The propene formation rate increased relatively linearly until 36.7 kPa where it leveled off. The reaction order was obtained by plotting a linear form of the graph in Figure 8.13B with the inclusion of the overall rate using logarithm of reaction rate and logarithm of ethene partial pressure as shown

in Figure 8.13C. The overall, linear butene, propene and iso-butene formation rate reaction orders were 1.5, 1.7, 1.2 and 2.0 respectively.

The effect of ethene partial pressure for the reaction over the H-SSZ-24 was also studied at 748 K. Figure 8.14A shows the selectivity versus ethene partial pressure at 748 K. Selectivity to linear butene increased from 38 to 59 % between 16.7 and 25 kPa and then decreased to 33 % 41.7 kPa. Propene selectivity decreased in opposite direction to that of linear butenes from 43 to 31 % and increased to 56 %. Selectivity to iso-butene increased and decreased slightly from 10 to 13 % and back to 10 % at similar pressures. Some selectivity to methane, n-butane and C_6s were observed. 10 % selectivity to C_6s was observed at 16.7 kPa but quickly disappeared with ethene partial pressure. The selectivities of the rest of the minor products totaled about 4 % with ethene partial pressure.

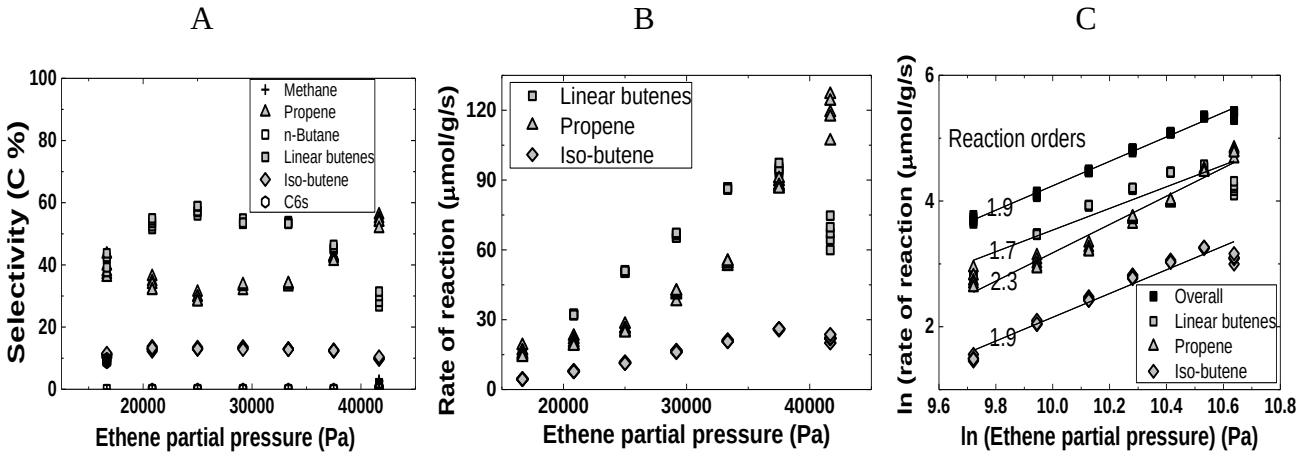

Figure 8.14: Effect of ethene partial pressure on selectivity (A), rate (B) and log-log plot of (B) as (C): H-SSZ-24 mass=20 mg, $Flow_{total}$= 24 ml/min, $Flow_{total}$= 12-30 ml/min, P_{Ethene}= 16.7-41.7 kPa, T = 748 K, WHSV= 4.66-11.64 h^{-1}

Figure 8.14 B shows the rate of formation of the main products versus ethene partial pressure at 748 K. The propene formation rate increased slightly more exponentially than the other main products. The order of reaction was obtained by plotting the logarithm of the reaction rates versus logarithm of ethene partial pressure as shown in Figure 8.14C with inclusion of the overall rate of reaction. The reaction orders within 16.7-41.7 kPa were 1.9, 1.7, 2.3 and 1.9 for the overall, linear butene, propene and iso-butene formation rates respectively. The orders of reaction at 748 K over the H-SSZ-24 were generally lower than that observed over H-SAPO-5 except for propene.

8.1.2.4 Effect of temperature on activity

The effect of the reaction temperature on the reaction was also studied over H-SSZ-24. This was done between 673 to 823 K at 33.3 kPa ethene partial pressure and 6.98 h^{-1} WHSV where conversions were below 1 %. Figure 8.15A shows the selectivity versus temperature. Selectivity to linear butene increased from 50 to 60 % between 673 and 723 K (low temperature region) and then decreased to 48 % at 823 K (high temperature region). Propene selectivity at similar temperatures varied in opposite direction to linear butenes such that it decreased from 35 to 26 % and increased to 34 %. Selectivity to iso-butene remained relatively stable at about 16 %. Up to 8 % C_6s at 673 K and 3 % of C_5s at 823 K were observed at the exact temperatures when propene selectivity was highest.

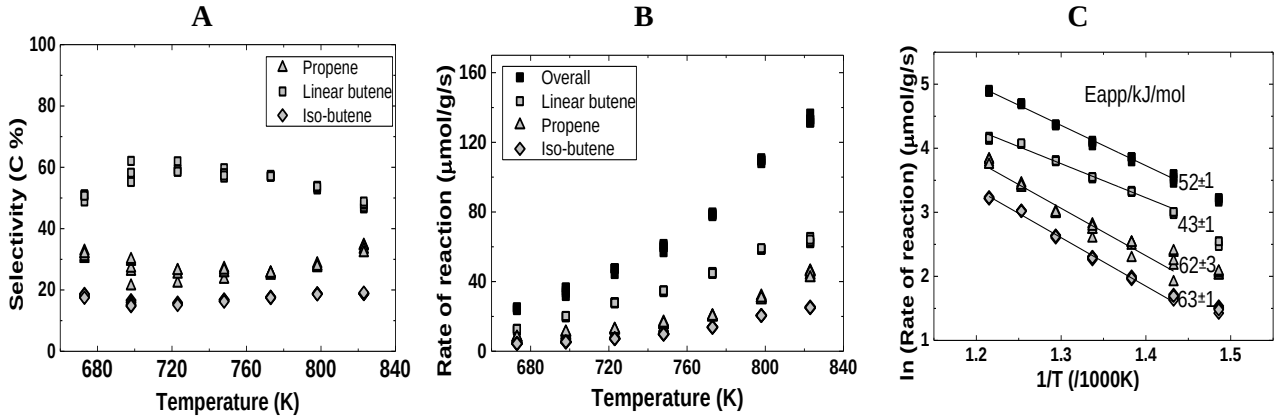

Figure 8.15: Effect of temperature on selectivity (A), rate (B) and log-log plot of (B) as (C): H-SSZ-24 mass=20 mg, $Flow_{total}$= 18 ml/min, P_{Ethene}= 33.3 kPa, T= 673-823 K, WHSV= 6.98 h^{-1}

Figure 8.15B shows the rate of reaction versus temperature. Generally, the overall reaction and the main products formation rates increased exponentially with temperature similar to what was observed over H-SAPO-5. Figure 8.15C shows a plot of the logarithm of the rate versus the reciprocal of the temperature. The apparent activation energy from the Arrhenius plot for the overall reaction, linear butene, propene and iso-butene formation rates between 698 and 823 K were 52±1, 43±1, 62±3 and 63±1 kJ/mol respectively. The estimate was made with 698 and 823 K just as was done over H-SAPO-5 for comparison.

8.2 Discussion

The results discussed in Sections 8.1.1 and 8.1.2 showed that the main products in ethene alkylation reaction over H-SAPO-5 and H-SSZ-24 are linear butene, propene and iso-butene. Propene, pentenes and iso-butene have already been observed as the main product when cis-2-butene was fed alone in Chapter 6 and also when co-reacted with ethene in Chapter 7. The propene and iso-butene were also observed as main product while pentene was a minor product during the ethene reaction. This indicates that, the ethene reaction can directly be linked to our earlier discussion particularly because similar products are involved. Also linear butene was observed as primary products in the ethene reaction. In the co-reaction, the influence of ethene was generally low even up to $\frac{P_{ethene}}{P_{cis-2-butene}} = 5$ at 748 K. This indicates that the linear butenes were very important intermediate in the ethene alkylation mechanism. This discussion will therefore be based on the role of ethene dimerization in the mechanism and a link to the secondary reactions over H-SAPO-5 and then H-SSZ-24.

8.2.1 Ethene reaction over H-SAPO-5

Generally very low ethene conversions were observed over H-SAPO-5 with linear butene, propene and iso-butene as the main products. The low ethene conversion was not surprising since the reaction involves ethyl carbenium ion [3], a primary carbenium ion which is less stable compared to other carbenium ions [33]. Despite this, conversions observed over H-SAPO-5 were still lower than other molecular sieves as reported by Lin et al [36] at nearly similar reaction conditions. This difference may be due to difference in pore dimensions, differences in acid strength and densities of the molecular sieves. The main products we observed were quite similar to theirs, with the exception of aromatics which were observed over H-ZSM-5. Large pore zeolites are reported to form poly aromatics quickly which are retained in the pores and are usually not observed [46]. Hence that could explain why aromatics were not observed over the H-SAPO-5 (and also H-SSZ-24).

Autocatalytic effect was observed (Figure 8.3) and the linear butenes decreased while propene increased and also a slightly increase in iso-butene selectivity with conversion over H-SAPO-5. This was in contrast to the cis-2-butene and co-reaction (Figures 6.4 and 6.7), where conversion increased linearly with contact time (no autocatalysis) coupled with relatively high conversions. For example cis-2-butene conversion at 0.004 h contact time and 4.5 kPa partial pressure was 3 % while ethene conversion at 1 h contact time and 33.3 kPa partial pressure was 0.7 %. Moreover, the co-reaction between ethene and cis-2-butene particularly at 748 and 823 K showed quite similar behavior as was observed for cis-2-butene reactions except for an increase in propene selectivity. This all points towards propene and iso-butenes as secondary products formed from linear butenes formed in ethene alkylation reaction.

In Chapters 6 and 7, it was suggested that the propene and iso-butene formation followed different pathways. When we join that of ethene reactions, the overall mechanism will be such that; from ethene to propene is ethene alkylation and cracking while iso-butene is via isomerization of ethene alkylate (linear butene). Scheme 8.1 shows a summary of the proposed mechanism for ethene alkylation. This is in agreement with the scheme shown earlier (Scheme 3.2) based on literature. It has already been suggested in literature that ethene oligomerizes into hexene and further cracks to form propene over zeolites [34, 36]. IR spectroscopy study has also revealed that iso-butene are formed as secondary products in ethene oligomerization over H-ZSM-5[37]. Our observation of minor products such as methane, pentenes (C_5s) and hexenes (C_6s) is an indication of random scission[7] of ethene alkylate.

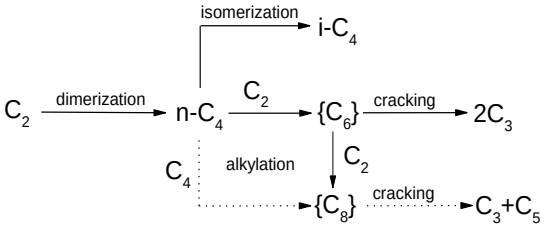

Scheme 8.1

Based on our data, sequence of reaction steps can be generated for the mechanism over H-SAPO-5. These steps will focus only the main products observed during the ethene feed reaction. We will also use similar assumptions as was made in Chapters 6 and 7. A second order of reaction was observed for the overall reaction and also for the formation of the main products at 673 and 748 K. Lin et al[36] also observed second order under similar conditions over H-ZSM-5. This suggested that the reaction depends on more than a single ethene. We can assume then that ethene adsorbs on a Brønsted acid site (HB) and the other near-by site we assumed to be a sort of 'Lewis site' (L) and

are illustrated in Equations 8.1 and 8.2 and subsequently reacts to form a linear butene, C_4 (Equation 8.3).

$$C_2 + HB = C_2HB \quad 8.1$$

$$C_2 + L = C_2B \quad 8.2$$

$$C_2HB + C_2L \rightarrow n - C_4HB + L \quad 8.3$$

The next step is the transformation of linear butene into iso-butene and propene. The iso-butene is formed via the skeletal isomerization of the linear butene (Equation 8.4) and C_6s via alkylation (Equation 8.5). It is also possible that ethene can alkylate iso-butene, however since it was observed not to be dominating during the co-reaction (Figure 7.27), we can assume it not as an initial reaction.

$$n - C_4HB \rightarrow i - C_4HB \quad 8.4$$

$$n - C_4HB + C_2L \rightarrow C_6H - B + L \quad 8.5$$

Desorption from the catalyst surface then gives the main products as indicated below. Since C_6s were observed in minor amount we assumed that they crack on desorption to form propene.

$$i - C_4HB = i - C_4 + HB \quad 8.6$$

$$C_6HB = 2C_3 + HB \quad 8.7$$

$$n - C_4HB = n - C_4 + HB \quad 8.8$$

If we assume that all the adsorption and desorption steps are in fast equilibrium, that is Equations 8.1, 8.2, 8.6 to 8.8, then coverage, θ can be written using Langmuir adsorption isotherm as follows;

$$\theta_{C_2HB} = \frac{K_1P_{C_2}}{1 + K_1P_{C_2} + K_{-6}P_{i-C_4} + K_{-7}{P_{C_3}}^2 + K_{-8}P_{n-C_4}} \quad 8.9$$

$$\theta_{HB} = \frac{1}{1 + K_1P_{C_2} + K_{-6}P_{i-C_4} + K_{-7}{P_{C_3}}^2 + K_{-8}P_{n-C_4}} \quad 8.10$$

$$\theta_{C_2L} = \frac{K_2P_{C_2}}{1 + K_2P_{C_2}} \quad 8.11$$

$$\theta_L = \frac{1}{1 + K_2P_{C_2}} \quad 8.12$$

The symbols mean the same as was stated in Chapter 6, except that the equilibrium/rate constants are written such that Equations 8.1- 8.8 corresponds to subscript 1-8 respectively. Previous experiments in Chapter 6 have already dealt with the formation of the secondary products (iso-butene and propene), hence we will only focus on the rate expression for the overall reaction, which turns to be determined by the formation of linear butenes in Equation 8.3.

The conversions per contact times (CT) for the cis-2-butene and the ethene reaction can be compared. While the highest ethene conversion was 0.7 % at 1.02 h.g/g CT, the lowest cis-2-butene conversion was 2.8 % at 0.0042 h.g/g CT. This represents a rate close to a 1000 faster in the cis-2-butene reaction than the ethene reaction despite just about one-seventh cis-2-butene (4.5 kPa) to ethene partial pressures used (33.3 kPa). Furthermore, the rate constants for the ethene reaction can be determined. Table 8.1 shows the reaction rate constant for the ethene reaction at 748 K. When a comparison is made with the cis-2-butene reaction (Table 6.2), propene formation for example rate constant was about 12000 higher than in the ethene reaction. Although the overall reaction as well as the iso-butene rate constants also show even larger order of magnitude difference, the units are not the same for both reactions. Hence the dimerization step which leads to the linear butene is the slowest step while the secondary reactions proceed faster.

Table 8.1: Reaction rate constant over H-SAPO-5 at 748 K and 33.3 kPa ethene partial pressure

$k_x = \frac{x\ reaction\ rate}{P_{C_2}{}^2}$	k / µmol/(gsPa^2)
$k_{over\ all}$	3.7 x10^{-9}
k_{C3}	1.2 x10^{-9}
k_{i-C4}	5.6 x10^{-10}
k_{n-C4}	1.7 x10^{-9}

We can therefore derive rate expression for the reaction by considering the Equation 8.3 as the slowest step, such that the overall rate is expressed in Equation 8.16, which will dominate when conversions are much lower than equilibrium conversions.

$$rate = k_3\theta_{C_2HB}\theta_{C_2L} = k_3K_1K_2P_{C_2}{}^2\theta_{HB}\theta_L \qquad 8.16$$

By this expression, the rate of reaction is second order dependent on ethene. Unlike the cis-2-butene reaction where the reaction order differed with the products of the two main pathways, here all products were second order. Another difference is that, temperature variations did not show so much distinction in the products distribution and so no strict adsorption site discrimination was observed compared to the cis-2-butene reactions. Hence whether Lewis sites were involved or not

in the ethene overall reaction expression will not matter so much, however since this effect was observed in the cis-2-butene reactions we will leave it as such. This also implies that the isomerization and alkylation-cracking processes were faster than the ethene dimerization since iso-butene and propene formations were similarly sensitive to coverage. When the rate expression is differentiated with temperature, an apparent activation energy (Eapp) expression that relates to the intrinsic activation energy (Ea) to adsorption enthalpies and coverage is obtained as shown in Equation 8.17.

$$Eapp = Ea_3 + \left(1 - \theta_{C_2HB}\right)\Delta H_1 + (1 - \theta_{C_2L})\Delta H_2 + \Delta H_6\theta_{i-C_4HB} + \Delta H_7\theta_{C_6HB} + \Delta H_8\theta_{n-C_4HB} \qquad 8.17$$

Table 8.2: Summary of apparent activation energies over H-SAPO-5 between 698-823 K in kJ/mol

Overall	Linear butene	Propene	Iso-butene
80±3	64±3	83±4	92±4

Table 8.2 shows a summary of the Eapp energy for the overall reaction as well as for the main products formation. The intrinsic activation energy for dimerization (Ea_3) is expected to be higher if the coverage and enthalpies are accounted for. Moreover, the Eapp for the ethene overall reaction is about twice that for the cis-2-butene reaction (Table 6.1) when compared at high temperatures. This explains why the rate of linear butene reactions was much faster than that of ethene. This indicates that higher energy is required for ethene to dimerize before the secondary reactions can proceed. The Eapp for the linear butenes was lower than those for propene and iso-butene. This also confirms the dependency of propene and iso-butene on linear butenes. Also, the Eapp for the formation of propene and iso-butene in the ethene reaction were much closer compared to what was observed when cis-2-butene was the reactant. This implies that after the formation of linear butenes, propene and iso-butene formations occur faster such that their distinction is minimized. This also supports the view that linear butene is formed first before the iso-butene and propene are formed.

8.2.2 Influence of acid strength on ethene reactions (H-SAPO-5 and H-SSZ-24 compared)

To compare the stability of the H-SAPO-5 and H-SSZ-24, the amounts of ethene accumulated per gram catalyst over 500 min TOS at 748 K versus ethene conversion % at different WHSVs were

plotted as shown in Figure 8.16. Initially, the conversion over H-SAPO-5 at 0.47 h^{-1} was lower than the conversion over H-SSZ-24 at 8.2 h^{-1} WHSV though they eventually crossed at a point. The H-SSZ-24 deactivated faster than H-SAPO-5 just at the initial time on stream but eventually deactivation was similar in both catalysts. Also the WHSVs needed for comparable conversion suggested that H-SSZ-24 was 17 times more active than H-SAPO-5. As suggested earlier, this was mainly due to the differences in acid strength rather than densities of the acids. Ding et al [90] reported that acid densities have a linear relationship on ethene oligomerization over H-ZSM-5. Since the estimated acid densities were 1 H-SAPO-5: 1.5 H-SSZ-24, it can be inferred that the acid strength increased ethene alkylation reaction to about 11 times.

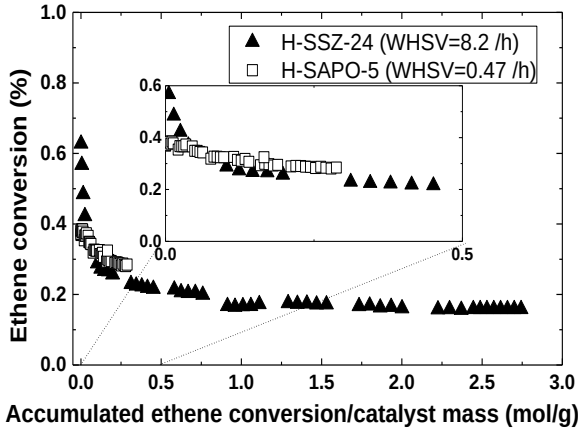

Figure 8.16: Ethene conversion over H-SAPO-5 and H-SSZ-24 versus accumulated ethene per catalyst mass over 500 min TOS

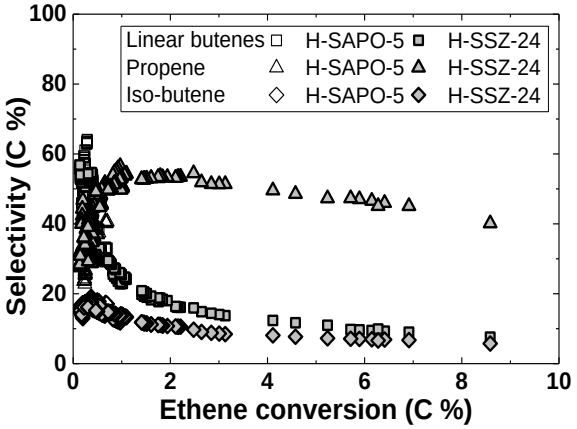

Figure 8.17: Selectivity versus ethene conversion over H-SAPO-5 and H-SSZ-24 P_{Ethene}= 33.3 kPa, T= 748 K

Over the H-SSZ-24, ethene alkylation showed autocatalytic effect similar to the observations over the H-SAPO-5 despite the difference in activity. Figure 8.17 shows the main product selectivity versus ethene conversion over both catalysts. The product distribution followed similar trend within the similar conversions (below 1 %). This confirms that the difference in acid strength did not significantly change the mechanism similar to the conclusion made for the cis-2-butene reactions (Chapter 6). This is also in agreement with the Lin et al[36] report that when H-ZSM-5 acidity was modified by phosphorus, only the activity for ethene conversions changed but no significant influence on product selectivity was observed.

The rate constant can also be estimated based on the pressure experiments. Over both H-SSZ-24 and H-SAPO-24 second order ethene dependence of the main products was observed. Table 8.3

shows the reaction rate constants over H-SAPO-5 and H-SSZ-24 based on the reaction rates and dependence on ethene partial pressure. Generally, the rate constants were very low for the ethene reaction (< 1000 times) for both catalysts compared to the linear butene reactions. In the ethene reaction, the rate constants were highest for linear butene, followed by propene and then iso-butene, an indication that linear butene formed faster than the other main products. The rate constant for the overall reaction rate over H-SSZ-24 was more than 39 times higher than the same over H-SAPO-5. This shows that the stronger the acid strength, the faster ethene alkylates.

Table 8.3: Reaction rate constant in µmol/(gsPa^2) over H-SAPO-5 at 748 K and 33.3 kPa ethene partial pressure

$k_x = \frac{x\ reaction\ rate}{P_{C_2}{}^2}$	H-SAPO-5	H-SSZ-24	$\frac{H-SSZ-24}{H-SAPO-5}$
$k_{over\ all}$	3.7 x10^{-9}	1.5 x10^{-7}	39
k_{C3}	1.2 x10^{-9}	4.9 x10^{-8}	39
k_{i-C4}	5.6 x10^{-10}	1.9 x10^{-8}	34
k_{n-C4}	1.7 x10^{-9}	7.8 x10^{-8}	45

Once again our observations can be compared with thermodynamics, similar to what was done in the linear butene reactions to see whether the reaction was controlled by thermodynamics at such a low rate constant. To do this, the inter-conversion of linear butene to propene can be analyzed as shown in Equations 8.18, the quotient Q calculated based on the concentration of the propene and linear butenes such as illustrated in Equation 8.19 and equilibrium constant, K_{eq} illustrated in Equation 8.20 and calculated from standard Gibbs free energy values[81]. A factor of 300 was multiplied as a pressure component ($\{P_{partial}/P_{total}\}^{3-4}$) in the *Q* expression because of the difference in stoichiometry in Equation 8.18. The ethene partial pressure was one-third of the total pressure and conversions were about 1 % for the results (temperature variation experiment) used for this analysis.

$$3n - C_4 = 4C_3 \qquad 8.18$$

$$Q = \frac{[C_3]^4}{[C_4]^3} \times \left(\frac{0.33}{100}\right)^{-1} \qquad 8.19$$

$$K_{eq} = e^{-(4\Delta G_{C3} - 3\Delta G_{C4})/RT} \qquad 8.20$$

Figure 8.18 shows the Q versus temperature over H-SAPO-5 and H-SSZ-24 compared with the K for the inter-conversion of linear butene to propene. The observed inter-conversion followed similar trend just as thermodynamics with increasing temperature. This implies that the distributions of products in the ethene reaction were controlled by thermodynamics. In that case, the stability of the products determines their distribution. This reasonable as the relative rates in dimerization is much lower compared with the faster secondary reactions. This could also explain why at high conversions in Figure 8.17 propene selectivity decreased while butene selectivity approached some stability, to approach a possible thermodynamic distribution.

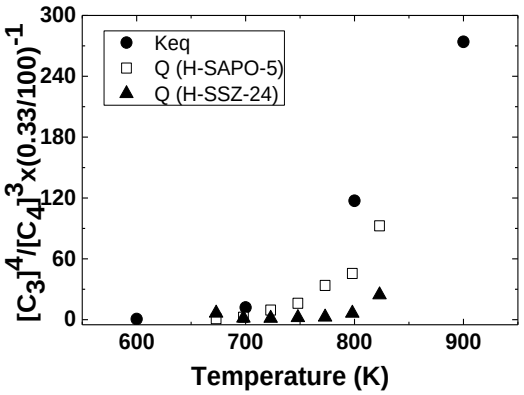

Figure 8.18: Q and K versus temperature

Table 8.4: Summary of apparent activation energies over H-SAPO-5 and H-SSZ-24, within 698-823 K

H-SAPO-5				H-SSZ-24			
Over all	**Linear butene**	**Propene**	**Iso-butene**	**Over all**	**Linear butene**	**Propene**	**Iso-butene**
80±3	64±3	83±4	92±4	52±1	43±1	62±3	63±1

The temperature variation experiment showed similar trends in product distribution over both catalysts. Table 8.4 shows a summary of the Eapp energy for the overall reaction as well as for the main products formation over both catalysts. Generally the Eapp over H-SSZ-24 was lower than what was observed over H-SAPO-5 which was also observed during the linear butene reaction and was attributed to the acid strength difference which allows for stronger adsorption in the H-SSZ-2. The Eapp for propene and iso-butene were almost the same over H-SSZ-24. This supports the view that acid strength influences dimerization of ethene but does not significantly discriminate between isomerization and alkylation-cracking. Also, the differences in Eapp support the view that the iso-butene and propene are formed from linear butene.

8.3 Summary

The kinetics studied over H-SAPO-5 for ethene alkylation reaction showed that linear butene is the primary product which either isomerizes to form iso-butene or alkylates and cracks to form propene. Autocatalytic effects as well as a second order rate in P_{ethene} with respect to linear butene, propene and iso-butene formation were observed. This coupled with linear butene reaction which was not autocatalytic suggested that ethene dimerization is a very important step in the mechanism. Moreover, the rate constant for formation of propene was observed to be about 1200 times larger in linear butene reaction compared with that of the ethene reaction. Kinetic rate expression was proposed for the overall reaction based on our data. No significant influence of temperature on the propene and iso-butene selectivities were observed in the ethene reaction compared with the significant difference during the linear butene reactions. This confirmed that the isomerization and alkylation-cracking reactions were much faster than the dimerization reactions. The apparent activation energies for the overall reaction, linear butene, propene and iso-butene formations between 698 and 823 K were 80, 64, 83 and 92 kJ/mol respectively.

Over H-SSZ-24, the product distributions when the various kinetic parameters were changed were very similar to what was observed over H-SAPO-5. The major difference was the activity, which was about 11 times faster than over H-SAPO-5, per number of acid sites. The rate constant for the overall reaction was 39 times higher in H-SSZ-24 than H-SAPO-5 at 748 K. The reactions over both catalysts were also observed to be controlled by thermodynamics with increasing temperature. The apparent activation energy over H-SSZ-24 for the overall reaction, linear butene, propene and iso-butene formations between 698 and 823 K were 52, 43, 62 and 63 kJ/mol respectively. These were lower than what was observed over H-SAPO-5 but followed similar trend. The virtually equal apparent activation energy of propene and iso-butene confirms that they are rapidly formed after ethene dimerization.

9. CONCLUSION AND FURTHER WORK

The kinetics of ethene alkylation reaction has been studied over H-SAPO-5 and H-SSZ-24 catalyst. These catalysts were used because they are one dimensional and have large pore size to minimize transition state or product restrictions. The main difference in these catalysts is their Brønsted acid strength which is stronger in H-SSZ-24 than H-SAPO-5 based on FTIR of CO adsorption. Moreover, their elemental composition based on Energy Dispersive Spectrometer was used to estimate their acid site density to be 1 H-SAPO-5: 1.5 H-SSZ-24.

The ethene reaction over H-SAPO-5 was very slow, autocatalytic and second order with respect to the main products formation at 673 and 748 K. The main products were linear butenes, propene and iso-butenes in that order. Contact time variation showed that the propene and to some extent iso-butene depended on linear butene formation. To investigate the importance of linear butene in the reaction, cis-2-butene was used as reactant. Here, no autocatalysis was observed coupled with iso-butene, propene and pentenes as the main products. Iso-butene was first order suggesting a direct isomerization of linear butenes while propene and pentenes were second order suggesting a dimerization-cracking of linear butenes. Temperature variation distinguished the two pathways such that at higher temperature the formation rates of iso-butene deviated from that of propene and pentenes. The apparent activation energies for the cis-2-butene reaction between 748 and 823 K were; iso-butene = 83 kJ/mol, propene = - 17 kJ/mol, pentene = -11 kJ/mol, and then; iso-butene = 42 kJ/mol, propene= 32 kJ/mol, pentene= 24 kJ/mol between 673 and 723 K. The differences in Eapp were attributed to differences in coverage at the different temperatures. This was different from the observations when ethene was the reactant, where there was less discrimination for the formation of propene and iso-butene. The apparent activation energies for the ethene reaction were; overall reaction = 80 kJ/mol, linear butene = 64 kJ/mol, propene = 83 kJ/mol and iso-butene = 92 kJ/mol between 698 and 823 K. This confirmed that linear butene formation determines the rate of ethene alkylation reaction.

Furthermore, co-reaction of ethene and cis-2-butene showed that ethene showed a significantly influenced propene formation after $\frac{P_{ethene}}{P_{cis-2-butene}} = 4$ at 748 and 823 K. The high concentration of ethene required before it influenced cis-2-butene further indicated the importance of linear butene in

ethene alkylation as well as alkylation-cracking leading to propene formation. In all cases, rate expressions were derived which correlated well with our data. Hence the mechanisms proposed for the ethene alkylation over H-SAPO-5 are as follows:

1. Ethene alkylates to form linear butenes which is the slowest step
2. Linear butene isomerizes to iso-butene
3. Further alkylation of linear butenes and cracking leads to propene and some pentenes.

Over H-SSZ-24, ethene, cis-2-butene and their co-reaction product distribution were very similar to the reactions observed over H-SAPO-5 at comparable conversions. The main difference was the activity which was very high in H-SSZ-24. When the acid densities of the two are considered as having a linear dependence on the activity, H-SSZ-24 is between 9 to 11 times more active than H-SAPO-5 for the ethene alkylation reactions. When the two catalyst selectivities where compared for cis-2-butene reactions, H-SSZ-24 was found to favour isomerization over dimerization-cracking more than H-SAPO-5 with about the same proportions as their acid densities. This indicated that acid strength favours both pathways without any particular preference. The apparent activation energies (Eapp) estimated for ethene reaction over the H-SSZ-24 between 698 and 823 K were 52, 43, 62 and 63 kJ/mol for the overall reaction, linear butenes, propene and iso-butene formations respectively. This was generally lower than what was observed over H-SAPO-5 with even closer Eapp for propene and iso-butene formation. This confirmed that propene and iso-butene formation are rapid provided linear butenes are formed when ethene is the reactant. The conclusion therefore is that acid strength only influences the rate of ethene alkylation reaction.

The ethene alkylation studied in this thesis is part of an on-going ethene oligomerization project in the Catalysis group. Other scientists in the group are studying other aspects to further understand the reaction. The following are some suggestions for continuation in relation with what was done in this thesis.

1. **Elemental analysis**: Other methods of elemental analysis will be important since the uncertainties in the EDS analysis from our observation were quite high. Atomic/Optical Emission Spectroscopy for example can be used to verify the elemental composition with better certainty.

2. **Acid site density determination**: The calculation of acid density was based on the elemental compositions rather than the specific concentration of acid sites. However, is it all the elements present that contribute to the creation of the acid site? FT-IR pyridine adsorption experiment for example can be used to measure the amount of the specific type of acid site present.
3. **Nature of AlOH in H-SSZ-24:** The exact nature of the AlOH was not known even though there were some suggestions. NMR for example can be used to probe the exact nature of this extra framework.
4. **Other site responsible for the dimerization:** In the linear butene experiment a second site other than Brønsted acid site was assumed to aid in dimerization. It will be interesting to probe this further. Was there really a second site? What is the nature of this site? How different is this site from the conventional Lewis acid site associated with defects? Further treatment of the catalyst and systematic follow-up with FTIR spectroscopy coupled with testing can give some valuable insight about this.
5. **Contact time experiment over H-SSZ-24**: We observed that contact time variation over H-SSZ-24 for the linear butene and co-reactions did not really follow a logical trend. Was this just a problem with deactivation or is it the actual case? It will be interesting to use H-SSZ-24 catalyst with relatively less acid sites than what was used here to analyse this further.
6. **Labelling experiment:** Labelled ethene ($^{13}CCH_4$) and unlabelled butene co-reaction can be used to verify the mechanism of propene formation. During the co-feed reaction at 673 K and $\frac{P_{ethene}}{P_{cis-2-butene}} > 6$, a gentle rise of isobutene and pentenes formation relative to the rapid decline of propene was observed. A labelled experiment will also help to substantiate the nature of the extra iso-butene and pentenes formations which can help better explain that observation.
7. **Influence of aromatics on the mechanism:** Despite the conclusion that aromatics do not take part in the skeletal isomerization of linear butenes, co-feeding an aromatic such as styrene with linear butenes can verify this. However, care must be taken since the catalysts used here deactivated relatively fast. If aromatics play a role, is it just for skeletal isomerization or does it restrict the formation of propene and pentenes or both?
8. **Coke analysis:** Despite no soluble coke observed in the H-SAPO-5 and H-SSZ-24, other methods can be used such as thermogravimetric analysis to estimate the amount of coke formed. CO and N_2 adsorption experiments can also help to know the available sites after the deactivation.

9. **Systematic analysing of coke:** All the coke analyses were done after an entire experiment which lasted more than 500 min TOS since parameters were varied on stream. However the changes in selectivity occurred mostly within 60 min TOS, a systematic analysis at shorter TOS at different reaction temperature will help to identify and distinguish between the nature of coke formed.

APPENDIX

A List of Chemicals used

All chemicals were from AGA.

During testing

Chemical	Purity
Ethene (2.5)	99.5
Cis-2-butene	99.0
Neon (4.5)	99.995
Helium (5)	99.999
Argon (4.6)	99.999

Calibration mixture composition/%

	Mixture 1	Mixture 2		Mixture 1	Mixture 2
He	5	5	Propene	2	2
Ar	67	67	N-butane	2	-
CO	-	5	Iso-butane	2	-
CO_2	-	2	Trans-2-butene	2	-
Methane	-	2	1-Butene	2	-
Ethene	10	5	Cis-2-butene	2	-
Ethane	1	10	Iso-butene	2	-
Propane	1	2	1,3-butadiene	2	-

Estimating relative retention times for C_5+ (% purity)

N-pentane	99	N-hexane	>97	Octane	>97
Iso-pentane	>99	2-methyl-2-pentane	>97	Benzene	99.9
1-Pentene	97	4-Methyl-1-pentene	98	p-Xylene	99
2-Methyl-2-butene	>99	N-heptane	99.5	m-Xylene	>99

B List of catalytic tests presented in this thesis

1. Cis-2-butene reactions

Parameter varied	Catalysts	Mass /mg	Total flow /mlmin^{-1}	WHSV / h^{-1}	P_{feed} /kPa	T /K
Contact time	H-SAPO-5	50	20-200	0.12-1.17	4.5	748
	H-SSZ-24	5	‘’	1.2-11.7	‘’	‘’
Pressure	H-SAPO-5	50	100	0.23-1.17	1.8-8.1	673
	H-SAPO-5	‘’	‘’	0.12-1.17	0.9-8.1	748
	H-SAPO-5	‘’	‘’	‘’	‘’	823
	H-SSZ-24	5	140	2.9-11.7	1.6-6.4	673
	H-SSZ-24	‘’	‘’	‘’	‘’	748
	H-SSZ-24	‘’	‘’	‘’	‘’	823
Temperature	H-SAPO-5	50	100	0.59	4.5	673-823
	H-SSZ-25	5	140	8.2	‘’	‘’

2. Ethene and cis-2-butene co-reaction

Parameter varied	Catalysts	Mass /mg	Total flow /mlmin^{-1}	WHSV / h^{-1}	P_{ethene} /kPa	$P_{cis\text{-}2\text{-}butene}$ /kPa	T /K
Contact time	H-SAPO-5	50	20-100	0.8-3.9	10	4.5	748
	H-SSZ-24	5	‘’	7.8-39	‘’	‘’	‘’
Pressure	H-SAPO-5	50	100	2.9-4.9	10	0.9-8.1	673
	H-SAPO-5	‘’	‘’	‘’	‘’	‘’	748
	H-SAPO-5	‘’	‘’	‘’	‘’	‘’	823
	H-SAPO-5	‘’	25	0.5-2.9	4-40	3.6	673
	H-SAPO-5	‘’	‘’	‘’	‘’	‘’	748
	H-SAPO-5	‘’	‘’	‘’	‘’	‘’	823
	H-SSZ-24	5	100	29-49	10	0.9-8.1	673
	H-SSZ-24	‘’	‘’	‘’	‘’	‘’	748
	H-SSZ-24	‘’	‘’	‘’	‘’	‘’	823
	H-SSZ-24	5	25	7.8-29	8-40	3.6	673
	H-SSZ-24	‘’	‘’	‘’	‘’	‘’	748
	H-SSZ-24	‘’	‘’	‘’	‘’	‘’	823
Temperature	H-SAPO-5	50	60	2.3	10	4.5	673-823
	H-SSZ-25	5	‘’	23	‘’	‘’	‘’

3. Ethene reaction

Parameter varied	Catalysts	Mass /mg	Total flow /mlmin^{-1}	WHSV / h^{-1}	P_{feed} /kPa	T /K
Contact time	H-SAPO-5	300	9-30	0.23-0.78	33.3	748
	H-SSZ-24	20,30,100	‘’	1.2-11.7	‘’	‘’
Pressure	H-SAPO-5	200	15	0.12-1.16	6.7-67	673
	H-SAPO-5	‘’	‘’	0.23-1.05	13.3-60	748
	H-SSZ-24	20	24	4.7-11.6	16.7-42	673
	H-SSZ-24	‘’	‘‘	‘’	‘’	748
Temperature	H-SAPO-5	200	12	0.47	33.3	673-823
	H-SSZ-25	5	18	6.98	‘’	‘’

C Temperature Profile

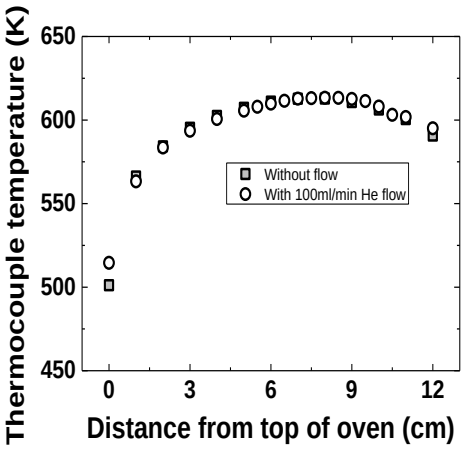

Figure C1: Temperature profiling diagram of the reactor at 623 K

Temperature profiling of the reactor was done to determine the isothermal zone in the oven before testing. This was done by lowering the thermocouple from the top of the oven down to the bottom and the corresponding temperatures measured. Figure C1 shows a plot of the temperature profile with and without gas flow at 623 K set-point temperature. The isothermal region was found to be between 7 and 8.5 cm from the top of the oven. The reactor bed was therefore positioned at 8 cm below the top of the oven.

D Normalization for deactivation

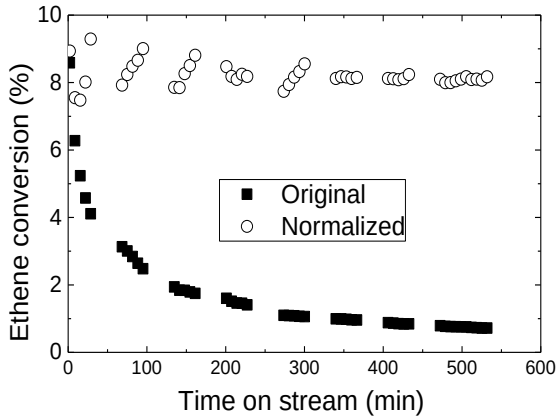

Figure D1: Original and normalized conversion versus TOS over H-SSZ-24

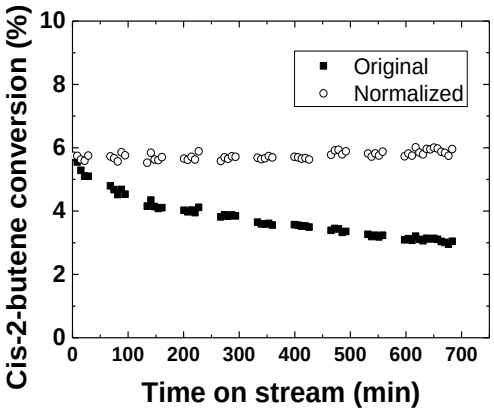

Figure D2: Original and normalized conversion versus TOS over H-SAPO-5

This was done by finding the slope (m) between two set of standards assuming to it to be a straight line with intercept (I_t). Then the original conversion (C_o) was normalized (C_N) within the particular time (t) on stream with the slope m_t and intercept (I_0) at 0 min time on stream given as:

$$C_N = \frac{(m_t \times t + I_t)I_0}{C_o}$$

E Testing for external diffusion

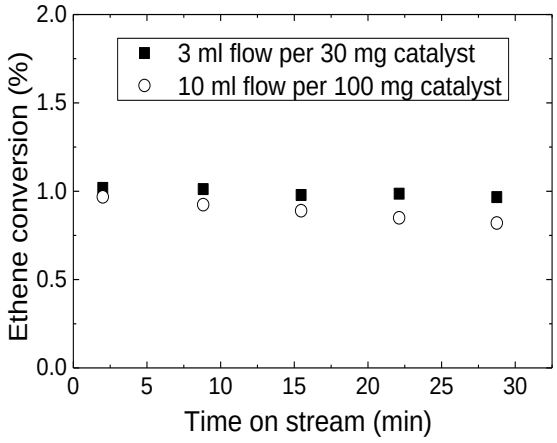

Figure E1: Conversion at similar WHSV over H-SSZ-24, H-SSZ-24, T= 748 K, WHSV= 0.70 h^{-1}, P_{ethene}= 33.3 kPa

Figure E1 shows ethene conversion versus TOS at different flow rate. The conversions were not dependent on flow velocity, an indication of minimal external diffusion limitation on the bed of the reactor.

F Typical butene selectivity over 650 min TOS

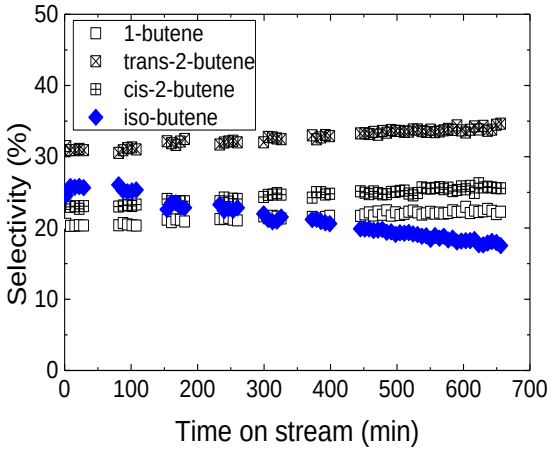

Figure F1: Typical linear butene composition H-SAPO-5 at 748 K, P_{Ethene}=33.3 kPa, WHSV = 0.47 h^{-1}

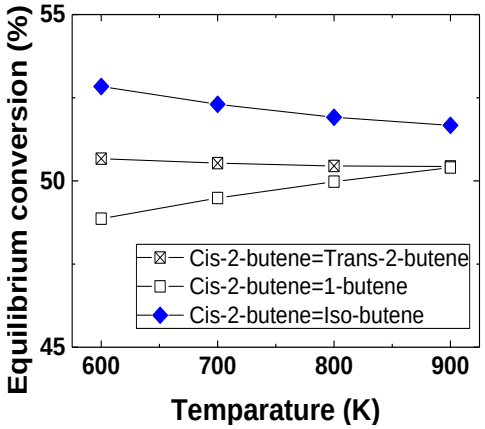

Figure F2: Thermodynamic equilibrium butene inter-conversion versus temperature

Figure F1 shows typical butene selectivity versus time on stream and Figure F2 is the thermodynamic equilibrium conversion of butenes. The linear butenes were in thermodynamic equilibrium, an indication that linear butene fast isomerization to equilibrium. Meanwhile iso-butene deviated from the linear butenes with relatively lower amount compared to the equilibrium conversions.

G Typical C_5s selectivity over 550 min TOS at 748 and 823 K

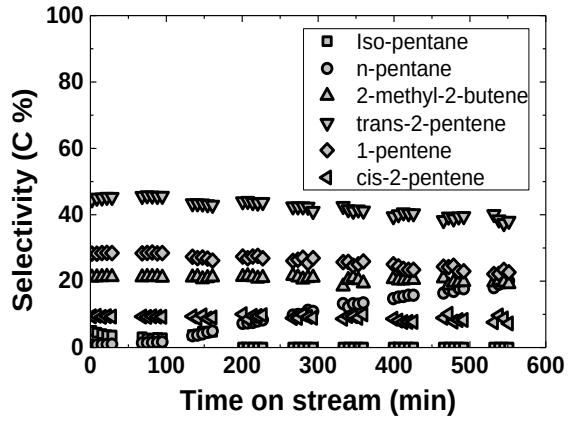

Figure G1: typical C5s composition at 748 K

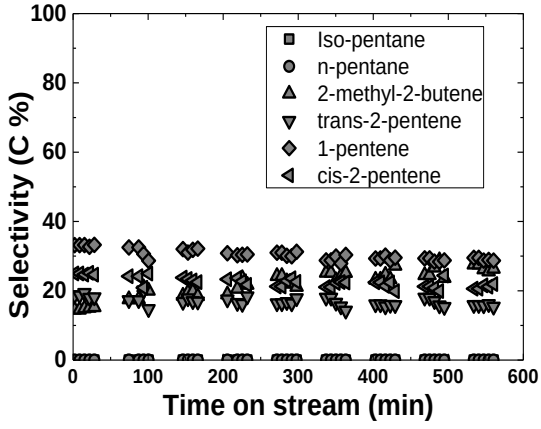

Figure G2: typical C5s composition at 823 K

Figures G1 and G2 show typical C5s selectivities versus TOS at 748 and 823 K over H-SAPO-5. The C_5s were made up of more than 80 % pentenes at all TOS. At 823 K, there were no pentanes.

H Mass balance for butene test within 673-823 K

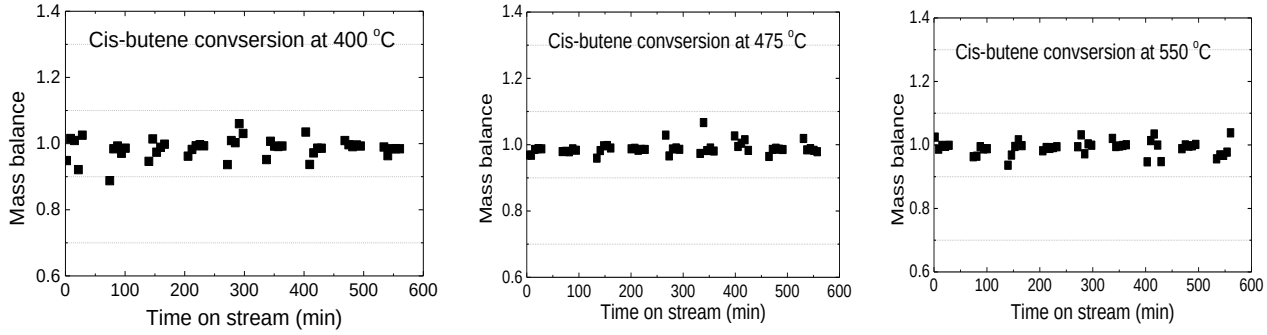

Figure H1: Mass balance over H-SAPO-5, conversion between 10-0.2 %

Figure H1 shows the mass balance of conversion over H-SAPO-5 at 673, 748 and 823 K. The mass balance was about 1±0.1 which indicated that roughly all products were accounted.

I Activity of catalyst before and after regeneration

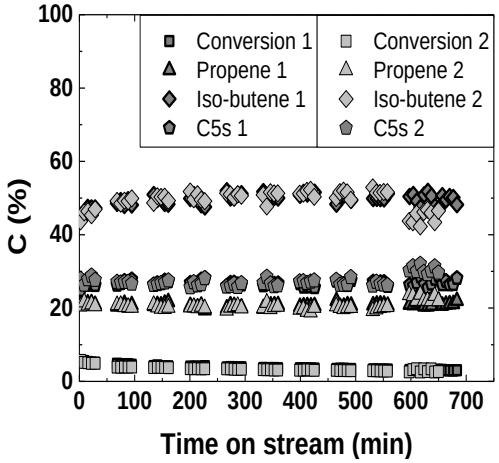

Figure I1: H-SAPO-5 at 748 K, 4.5 kPa.

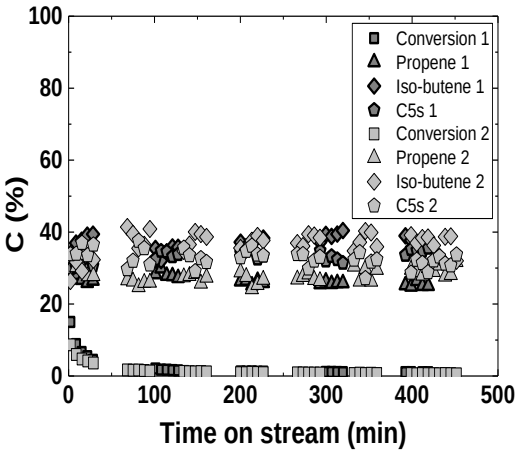

Figure I2: H-SSZ-24 at 748 K, 4.5 kPa.

Figures I1 and I2 show the activity versus TOS over H-SAPO-5 and H-SSZ-24 respectively before (1) and after (2) regeneration at 823 K in O_2. This indicated that the catalysts reproduce similar results after regeneration.

J Co-feed reaction at 673 K

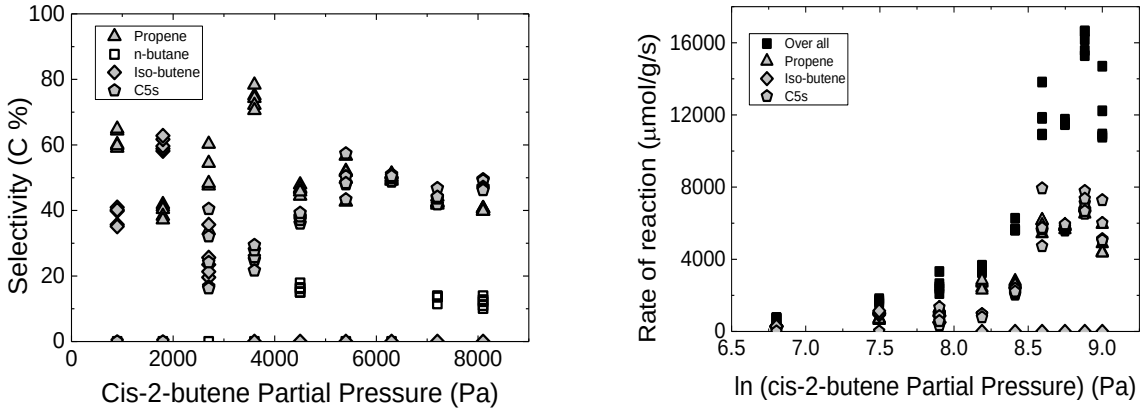

Figure J1: Cis-2-butene variation in co-feed reaction over H-SSZ-24

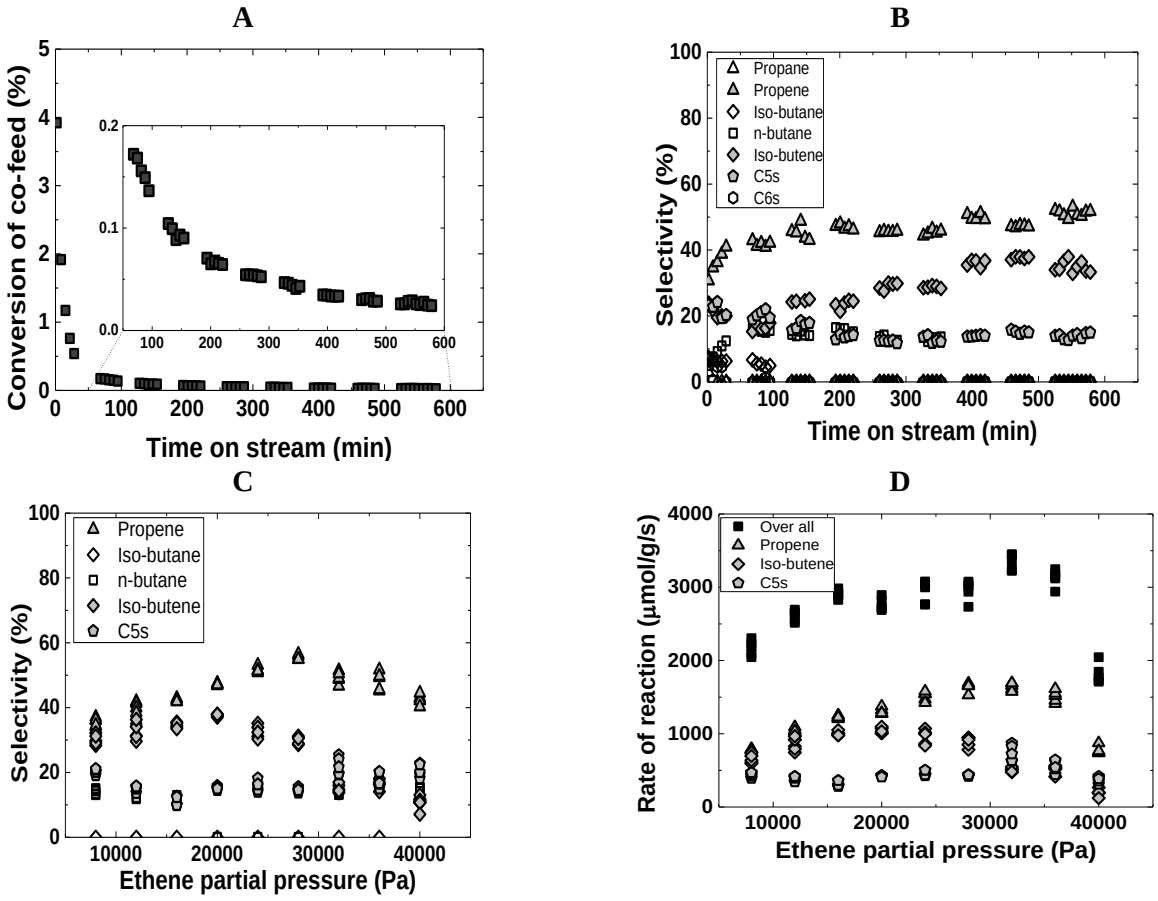

Figure J2: Ethene variation in CO-feed experiment over H-SSZ-24

REFERENCES

[1] Key World Energy Statistics, International Energy Agency, 2010.

[2] J.C. Mol, Journal of Molecular Catalysis A: Chemical, 213 (2004) 39-45.

[3] J.A. Moulijn, M. Makkee, A.V. Diepen, Chemical Process Technology, John Wiley & Sons, 2001.

[4] U.S. Energy Information Administration http://www.eia.gov/energy_in_brief/article/about_shale_gas.cfm, (Accessed: 11.05.14).

[5] A.H. Tullo, Chemical and Enginering News, 2012.

[6] J. Skupinska, Chemical Reviews, 91 (1991) 613-648.

[7] M. Iwamoto, Molecules, 16 (2011) 7844-7863.

[8] H. Oikawa, Y. Shibata, K. Inazu, Y. Iwase, K. Murai, S. Hyodo, G. Kobayashi, T. Baba, Applied Catalysis A: General, 312 (2006) 181-185.

[9] A. Ito, H. Maekawa, H. Kawagoe, K. Komura, Y. Kubota, Y. Sugi, Bulletin of the Chemical Society of Japan, 80 (2007) 215-223.

[10] S. Upadhyayula, Journal of Chemical Sciences, 121 (2009) 199-207.

[11] G.A. Somorjai, Introduction to Surface Chemistry and Catalysis, John Wiley & Sons, Inc., 1994, pp. 444-446.

[12] I. Chorkendorff, J.W. Niemantsverdriet, Concepts of Modern Catalysis and Kinetics, 2nd ed., WILEY-VCH Verlag GmbH & Co, 2007, pp. 1-69, 185-190.

[13] E. Farnetti, R. Di Monte, J. Kaspar, Homogeneous and Heterogeneous Catalysis in Inorganic and Bio-inorganic Chemistry :http://www.eolss.net/sample-chapters/c06/e6-100-10-00.pdf, Encyclopedia of Life Support Systems, 2000s (Accessed: 13.05.13).

[14] S. Svelle, M. Bjørgen, in: S.B. A. Zecchina, E. Groppo (Ed.) Selective Nanocatalysts and Nanoscience, Wiley-VCH Verlag GmbH & Co. KGaA, 2011, pp. 241-247.

[15] C. Baerlocher, L.B. McCusker, D.H. Olson, Atlas of Zeolite Framework, 6th Revised ed., Elsevier, 2007.

[16] C. Baerlocher, L.B. McCusker, Database of Zeolite Structures: http://www.iza-structure.org/databases/, (Accessed: 30.04.14).

[17] L.B. McCusker, C. Baerlocher, Introduction to Zeolite Science and Practice, Elsevier B. V., 2007, pp. 13-37.

[18] P. Payra, P. Dutta, in: K.A.C. S. M. Auerbach, P. K. Dutta (Ed.) Handbook of Zeolite Science and Technology, Marcel Dekker, Inc., 2003, pp. 1-19.

[19] A. Feller, A. Guzman, I. Zuazo, J.A. Lercher, Journal of Catalysis, 224 (2004) 80-93.

[20] S.T. Wilson, B.M. Lok, C.A. Messina, T.R. Cannan, E.M. Flanigen, Journal of the American Chemical Society, 104 (1982) 1146-1147.

[21] M. Bennett J, P. Cohen J, M. Flanigen Edith, J. Pluth J, V. Smith J, Intrazeolite Chemistry, American Chemical Society, 1983, pp. 109-118.

[22] B.M. Lok, C.A. Messina, R.L. Patton, R.T. Gajek, T.R. Cannan, E.M. Flanigen, Journal of the American Chemical Society, 106 (1984) 6092-6093.

[23] A. Van Nordstrand Robert, S. Santilli Don, I. Zones Stacey, Perspectives in Molecular Sieve Science, American Chemical Society, 1988, pp. 236-245.

[24] R.M. Barrer, C. Marcilly, Journal of the Chemical Society A: Inorganic, Physical, Theoretical, (1970) 2735-2745.

[25] J. Yu, Introduction to Zeolite Science and Practice, Elsevier B. V., 2007, pp. 39-48.

[26] E.M. Flanigen, B.N. Lok, L.R. Patton, S.T. Wilson, Pure and Applied Chemistry, 58 (1986) 1351-1358.

[27] M. Westgård Erichsen, S. Svelle, U. Olsbye, Catalysis Today, 215 (2013) 216-223.

[28] J. McMurry, Organic Chemistry a biological approach, ThomsonBrooks/Cole, 2007, pp. 239-250.

[29] L. Domokos, L. Lefferts, K. Seshan, J.A. Lercher, Journal of Catalysis, 197 (2001) 68-80.

[30] D.S. McGuinness, Chemical Reviews, 111 (2010) 2321-2341.

[31] H. You, W. Long, Y. Pan, Petroleum Science and Technology, 24 (2006) 1079-1088.

[32] T. Baba, H. Sawada, Physical Chemistry Chemical Physics, 4 (2002) 3919-3923.

[33] E.V. Anslyn, D.A. Dougherty, Modern Physical Organic Chemistry, University Science Books, 2006, pp. 52-59,87-112.

[34] H. Zhou, Y. Wang, F. Wei, D. Wang, Z. Wang, Applied Catalysis A: General, 348 (2008) 135-141.

[35] J.M. Thomas, W.J. Thomas, Principles and Practice of Heterogeneous Catalysis, VCH Verlagsgesellschaft mbH, 1996, pp. 65-125, 295-314.

[36] B. Lin, Q. Zhang, Y. Wang, Industrial & Engineering Chemistry Research, 48 (2009) 10788-10795.

[37] G. Spoto, S. Bordiga, G. Ricchiardi, D. Scarano, A. Zecchina, E. Borello, Journal of the Chemical Society, Faraday Transactions, 90 (1994) 2827-2835.

[38] H.H. Mooiweer, K.P. de Jong, B. Kraushaar-Czarnetzki, W.H.J. Stork, B.C.H. Krutzen, Studies in Surface Science and Catalysis, 84 (1994) 2327-2334.

[39] M. Guisnet, P. Andy, N.S. Gnep, E. Benazzi, C. Travers, Journal of Catalysis, 158 (1996) 551-560.

[40] M. Guisnet, P. Andy, N.S. Gnep, C. Travers, E. Benazzi, Journal of the Chemical Society, Chemical Communications, (1995) 1685-1686.

[41] P. Andy, N.S. Gnep, M. Guisnet, E. Benazzi, C. Travers, Journal of Catalysis, 173 (1998) 322-332.

[42] J. Houžvička, O. Diefenbach, V. Ponec, Journal of Catalysis, 164 (1996) 288-300.

[43] J. Houžvička, V. Ponec, Catalysis Reviews, 39 (1997) 319-344.

[44] P. Meriaudeau, R. Bacaud, L.N. Hung, A.T. Vu, Journal of Molecular Catalysis A: Chemical, 110 (1996) 177-179.

[45] J. Čejka, B. Wichterlová, P. Sarv, Applied Catalysis A: General, 179 (1999) 217-222.

[46] J. Houžvička, S. Hansildaar, V. Ponec, Journal of Catalysis, 167 (1997) 273-278.

[47] G. Seo, M.Y. Kim, J.H. Kim, Catalysis Letters, 67 (2000) 207-213.

[48] J.I. Villegas, N. Kumar, T. Heikkilä, V.P. Lehto, T. Salmi, D.Y. Murzin, Top Catal, 45 (2007) 187-190.

[49] J.W. Niemantsverdriet, Spectroscopy in Catalysis, An introduction, 3rd Completely Revised and Enlarge ed., Wiley-VCH, 2007.

[50] E.R. Morris, P.S. Wheatley, Introduction to Zeolite Science and Practice Elsevier B. V., 2007, pp. 380-391.

[51] A.W.B. Skilbred, H. Fjeld, R. Strandbakke, Lecture notes for SEM module, University of Oslo, 2012.

[52] S. Brunauer, P.H. Emmett, E. Teller, Journal of American Chemical Society 60 (1938) 309-319.

[53] M. Westgård Erichsen, M. Sc. thesis, University of Oslo, 2010.

[54] K.S.W. Sing, R.A.W. Haul, L. Moscou, R.A. Pierotti, J. Rouquérol, T. Siemieniewska, Pure and Applied Chemistry, 57 (1985) 603-619.

[55] J.A. Lercher, A. Jentys, Introduction to Zeolite Science and Practice Elsevier B. V., 2007, pp. 448-452.

[56] A. Maczek, Statistical thermodynamics, Oxford University Press, 1998, pp 58.

[57] K. Gable, Oregon State University: http://chemistry.oregonstate.edu/courses/ch361-464/ch362/irinstrs.htm, (Accessed: 26.02.14).

[58] M. Westgård Erichsen, S. Svelle, U. Olsbye, Journal of Catalysis, 298 (2013) 94-101.

[59] M.M.J. Treacy, J.B. Higgins, Database of Zeolite Structures: http://www.iza-structure.org/databases/, (Accessed: 24.02.14).

[60] M. Briend, A. Shikholeslami, M.-J. Peltre, D. Delafosse, D. Barthomeuf, Journal of the Chemical Society, (1989) 1361-1362.

[61] I. Petrovic, A. Navrotsky, M.E. Davis, S.I. Zones, Chemistry of Materials, 5 (1993) 1805-1813.

[62] J. Martinez-Triguero, M.J. Diaz-Cabañas, M.A. Camblor, V. Fornẽs, L.M. Maesen, A. Corma, Journal of Catalysis, 182 (1999) 463-469.

[63] S.G. Hedge, P. Ratnasamy, L.M. Kustov, V.B. Kazansky, Zeolites, 8 (1988) 137-141.

[64] F. Schueth, D. Demuth, B. Zibrowius, J. Kornatowski, G. Finger, Journal of the American Chemical Society, 116 (1994) 1090-1095.

[65] C. Halik, J.A. Lercher, H. Mayer, Journal of the Chemical Society, Faraday Transactions 1: Physical Chemistry in Condensed Phases, 84 (1988) 4457-4469.

[66] Y. Matsunaga, H. Yamazaki, T. Yokoi, T. Tatsumi, J.N. Kondo, The Journal of Physical Chemistry C, 117 (2013) 14043-14050.

[67] A. Zecchina, F. Geobaldo, C. Lamberti, S. Bordiga, G. Turnes Palomino, C. Otero Areán, Catalysis Letters, 42 (1996) 25-33.

[68] A. Zecchina, S. Bordiga, G. Spoto, D. Scarano, G. Petrini, G. Leofanti, M. Padovan, C.O. Arean, Journal of the Chemical Society, Faraday Transactions, 88 (1992) 2959-2969.

[69] K. Chakarova, K. Hadjiivanov, The Journal of Physical Chemistry C, 115 (2011) 4806-4817.

[70] H.G. Karge, Microporous and Mesoporous Materials, 22 (1998) 547-549.

[71] T.H. Ballinger, J.T. Yates, Langmuir, 7 (1991) 3041-3045.

[72] M.A. Makarova, K.M. Al-Ghefaili, J. Dwyer, Journal of Chemical Society, Faraday Transactions, 90 (1994) 383-386.

[73] P. Warfvinge, Lund of University, Department of Chemical Engineering, 2009, pp. 41-43, 51-72.

[74] M.K. Stenstrom, D. Rosso, in: UCLA (Ed.) http://www.seas.ucla.edu/stenstro/Reactor.pdf, (Accessed: 04.03.14) 2003, pp. 1-5.

[75] H.A. Jakobsen, in: NTNU (Ed.) Department of Chemical Engineering, 2011, pp. 3-13.

[76] F.M. Dautzenberg, in: M.J.G. S. A. Bradley, R. J. Bertolacini, (Ed.) Characterization and Catalyst Development, American Chemical Society, 1989, pp. 99-119.

[77] P. Atkins, d.J. Paula, Atkins' Physical Chemistry, 8th ed., Oxford Press, 2006.

[78] P. Houston, Chemical Kinetics and Reaction Dynamics, Dover Publications, Inc., 2001.

[79] D. Harvey, Modern Analytical Chemistry, The McGraw-Hill Co., Inc., 2000, pp. 549-577.

[80] W.A. Dietz, Journal of Gas Chromatography, 5 (1967) 68-71.

[81] NIST, Thermodynamics Research Center, Standard Reference Database 85, Version 1.5 software, 2001.

[82] B. de Ménorval, P. Ayrault, N.S. Gnep, M. Guisnet, Applied Catalysis A: General, 304 (2006) 1-13.

[83] S.M. Babitz, B.A. Williams, J.T. Miller, R.Q. Snurr, W.O. Haag, H.H. Kung, Applied Catalysis A: General, 179 (1999) 71-86.

[84] M. Misk, G. Joly, P. Magnoux, S. Jullian, M. Guisnet, Zeolites, 16 (1996) 265-270.

[85] S. Svelle, P.O. Rønning, U. Olsbye, S. Kolboe, Journal of Catalysis, 234 (2005) 385-400.

[86] B. Wichterlová, N. Žilkova, E. Uvarova, J. Čejka, P. Sarv, C. Paganini, J.A. Lercher, Applied Catalysis A: General, 182 (1999) 297-308.

[87] B.A. De Moor, M.-F.o. Reyniers, O.C. Gobin, J.A. Lercher, G.B. Marin, The Journal of Physical Chemistry C, 115 (2010) 1204-1219.

[88] E. Yoda, J.N. Kondo, K. Domen, The Journal of Physical Chemistry B, 109 (2005) 1464-1472.

[89] F. Eder, M. Stockenhuber, J.A. Lercher, The Journal of Physical Chemistry B, 101 (1997) 5414-5419.

[90] X. Ding, S. Geng, C. Li, C. Yang, G. Wang, Journal of Natural Gas Chemistry, 18 (2009) 156-160.